Propulsive Abort Trajectory Options for a Reconnaissance Human Mars Mission

MSc Thesis Report

Palash Patole

February 20, 2020

Delft University of Technology

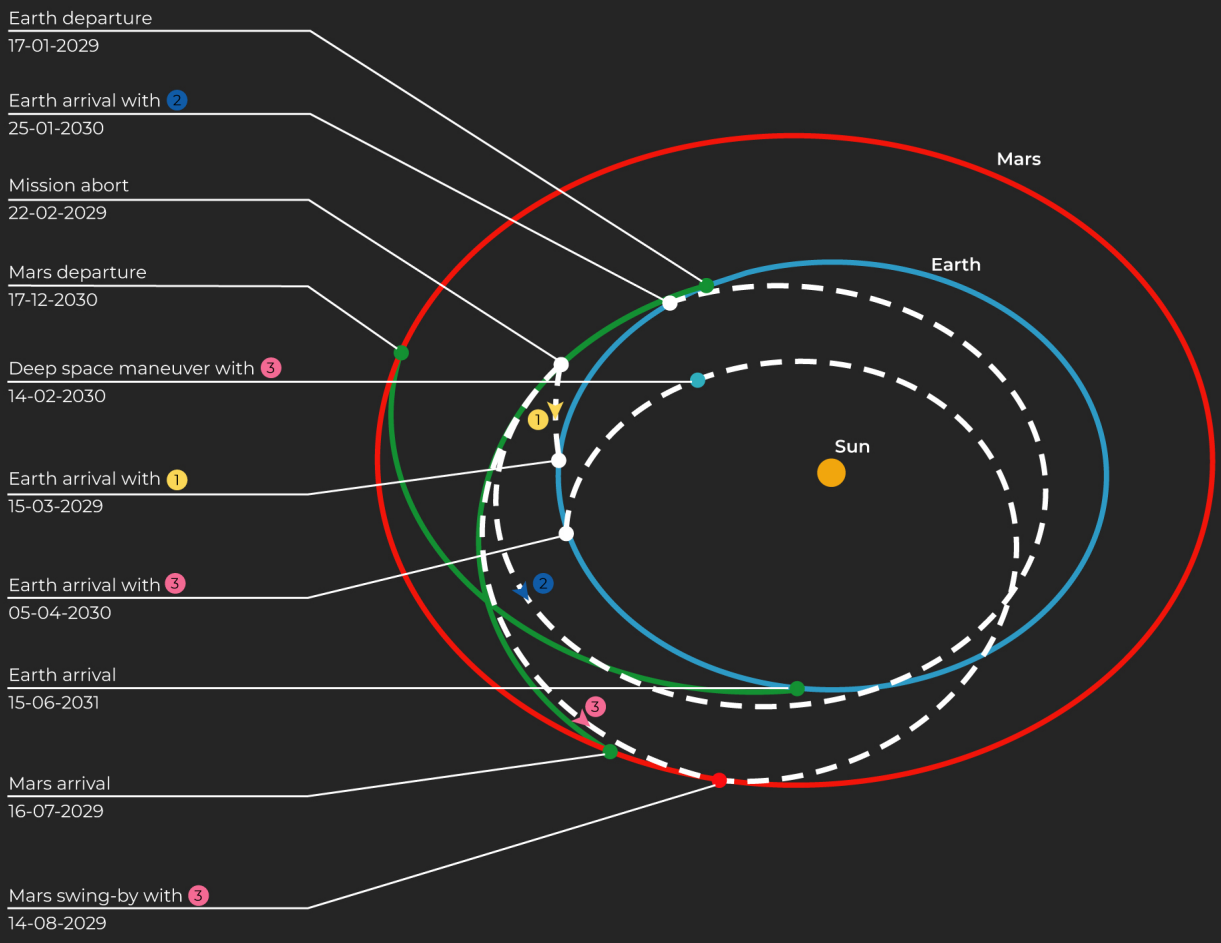

TU Delft Delft University of Technology

Challenge the future

Propulsive Abort Trajectory Options for a Reconnaissance Human Mars Mission

MSc Thesis Report

by

Palash Patole

in partial fulfillment of the requirements for the degree of

Master of Science
in Aerospace Engineering

at the Delft University of Technology,
to be defended publicly on Thursday February 20, 2020.

Student number:	4721284	
Supervisor:	ir. R. Noomen,	TU Delft
Thesis committee:	Dr. D. M. Stam,	TU Delft
	ir. B.T.C. Zandbergen,	TU Delft

This thesis is confidential and cannot be made public until February 20, 2022.

TU Delft Delft University of Technology

Preface

In recent years, the global space sector has witnessed an emergence of private industries that are undertaking complex spaceflight projects while competing with national space agencies or traditional contractors having bigger budgets. Often dubbed as *NewSpace* or *Space 2.0*, this age of space exploration is influenced by the commercial interests of these private companies to develop, test and deploy a range of technologies, and such ventures are changing the landscape of our capabilities for space exploration. While the dream of leaving our footprints on Martian soil has existed from even before the *Apollo* missions, the recent developments might lead to the actual execution of human Mars exploration plans within the next few decades.

As a graduate student who developed a keen interest in the field of astrodynamics and space mission design, I have decided to focus my thesis research on finding optimal interplanetary trajectory solutions having a fail-safe Earth-return provision that can be used for a reconnaissance human Mars mission. Through this work, I have computed some of the important trajectory parameters associated with such optimal solutions and tried to understand the effect of their values on the mission requirements. This thesis research represents an application of my academic and technical skill-set, so far obtained as an aerospace engineer, while making a small contribution to the existing body of knowledge.

I am grateful to my supervisor - Ron Noomen - for our weekly meetings and his continuous guidance and support throughout the period of two years. Without him playing the *devil's advocate* and providing me the valuable suggestions, this research would not have achieved its full potential. I would like to thank my parents and my sister, for providing me the opportunity to step into a bigger world and grow as an individual through such an experience. I am equally grateful to my family in the Netherlands - Amey, Sharayu, Nihar, Hetal, Maneesh and Anmol - for all the love and great memories, and to my friends from the 9th floor for providing me an encouraging and joyful environment. Finally, special thanks to Shubham - a good friend for years and one of the most creative product designers I have ever met - for providing a nice illustration for the cover page.

Palash Patole
Delft, February 2020

Abstract

For a human Mars exploration mission, it is required to minimize the time-of-flight of the interplanetary trajectories to mitigate the adverse effects of the radiation environment and prolonged weightlessness conditions on the health of the crew. Moreover, having a fail-safe provision to return the crew back to Earth in case of a mission abort situation is highly desirable. This thesis research investigated several optimal/sub-optimal and feasible solutions for the high-thrust interplanetary transfer and abort trajectories of a reconnaissance human Mars mission. A conjunction-class mission architecture has been analyzed to transport the crew to and from Mars during the transfer opportunities in 2028 and 2030, respectively. Baseline requirements of such a mission were defined by finding the optimal ballistic Earth-to-Mars and Mars-to-Earth transfer trajectory solutions. A number of propulsive abort trajectory solutions were then computed that can return the crew back to Earth when the nominal mission is aborted either during the Earth-to-Mars transfer or during the Mars surface stay period. A semi-analytic trajectory model was used for the design of such abort trajectories that can include one or two deep space maneuvers and a powered Mars swing-by. With the use of a meta-heuristic global optimization algorithm, multi-objective optimization problems were solved to minimize the ΔV cost and the interplanetary transit duration of the mission. By comparing the transfer and abort trajectory solutions, it was concluded that various abort trajectory options can be provided for a reconnaissance human Mars mission, that also satisfy the imposed constraint on the arrival excess velocity. The effects of such abort trajectory options on the ΔV cost and other baseline mission requirements (such as the total mission duration) were analyzed. Critical challenges of such a safe human Mars mission architecture have been identified and discussed.

Contents

List of Abbreviations

CP	Chemical Propulsion
DE	Differential Evolution
DRM	Design Reference Mission
DSM	Deep Space Maneuver
EP	Electric Propulsion
GCR	Galactic Cosmic Rays
GPS	Global Positioning System
HECRF	Heliocentric Ecliptic Reference Frame
ICRF	International Celestial Reference Frame
IMLEO	Initial Mass in (or Injected Mass to) Low Earth Orbit
ISRU	In-situ Resource Utilization
JD	Julian Date
JPL	Jet Propulsion Laboratory
LEO	Low Earth Orbit
LGA	Lunar Gravity Assist
LMO	Low Mars Orbit
MATLAB	Matrix Laboratory
MGA	Multiple Gravity Assists/Assisted
MGA-1DSM-PF	Multiple Gravity Assist with 1 Deep Space Maneuver per leg, using the Position Formulation approach
MGA-1DSM-VF	Multiple Gravity Assist with 1 Deep Space Maneuver per leg, using the Velocity Formulation approach
MJD2000	Modified Julian Date relative to the J2000 epoch
MOEA/D	Multi-objective Evolutionary Algorithm by Decomposition
NASA	National Aeronautics and Space Administration
NEP	Nuclear Electric Propulsion
NSGA-II	Non-dominated Sorting Genetic Algorithm
NTP	Nuclear Thermal Propulsion
NTR	Nuclear Thermal Rocket
PaGMO	Parallel Global Multi-objective Optimizer
S/C	Spacecraft

SEP	Solar Electric Propulsion
SOI	Sphere of Influence
SPE	Solar Particle Event
TCM	Trajectory Correction Maneuver
TEI	Trans-Earth Injection
TMI	Trans-Mars Injection
TOF	Time of Flight
TRL	Technology Readiness Level
TT	Terrestrial Time
Tudat	TU Delft Astrodynamics Toolbox
TV	Transfer Vehicle

List of Symbols

In the following tables, the lists of symbols used in this report are presented to explain their meanings. A list of the Roman symbols and a list of the Greek symbols are first presented. This is followed by a list of subscripts that are often used with such symbols. Finally, a list of symbols for the various propulsive maneuvers associated with the trajectory solutions of this thesis is also provided.

Roman Symbols

Symbol	Meaning	SI Unit
A_B	Bond albedo	[-]
a	Semi-major axis	[m]
b_{incl}	Three dimensional rotation inclination angle	[rad]
C_3	Departure energy or injection energy	$[m^2 \cdot s^{-2}]$
E	Elliptic eccentric anomaly	[rad]
e	Eccentricity	[-]
F	Hyperbolic eccentric anomaly	[rad]
G	Gear ratio	[-]
g_0	Standard acceleration due to gravity	$[m \cdot s^{-2}]$
h_{cm}	Altitude of the circular parking orbit around Mars	[m]
h_p	Altitude of the pericenter	[m]
I_0	Solar constant	$[W \cdot m^{-2}]$
I_{sp}	Specific impulse	[s]
i	Index of a generation	[-]
i_{buffer}	Minimum number of generations after detecting the convergence	[-]
i_{max}	Maximum number of generations	[-]
i_{min}	Minimum number of generations	[-]
K	Inert mass fraction for a propulsion system	[-]
M	Elliptic mean anomaly	[rad]
$\bar{M}$	Hyperbolic mean anomaly	[rad]
$m_{heat-shield}$	Mass of the heat-shield for a taxi vehicle	[kg]
m_{landed}	Landed mass of a taxi vehicle	[kg]
Obj_1	Objective I of the optimization problem	[-]
Obj_2	Objective II of the optimization problem	[-]
q	Mass ratio	[-]
R_m	Average radius of Mars	[m]
r	Position in space from the origin	[m]
r_p	Pericenter radius	[m]
$r_{Sun-min}$	Minimum distance to the Sun	[m]
T_{eq}	Equilibrium or effective black-body temperature	[K]
T_i	TOF of ith leg in a trajectory model	[s]
$T_{mission}$	Total duration of the mission	[s]
$T_{nom-surf}$	Nominal Mars surface stay period	[s]
t	Time/Epoch	[s]
$t_{DSM,i}$	Epoch of application of a DSM during ith leg of a trajectory model	[s]
t_i	Epoch of a planetary encounter during ith leg of a trajectory model	[s]
t_{nom-ED}	Nominal Earth-departure epoch	[s]
t_{nom-MA}	Nominal Mars-arrival epoch	[s]

Roman Symbols

Symbol	Meaning	SI Unit
V	Velocity	$[m \cdot s^{-1}]$
V_∞	Hyperbolic excess velocity	$[m \cdot s^{-1}]$
$V_{\infty-EA}$	V_∞ when the S/C arrives at Earth	$[m \cdot s^{-1}]$
V_p	Velocity at pericenter	$[m \cdot s^{-1}]$
W_i	Weighing factor in the penalty function (i = 1, 2, 3,and 4)	[-]
x	X-coordinate	[m]
$\bar{x}$	Arithmetic mean	various
y	Y-coordinate	[m]
	Variable	various
z	Z-coordinate	[m]

Greek Symbols

Symbol	Meaning	SI Unit
α	Total bending angle during the gravity assist	[rad]
ΔV	Change in the spacecraft's velocity	$[m \cdot s^{-1}]$
$\Delta\theta$	Heliocentric transfer angle	[rad]
$\delta/2$	Bending angle of a leg during the gravity assist	[rad]
η_{abort}	Abort fraction	[-]
η_i	Fraction of the TOF at which a DSM is performed (during ith leg of a trajectory model)	[-]
θ	True anomaly	[rad]
	In-plane angle of the V_∞	[rad]
λ	Payload ratio	[-]
μ	Gravitational parameter	$[m^3 \cdot s^{-2}]$
$\Sigma\Delta V$	Sum of all the relevant ΔVs	$[m \cdot s^{-1}]$
σ	Standard deviation	[various]
	Stefan-Boltzmann constant	$[W \cdot m^{-2} \cdot K^{-4}]$
ϕ	Out-of-plane angle of the V_∞	[rad]

Common subscripts used with the Roman/Greek Symbols

Subscript	Meaning
f	Final
GA	Gravity assist
i	Initial
in	Incoming
nom	Nominal
o	Initial
out	Outgoing
pl or *planet*	Planet

Symbols for the propulsive maneuvers

Symbol	Meaning	SI Unit
ΔV_1	ΔV for the departure from the parking orbit around Earth (ΔV for the TMI)	$[m \cdot s^{-1}]$
ΔV_2	ΔV for the capture into the parking orbit around Mars	$[m \cdot s^{-1}]$
ΔV_3	ΔV for the departure from the parking orbit around Mars (ΔV for the TEI)	$[m \cdot s^{-1}]$
ΔV_4	ΔV for the abort during the Earth-to-Mars transfer	$[m \cdot s^{-1}]$
ΔV_5	ΔV for the DSM during the Earth-to-Mars transfer	$[m \cdot s^{-1}]$
ΔV_6	ΔV for the powered gravity assist at Mars	$[m \cdot s^{-1}]$
ΔV_7	ΔV for the DSM during the Mars-to-Earth transfer	$[m \cdot s^{-1}]$

1

Introduction

One of the hardest technological challenges that humans can possibly undertake in the 21st century is a human Mars mission, with a long-term goal to establish a sustainable surface base. Going to the *Red Planet* implies taking our intellectual, physical and psychological capabilities to the next level. Such a complex mission would have to be executed with manageable financial expenditure and would require a number of provisions for the safety of the astronauts. This thesis work aims to find optimal, safe and feasible interplanetary high-thrust transfer and abort trajectory solutions for a mission in the early stages of human Mars exploration (which is referred to as a reconnaissance mission). Finding such trajectory solutions will account for the knowledge gap that had been identified in the earlier literature study phase. The primary research question for this thesis work can be stated as follows.

- Is it possible to include an option of returning to Earth when a reconnaissance human Mars mission is aborted?

This primary research question can be split into four logical research sub-questions as follows.

1. What are the optimum high-thrust interplanetary trajectory solutions for Earth-to-Mars and Mars-to-Earth transfers in a reconnaissance human Mars mission, considering the total time of flight (TOF) and the total ΔV requirement?
2. What are the feasible high-thrust Earth-return abort trajectory options with and without the use of a Mars swing-by, if such a reconnaissance human Mars mission is aborted during the nominal Earth-to-Mars transfer?
3. What are the feasible high-thrust Earth-return abort trajectory options if such a reconnaissance human Mars mission is aborted during the nominal Mars surface stay period?
4. How do the important trajectory parameters of the investigated abort trajectory options compare with those of the nominal transfer trajectory options?

While addressing the above research sub-questions, the feasibility and optimality of the trajectory solutions are analyzed from a technical perspective and other aspects such as the financial feasibility are not taken into account. The relevant aspects have been presented in different chapters of this report. Existing literature for the interplanetary trajectory design of a Mars mission was first studied to define the scope of this novel research work. Important conclusions of this study have been summarized in Chapter 2, along with the rationale for a reconnaissance mission and the use of high-thrust propulsion. The subsequent chapter presents an overview of the methodology followed to find the trajectory solutions and also describes the underlying foundation for the trajectory optimization problems to be solved. Chapters 4 to 6 elaborate on three building blocks of the research methodology viz. methods for the solution of a transfer trajectory problem, methods for the solution of an abort trajectory problem, and the process of optimization, respectively. Results obtained for various transfer and abort trajectory scenarios are presented and discussed in Chapter 7 while Chapter 8 provides results for the sensitivity analysis. In the subsequent chapter, the conclusions of this thesis research have been presented. This report is concluded with Chapter 10, where recommendations for future research have been provided.

2

Heritage

The problem of finding optimum interplanetary trajectory solutions for a human Mars mission is not novel in itself. According to one study which has documented important details of human Mars mission plans of the past 60+ years [1], there have been more than 1000 human Mars mission studies performed by space agencies like the National Aeronautics and Space Administration (NASA), industry study teams, private organizations, etc. between about 1950 and 2000 itself. While it is not possible to study the trajectory design aspects of all these studies due to time constraints, important ideas and architectures have been studied and summarized in this chapter.

In Section 2.1, key mission architectures will be described which are used by several proposed trajectory designs of interest. The subsequent section describes a number of relevant technologies associated with a human Mars mission that can influence the selection of the mission architecture and/or improvise the performance of a selected architecture. Section 2.3 describes some of the important challenges of a human Mars mission from the trajectory design perspective. Based on all this information, Section 2.4 provides the rationale for the research questions of this thesis work.

2.1. Mission Architectures

In the context of this thesis report, a mission architecture refers to the specific placement and transportation of various mass elements of the mission (such as the crewed spacecraft (S/C)[1], Mars surface habitat, Mars ascent vehicle, Earth return taxi vehicle) in/through various orbits such as the parking orbit, a flyby trajectory. Seven mission architectures are discussed in this section.

2.1.1. Conjunction and Opposition Class

Interplanetary transfer trajectories are often termed as conjunction class or opposition class solutions, depending upon the geometry of Earth and Mars when the S/C departs for interplanetary transfer. For a conjunction class mission[2], Earth and the target planet are close to each other when the S/C departs Earth and are on the opposite sides of the Sun when the S/C reaches the target planet. Opposition class missions or short-stay missions have Earth and the target planet on the same side of the Sun at arrival. Representative trajectory visualizations for these two classes of missions with Mars as the target planet are shown in Figure 2.1.

Conjunction class missions have a shorter in-space duration but a longer surface duration compared to the opposition class missions [2]. For missions from Earth to Mars and back, both outbound and inbound transfer trajectories of conjunction class missions would lie outside the (average) Earth orbit around the Sun. On the other hand, for the opposition class missions, there exists a longer transit leg.

[1] Crewed S/C is the spacecraft that transports the astronauts between Earth and Mars. It is also referred to as a transfer vehicle (TV) in many studies, including this report. Interplanetary transfer trajectories followed by such a crewed S/C are to be optimized in this thesis work.

[2] Conjunction class missions are also referred to as Hohmann transfer missions or long-stay missions in the literature.

If such longer transit legs are used to come back to Earth from Mars, it will cross the (average) Earth orbit and a Venus flyby can be used in such a case [1] [3].

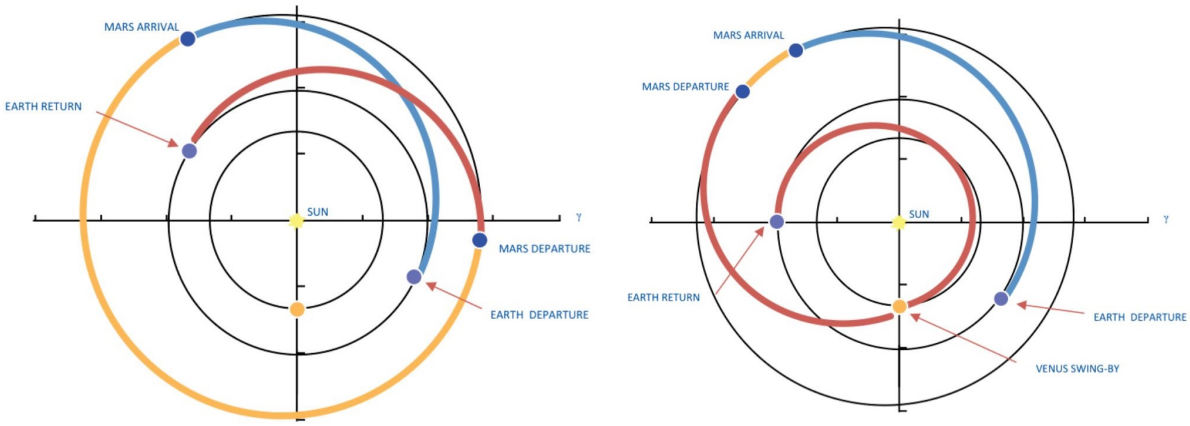

Figure 2.1: Trajectory visualizations for the conjunction class (*left*) and the opposition class (*right*) missions [3].

While comparing these two mission architectures with each other, [3] mentions that greater risks are associated with human health due to close passage to the Sun in the case of opposition class missions. Opposition class missions also require higher ΔV which varies from opportunity to opportunity [1]. However, these higher ΔV requirements might not translate into a higher propellant requirement as a major fraction of the total ΔV would be spent for the lighter S/C returning to Earth [3].

Depending upon whether the crew starts from/ descends to the planetary surface directly using the transfer vehicle (TV) or uses a taxi vehicle to travel to/ from the TV orbiting Earth or the target planet in the parking orbit, these mission architectures can be called direct, semi-direct or stop-over. Figure 2.2 explains the differences between these architectures. NASA *Design Reference Missions (DRM)* such as *DRM-1*, *DRM-3* use the stop-over mission architecture [4].

Architecture	Earth encounter	Mars encounter	Schemata
Direct	Surface	Surface	
Semi-direct	Surface	Parking orbit	
Stop-over	Parking orbit	Parking orbit	
M–E semi-cycler	Flyby	Parking orbit	
E–M semi-cycler	Parking orbit	Flyby	
Cycler	Flyby	Flyby	

Figure 2.2: Schemata for some of the human Mars mission architectures found in literature [4].

2.1.2. Cycler Missions

The cycler mission architecture has the heliocentric trajectory planned such that the S/C encounters Earth and Mars on a regular basis. To avoid the need to launch the TV or capture such TV in parking orbits every time the crew has to be transferred between these two planets, taxi vehicles are utilized to ascend from/descend to the departure/target planet and perform a rendezvous with the TV. On planetary encounters, the TV uses planetary swing-bys to change its direction and additional Deep Space Maneuvers (DSM) might be used to maintain the cycler orbit. A representative trajectory visualization of a cycler mission architecture is shown in Figure 2.3. This architecture concept was introduced by astronaut Buzz Aldrin in 1985 and it has been widely researched and documented such as in [5] [6] [7].

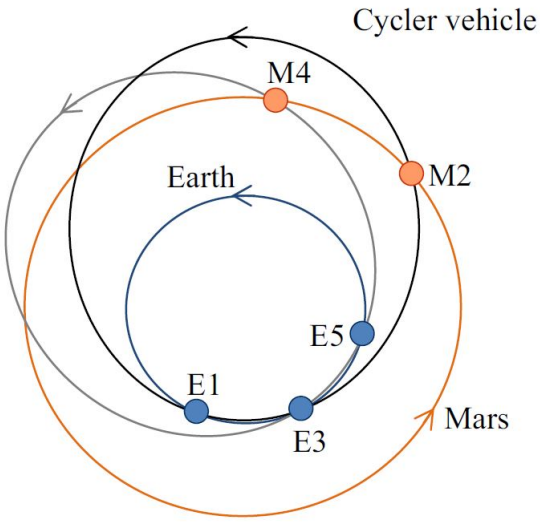

Figure 2.3: Trajectory visualization for a cycler mission architecture [7]. The order of flybys is: Earth(E1)-Mars(M2)-Earth(E3)-Mars(M4)-Earth(E5).

Schemata of this mission architecture compared to others can be seen in Figure 2.2. Use of a single TV leads to a total Earth-Mars-Earth trip time of about two synodic periods[3] while using two TVs, this trip time can be reduced to about a synodic period [7]. The cycler mission architecture can be an attractive choice when a long-term/multi-mission human Mars exploration plan is committed. However, there are two primary disadvantages of this architecture.

As the TV approaches a planet in this architecture, its excess velocity (V_∞) with respect to the planet can have high values. In the case of a Mars encounter, this can be as high as 12 km/s. A higher value of V_∞ will lead to a higher entry velocity for the taxi vehicle, requiring increased mass for the heat shield to withstand thermal loads and for the structure to withstand deceleration loads [7]. One of the solutions to this problem is proposed in [9] where a cycler trajectory derived from a semi-cycler trajectory is used for the Mars-to-Earth transfer and the DSM that such a trajectory uses has an extra ΔV of about 1.8 km/s.

Moreover, the taxi vehicle involved in this mission architecture has to perform a hyperbolic rendezvous with the TV. Not only the velocities required for such maneuvers are higher, but also the time available for executing such operation is smaller, unlike a circular or elliptical orbit rendezvous. The limited duration of the taxi vehicle's life support capacity can make this rendezvous aspect a risky step of the mission [7].

[3]The synodic period is defined as the period after which relative configuration of two planets such as Earth and Mars is *almost* repeated [8]. For Earth and Mars orbits, this period is 2.135 years or about 26 months. Due to eccentricity and inclination of their orbits, the relative configuration of Earth and Mars will not *exactly* repeat after a synodic period, but after 7 to 8 synodic periods.

2.1.3. Semi-cycler Missions

The semi-cycler mission architecture is inspired by the necessity of having a smaller V_∞ value in the cycler architecture [7]. Two types of semi-cycler mission architectures exist viz. Mars-Earth semi-cycler and Earth-Mars semi-cycler [6]. Schemata for these architectures are shown in Figure 2.2. For a Mars-Earth semi-cycler mission, the TV departs from the parking orbit around Mars, performs a swing-by at Earth to drop off the crew returning from their Mars mission, and orbits the Sun to re-counter Earth again. It then picks up the crew for the next Mars mission and travels towards Mars to be captured in an orbit and stays parked in this orbit until the next transfer opportunity. For an Earth-Mars semi-cycler mission, a similar sequence is followed but the TV is parked in an orbit around Earth. As in the case of a cycler mission, taxi vehicles are used in this architecture to ascend from/descent to the planetary surface and DSMs are used to achieve the desired trajectory.

As described in [10], trajectory types can be defined for a semi-cycler mission depending upon the ratio of Earth's revolutions to the TV's revolutions. For example, in a 7:5 trajectory Earth-Mars semi-cycler mission, during seven revolutions of Earth, the TV completes five revolutions. As the TV arrives at Earth seven years after it had initially departed, this S/C will not be available for use in the next three launch opportunities (based on the synodic period). Thus, at least four TVs are required to provide short outbound and inbound transit durations every synodic period.

Based on the comparative assessment of various mission architectures and technologies for a human Mars mission, [4] concludes that for a given technology base, the Earth-Mars semi-cyclers and the cycler architectures require a smallest Initial Mass in Low Earth Orbit (IMLEO) compared to other architectures when recurring launches are considered, as seen in Table 2.1.

	Propulsion system[a]	**ISRU**	**Trajectory architecture**					
	$U_E L_M U_M T$[b]		Direct	Semi-direct	Stop-over	M-E S-C	E-M S-C	Cycler
1	MMMM	No	1170	435	530	582	447	456
2	HHHH	No	801	337	388	413	321	353
3	MMMM	Yes	324	287	323	300	203	197
4	E_{50}MMM	Yes	200	153	162	209	121	165

Table 2.1: Comparative assessment of the six mission architectures using a several technologies [4]. Recurring IMLEO values (in ton) to transfer a crew of four without any cargo for every synodic opportunity are presented. M-E S-C refers to the Mars-Earth semi-cycler while E-M S-C refers to the Earth-Mars semi-cycler. All the missions have a TOF of 210 days, the taxi capsule mass of six ton and the transfer vehicle cabin mass of 24 ton. 20 kg of the consumables are required per day. Three propulsion types are considered [a] : M = LOX/CH_4, H = LOX/LH_2, E_{50} = Electric propulsion with the specific mass / the jet efficiency = 50 kg/kW. Four stages of the propulsion system [b] : U_E = Earth upper stage, L_M = Mars launch vehicle, U_M = Mars upper stage, T = transfer vehicle. ISRU at Mars is used for the propellant production when marked as 'Yes'.

Another study [10] has concluded that the IMLEO value of the Earth-Mars semi-cycler architecture can be $10-50\%$ lower than that of the semi-direct mission architecture when both missions use either the Chemical Propulsion (CP) or the Nuclear Thermal Propulsion (NTP) along with other technologies such as the aerocapture or the In-Situ Resource Utilization (ISRU). It should be noted that these savings in IMLEO do not occur with the first mission itself but after several missions, and this makes the semi-cycler mission an attractive choice when a multi-mission human Mars exploration plan is to be executed.

One of the disadvantages of this architecture is the requirement of extra safety checks of the TV which is continuously operated, often with the periods having no humans on-board [10]. As an unforeseen problem can not be fixed manually, more functional and robust automated systems are required. In-flight demonstration of such systems to achieve the desired Technology Readiness Level (TRL) might take months if not years.

2.1.4. Stop-over Cycler Missions

In Figure 2.2, the schemata of the stop-over architecture is shown where the TV travels between parking orbits around both Earth and Mars. One of the studies [11] refers to such an architecture as a stop-over cycler. The use of two TVs is proposed which are parked in a highly elliptical orbit around

Earth and Mars when not transferring the crew. The name stop-over cycler is justified in the study as the TVs are refueled and they often shuffle between the parking orbits around both planets.

Important advantages of this architecture highlighted in the study are low departure and arrival velocities, flexibility about launch and arrival epochs, elliptical orbit rendezvous rather than challenging hyperbolic rendezvous similar to the cycler/semi-cycler missions, possible use of the TVs for alternative purposes such as an orbiter mission when parked around either planet, easier in-orbit propellant re-fueling for the TV compared to the cycler/semi-cycler missions.

A direct quantitative comparison between this architecture and others was not found in literature. However, as this architecture is essentially a stop-over architecture, based on Table 2.1 it can be concluded that it has higher IMLEO values compared to that of the cycler and the Earth-Mars semi-cycler architectures.

2.1.5. Flyby and Free-return Trajectories

Robotic exploration of Mars was started with flyby missions such as the Soviet mission *Marsnik 1* (1960) and NASA's mission *Mariner 3* (1964), and eventually orbiter and lander missions were undertaken. It can be argued that human exploration of Mars should start with a flyby mission as by eliminating the need to land on the Martian surface, the mission design can be simplified to focus on the risks assessment of the human interplanetary spaceflight and the study of other aspects. Benefits of a human Mars flyby mission have to be traded off against the lower scientific and operational output of such a mission and against those risks which are present in the mission. For a Mars flyby mission, if a shorter outbound trajectory is used then the relative motion of Earth and Mars forces the inbound trajectory to be longer [12].

Three mission architectures belonging to the flyby class of missions have been proposed in [12] viz. the dual habitat trajectory model, the loitering habitat model, and the hybrid dual loitering habitat model. Through the careful design of flyby trajectories and the use of transfer vehicles, all these architectures resolve the issue of generating less scientific/operational output through a flyby mission. An illustration of how the dual habitat trajectory model works and a trajectory visualization for the loitering habitat trajectory model are shown in Figures 2.4 and 2.5 respectively.

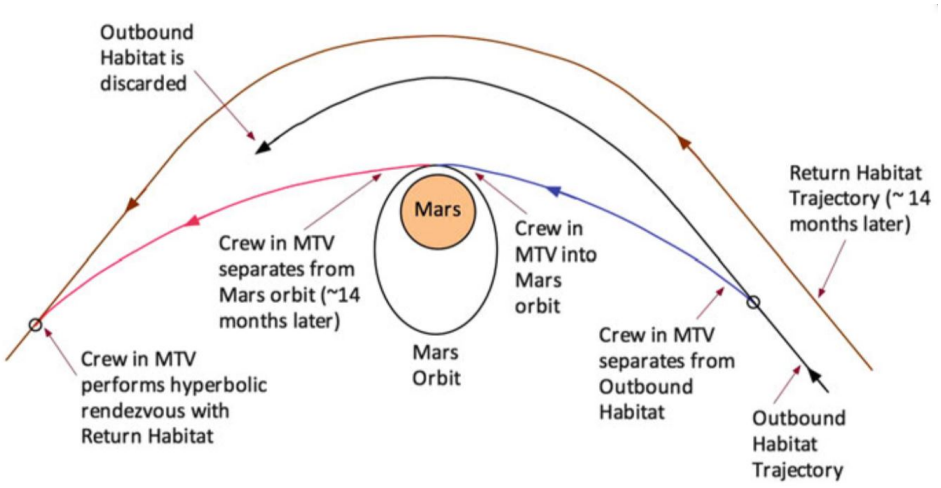

Figure 2.4: Operations during a Mars flyby in the dual habitat trajectory model [1].

The dual habitat trajectory model has two S/C used by the crew during the outbound/inbound transfers to/from Mars, and both of these habitats perform a Mars flyby at Mars at two epochs separated by a considerable period of operation at Mars. On the other hand, the loitering habitat model uses a single S/C or TV for both legs of the mission. Figure 2.5 shows one free-return trajectory possible with this model where the S/C performs two consecutive flybys at Mars before returning to Earth. Inclusion of a DSM in this model allows for more trajectory solutions.

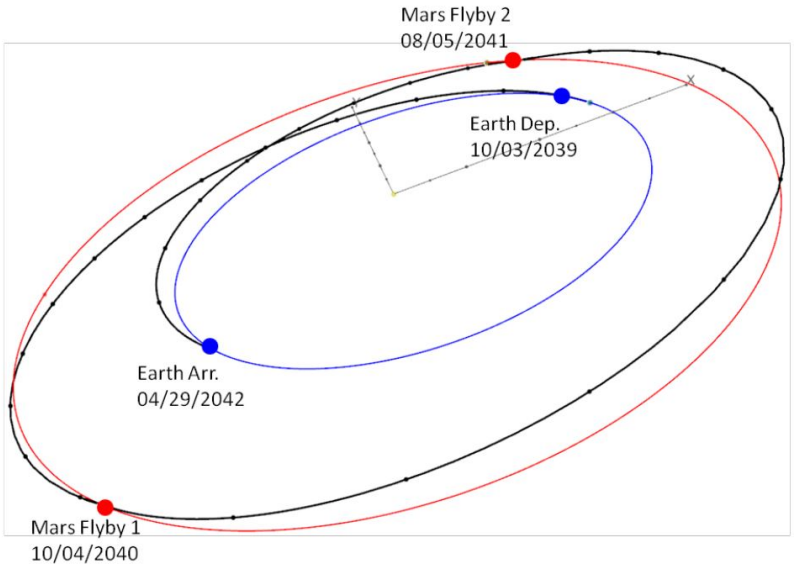

Figure 2.5: Flyby trajectory visualization for the loitering habitat model [12]. A ballistic free-return Earth-Mars-Mars-Earth trajectory for the October 2039 launch opportunity is shown.

The hybrid dual loitering habitat model, as the name suggests, uses two TVs similar to the dual habitat model but both TVs perform two Mars flybys between the epochs of departure from Earth and the epochs of arrival at Earth. By accurately timing the epochs of such flybys at Mars and including DSMs for required corrections, this model provides redundancy as it offers more than one Earth-return opportunity to the crew.

A mission architecture involving a free-return trajectory is important considering a mission abort scenario. With the trajectory of this model, it is possible to abort the mission at Mars arrival and return to Earth after an unpowered gravity assist[4]. Figure 2.6 shows a trajectory visualization for a free-return trajectory mission which has followed a conjunction-class outbound trajectory to Mars. Free-return trajectories exploit resonance in their orbital period and the orbital period of Earth, and in practice also require some mid-course corrections [2].

One of the disadvantages identified for the free-return Mars mission that has been proposed by the *Inspiration Mars Foundation* is the high excess velocity at its Earth arrival which leads to problems such as questionable g-forces for the crew taxi vehicle [1]. As mentioned in [2], the shortest Earth-Mars-Earth trip time associated with a practically possible free-return trajectory architecture is two years. Moreover, such two-year free-return trajectories suffer in terms of high Mars entry velocities in many opportunities between 2020 and 2037. The one-year period for a free-return trajectory drives the perihelion significantly inside Earth's orbit which will result in higher Earth departure ΔV.

2.1.6. Propulsive Abort Trajectories

One of the studies [2] has proposed a human Mars mission architecture using propulsive abort trajectories that allow aborting the mission through a propulsive maneuver. These trajectory solutions differ from the free-return trajectories in the sense that an additional ΔV is provided to the TV when it performs the Mars swing-by. The propulsive-abort trajectory solutions found in this particular study not only decrease the Mars entry velocities but also offer an additional benefit of decreasing the associated Earth departure ΔV. However, the inclusion of an extra ΔV neither reduces the trip time of such trajectories nor it affects the Earth entry velocity compared to free-return trajectories by a large margin. As seen in Figure 2.7, these trajectories have almost the same trip time as that of a two-year

[4]Powered and unpowered gravity assist maneuvers are explained in Chapter 5. It should be noted that a gravity assist is also sometimes referred to as a gravitational slingshot or a swing-by.

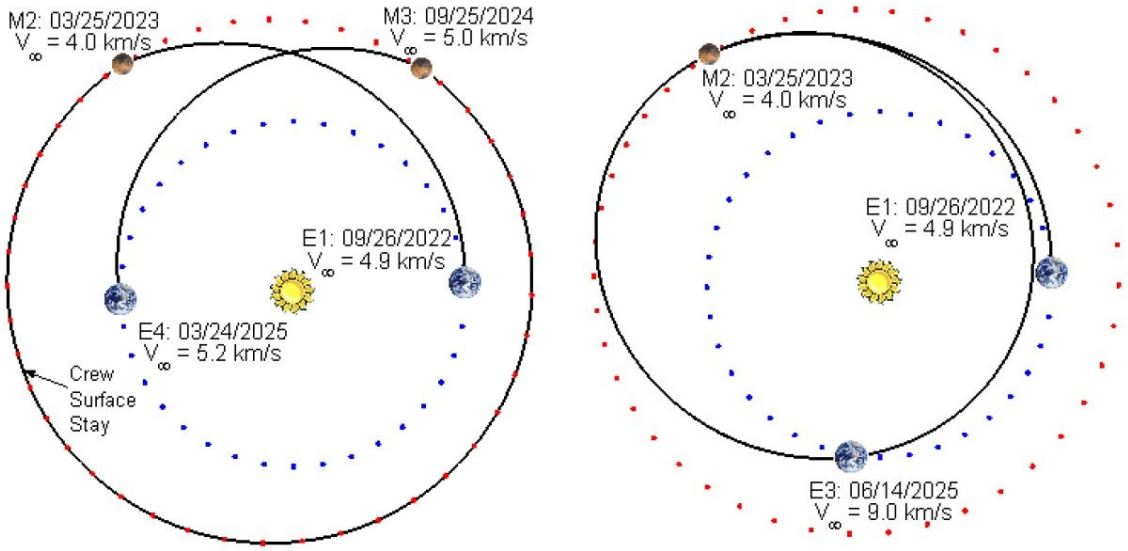

Figure 2.6: Trajectory visualizations for the conjunction class and the free-return architecture [13]. (*Left*) trajectories of outbound and inbound legs of a conjunction class mission to Mars. (*Right*) Mars free-return trajectory with near 3:2 resonance from E1:E3, associated with the conjunction class outbound trajectory (on the left). In case of a mission abort scenario after reaching Mars, the crew can return back to Earth, along M2- E3, instead of a surface stay M2-M3 (on the left).

free return trajectory, and the trip times only gradually increase with an increase in the value of ΔV applied during the Mars flyby.

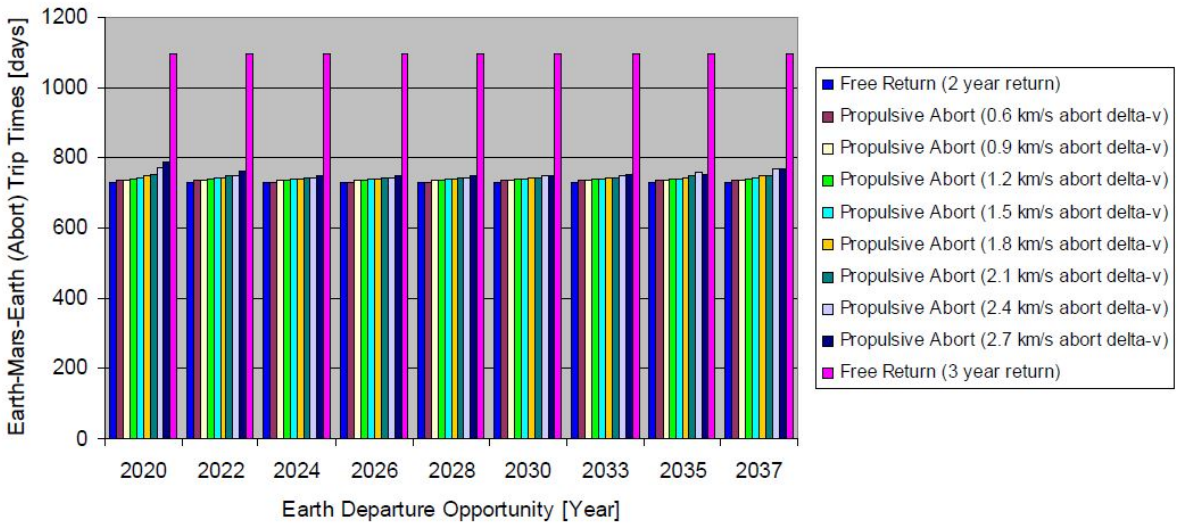

Figure 2.7: Total trip times for the free-return trajectories and propulsive abort trajectories over Earth departure opportunities from 2020 to 2037, when the abort decision is taken at Mars arrival. Results presented are for the trajectories investigated in [2] and the above figure is adopted from the same source.

It should be noted that for the propulsive abort trajectory investigated in the study [2], the decision to abort the mission and to return to Earth is taken only after completing the nominal outbound Earth-to-Mars transfer. After such a decision, a ΔV from 0.6 to 2.7 km/s has been applied during the Mars swing-by but no DSMs are applied during the inbound return trajectory of this architecture.

2.1.7. Continuous-thrust Trajectories

The mission architectures discussed so far in this chapter have a number of impulsive maneuvers involved. However, it is possible to apply thrust of a relatively smaller value over non-negligible periods of time (in comparison with the TOF of the trajectory). Mission architectures that involve such continuous-thrust trajectories can utilize technologies such as solar electric propulsion (SEP) or nuclear electric propulsion (NEP).

An investigation of some of the continuous-thrust transfer trajectories to Mars is presented in [14]. For launch opportunities between 2009 and 2022, such trajectories have a TOF between 180 to 270 days, and their performance has been evaluated for two cases - powered capture and aero-assisted arrival at Mars. Assuming that thrust and specific impulse (I_{sp}) are constant and aero-assisted transfers have a moderate V_∞, the study found that thrust usually of the order of a few Newtons and one Newton per metric ton of payload are required for these two cases respectively.

In another study [7], the use of a continuous-thrust stop-over mission architecture has been suggested, having a repeat time of one synodic period. All the components of this architecture such as the Mars taxi, the Earth taxi, the crew cabin are synodic payloads except the NEP power generator. Continuous-thrust propulsion is used for i. elliptically spiraling out the TV before the Earth taxi carrying the crew performs a rendezvous with it ii. the interplanetary trajectory of the TV, and iii. circularly spiraling in the TV after the crew leaves for Earth's surface using the taxi vehicle on its arrival. The total IMLEO of the infrastructure (power generator and synodic payloads) has been optimized for seven consecutive round-trip Mars missions by assuming that NEP can provide a thrust of 145.8 N, having a power as high as 11 MW[5].

With such assumptions regarding the NEP system, all the missions in this architecture have a round-trip duration of 751 days and an IMLEO based on the synodic payload of 296.6 ton (for the most massive launch in 2024). In another study [15], SEP is utilized instead of NEP along with CP, and a hybrid architecture for a conjunction class human Mars mission is proposed. A schematic explaining the steps involved in this architecture is presented in Figure 2.8, where it can be seen that powered Lunar gravity assist (LGA) is used for departing from Earth.

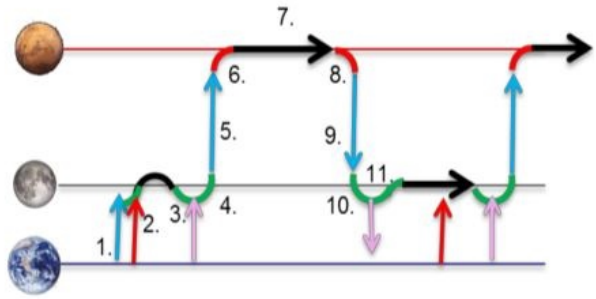

1. Deploy to cis-lunar space
2. Re-fuel and outfit
3. Crew and final logistics rendezvous
4. Powered Lunar Gravity Assist (LGA) for Earth departure
5. Solar Electric Propulsion (SEP) thrusting to Mars
6. Chemical Propulsion (CP) burn at Mars close approach to insert into parking orbit
7. Mars destination operations
8. CP burn and periapsis for Mars departure
9. SEP thrusting to Earth
10. LGA for Earth capture into cis-lunar space
11. Crew return to Earth surface

Repeat steps 2-11 for each crew Mars mission

Figure 2.8: Schematic of the hybrid mission architecture for the continuous-thrust trajectories that also uses chemical propulsion [15].

[5]Other important assumptions for the NEP system of this study are: overall efficiency of 65%, I_{sp} of 10000 s and propellant flow rate of $1.487 \cdot 10^{-3}$ kg/s. The total mass of the power generator infrastructure consisting of the nuclear reactor, the power conditioning system, the heat radiator and the radiation shield for the crew is 90 ton.

2.2. Relevant Technologies

A number of key technologies exist that can affect the mission characteristics such as IMLEO, trip times, system and mission complexity after their successful deployment for a human Mars mission. A list of such technologies along with their relative TRLs is presented in Table 2.2. One of the key technologies which is not present in this table (adopted from a study in 2009) but worth to mention is the reusability of launch vehicles. While comments about only three such technologies are presented in this section, [16] has provided good remarks on technology development for human Mars exploration.

Technology	Relative TRL	Definition
Chemical propulsion	9	System flight proven
Parking orbit rendezvous (Earth)	9	
Parking orbit rendezvous (Mars)	8	System flight qualified
Refuel in orbit (Earth)	8	
Cargo electric propulsion (EP)	7	Prototype in space
Refuel in orbit (Mars)	7	
Hyperbolic rendezvous (Earth)	7	
Hyperbolic rendezvous (Mars)	6	Protype demonstration
Nuclear thermal rocket (NTR)	6	
Reusable Mars launch vehicles	5	Component demonstration
Aerocapture	5	
Transfer vehicle electric propulsion[a]	5	
In-situ propellant production	5	
Mars launch vehicle NTR	4	Component in laboratory
Mars water excavation	3	Proof of concept

Table 2.2: Relative technology readiness level (TRL) of key technologies relevant to the human Mars missions. This table is regenerated from [4] which has been published in October 2009. [a]The TRL values correspond to nuclear electric propulsion, but the IMLEO values are applicable to both solar and nuclear electric systems.

2.2.1. Aeroassist

Aeroassist technologies utilize aerodynamic drag and lift forces to reduce the requirements from the propulsion system i.e. the ΔV associated with the trajectories. Three such technologies are aeromaneuver, aerocapture, and aerobraking. Such maneuvers are relevant for departure/arrival at both Earth and Mars, as both planets have an atmosphere (even though the latter has a relatively very thin atmosphere). Aeromaneuvers are used to land at a specific site through the use of drag and lift forces [17] and one clear example is the landing of the *Space Shuttle orbiter*.

In the case of aerocapture, aerodynamic drag is utilized to get the S/C captured into an initially elliptical parking orbit around the planet. With the use of aerocapture, the heat shield replaces the propulsion system required for orbit capture and such replacement can have a considerable mass benefit. [1] has identified two issues with aerocapture - unacceptable mechanical loads due to rapid deceleration and a very large diameter of the shroud required due to the large size of the aeroshell. The use of an aerocapture maneuver was suggested in NASA's *Design Reference Architecture-5* [16], but it has not been attempted for any mission to date [4].

An aerobraking maneuver uses the atmospheric forces to reduce the apoapsis altitude of an elliptical orbit around the planet when the periapsis passes are made through the atmosphere of the planet. Studies at NASA during 1963-65 showed the potential of reducing IMLEO for Mars missions through aerobraking [1]. Robotic missions to Mars - the *Mars Global Surveyor*, *Mars Odyssey*, *Mars Reconnaissance Orbiter*, and *ExoMars Trace Gas Orbiter* - all have used aerobraking at Mars. The aerobraking maneuver is a time-consuming process that demands human supervision and continuous maintenance for a number of months [1].

2.2.2. Propellant Production through ISRU

The Martian atmosphere has an abundance of carbon dioxide (95.3%) [18]. During 1996-2013, under the science theme *Follow the Water*, NASA's robotic missions such as the *2001 Mars Odyssey*, *Mars Exploration Rovers*, *Mars Reconnaissance Orbiter*, *Mars Phoenix Lander* provided information about water on Mars [19]. Through in-situ utilization of these resources, propellants can be generated at Mars.

Through electrolysis of Martian water or by using the hydrogen feed-stock brought from Earth to react with Martian carbon-dioxide, the Sabatier reaction can be performed which produces methane as a by-product[6]. Liquid oxygen and liquid methane can then be used as propellants for the ascent spacecraft to be used by the crew returning to Earth after a Mars surface mission. This will reduce the IMLEO to be launched from Earth.

After production of cryogenic propellants, it is required to store them on the Martian surface for months before they are used by the ascent taxi vehicle. An active cooling system might be required to prevent boil-off losses. Moreover, cryogenic fluid management technologies such as thermodynamic vent system and liquid acquisition devices need to Sabatier for storing the in-situ produced propellant [16].

Propellant production through Mars ISRU can be strategically combined with other options for a human Mars mission, as suggested in [1]. If the parking orbit around Mars is elliptical, it would reduce the ΔVs required by the TV for orbit insertion and Trans-Earth Injection (TEI). The increased ΔV cost of the ascent taxi vehicle can be met through the propellant production at Mars, without depending upon propellants from Earth.

2.2.3. Hyperbolic Rendezvous

While discussing the cycler and semi-cycler mission architectures in Sections 2.1.2 and 2.1.3 respectively, a rendezvous maneuver to be performed by a taxi vehicle for the rendezvous with the TV was mentioned. This is an essential requirement for these architectures but it is a risky maneuver. The taxi vehicle has only one opportunity to accomplish such a rendezvous as the TV would be on a hyperbolic orbit around the planet [4].

In a recent study, hyperbolic rendezvous trajectories for the cycler architecture have been optimized for the taxi vehicle considering two/three/four impulsive maneuvers by a high-thrust propulsion system or maneuvers by a continuous-thrust propulsion system. It has been concluded that without any constraints on TOF and intermediate arcs of the transfer trajectory, a four-impulsive-maneuver option is the most fuel-efficient between high-thrust options, while the continuous-thrust hyperbolic rendezvous might prove superior to the high-thrust alternatives in the future [20]. Nevertheless, this technology needs a successful in-flight demonstration similar to aerocapture.

2.3. Challenges of Human Mars Mission

The study of the available literature for human Mars missions revealed a number of challenges associated with such missions. These challenges should be kept in mind while designing a reconnaissance mission. Some of the relevant challenges are described as follows.

1. **High IMLEO**
   A human Mars mission architecture requires a large number of mass elements to be placed at the desired locations and to function for the desired time. Apart from basic elements such as the life-support systems, consumables, crew quarters which provide enough volume on-board the TV for the crew, there are other elements to be accounted for such as the radiation protection shielding and any possible measures to mitigate hazardous health effects caused by prolonged weightlessness. Moreover, for the reconnaissance mission to Martian surface, a Mars taxi vehicle, Mars ascent vehicle, surface stay habitat, surface power plant, ISRU units etc. might be required.

[6] Propellant production options at Mars through ISRU can be categorized as - the solid oxide electrolysis process, Sabatier/electrolysis process with indigenous Mars H_2O and Sabatier/electrolysis process with H_2 brought from Earth [1].

The necessity of these elements leads to high IMLEO values associated with the human Mars mission. As seen in the list of crewed Mars mission proposals [21], almost all human Mars mission plans have an IMLEO estimation in the order of hundreds of metric tons. The widely discussed Mars mission plan of the *SpaceX Corporation* aims to land the first crewed S/C on the Martian surface by 2024 [22]. This mission would use a fully reusable transportation system named *Starship* which has payload capability of at least 100 metric tons when loaded with 1200 metric tons of the propellant [23].

2. **Need for companion cargo missions**
The high IMLEO values of the human Mars mission architecture might lead to the division of elements that can be then launched with more than one heavy-lift launcher. This is referred to as a split mission strategy, which is often advocated in many proposals. For example, the NASA DRM-1 mission proposed in 1993-94 had the *Infrastructure Cargo Vehicle*, the *Habitat Landing Vehicle* etc. apart from the crewed TV [1].

   As it was proposed for this particular mission, the cargo elements required for supporting the crew on the Martian surface can be launched before the crew starts their journey towards Mars. Other reasons for a companion cargo missions include the pre-placement of ISRU infrastructure or placing an Earth-return vehicle in a parking orbit around Mars. If such missions are to be included in the overall human reconnaissance Mars mission architecture, interplanetary trajectories of such missions should be optimum (or sub-optimum but feasible) and consistent with the human mission.

3. **Limitation on transit duration**
Two major risks associated with the prolonged human interplanetary spaceflight are the risk due to radiation exposure and the risk due to prolonged weightlessness conditions. While the latter problem can be at least partially solved through generation of an artificial gravity environment, the former problem poses a critical challenge. To limit the radiation exposure, proposals such as [2] [14] [24] do not recommend transit duration/TOF of the mission of more than 180 days. For transfer trajectories to have an heliocentric transfer angle of less than 180°, the maximum TOF is 270 days [2].

   Harmful effects of radiation and weightlessness can be reduced by limiting the transit duration at the cost of a higher ΔV, which would lead to a higher IMLEO requirement [4]. Thus, there exists a trade-off between energy requirements of the mission and risks associated with the mission. While designing the trajectory which allows the abort option(s), it should be noted that the transit duration of the TV is most likely to be increased compared to the nominal mission. In such a case, the TV should be equipped to support the crew for an extended duration in space.

4. **Limitation on mission duration**
Similar to the transit duration, the total Earth-Mars-Earth trip time or the mission duration can be defined by/limited due to a number of factors. Few such factors are the life support available to the crew for surface missions, the choice of launch opportunities, expected scientific/operational output of the mission, the type of architecture chosen (for example, conjunction class missions usually have a longer mission duration compared to that of the opposition class missions [1]). If physical health and psychological considerations for the crew are considered, then a shorter mission duration would be preferred.

5. **Limitation on arrival/entry velocity**
A limit on the hyperbolic excess velocity at Mars might be required because very high excess velocity values would translate to high values of entry velocity. This would increase the mechanical and heat loads, creating issues for the safety of the crew and for the structure of the Mars descent vehicle. A restriction of 8.7 km/s for Mars entry velocity has been suggested in [24] which corresponds to V_∞ of 7.167 km/s (for an entry altitude of 125 km). NASA's *Design Reference Architecture* has a similar value of the constraint on V_∞ at Mars : 7.6 km/s [7].

Similarly for a safe re-entry at Earth, [24] has suggested that the Earth-arrival excess velocity should not be greater than 9.36 km/s. This value is also based on an entry altitude of 125 km when Earth entry velocity is limited to 14.5 km/s. This value of Earth entry velocity matches with another study [2], which has suggested that Earth entry velocities up to 14.7 km/s would be required if the crewed S/C has to return from Mars in 180 days.

6. **Inclusion of mission abort options**
Safety is a very important element of any human spaceflight project. Unforeseen circumstances arising from the failure of any of the thousands of technologies/systems/plans involved, during various phases of the mission, dictate that for crewed missions beyond low Earth orbit (LEO), an option to return the astronauts back to Earth is always desirable. During the *Apollo 13* mission, the use of a free-return trajectory allowed the crew to return to Earth despite the failure of the service module of the spacecraft. The aftermath of a fatal accident not only imparts negative notion to the spirit of everyone but also can result in the suspension of follow-up plans for the project, as experienced with major accidents in human spaceflight such as *Apollo-1*, *Challenger* and *Columbia*. Thus, it can not be argued more that for a reconnaissance human Mars mission, mission abort options should be included during the design phase.

2.4. Rationale for Research Questions

In the previous chapter, four research sub-questions for this thesis work were listed. These questions have been formulated at the end of the literature study phase and important findings of that phase have been presented in the previous sections of this chapter. In this section, the rationale for the research sub-questions will be explained. For better readability, these questions are listed again as follows.

- What are the optimum high-thrust interplanetary trajectory solutions for Earth-to-Mars and Mars-to-Earth transfers in a reconnaissance human Mars mission, considering the total TOF and the total ΔV requirement?
- What are the feasible high-thrust Earth-return abort trajectory options with and without the use of a Mars swing-by, if such a reconnaissance human Mars mission is aborted during the nominal Earth-to-Mars transfer?
- What are the feasible high-thrust Earth-return abort trajectory options if such a reconnaissance human Mars mission is aborted during the nominal Mars surface stay period?
- How do the important trajectory parameters of the investigated abort trajectory options compare with those of the nominal transfer trajectory options?

For the analysis in this thesis work, a reconnaissance human Mars mission is selected, that aims to transport the astronauts from Earth to Mars and back during the selected launch opportunities between 2020 and 2040. Unlike the robotic missions to Mars to date, this mission will have much higher scientific output and it will help in establishing a sustainable surface base at Mars. A number of technologies can be matured and valuable information can be obtained through such a one-shot reconnaissance mission during the early phase of human Mars exploration. This will eventually lead to more efficient and safer designs for several successive Mars exploration missions (possibly during the colonization phase). Details such as the crew size, the specific launch opportunities within the 2020-2040 time-frame will be discussed in Chapter 3.

For such a reconnaissance human Mars mission, there is a need to obtain Earth-to-Mars and Mars-to-Earth transfer trajectory solutions which are optimum or close to optimum considering the IMLEO and total trip and/or transit duration for the mission. IMLEO is primarily driven by the ΔV requirements and it translates to the launch cost of the mission. Trip and transit times define a number of mission characteristics including the level of risk associated with the health of the crew. These two parameters (ΔV and trip time) are often inversely proportional to each other. Therefore, it is required to present the trade-off between the values of these parameters while presenting the transfer trajectory solutions so that mission planners and managers can choose the solution that meets the requirements of all

stakeholders. A number of solutions already exist in literature and they use one of the mission architectures described in this chapter.

Conjunction and opposition class mission architectures are simpler compared to others. A number of trajectory solutions using these architectures are found in literature that often investigate the ballistic transfers[7]. For example, optimum ballistic transfer solutions having a minimum initial mass for piloted missions during the 2009-2024 time-frame have been presented in NASA's interplanetary mission design handbook [24]. A similar investigation is presented in [8] for mission opportunities between 2026-2045, but quantitative results are provided only for the Earth-to-Mars ballistic transfers with either minimum departure energy or minimum arrival V_∞ at Mars. Another study [11] has optimized Earth-to-Mars and Mars-to-Earth transfers separately for the ballistic missions between 2011 and 2025.

Due to their shorter transit times and relatively smaller ΔV requirements, the conjunction class architecture is preferable to the opposition class architecture, for a reconnaissance human Mars mission which aims to reduce the risks associated with prolonged interplanetary spaceflight. Moreover, while investigating ballistic transfer solutions, both legs of the mission should be optimized together to estimate minimum total ΔV requirement (relates to minimum IMLEO) and minimum possible total transit time having a feasible ΔV value. For ballistic transfers, trajectories having minimum hyperbolic velocities at arrival are often different than those having minimum launch energies [25]. Combining all the relevant ΔVs and optimizing solution for this value is expected to lead to the best trade-off for both transfer legs of the mission.

Continuous-thrust trajectories are very energy-efficient compared to high-thrust trajectories. However, for the heavier payload mass expected for a human Mars mission, the power-to-mass ratio (specific power) of the propulsion system becomes a significant parameter and it is advised to utilize a power source of a higher power rating [7]. Neither SEP nor NEP with the desired power level have been developed so far. The longer transit duration with continuous-thrust trajectories and the on-board radiation hazard possible with NEP are other reasons why the continuous-thrust mission architecture is less preferable for a human Mars mission. However, this architecture has potential for the cargo missions to Mars.

Considering the time-frame and requirements of a reconnaissance human Mars mission of interest, it makes sense to use a high-thrust chemical propulsion system for the crewed S/C. Such a propulsion system provides an advantage in terms of the mission duration and can also be scaled up and improvised (through reusability, in-situ propellant production, etc.) to meet the demands of a human Mars mission. Various super heavy-lift launch vehicles are under development (such as the *SLS*, *Starship*, *Long March 9*), which will rely on the high-thrust chemical propulsion for the missions beyond LEO in near-future. Selected high-thrust propulsion system(s) can be used to provide the impulsive maneuvers for the Mars mission architectures such as the cycler mission, the flyby mission, the architecture that uses the propulsive abort trajectories.

As mentioned before, cycler and semi-cycler architectures have been proven beneficial in theory compared to other architectures when a number of Mars missions are considered. As these architectures eliminate the need to launch the TV every time the crew wants to go to Mars/Earth, recurring IMLEO values with a set of missions executed by these architectures are considerably smaller than those executed by other mission architectures. However, these promising architectures require successful development and deployment of critical/risky technology such as hyperbolic rendezvous along with reliable autonomous systems for maintenance and operation. Committing to an expensive Mars exploration program for decades (such as Mars colonization) will surely make these architectures attractive choices. However, during the early stages of human Mars exploration, a reconnaissance mission is unlikely to utilize these architectures but most likely to use a simplified architecture that is safe, technologically feasible in near-future and has close-to-optimum trajectory options.

[7] For ballistic transfers, ΔV maneuvers are performed only for orbit departure and capture and no DSMs are considered. In practice, one or more trajectory correction maneuvers (TCM) are often applied to account for any deviation of the actual S/C trajectory from the ideal trajectory. Inclusion of one or more DSMs expands the design space for the trajectory design and it is sometimes possible to reduce overall ΔV.

Human Mars flyby missions have a lower scientific and operational output compared to the missions which stay in an orbit around Mars or on the Mars surface. The relative positions of Earth and Mars in their orbits can force the flyby missions to have one transit leg longer in duration. Some of the models based on the flyby architecture such as the dual habitat model require the hyperbolic rendezvous technology, similar to the cycler and semi-cycler architectures. Feasible free-return trajectories for a human Mars mission, which perform the Mars flyby in case of an abort, have total trip times as long as two years for the same reason. Thus, the Mars flyby or free-return architectures do not seem to be an attractive choice for a reconnaissance Mars mission.

As mentioned earlier, the safety of the crew is an important element to be considered and having a fail-safe provision to abort the mission and return the crew safely to Earth within the shortest period of time is desired. Therefore, along with nominal transfer trajectory options, abort trajectory options should be investigated for a reconnaissance human Mars mission. While free-return abort trajectories have limitations as mentioned earlier, the use of propulsive abort trajectories including DSMs can help to eliminate/reduce such limitations. Such abort trajectories can potentially utilize an unpowered or powered swing-by at Mars to their advantage. If such abort trajectory options are investigated over the total duration of a mission i.e. taking place at a number of epochs during the Earth-to-Mars transfer or during the Mars surface stay period then realistic conclusions about the feasibility and requirements of a safe reconnaissance mission can be drawn.

Finally, promising technologies such as propellant production through ISRU or aerocapture can enhance the performance of the chosen mission architecture. However, such technologies are still in development and the design of a reconnaissance human Mars mission should not be based on the condition that they would be indeed utilized during the mission. Therefore, research questions of this thesis work do not take into account the use of these technologies.

With the knowledge of mission heritage and research questions, it is now possible to develop the research methodology to be followed for this thesis work. An overview of this methodology and important aspects of the trajectory design problems are discussed in the next chapters.

3

Overview of Methodology

As discussed in earlier chapters, the research objective of this thesis work is to find optimum interplanetary transfer and abort trajectory solutions for a reconnaissance human Mars mission. To compute such trajectory solutions, various concepts from the subject of astrodynamics such as orbital perturbations, reference frames need to be understood. They have been studied during the literature study phase of the thesis. While all such concepts/methods are not explained in detail [1], this chapter presents an overview of the methodology followed to find trajectory solutions, by addressing various aspects of the problem and problem-solving methods.

Section 3.1 lists the assumptions of this thesis work. In the next section, five different mission scenarios are described along with relevant information. For the trajectory design problems under consideration, depending upon the mission scenario, a number of design parameters and constraints are applicable. Sections 3.3 and 3.4 discuss these two aspects respectively. Section 3.5 concludes this chapter by listing the methods from astrodynamics and the simulation tools/libraries used for this thesis work.

3.1. Assumptions

While finding the transfer and abort trajectory solutions, a number of assumptions are made. It is very important to keep these assumptions in mind while analyzing the results of this work as a change of certain assumptions can drastically affect the outcome of thesis work. The assumptions are as follows.

1. **Interplanetary trajectory design**
   A detailed design of a reconnaissance human Mars mission would involve trajectory design for different mass elements or groups of mass elements. Such trajectories include the departure trajectory from a parking orbit, interplanetary trajectories, trajectory for capture into a parking orbit, trajectory during Mars flyby, re-entry trajectory. This thesis work focuses only on the interplanetary trajectory design aspect - the trajectory of the crewed S/C or TV outside the sphere of influence (SOI) of Earth and Mars. The computation of ΔV values for trans-Mars injection (TMI) or TEI or powered gravity assist has been performed using excess velocity (V_∞) values of the heliocentric leg, but no detailed orbital dynamics is considered for the departure/flyby/capture trajectories.

2. **No orbital perturbations**
   The S/C trajectory design problem can be considered as a perturbed two-body problem in astrodynamics. Along with the gravitational force due to the central celestial body, a number of perturbative forces such as solar radiation pressure, atmospheric drag, third-body gravity are acting on the S/C, perturbing its ideal Kepler orbit motion around the central body. However, for the interplanetary trajectory design problem of this thesis, no orbital perturbations are considered. The research is intended to serve as a first-order estimation of the trajectory options, which are to be subjected to detailed analysis for future work. Therefore, the gravitational force

[1] Interested readers can refer to the literature study report [26] preceding this thesis work.

due to the Sun is the sole force to be taken into account, whose order of magnitude is at least four times higher than any second-largest perturbative forces - third-body gravity by Jupiter and Venus (neglecting increased perturbations due to Earth, Moon or Mars well within their SOI).

3. **Only Mars swing-by**
   In this thesis, ephemerides of Earth, Mars, and the Sun have been taken into account while finding transfer and abort trajectory solutions. A swing-by maneuver at any planet other than Mars is *never* considered even when an abort trajectory can sometimes reach distances similar to average Venus orbit. A Mars swing-by is used for finding abort trajectory solutions, *only when specified*.

4. **No capture ΔV on Earth arrival**
   It has been assumed that the TV carries an Earth return taxi vehicle similar to the *Soyuz* which performs ballistic re-entry on the arrival at Earth. As the TV is not inserted into a parking orbit around Earth on its arrival, a capture ΔV for the inbound leg is not to be computed.

5. **DE430 Ephemeris**
   DE430 planetary ephemerides data released by Jet Propulsion Laboratory (JPL) in 2013 are used for thesis work.

6. **Heliocentric Ecliptic Reference Frame**
   The reference frame used in this thesis work is referred to as the Heliocentric Ecliptic Reference Frame (HECRF). With the Sun as the origin, this frame uses the ecliptic plane as the fundamental plane and has an axes orientation similar to that of the International Celestial Reference Frame (ICRF).

7. **Launch Opportunity**
   It has been assumed that the reconnaissance human Mars mission under consideration has to be investigated for a particular launch opportunity for the conjunction-class Earth-to-Mars transfer within the 2020-2040 time-frame. It has been assumed that the inbound (Mars-to-Earth) transfer would take place when the relative positions of Earth and Mars allow a conjunction-class transfer again i.e. subsequent launch opportunity from Mars.

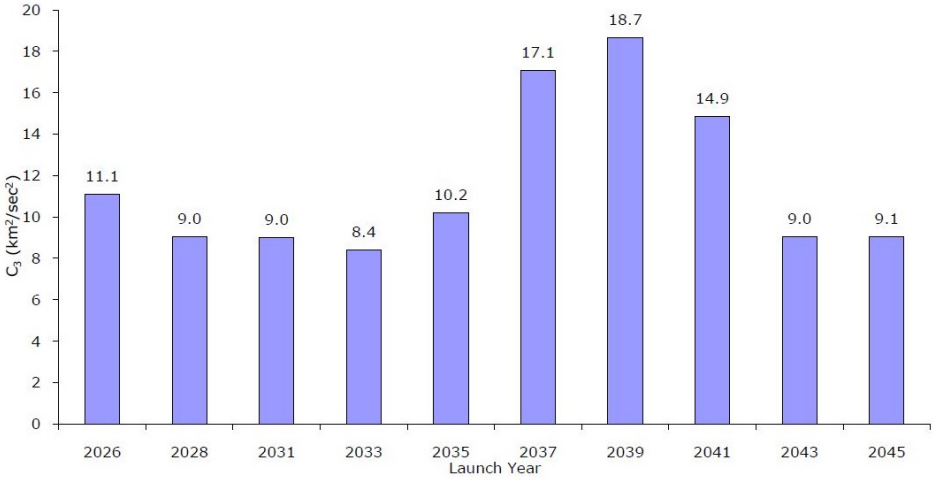

Figure 3.1: Departure energies for the optimum type I Earth-to-Mars transfers between 2026 and 2045 [8].

Departure energies[2] (C_3) associated with optimum Earth-to-Mars transfers for a number of launch opportunities between 2026 and 2045 are shown in Figure 3.1. Energy values for the type I trajectories[3] show that the launch opportunities from Earth such as those in 2028, 2031 and

[2]Departure energy or injection energy is the amount of specific launch energy required to escape a planet's SOI. It is equal to the square of the excess velocity of the escape hyperbolic trajectory. This terminology is often used in literature such as the interplanetary mission design handbooks [8] [24].

[3]Type I transfer trajectories have a heliocentric transfer angle of less than $180°$. For type II transfer trajectories, such an angle is between $180°$ and $360°$.

2033 are would have significantly smaller Earth-departure ΔV compared to other opportunities before 2043. Results for the type II trajectories show a similar trend [8]. For the transfer trajectory solutions of this thesis, it has been assumed that the Earth-to-Mars transfer would take place during the 2028 opportunity while the Mars-to-Earth transfer would take place during the subsequent launch opportunity (2030) from Mars.

8. **Payload mass and the propulsion system**
In this thesis, the computed trajectory solutions will be characterized based on their total ΔV values. However, it is also important to estimate the IMLEO of such trajectories in order to estimate the number of launches required from Earth (with a selected launch vehicle) and to comment upon their feasibility based on the cost of such a mission architecture. The IMLEO values are *not computed* and *not directly used* as one of the objectives during the optimization process[4], but such values are *estimated* after the optimization process has provided a set of optimal/sub-optimal trajectory solutions.(Section 7.5).

The total mass of the TV consists of the payload mass, the dry mass of the propulsion system, and the propellant mass. The payload of the TV includes the crew-cabin, consumables required for the total mission duration, a taxi vehicle for descending to the Martian surface and an Earth return taxi vehicle[5]. The crew-cabin refers to the system comprised of the living quarters, radiation shielding measures, any artificial gravity measures and the structural mass of elements of the power, life-support, thermal management and other systems (excluding the primary propulsion system).

While comparing various architectures for human Mars missions, [4] has presented a detailed discussion about the mass requirements of various relevant elements. Using the values from this study as a reference, the payload mass of the TV can be estimated as shown in Table 3.1, for a crew size of four astronauts. A crew size of four astronauts, similar to the reference study [4], is deemed sufficient for a reconnaissance human Mars mission. This assumption is based on the rationale that providing the consumables, protective measures and adequate living space for a total mission duration of 1200 days (in case of a contingency situation) to such a smaller size of the crew is preferable than providing limited resources to a larger crew size.

The mass of heat-shield ($m_{heat-shield}$) for the Mars descent and Earth return taxi vehicles can be estimated using a heuristic relationship of such a mass with the mass without a heat-shield i.e. the landed mass (m_{landed}), as given by Equation 3.1 [4]. The taxi vehicles are assumed to be designed for the values of V_∞ the same as the expected constraining values (discussed in Section 3.4).

$$\begin{aligned} m_{heat-shield}/m_{landed} &= 15\% && \text{if } V_\infty \leq 5 \text{ km/s} \\ &= 15\% + 2\% \times (V_\infty - 5 \text{ km/s})/(\text{km/s}) && \text{if } V_\infty > 5 \text{ km/s} \end{aligned} \tag{3.1}$$

As seen in Table 3.1, the payload mass of 70 metric tons has been assumed for this thesis work. To estimate the effective IMLEO for the trajectory solutions from this payload mass, two propellant combinations are to be considered for the high-thrust chemical propulsion system, as shown in Table 3.2. A typical range of values for the I_{sp} and the inert mass fraction (K) for the propulsion system that uses these propellants are shown in this table. K for a propulsion system can be defined as the ratio of total dry/inert mass of the propulsion system (consisting of thrusters, propellant tanks, plumbing, etc.) to the propellant mass.

[4] Such computations are not performed and the conclusions are not drawn based on the computed values as a number of assumptions are made regarding i. the mass of various elements (such as the taxi vehicles, the crew-cabin) involved in the mission architecture and ii. the performance characteristics of the selected propulsion system.

[5] It is assumed that other critical elements of the mission such as the Mars ascent taxi vehicle, the Mars surface habitat are delivered through the companion cargo missions of the mission architecture. Thus, such elements are not delivered as a payload by the TV itself, which transports the crew to Mars and back.

Mass Element	Reference value	Computed value	Description
Crew-cabin	6 t/person	24 t	For the crew size of four
Mars descent taxi vehicle	1.5 t/person	6	Mass without a heat-shield for the crew size of four
Heat-shield for the Mars descent taxi vehicle	Refer Equation 3.1	1.16	Extra mass for the heat-shield with V_∞ = 7.167 km/s
Earth return taxi vehicle	1.5 t/person	6	Mass without a heat-shield for the crew size of four
Heat-shield for the Earth return taxi vehicle	Refer Equation 3.1	1.42	Extra mass for the heat-shield with V_∞ = 9.36 km/s
Consumables (food, air, and water)	5 kg/day/person	24 t	When provided for 1200 days, for the crew size of four
Total		62.58 t	
Margin (10%)		6.26 t	
Total with the included margin		68.84 t	
Total payload mass (after round-off)		70 t	

Table 3.1: Estimation of the payload mass for the TV used in the reconnaissance human Mars mission. Reference values are obtained from [4]. Mass of various elements are shown in metric ton [t].

Propellants for the CP	I_{sp} [s]	K
CH_4/O_2	360 to 380	0.06 to 0.12
H_2/O_2	420 to 450	0.1 to 0.16

Table 3.2: Specific impulse (I_{sp}) and the inert mass fraction (K) for the two chemical propulsion (CP) systems, considered for the reconnaissance human Mars mission. The ranges of the values for these parameters are based on [1] [4].

3.2. Mission Scenarios

Five mission scenarios have been formulated for this thesis work as shown in Table 3.3 along with their identifiers. These identifiers have been used throughout the report to refer to the mission scenarios. Finding optimum/sub-optimum and feasible trajectory solutions and comparing the trajectory parameters for such solutions help to answer the research questions.

As seen in this table, the mission scenarios *MS-1* and *MS-2* have been proposed to investigate ballistic transfer trajectories that are related to the first research sub-question. The latter assumes an elliptical parking orbit around Mars which implies that Mars capture ΔV and TEI ΔV values would be smaller for the optimum solutions of this mission scenario compared to that of *MS-1*. Since the trajectory optimization problem would be solved for the same launch opportunity, it is expected to find optimum solutions that only differ in ΔV values over these scenarios. Investigation of these scenarios would also help to establish baseline results for other mission scenarios.

The computation of optimum solutions for mission scenarios *MS-3*, *MS-4* and *MS-5* provides propulsive abort trajectory solutions that lead to answering second and third research questions. It should be noted that the term 'mission abort' or 'abort' in this thesis work refers to the *execution* of the decision to terminate nominal mission operation and deploy the TV on an Earth-return abort trajectory. The epoch when this journey of the TV on such an Earth-abort return trajectory commences is referred to as an abort epoch. For *MS-3* and *MS-4*, such an abort epoch lies between the nominal Earth departure epoch and the nominal Mars arrival epoch. Abort epoch in case of *MS-5* lies between the nominal Mars arrival epoch and the nominal Mars departure epoch i.e. during the nominal Mars surface stay period.

Transfer/ Abort Trajectories	Mission Scenario Identifier	Description
Ballistic Transfer	*MS-1*	Earth-to-Mars and Mars-to-Earth transfers when a **circular** parking orbit around Mars is used
	MS-2	Earth-to-Mars and Mars-to-Earth transfers when an **elliptical** parking orbit around Mars is used
Propulsive Abort	*MS-3*	Mission abort occurs during nominal Earth-to-Mars transfer and **Mars swing-by** is used
	MS-4	Mission abort occurs during nominal Earth-to-Mars transfer and **no planetary swing-by** is used
	MS-5	Mission abort occurs during nominal Mars surface stay period and **no planetary swing-by** is used

Table 3.3: Description of the mission scenarios investigated in the thesis work.

For trajectory solutions of *MS-4* and *MS-5*, the TV would follow an abort trajectory that brings it directly back to Earth. While the initial position of the TV in the case of *MS-3* or *MS-4* would be somewhere in interplanetary space, the TV would start from Mars in the case of *MS-5*. As *MS-3* includes a Mars swing-by, the TV would first travel to Mars and then perform a swing-by to be placed on an Earth-return trajectory. One or two DSMs are considered for abort trajectory solutions. Propulsive maneuvers associated with high-thrust trajectories of this research have been listed and marked with indices in Table 3.4. The ΔV value associated with a maneuver having index 'x' is referred with the notation ΔV_x in this report, implying that the transfer trajectories of *MS-1* have only ΔV_1, ΔV_2, and ΔV_3.

Propulsive Maneuver Index	Description	Mission Scenario				
		MS-1	*MS-2*	*MS-3*	*MS-4*	*MS-5*
1	Departure from the parking orbit around Earth (TMI)	✔	✔	✔	✔	✔
2	Capture into the parking orbit around Mars	✔	✔	-	-	✔
3	Departure from the parking orbit around Mars (TEI)	✔	✔	-	-	✔
4	Abort on the outbound leg of mission	-	-	✔	✔	-
5	DSM on the outbound leg of mission	-	-	✔	-	-
6	Powered gravity assist at Mars	-	-	✔	-	-
7	DSM on the inbound leg of mission	-	-	✔	✔	✔

Table 3.4: Propulsive maneuvers associated with different mission scenarios.

3.3. Parameters

For the interplanetary transfer or abort trajectories associated with the mission scenarios discussed in the previous section, a number of design parameters exist. The choice of particular values for these parameters along with the assumptions listed earlier strongly influences the results computed for this research. The design parameters of interest and their chosen values are discussed as follows.

1. **Launch opportunity**
   As mentioned earlier, the 2028 launch opportunity has been selected for finding Earth-to-Mars transfer trajectory solutions. The 2030 launch opportunity has been selected for finding Mars-to-Earth transfer trajectory solutions. The exact values of the starting and ending epochs for these launch opportunities in terms of Gregorian date as well as in MJD2000[6] are presented in Table 3.5.

Launch Opportunity	**Starting epoch**		**Ending epoch**	
	Date	MJD2000	Date	MJD2000
2028 (Earth-to-Mars)	18 Aug 2028	10457.0	2 May 2029	10714.0
2030 (Mars-to-Earth)	9 Sep 2030	11209.0	25 May 2031	11467.0

Table 3.5: Details for selected launch opportunities, for the ballistic Earth-to-Mars and Mars-to-Earth trajectories investigated in the thesis work.

   For the abort trajectory solutions, one of the solutions obtained with the transfer trajectory mission scenarios (*MS-1* or *MS-2*) has to be selected and the TV would follow this nominal trajectory for this particular solution until the abort epoch.

2. **Parking orbits**
   For computing the values of ΔV_1 to ΔV_3, certain assumptions regarding the parameters of the parking orbit have been made. For both *MS-1* and *MS-2*, the circular parking orbit around Earth is assumed to have an altitude of 200 km. For *MS-1*, the circular parking orbit around Mars is assumed to have an altitude of 300 km. With *MS-2*, the elliptical parking orbit around Mars is assumed to have a periapsis altitude of 300 km and a period of 1 Earth day or 86400 seconds.

3. **Abort fractions**
   For mission scenarios *MS-3*, *MS-4* and *MS-5*, the abort epoch has to be specified as a design parameter. To investigate how available Earth-return abort trajectory options vary over the nominal Earth-to-Mars transit duration or nominal Mars surface stay duration, a number of epochs within these periods are selected. Such abort epochs are defined using the so-called abort fraction - the fraction of the nominal transfer or surface stay duration at which the mission abort takes place. An investigation for four abort fraction values (0.2, 0.4, 0.6 and 0.8) is to be performed at each of the above mission scenarios.

[6] MJD2000 refers to the modified Julian date relative to J2000 epoch. It is equal to the number of full days elapsed since 1 January 2000 12.00 Terrestrial Time (TT) or from Julian date (JD) = 2451545.0 TT. This unit has been used in NASA's interplanetary mission design handbook such as [8]. The selected trajectory design toolbox also uses this convention for specifying the epochs of interest.

3.4. Constraints

Transfer and abort trajectories for a reconnaissance human Mars mission are also subjected to a number of constraints. It is important to understand all the possible constraints while formulating the methodology, because the optimization model/method/process should be designed such that only those solutions which satisfy such constraints are permitted. For trajectory design problems of interest, the following constraints on the values of the design variable/parameter/output variables are applicable.

1. **Type I trajectory**
   Interplanetary transfer trajectory solutions to be obtained for *MS-1* and *MS-2* belong to the conjunction class architecture, which is superior to the opposition class architecture due to the reasons mentioned earlier. Moreover, it has also been decided to consider only type I ballistic transfer trajectory solutions. By constraining the value of the heliocentric transfer angle to less than $180°$, shorter transit times can be achieved at the cost of a relatively small increase in departure energy [25]. Such trajectories also have a lower error sensitivity compared to the type II transfers [8].

   The constraint regarding the type I trajectories is applicable only for *MS-1* and *MS-2* optimization problems.

2. **TOF**
   One of the challenges of human Mars missions is the requirement of a shorter transit duration, as discussed in Section 2.3. Therefore, both the Earth-to-Mars TOF and Mars-to-Earth TOF variables have to be constrained to have a value between 180 days and 270 days. With a TOF of 180 days, the solutions obtained have a moderate total ΔV, as observed during earlier stages of thesis work. The upper limit of 270 days is essential to meet the constraint regarding a type I trajectory.

   The constraint regarding the TOF is applicable only for *MS-1* and *MS-2* optimization problems.

3. **V_∞**
   The hyperbolic excess velocities at Mars arrival and Earth arrival have to be constrained to have values smaller than 7.167 and 9.36 km/s respectively, for the reasons mentioned earlier. These values are the same as those found in literature [24].

   The constraint regarding V_∞ at Earth arrival is applicable for all mission scenarios, except for some of the optimization problem cases (explained in Section 7.2.1). The constraint regarding V_∞ at Mars arrival is applicable for those mission scenarios which involve capture of the TV into the parking orbit around Mars (*MS-1*, *MS-2* and *MS-5*).

4. **Total ΔV**
   The total ΔV of the transfer or abort trajectory is one of the objectives to be optimized. Without any constraint on the value of this objective, sometimes trajectories can be obtained having attractive transit duration but require an unrealistically high total ΔV. Considering the feasibility of executing such solutions for a real mission, an appropriate limit on the value of total ΔV is to be applied wherever possible. This might lead to sub-optimal solutions in such cases.

   The constraint regarding total ΔV is to be applied for any of the five mission scenarios. Value for such a constraint is chosen according to the preliminary results obtained.

5. **Minimum flyby altitude at Mars**
   Mission scenario *MS-3* includes a Mars swing-by and it is desired to constrain the minimum flyby altitude to avoid adverse effects of atmospheric drag on the S/C trajectory. The minimum value of the Mars flyby altitude is equal to the value suggested in [27]: 257 km. This value is in agreement with the closest approach to the Mars surface during a flyby to date - by the *Rosetta* mission at about 250 km [28].

   The constraint regarding the minimum flyby altitude is applicable only for *MS-3* optimization problems.

3.5. Methods and Simulation Tools

Along with studying the mission heritage, the literature study phase of this thesis work (documented in [26]) also included the study and selection of various methods and the software/simulation tools that are to be used for the thesis work. The design of high-thrust trajectories such as those investigated in this research is an optimization problem having the aim to find the best solutions to the underlying trajectory design problem. A summary of selected methods to find optimum transfer/abort trajectory solutions for various mission scenarios is shown in Table 3.6.

Mission Scenario	**Trajectory design method(s)**	**Optimization algorithm(s)**
MS-1 and *MS-2*	Lambert targeting problem	MOAE/D and/or NSGA-II
MS-3 and *MS-4*	Kepler orbit propagation and MGA-1DSM-VF model	MOAE/D and/or NSGA-II
MS-5	MGA-1DSM-VF model	MOAE/D and/or NSGA-II

Table 3.6: Selected methods for trajectory design and optimization. MGA-1DSM-VF is a semi-analytic trajectory model for the analysis of high-thrust trajectories having multiple gravity assists with one DSM per transfer leg and it is based upon the velocity formulation approach. Multi-objective Evolutionary Algorithm by Decomposition (MOEA/D) and Non-dominated Sorting Genetic Algorithm (NSGA-II) are the meta-heuristic global optimization algorithms.

Based on the heritage regarding the use of a toolbox for similar applications, features available, the author's own experience and support available, three software tools have been selected for the thesis work. All trajectory design methods listed above are already implemented within the *TU Delft Astrodynamics Toolbox (Tudat)*. This open-source toolbox is well supported and familiar to the author and thus, it has been selected to solve the trajectory design problems.

Tudat also provides an optimization capability through an interface with the external tool - *Parallel Global Multi-Objective Optimizer (PaGMO)*. The *PaGMO2* library supports the meta-heuristics algorithms listed above and it has been selected for the optimization part of the research. A proprietary multi-paradigm numerical computing software - *Matrix Laboratory (MATLAB)* - has been chosen to post-process the results of the optimization process. A license for the academic use of this tool is provided by TU Delft to its students.

The subsequent three chapters of this report are aimed at providing more details about the methods and algorithms mentioned above. Various methods for the trajectory design are explained in Chapters 4 and 5. Aspects regarding the optimization such as the algorithms and tuning of the process are explained in Chapter 6.

4

Methods: Transfer Trajectories

Mission scenarios *MS-1* and *MS-2* of the thesis work focus on the optimum ballistic interplanetary transfer trajectory solutions. For the first-order estimation of high-thrust trajectories in this thesis work, it has been assumed that no orbital perturbations are acting on the S/C. The method of patched conics from astrodynamics becomes applicable without orbital perturbations, and the interplanetary motion of the S/C can be assumed to be under the sole gravitational influence of the Sun outside the SOI of the planets. For the interplanetary motion that represents Earth-to-Mars and Mars-to-Earth transfers of the S/C, the Lambert targeting problem method can be used.

In this chapter, three aspects of solving a transfer trajectory problem are described. First, the Lambert targeting problem is briefly explained in Section 4.1. Several approaches exist to solve the Lambert targeting problem and comments on some of these approaches are presented in Section 4.2. A script has been developed to solve the transfer trajectory problem using the chosen solution method for the Lambert targeting problem, and it has been validated as described in Section 4.3.

4.1. Lambert Targeting Problem

Originally proposed by Johann Heinrich Lambert in the 18th century, Lambert's problem is a boundary value problem in astrodynamics. It is a useful analytical formulation that can be used for solving the interplanetary trajectory design problem when Keplerian transfer orbits are considered (i.e. no perturbations are taken into account). With the Lambert targeting problem, the initial and final positions of the S/C are known. When a certain TOF is expected, the parameters such as the semi-major axis and eccentricity for a Keplerian transfer trajectory that connects these two points are to be determined. These parameters are determined by solving the following equation through an iterative approach [29].

$$TOF = t_2 - t_1 = \sqrt{\frac{a^3}{\mu}}\left[E_2 - E_1 - e(\sin E_2 - \sin E_1)\right] \tag{4.1}$$

The geometry associated with this method is illustrated in Figure 4.1 when an interplanetary transfer from the departure planet to the target planet is of interest. For this case, positions of the S/C correspond to the positions of the departing planet at departure and the position of the target planet at arrival. As the planetary positions at various epochs are known through the use of an ephemeris, the design variables for the implementation of Lambert targeting problem, for ballistic transfer between two planets, are reduced to the date of departure and date of arrival.

For the thesis work, the Lambert targeting problem has been utilized for finding the optimum interplanetary trajectory solutions in the mission scenarios *MS-1* and *MS-2*. As only ballistic transfers are investigated in these scenarios, the Lambert targeting problem completely defines the approach to be taken (method to be used) to solve the associated trajectory design problems. However, it should be noted that for the trajectory model described in the next chapter, the Lambert targeting problem

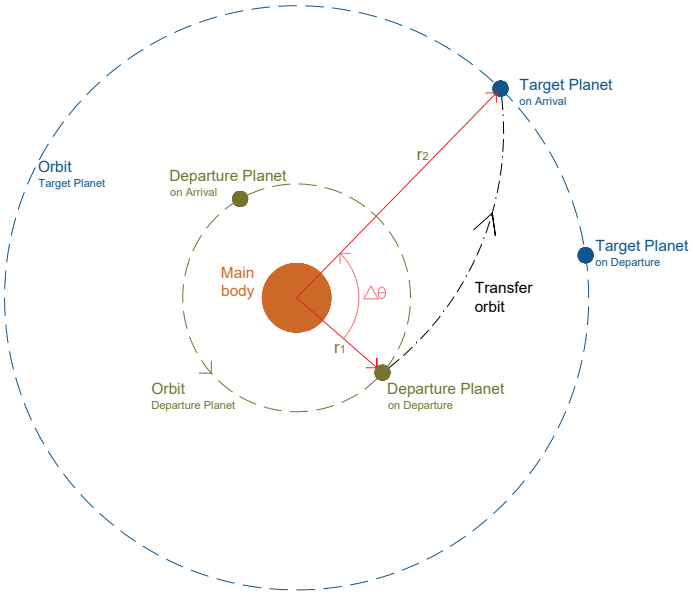

Figure 4.1: Geometry of the Lambert targeting problem.

method constitutes a part of the model and contributes to the process of finding solutions to the abort trajectory design problem.

4.2. Solution Methods

The Keplerian transfer trajectory in case of the Lambert targeting problem in a heliocentric frame can have the heliocentric transfer angle $\Delta\theta$ or $2\pi - \Delta\theta$ between two locations in the Solar System, depending upon the clockwise or counter-clockwise direction of motion. As the planets in the Solar System orbit in a counter-clockwise direction of motion, counter-clockwise transfers are preferred. Moreover, multiple revolutions around the Sun are also possible, increasing the transfer angle beyond 2π.

In literature, there are a number of formulations and methods available to solve the Lambert targeting problem. [30] has provided a useful classification for these formulations, where the groups are formed on the basis of the choice of the free parameter and major lines of research. This classification can be found in Appendix A.

Gooding's approach to solving the Lambert targeting problem has been considered as the most accurate and computationally efficient compared to other approaches by a number of studies, as mentioned in [31]. Based on the formulation of Lancaster and Blanchard, this approach evaluates an unknown parameter x using Halley's cubic iteration process and yields an accurate estimate in only three iterations [32].

Izzo's formulation for the solution of the Lambert targeting problem is also based on the work of Lancaster and Blanchard. This formulation leads to an algorithm that does not make use of heuristics for initial guess generation and uses a Householder iterative scheme instead of Halley's method. This algorithm has lower complexity and is considered as accurate as Gooding's method [31].

Choice of Algorithm

As the Lambert targeting problem has to be used for the transfer trajectory analysis of thesis work, a choice has to be made regarding the formulation for the solution of the Lambert targeting problem. While selecting a formulation, apart from the above-mentioned characteristics for the formulations, two other factors have been considered - heritage for its use in a similar trajectory design problem and

the availability of this formulation in the form of a computer algorithm within the selected tool - *Tudat*.

While finding high-thrust trajectory solutions for a mission to Neptune and Triton, [27] has used Gooding's method. [33] has compared the computational effort required by Izzo's method with that by Gooding's method, and has shown that the former requires less computational time on average when a number of samples having different values of $\Delta\theta$ are analyzed. Based on such rigorous verification in this study, [34] then used Izzo's method in his thesis focusing on the optimization of trajectories employing multiple gravity assists (MGA) and DSMs.

On the other hand, the following four algorithms have been implemented within *Tudat* so far.

1. Izzo's algorithm
2. Gooding's algorithm
3. Izzo's zero-revolution algorithm
4. Izzo's multi-revolution algorithm

Due to the advantages mentioned in literature for Izzo's method, Izzo's algorithm from *Tudat* has been selected for the thesis work. This algorithm is described in Appendix A. Using this algorithm, a script in C++ has been developed to solve the ballistic transfer trajectory design problems of the thesis work.

4.3. Validation

Before utilizing the Lambert targeting problem script for finding the ballistic transfer trajectory solutions for the mission scenarios *MS-1* and *MS-2*, validation of this script has been performed. The aim of this validation was to reproduce results available in literature, for a similar trajectory design problem. Such trajectory solutions are referred to as test cases in this thesis work. During the literature study phase of the thesis, the author had identified and defined two test cases for validation of the developed Lambert targeting problem script. These two test cases are referred with identifiers TC_1 and TC_2 in this thesis work and can be briefly described as follows.

- **TC_1**
  Energy-efficient ballistic transfer trajectory solutions for the human missions to Mars using a stop-over cycler architecture can be found in [11]. These solutions are obtained by solving the Lambert targeting problem. The period considered for such missions is from 2011 to 2024. In total, 14 trajectory solutions are provided, 7 for the outbound leg and 7 for the inbound leg of the mission.
- **TC_2**
  The interplanetary mission design handbook published by NASA provides a number of ballistic interplanetary trajectory solutions for the piloted missions to/from Mars between 2009 and 2024 [24]. These solutions have also been obtained by solving the Lambert targeting problem. Out of all the solutions presented in this handbook, 8 outbound and 8 inbound transfer trajectories having minimum departure excess velocity and initial mass are to be utilized for the validation. Moreover for the qualitative comparisons, departure energy (C_3) and arrival excess velocity at Mars (V_∞) contour plots for two mission opportunities (2009 and 2011) of this test case are to be regenerated.

It is important to note that when TC_1 and TC_2 are used for the quantitative validation of the Lambert targeting problem script, the values of the design variables - date of departure and date of arrival - are taken the same as the reference values for optimum transfer solutions. The objective of the validation phase is then to compute such values of the hyperbolic excess velocity at departure and arrival using the developed script, that are to be in agreement with the reference values (i.e any errors should be within an acceptable margin).

In the following sections, the results generated using the developed Lambert targeting script for these two validation test cases will be presented. Section 4.3.1 shows the regenerated so-called porkchop plots for two selected mission opportunities of TC_2. In Section 4.3.2, regenerated contours for the

arrival excess velocity at Mars for the same mission opportunities of TC_2 are presented. Section 4.3.3 describes quantitative results for the validation, where the errors between the reference values and the computed values for the departure and arrival excess velocities are tabulated. This quantitative comparison has been performed for all the chosen trajectory solutions of both test cases.

To regenerate the porkchop plot or the contours for arrival excess velocity, the Lambert targeting problem is solved multiple times over an equidistant grid defined for the design space of variables - date of departure and date of arrival. However, the Lambert targeting problem is solved a limited number of times to perform the quantitative validation, as mentioned earlier.

4.3.1. Porkchop Plots

The first step for the validation of the developed Lambert targeting script is an ability to regenerate the porkchop plots, usually found in the interplanetary mission design handbooks published by NASA. Through visual inspection of the regenerated porkchop plots and their comparison with the available porkchop plots, one can comment on the validity of the developed script.

For the 2009 and 2011 launch opportunities of TC_2, reference and regenerated porkchop plots for the ballistic Earth-to-Mars trajectories are shown in Figure 4.2. Through visual inspection and comparison, it can be concluded that the regenerated results are in agreement with the results from the reference [24].

4.3.2. Arrival Excess Velocity Contours

Similar to C_3, the arrival excess velocity is another parameter associated with the interplanetary transfer trajectory. Contour plots for the values of this parameter, over the design space defined by the departure and arrival dates, can also be found in the interplanetary mission design handbook. To supplement the qualitative validation performed through the regeneration of porkchop plots, regeneration of the arrival excess velocity contours has been performed.

Figure 4.3 shows the reference and regenerated arrival excess velocity contour plots for the ballistic Earth-to-Mars trajectories of the 2009 and 2011 launch opportunities. Similar to the earlier case of the porkchop plots, the regenerated contour plots can be observed to be in agreement with the reference contour plots.

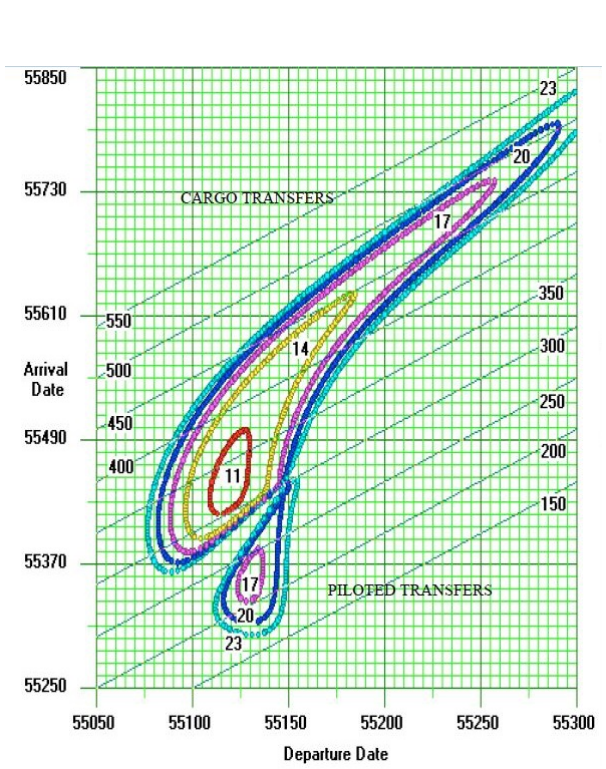

(a) 2009 Launch Opportunity (Reference)

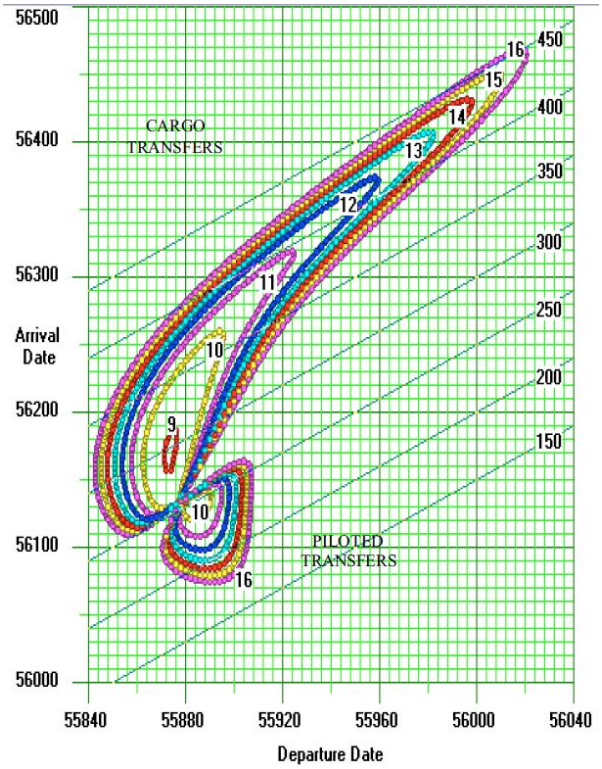

(b) 2011 Launch Opportunity (Reference)

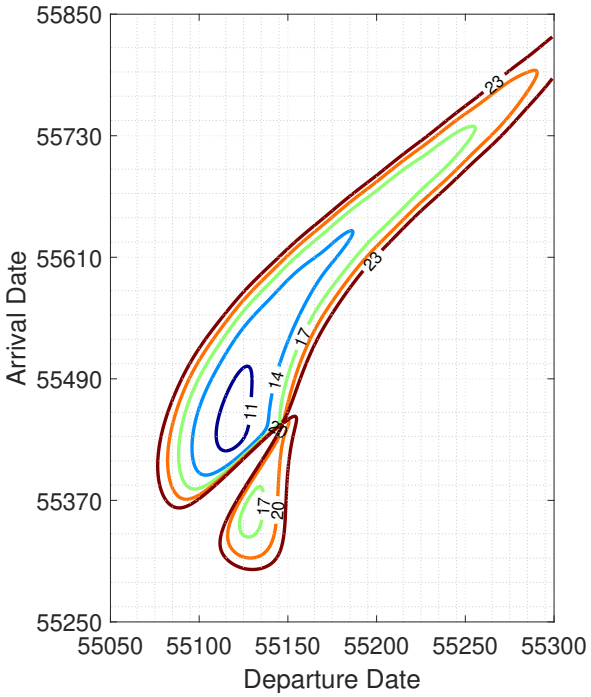

(c) 2009 Launch Opportunity (Regenerated)

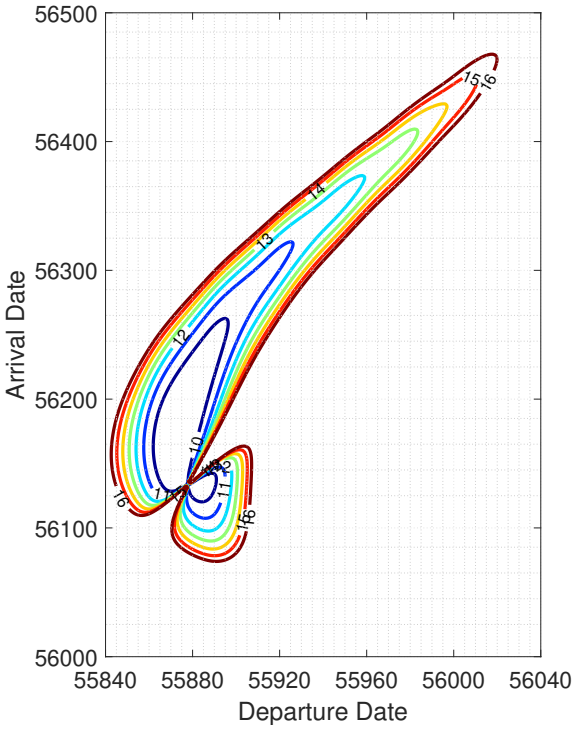

(d) 2011 Launch Opportunity (Regenerated)

Figure 4.2: Validation of the Lambert targeting script, through regeneration of porkchop plots. Figures (a) and (b) show the porkchop plots (departure energy (C_3) contours) provided in the NASA interplanetary mission design handbook [24], for ballistic Earth-to-Mars transfers during the 2009 and 2011 launch opportunity respectively. Similar plots are regenerated during the validation phase, as shown in Figures (c) and (d).

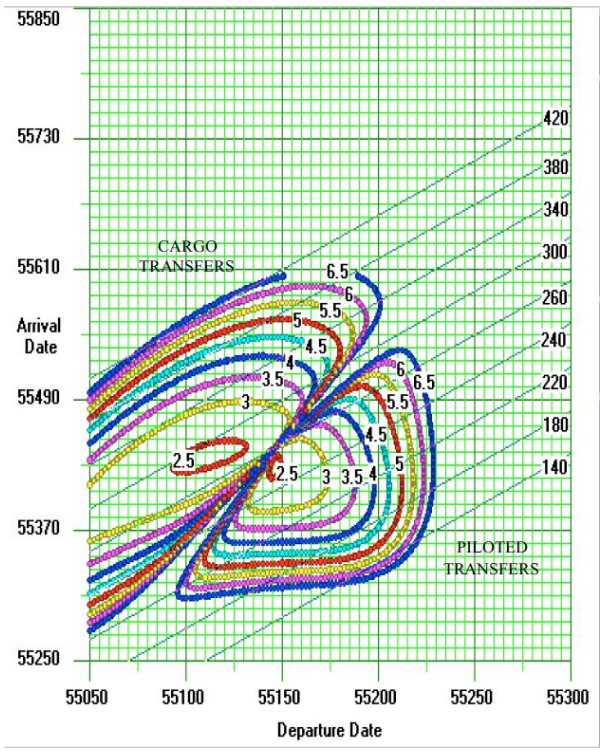

(a) 2009 Launch Opportunity (Reference)

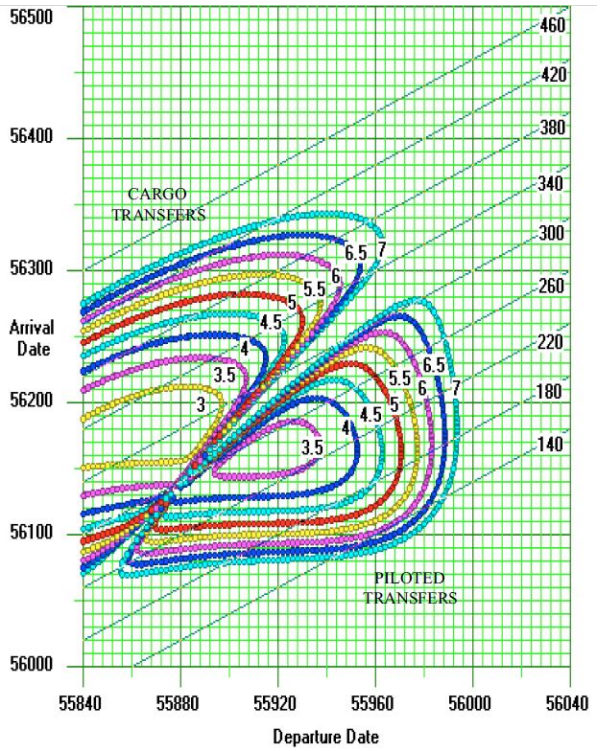

(b) 2011 Launch Opportunity (Reference)

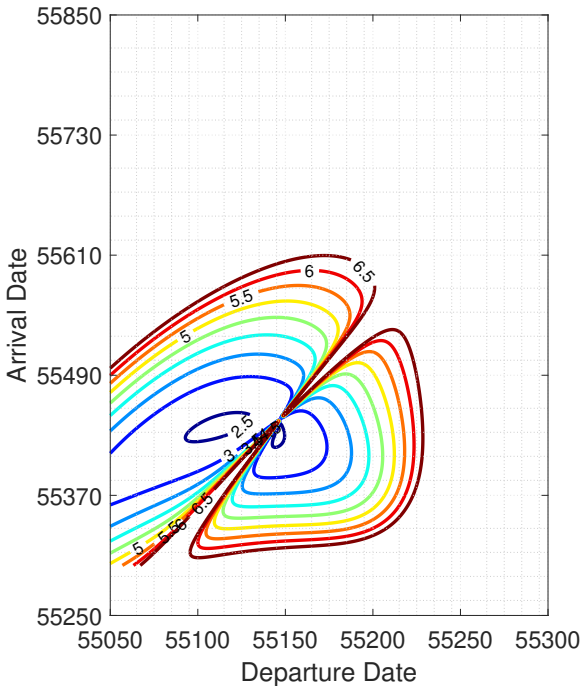

(c) 2009 Launch Opportunity (Regenerated)

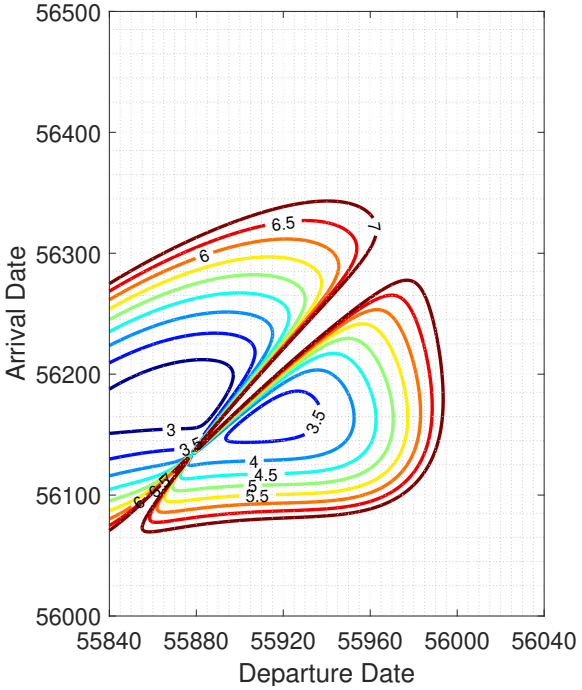

(d) 2011 Launch Opportunity (Regenerated)

Figure 4.3: Validation of the Lambert targeting script, through regeneration of arrival excess velocity contours. Figures (a) and (b) show the arrival excess velocity at Mars contours provided in the NASA interplanetary mission design handbook [24], for ballistic Earth-to-Mars transfers during the 2009 and 2011 launch opportunity respectively. Similar plots are regenerated during the validation phase, as shown in Figures (c) and (d).

4.3.3. Quantitative Validation

The previous two sections described the validation of the developed Lambert targeting script through a qualitative comparison with the reference results. However, there is a need to quantify the deviation of the generated results from the reference results. In this section, such a quantitative comparison is presented. Values of two parameters can be used for this purpose viz. hyperbolic excess velocity at the departure planet and hyperbolic excess velocity at the arrival planet.

As seen in Table 4.1, computed values of the hyperbolic excess velocities, both at departure and arrival, for both outbound and inbound trajectory solutions of TC_1 are in agreement with the reference values. The maximum deviation of the computed values from the reference values is 1.12%. It should be noted that the source for this test case does not specify the exact departure/arrival time on the day of departure/arrival and therefore, an approximation error for the input values of design variables is present.

			V_∞ at departure			V_∞ at arrival		
Date of departure	**Date of arrival**	**TOF [days]**	**Ref. value [m/s]**	**Comp. value [m/s]**	**% Error**	**Ref. value [m/s]**	**Comp. value [m/s]**	**% Error**
Earth-to-Mars ballistic transfer trajectories								
16-12-2011	13-07-2012	210	4365.78	4396.75	0.71	4309	4286.60	-0.52
21-01-2014	19-08-2014	210	3905.12	3934.84	0.76	4103	4086.64	-0.40
09-03-2016	05-10-2016	210	3567.91	3572.11	0.12	3763	3757.33	-0.15
10-05-2018	06-12-2018	210	2812.47	2800.09	-0.44	2969	2970.01	0.03
25-07-2020	20-02-2021	210	3737.65	3741.80	0.11	2591	2586.09	-0.19
18-09-2022	16-04-2023	210	4469.90	4483.75	0.31	3136	3121.52	-0.46
28-10-2024	26-05-2025	210	4687.22	4706.44	0.41	3911	3890.33	-0.53
Mars-to-Earth ballistic transfer trajectories								
24-10-2011	21-05-2012	210	4082.89	4105.62	0.56	4944	4898.68	-0.92
03-12-2013	01-07-2014	210	3782.86	3803.81	0.55	4641	4605.62	-0.76
14-01-2016	11-08-2016	210	2851.32	2864.51	0.46	4203	4182.24	-0.49
20-03-2018	16-10-2018	210	2473.86	2475.32	0.06	3177	3174.45	-0.08
21-05-2020	17-12-2020	210	3514.26	3517.52	0.09	3404	3401.06	-0.09
26-07-2022	21-02-2023	210	3931.92	3940.69	0.22	3708	3677.68	-0.82
07-09-2024	05-04-2025	210	4062.02	4079.10	0.42	4071	4025.30	-1.12

Table 4.1: Validation of the Lambert targeting script through computation of results for 14 transfer trajectories of TC_1. Reference (Ref.) values for the hyperbolic excess velocities (V_∞) are obtained from [11]. Computed (Comp.) values for both Earth-to-Mars and Mars-to-Earth ballistic trajectories are shown.

Similar conclusions can be drawn for the validation of TC_2 results through observation of Table 4.2. The maximum deviation of the computed values from the reference values is 0.85 %. The source for this test case also does not specify the exact departure/arrival time on the day of departure/arrival and a similar approximation error exists .

The values of $\%$ errors are considered acceptable because some of the assumptions for the solutions of the Lambert targeting problem in the reference literature are unknown. One of the potential causes of error is the use of different ephemerides data than the one selected for this thesis work (mentioned as one of the design parameters, in Section 3.3).

Based on this quantitative validation and results presented in earlier sections, the Lambert targeting problem script is considered to be validated for its use. Such a script will be used with the optimization algorithm and optimization parameters (described in Chapter 6) to find optimum transfer trajectory solutions. In the next chapter, the methods used to solve the relevant abort trajectory problem will be presented.

Date of departure	Date of arrival	TOF [days]	V_∞ at departure			V_∞ at arrival		
			Ref. value [m/s]	Comp. value [m/s]	% Error	Ref. value [m/s]	Comp. value [m/s]	% Error
Earth-to-Mars ballistic transfer trajectories								
30-10-2009	28-04-2010	180	4478.84	4490.24	0.25	6511	6537.08	0.40
02-12-2011	30-05-2012	180	3989.99	3990.46	0.01	7073	7059.08	-0.20
04-01-2014	03-07-2014	180	3322.65	3313.15	-0.29	6785	6793.79	0.13
20-02-2016	19-08-2016	181	2978.25	2989.34	0.37	5297	5271.05	-0.49
08-05-2018	04-11-2018	180	2847.81	2845.01	-0.10	3256	3252.33	-0.11
19-07-2020	15-01-2021	180	3664.70	3653.11	-0.32	3154	3164.88	0.34
10-09-2022	09-03-2023	180	4430.58	4443.85	0.30	4621	4615.21	-0.13
17-10-2024	15-04-2025	180	4566.18	4579.55	0.29	6090	6106.90	0.28
Mars-to-Earth ballistic transfer trajectories								
16-10-2011	13-04-2012	180	4161.00	4159.35	-0.04	9360	9406.99	0.50
19-11-2013	18-05-2014	180	3688.00	3688.42	0.01	9312	9381.31	0.74
07-01-2016	05-07-2016	180	2989.00	2990.02	0.03	7342	7395.78	0.73
25-03-2018	21-09-2018	180	2642.00	2643.73	0.07	4012	4046.04	0.85
12-06-2020	09-12-2020	180	3419.00	3420.61	0.05	3498	3509.09	0.32
31-07-2022	27-01-2023	180	4048.00	4049.21	0.03	5282	5305.39	0.44
02-09-2024	01-03-2025	180	4279.00	4278.27	-0.02	7618	7587.77	-0.40
02-10-2026	31-03-2027	180	4251.00	4251.24	0.01	9248	9315.94	0.73

Table 4.2: Validation of the Lambert targeting script through computation of results for 16 transfer trajectories of TC_2. Reference (Ref.) values for the hyperbolic excess velocities (V_∞) are obtained from [24]. Computed (Comp.) values for both Earth-to-Mars and Mars-to-Earth ballistic trajectories are shown.

5

Methods: Abort Trajectories

Abort trajectory solutions are to be obtained in this thesis work by investigation of mission scenarios *MS-3*, *MS-4* and *MS-5*. According to the definition of these mission scenarios, corresponding high-thrust propulsive abort trajectories can include one or more DSMs or can even benefit from a Mars swing-by maneuver. Due to these added propulsive maneuvers, the number of design variables increases and the method of the Lambert targeting problem discussed in the previous chapter is not sufficient to solve the abort trajectory design problem. Instead, other methods are to be used to solve such a problem.

In this chapter, methods used to solve the problem of abort trajectory design are described. The comparatively simpler but an essential method of propagating a Kepler orbit of the S/C is explained in Section 5.1. Section 5.2 briefly explains the concept of a gravity assist maneuver and presents the propagation scheme for the powered gravity assist. Section 5.3 describes the semi-analytic trajectory model of interest and the computation scheme for the mission scenarios that investigate abort trajectory solutions.

5.1. Kepler Orbit Propagation

Kepler orbit propagation is an analytical method that can be used to obtain the state of the S/C (or a celestial body) at any epoch if its initial state is known and if its motion is affected by only the central body's gravitational force. Since all orbital perturbations are neglected for the heliocentric interplanetary trajectory of the S/C in this thesis, its final state at any subsequent epoch can be determined using the method of Kepler orbit propagation and knowledge of its initial state, provided that no discontinuities in motion are present due to the propulsive maneuvers.

Thus, if $\boldsymbol{r}_i$ and $\boldsymbol{V}_i$ represent the initial position vector and initial velocity vector[1] at time t_i, then the position vector $\boldsymbol{r}_f$ and velocity vector $\boldsymbol{V}_f$ at time t_f can be computed through the Kepler orbit propagation. As the first step of this method, the initial state of the S/C in Cartesian coordinates $[\boldsymbol{r}_i, \boldsymbol{V}_i]$ can be converted into equivalent Keplerian elements. Without any perturbation forces, five out of six Keplerian elements would remain constant throughout the motion of the S/C from t_i to t_f. Only the true anomaly is a time-dependent element and it needs to be updated to obtain the final state of the S/C in Keplerian elements.

Depending upon the type of Kepler orbit - elliptical or parabolic or hyperbolic - appropriate conversion formulas are used to update the true anomaly. Since parabolic orbits are rarely encountered in any analysis, the relevant calculation scheme is not discussed here but it can be found in literature. For elliptical or hyperbolic orbits, the initial true anomaly (θ_i) is converted into the initial elliptic eccentric anomaly (E_i) or the initial hyperbolic eccentric anomaly (F_i).

E_i or F_i are then converted into initial elliptic mean anomaly (M_i) or initial hyperbolic mean anomaly ($\bar{M}_i$). The final mean anomaly can be computed using knowledge of $(t_f - t_i)$ and the initial mean

[1] In this report, vectors are represented in boldface.

anomaly. After such a computation, the final mean anomaly is converted into the equivalent final eccentric anomaly which is then converted into equivalent final true anomaly (θ_f). With knowledge of θ_f, the final state of the S/C in Keplerian elements is known which can be transformed to equivalent Cartesian coordinates.

The mathematical formulae associated with orbital element conversions or conversion of different anomaly types into each other are not presented here due to space constraints. However, such formulae can be found in astrodynamic textbooks such as [29]. More importantly, *Tudat* has an implementation of algorithms for relevant orbital element conversions and the Kepler orbit propagation method.

As mentioned in Chapter 3, the method of Kepler orbit propagation has been used with the mission scenarios *MS-3* and *MS-4*. In these scenarios, the mission is aborted during Earth-to-Mars transfer. Since a ballistic transfer trajectory is followed until the abort epoch, the state of the S/C at this abort epoch can be known by using the method of Kepler orbit propagation. Knowledge of the initial state in such cases comes from the trajectory parameters for the selected ballistic transfer trajectory solution, analyzed earlier through *MS-1* or *MS-2*.

The Kepler orbit propagation also constitutes a part of the trajectory model described in Section 5.3. As this trajectory model is used for the mission scenarios *MS-3*, *MS-4* and *MS-5*, this method is, in fact, relevant for all abort trajectory solutions investigated in this thesis work.

5.2. Gravity Assist

A gravity assist (or swing-by or flyby) is a maneuver used in the interplanetary trajectory design where the S/C is made to interact with the gravitational field of a planet to increase its orbital energy. Through conservation of total momentum in such an interaction, magnitude and direction of the heliocentric velocity of the S/C is changed to eliminate/reduce the requirement of ΔV from the onboard propulsion system to achieve the same effect. Two major types of gravity assist are unpowered gravity assist and powered gravity assist, and they are described in Sections 5.2.1 and 5.2.2 respectively.

The concept of gravity assist and the associated mathematical formulation can be found in textbooks such as [29]. This was studied during the literature study phase and only essential elements of this study are presented in this section.

5.2.1. Unpowered Gravity Assist

The geometry and velocity vector diagram associated with an unpowered gravity assist is shown in Figure 5.1. With such a maneuver, the S/C follows a hyperbolic trajectory without any propulsive maneuver within the SOI of the planet. Incoming and outgoing hyperbolic excess velocities ($\boldsymbol{V}_{\infty,in}$ and $\boldsymbol{V}_{\infty,out}$) of the S/C have the same magnitude but different directions in the planetocentric reference frame. As a result of the planet's velocity component in the plane of the orbital motion of the S/C ($\boldsymbol{V}_{planet}$), the heliocentric velocity of the S/C changes from $\boldsymbol{V}_{in}$ to $\boldsymbol{V}_{out}$. With a proper geometric configuration for this maneuver, the amount and direction of heliocentric velocity change can be adjusted to achieve the desired effect without requiring a ΔV maneuver.

A gravity assist maneuver is possible only if the pericenter radius of the planetocentric hyperbolic trajectory is greater than the radius of the planet. Moreover, a dense atmosphere of the planet can limit how deep the S/C can penetrate inside such an atmosphere without excessive degradation of the trajectory. Aero-gravity assist maneuvers utilize the effect of the atmosphere during a gravity assist to their advantage.

5.2.2. Powered Gravity Assist

With the inclusion of a propulsive maneuver in a gravity assist, a greater change in the heliocentric velocity of the S/C can be achieved. The pericenter of the planetocentric hyperbola followed by the S/C is the most efficient location to apply such a propulsive maneuver. The resultant trajectory of the S/C consists of two legs having different bending angles and hyperbolic excess velocities - $\boldsymbol{V}_{\infty,in}$ and $\boldsymbol{V}_{\infty,out}$ - can have a different magnitude.

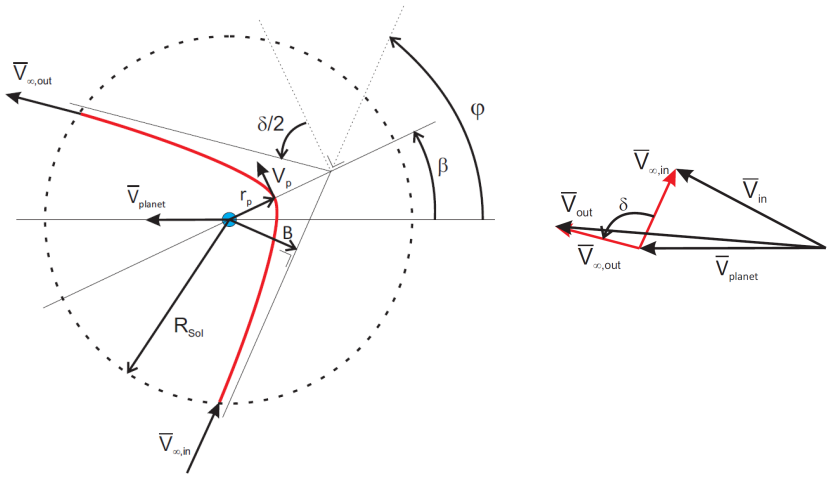

Figure 5.1: Geometry of planetocentric hyperbolic trajectory in the case of unpowered gravity assist (*left*) and associated velocity vector diagram (*right*) [35].

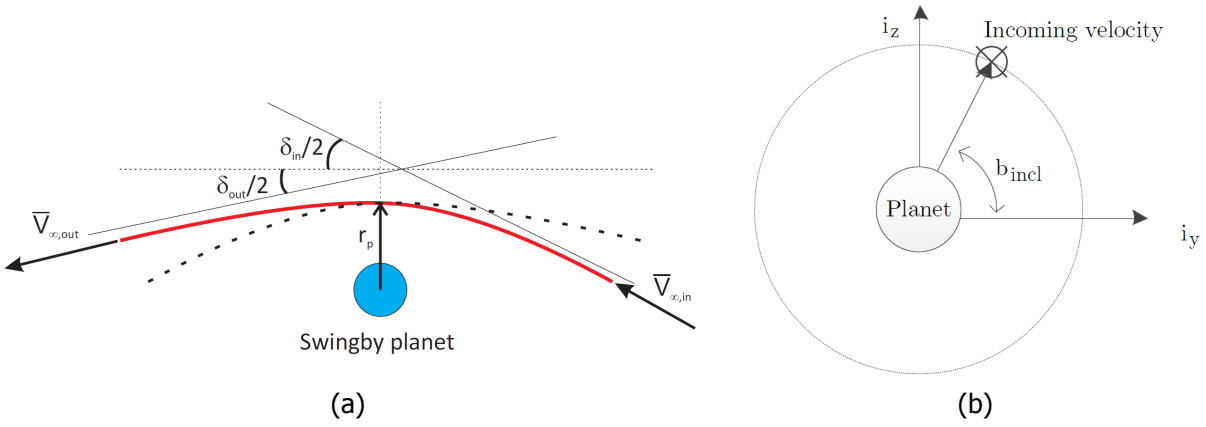

Figure 5.2: (a) Geometry of a powered gravity assist maneuver [35]. (b) Definition of the 3D rotation inclination angle b_{incl} [34].

The two-dimensional geometry of a powered gravity assist maneuver is shown in Figure 5.2. The trajectory model discussed in Section 5.3.1 uses a powered gravity assist maneuver and the propagation scheme for the same is explained as follows. This propagation scheme is based on the description provided in [34].

Propagation Scheme

The problem for the powered gravity assist propagation can be formulated as: Given values for the pericenter radius (r_p), inclination angle (b_{incl}), propulsive maneuver applied for powered gravity assist (ΔV_{GA}), and incoming heliocentric velocity ($\boldsymbol{V}_{in}$), compute the outgoing the heliocentric velocity ($\boldsymbol{V}_{out}$).

The first step is to determine the planetocentric velocity ($\tilde{\boldsymbol{V}}_{in}$) and eccentricity ($e_{in}$) for the incoming leg using Equations 5.1 and 5.2. Here, μ_{pl} and $\boldsymbol{V}_{pl}$ are the gravitational parameter and heliocentric velocity for the planet.

$$\tilde{\boldsymbol{V}}_{in} = \boldsymbol{V}_{in} - \boldsymbol{V}_{pl} \tag{5.1}$$

$$e_{in} = 1 + \frac{r_p |\tilde{\boldsymbol{V}}_{in}|^2}{\mu_{pl}} \tag{5.2}$$

The computation of the incoming planetocentric velocity vector leads to the definition of a coordinate frame in which the outgoing planetocentric velocity can be represented. Such a coordinate frame is defined using Equation 5.3. The 3D rotation inclination angle (b_{incl}) relates with this coordinate frame as shown in Figure 5.2.

$$\boldsymbol{i}_x = \frac{\tilde{\boldsymbol{V}}_{in}}{|\tilde{\boldsymbol{V}}_{in}|} \tag{5.3a}$$

$$\boldsymbol{i}_y = \frac{\boldsymbol{i}_x \times \boldsymbol{V}_{pl}}{|\boldsymbol{i}_x \times \boldsymbol{V}_{pl}|} \tag{5.3b}$$

$$\boldsymbol{i}_z = \boldsymbol{i}_x \times \boldsymbol{i}_y \tag{5.3c}$$

The bending angle of the incoming leg can be determined using Equation 5.4.

$$\frac{\delta_{in}}{2} = \arcsin \frac{1}{e_{in}} \tag{5.4}$$

The magnitude of the pericenter velocities for the incoming and outgoing legs ($V_{p,in}$ and $V_{p,out}$) are then calculated using Equations 5.5 and 5.6.

$$V_{p,in} = \sqrt{|\tilde{\boldsymbol{V}}_{in}|^2 \cdot \frac{e_{in}+1}{e_{in}-1}} \tag{5.5}$$

$$V_{p,out} = V_{p,in} + \Delta V_{GA} \tag{5.6}$$

The magnitude of outgoing planetocentric velocity $\tilde{V}_{out}$ is determined using Equation 5.7.

$$\tilde{V}_{out} = \sqrt{V_{p,out}^2 - \frac{2 \cdot \mu_{pl}}{r_p}} \tag{5.7}$$

Subsequently, the eccentricity (e_{out}) and bending angle of the outgoing leg ($\delta_{out}/2$) are determined using Equations 5.8 and 5.9.

$$e_{out} = 1 + \frac{r_p |\tilde{\boldsymbol{V}}_{out}|^2}{\mu_{pl}} \tag{5.8}$$

$$\frac{\delta_{out}}{2} = \arcsin \frac{1}{e_{out}} \tag{5.9}$$

The total bending angle is then calculated using Equation 5.10. The outgoing planetocentric velocity vector $\tilde{\boldsymbol{V}}_{out}$ is computed in the coordinate frame discussed earlier, using Equation 5.11.

$$\alpha = \frac{\delta_{in}}{2} + \frac{\delta_{out}}{2} \tag{5.10}$$

$$\tilde{\boldsymbol{V}}_{out} = \tilde{V}_{out} \cdot (\cos\alpha \cdot \boldsymbol{i}_x + \cos b_{incl} \cdot \sin\alpha \cdot \boldsymbol{i}_y + \sin b_{incl} \cdot \sin\alpha \cdot \boldsymbol{i}_z) \tag{5.11}$$

Finally, the outgoing heliocentric velocity vector $\boldsymbol{V}_{out}$ is computed using Equation 5.12.

$$\boldsymbol{V}_{out} = \boldsymbol{V}_{pl} + \tilde{\boldsymbol{V}}_{out} \tag{5.12}$$

5.3. Trajectory Models

As mentioned earlier, high-thrust propulsive abort trajectories of this research can include one or more DSM(s) and utilize the Mars-swingby maneuver. In the past, a semi-analytic trajectory model had been developed by researchers to investigate high-thrust trajectories that employed only gravity assist maneuvers. Known as the multiple gravity assisted (MGA) trajectory model, no propulsive maneuvers were assumed in-between planetary encounters and the method of the Lambert targeting problem was used to solve the trajectory problem [34].

More complex semi-analytic trajectory models can be found in literature for the interplanetary trajectory analysis in the absence of orbital perturbations, that allow the inclusion of DSM(s) along with gravity assists. Depending upon the approach to define the position of the DSM, these models usually fall into two categories - Position Formulation (PF) models and Velocity Formulation (VF) models. In the case of the former model, the position of a DSM is directly specified using an independent parameter such as the dimensionless radial distance of the DSM. On the other hand, VF models specify the velocity after the last planetary encounter and propagate the Kepler orbit until the epoch of DSM to obtain the associated position [34].

While optimizing high-thrust trajectories that include gravity assists at several planets and also include DSMs, [34] has presented a comprehensive description, analysis, and application of semi-analytic trajectory models that utilize the VF or PF approach and include one DSM per transfer leg between two planetary encounters. These models are referred to as MGA-1DSM-VF (Multiple Gravity Assist with 1 Deep Space Maneuver per leg, using the Velocity Formulation approach) and MGA-1DSM-PF (Multiple Gravity Assist with 1 Deep Space Maneuver per leg, using the Position Formulation approach).

Both these models have been implemented in *Tudat* through the *Trajectory Class* [36]. Through a review of literature for these models and documentation for such implementation, it has been concluded that the MGA-1DSM-VF model is more suitable for investigating abort trajectories in this thesis work. Important theoretical elements of this model including the generic computation scheme are described in Section 5.3.1. A modified computation scheme based on this trajectory model is presented in Section 5.3.2, which also defines the design variables for different mission scenarios.

While the MGA-1DSM-VF model restricts the use of only one DSM per transfer leg, there are other semi-analytic models that can allow the inclusion of more than one DSM. However, as the definition of mission scenarios of this research does not require more than one DSM per leg between Earth and Mars, the study of more complex analytic models has not been performed.

5.3.1. MGA-1DSM-VF Model

A detailed theoretical description of the MGA-1DSM-VF trajectory model can be found in [34]. Based on this literature, only important information about this model is presented in this section[2].

The MGA-1DSM-VF model described in [34] and implemented in *Tudat* allows the use of powered gravity assist maneuvers unlike other similar models found in literature that permit using only unpowered gravity assist maneuvers. The assumptions of this trajectory model are as follows.

- Orbital perturbations are neglected and the method of patched conics is applicable.
- Order of planetary encounter is fixed.
- Only a single revolution and counter-clockwise transfers are considered while using the method of the Lambert targeting problem in this model.
- Only one DSM is applied.

The first assumption for this trajectory model is in agreement with a similar assumption for this thesis work, mentioned in Section 3.1. Since the definitions of the mission scenarios for this thesis work

[2] As [34] has developed a generic architecture for three trajectory models - the MGA-trajectory model, MGA-1DSM-VF trajectory model, and MGA-1DSM-PF trajectory model, some of the elements discussed in this section are common to all three models.

are also consistent with other assumptions mentioned above, this trajectory model can be utilized for research.

The MGA-1DSM-VF trajectory model decomposes the problem of interplanetary trajectory design into several parts, referred to as legs. Within the context of description and implementation of this model, three leg types have been identified as illustrated in Figure 5.3 and defined in Table 5.1. This table also shows the usage of three different leg types with mission scenarios concerning abort trajectory design.

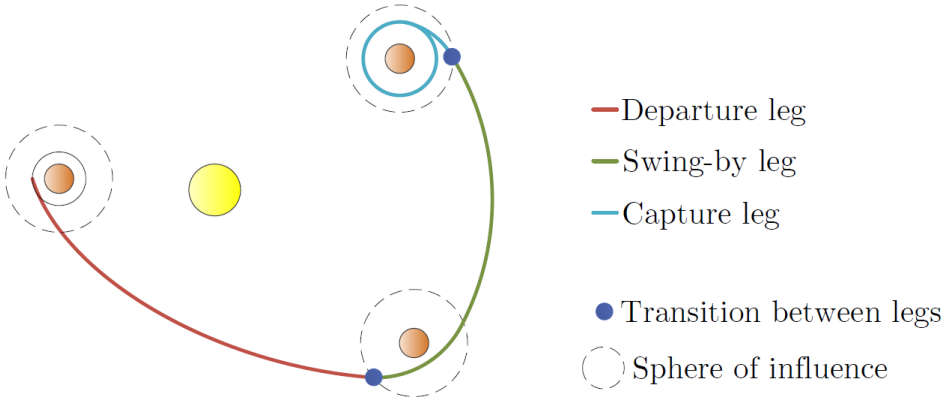

Figure 5.3: Schematic representation of three leg types with the MGA-1DSM-VF trajectory model [34]. There can be more than one swing-by leg between a departure leg and a capture leg when a sequence of planetary flybys exists in the trajectory. The capture leg can also be followed by a departure leg, when after a finite capture period at the planet, the S/C travels to another planetary destination.

Leg type	**Definition**	**Mission scenarios**		
		MS-3	*MS-4*	*MS-5*
Departure leg	Starts from a parking orbit around the departure planet and lasts until the SOI of the target planet is reached	✔	✔	✔
Swing-by leg	Starts after entering the SOI of the swing-by planet to perform a swing-by maneuver and lasts until the SOI of the next target planet is reached	✔	-	-
Capture leg	Starts after entering the SOI of the capture planet and can last until a possible departure from the parking orbit again	✔	✔	✔

Table 5.1: Definitions of three leg types for the MGA-1DSM-VF trajectory model and their usage with three mission scenarios - *MS-3*, *MS-4* and *MS-5*. Based on the information from [34] [36].

With this trajectory model, multiple legs belonging to one of the three types in Table 5.1 are concatenated with each other to form the desired interplanetary trajectory. Such a set of legs should have the departure leg type at the start and the capture leg type at the end. Between these two extremes, there can be multiple swing-by legs. Multiple capture legs and departure legs can be used, provided an intermediate departure leg is always preceded by a capture leg.

For the departure leg type, the following four variables are used in this model:

- V_∞: Magnitude of the relative velocity of the S/C with respect to the velocity of departure planet (hyperbolic excess velocity at the start)

- θ: the in-plane angle of the relative velocity V_∞
- ϕ: the out-of-plane angle of the relative velocity V_∞
- η_i: the fraction of TOF at which a DSM is performed during this leg

For the swing-by leg type, the following four variables are used in this model:

- r_p: the pericenter radius of the gravity assist maneuver at the relevant planet
- b_{incl}: the rotation angle of the gravity assist maneuver
- ΔV_{GA}: the magnitude of the ΔV applied at pericenter for the powered gravity assist maneuver
- η_i: the fraction of TOF at which a DSM is performed during this leg

An essential element required to use the above legs in a trajectory model is the knowledge of positions and velocities of planets at the epochs of any planetary encounter. This data can be derived from the selected planetary ephemerides (DE430) for the thesis[3]. Having access to the knowledge of planetary positions and velocities for a given sequence of planetary encounters and chosen values for design parameters such as parking orbit parameters, this trajectory model can be solved as follows.

1. For a given initial epoch (t_0) for the interplanetary trajectory concatenated from leg types described above, TOF (T_i) of all legs should be specified. By adding such TOF to the initial epoch according to the following equation, the epochs of the planetary encounters (t_i) are computed.

$$t_i = t_0 + \sum_{j=1}^{i-1} T_j \tag{5.13}$$

2. With known values for the epochs of the planetary encounters, the planetary positions are determined using the ephemeris data.

3. The heliocentric velocity after leaving the departure planet is determined.

   - If it is a departure leg:

     (a) Compute the departure ΔV with known values for the semi-major axis a and eccentricity e for the parking orbit around the departure planet:

$$\Delta V = \sqrt{\frac{2\mu}{a(1-e)} + V_\infty^2} - \sqrt{\frac{2\mu}{a(1-e)} - \frac{\mu}{a}} \tag{5.14}$$

     In above equation, μ is the gravitational parameter for the departure planet.

     (b) Compute the relative velocity vector $\boldsymbol{V_0}$[4]:

$$\boldsymbol{V_0} = \begin{bmatrix} \cos\theta \cdot \cos\phi \\ \sin\theta \cdot \cos\phi \\ \sin\phi \end{bmatrix} \cdot V_\infty \tag{5.15}$$

     Add the velocity of the departure planet to this relative velocity $\boldsymbol{V_0}$ to compute the heliocentric velocity.

   - If it is a swing-by leg, use the powered gravity assist propagation scheme as described in Section 5.2.2, to determine such a heliocentric velocity.

[3] For the high-thrust trajectory analysis using the MGA-1DSM-VF trajectory model, [34] had used the ephemerides data having approximate positions for the planets. On the other hand, this thesis uses more accurate three-dimensional ephemerides, obtained by the 6th order Lagrange interpolation of the published DE430 ephemerides data.

[4] $\boldsymbol{V_0}$ should be defined in such a way that its X-direction aligns with the heliocentric velocity of the departure planet, the Z-direction is normal to the orbital plane of the departure planet while the Y-direction completes a right-handed coordinate frame. Values of θ and ϕ should be specified considering this definition.

4. Compute the epoch of application of a DSM:

$$t_{DSM,i} = t_0 + \sum_{j=1}^{i-1} T_j + \eta_i \cdot T_i \tag{5.16}$$

5. Use the Kepler orbit propagation method described in Section 5.1, to propagate the trajectory up to $t_{DSM,i}$. The position of the DSM will be known after such a propagation.

6. Use the method of the Lambert targeting problem to find the trajectory from the position of the DSM until the next target planet. The solution of the Lambert targeting problem will provide the heliocentric velocity after the DSM and the heliocentric velocity on arrival at the target planet.

7. The ΔV for the DSM can be computed from the known values for the velocity before and the velocity after the epoch of application of such a DSM.

8. If it is a capture leg, compute the capture ΔV with Equation 5.14 using the parameters of the parking orbit around the capture planet and the gravitational parameter for this planet.

This computation scheme is illustrated in Figure 5.4.

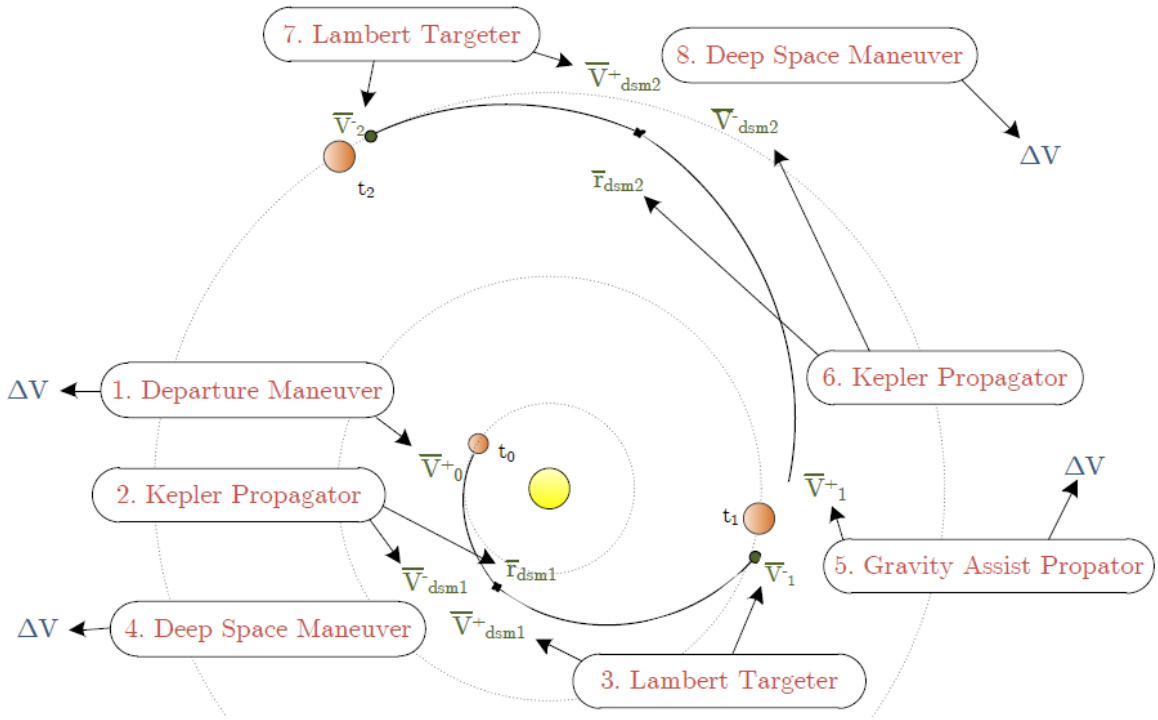

Figure 5.4: Schematic representation of the computation scheme for the MGA-1DSM-VF trajectory model, having one departure leg and one swing-by leg [34]. The Kepler propagator in this schematic corresponds to the method of Kepler orbit propagation.

With this trajectory model, the following four types of ΔV contributions are associated with the complete heliocentric trajectory:

- Departure ΔV: the ΔV required to achieve desired the V_∞ with respect to the departure planet
- DSM ΔV: the ΔV applied at the location of a DSM to match the heliocentric velocities before and after the epoch of application of the DSM
- ΔV_{GA}: the ΔV applied at the pericenter during a powered gravity assist maneuver. Constraining this to the value of 0 would indicate the use of only unpowered gravity assist maneuver(s).

- Capture ΔV: the ΔV required to get captured into a parking orbit around the capture planet after the execution of earlier legs of the mission

Two parameters of a gravity assist maneuver - pericenter radius (r_p) and magnitude of propulsive maneuver (ΔV_{GA}) - are used as variables in this trajectory model. By choosing only practical/feasible values for these variables, only feasible trajectory solutions can be allowed from the search space, when this model is used in combination with the meta-heuristic optimization algorithms during the optimization process. However, a disadvantage of the MGA-1DSM-VF model is that unlike its PF counterpart each leg of this model depends upon all previous legs and velocities at the end of a leg are propagated in the subsequent leg.

5.3.2. Computation Scheme: *MS-3*, *MS-4* and *MS-5*

A generic computational scheme for solving any interplanetary trajectory design problem using the MGA-1DSM-VF trajectory model has been discussed in the previous section. However, when this model is used to find the abort trajectory solutions for mission scenarios *MS-3*, *MS-4* and *MS-5* at various abort fractions, the process followed is slightly different. Such differences are highlighted in this section.

Unlike a conventional problem that can be solved using the MGA-1DSM-VF trajectory model (where the S/C departs from a planet on an interplanetary trajectory to visit other planets), abort trajectories investigated for *MS-3* and *MS-4* do not start at either Earth or Mars. These mission scenarios have the abort epoch during the nominal Earth-to-Mars transit duration (TOF_{nom}) implying that associated abort trajectories would start from a location in interplanetary space between the orbits of Earth and Mars. For *MS-5*, the S/C would indeed start from a parking orbit around Mars. These differences in the encounter sequence after abort are presented in Table 5.2.

	MS-3	***MS-4***	***MS-5***
Encounter sequence after abort	Abort location - Mars - Earth	Abort location - Mars - Earth	Mars - Earth
Methods	Kepler orbit propagation, then MGA-1DSM-VF model	Kepler orbit propagation, then MGA-1DSM-VF model	MGA-1DSM-VF model
Design variables with relevant legs of the MGA-1DSM-VF model			
Departure leg	T_1, V_∞, θ, ϕ, η_1	T_1, V_∞, θ, ϕ, η_1	T_1, V_∞, θ, ϕ, η_1
Swing-by leg	T_2, r_p, b_{incl}, ΔV_{GA}, η_2	-	-
Capture leg -	-	-	-
Design parameters with relevant legs of the MGA-1DSM-VF model			
Initial epoch (t_0)	t_{nom-ED} $+\eta_{abort} \times TOF_{nom}$	t_{nom-ED} $+\eta_{abort} \times TOF_{nom}$	t_{nom-MA} $+ \eta_{abort} \times T_{nom-surf}$
Parking orbit at departure	$a = \infty$ $e = 0$	$a = \infty$ $e = 0$	$a = R_m + h_{cm}$ $e = 0$
Parking orbit at capture	$a = \infty$ $e = 0$	$a = \infty$ $e = 0$	$a = \infty$ $e = 0$

Table 5.2: Design variables and parameters with three mission scenarios *MS-3*, *MS-4*, and *MS-5*.

Therefore, the knowledge of planetary positions and velocities through the planetary ephemerides is not sufficient but the state of the S/C at the abort epoch should be known too. As mentioned earlier in Section 5.1, such a state can be obtained using the method of Kepler orbit propagation because prior to the abort epoch, the S/C follows a ballistic transfer trajectory which would take it to Mars if the mission were not aborted. After such a state of the S/C is obtained, the MGA-1DSM-VF trajectory

model can be used for the abort trajectory design. The knowledge of ephemerides of Mars and Earth is sufficient for the *MS-5* problems and the Kepler orbit propagation method is not required.

The abort epochs of the abort trajectories would correspond to the initial epoch (t_0) of the trajectory model and their values can be computed as shown in Table 5.2. Four trajectory parameters associated with the selected nominal ballistic transfer solution are required for these computations viz. the nominal Earth-departure epoch (t_{nom-ED}), nominal Mars-arrival epoch (t_{nom-MA}), nominal Earth-to-Mars TOF (TOF_{nom}) and nominal Mars surface stay period ($T_{nom-surf}$). With assumed values of 0.2, 0.4, 0.6, and 0.8 for the abort fraction (η_{abort}), t_0 can be determined.

Two other design parameters are changed for the computation scheme - the semi-major axes (a) and eccentricities (e) for the parking orbits at the departure and at the capture. The values shown in Table 5.2 for these design parameters affect the ΔV values calculated using Equation 5.14. Since there neither an actual departure planet nor a parking orbit with *MS-3* and *MS-4*, setting the value of ∞ for a, reduces ΔV to V_∞. In this case, V_∞ represents the initial velocity of the S/C after the abort epoch relative to its own velocity before the abort epoch and thus, it represents the abort ΔV for the mission.

As the S/C departs from Mars with *MS-5*, values of the Mars parking orbit parameters discussed earlier in Section 3.3 are to be used. For the circular parking orbit at Mars, a can be computed using the average Mars radius (R_m) and the chosen altitude for such orbit (h_{cm}). As ballistic re-entry of an Earth-return taxi vehicle is assumed for this thesis, capture ΔV is not to be included in the total ΔV computation. Values of a and e for the parking orbit at the capture, shown in Table 5.2, would lead to the computation of V_∞ at Earth-arrival which has to be checked for the relevant constraint violation.

The types of legs present in the concatenated heliocentric abort trajectories for *MS-3*, *MS-4* and *MS-5* have been marked in Table 5.1. For *MS-3*, the abort trajectory consists of a departure leg, followed by a swing-by leg and then a capture leg. For *MS-4* and *MS-5*, the abort trajectories have only a departure leg followed by a capture leg. Use of these legs lead to a set of design variables shown in Table 5.2. With *MS-3*, a total of 10 design variables define an abort trajectory. The Number of design variables reduces to five for both *MS-4* and *MS-5* abort trajectories.

With such a modified computation scheme, abort trajectories have been computed in this thesis work. The task of the optimization process is to find the best possible values for the design variables of each mission scenario. The ΔV contributions of an abort trajectory are added together to use as one of the objectives of the optimization. With *MS-3*, the TOF of the departure and swing-by legs are added together ($T_1 + T_2$) to use as the second objective of the optimization. With *MS-4* and *MS-5*, the TOF of the departure leg (T_1) is used as the second objective of the optimization. The next chapter describes the optimization elements of this thesis.

6

Optimization

The previous two chapters described the methods that have been used in the thesis to solve the transfer and abort trajectory design problems. However, to optimize one or more objectives associated with such trajectories, an optimization process has to be performed using suitable optimization method(s). A study of basic concepts regarding optimization such as local vs global optimization, convex/concave nature of a function along with a survey of different optimization methods has been performed during the literature study phase and documented in [26].

In this chapter, the most relevant element of the literature study phase - global optimization methods - are summarized in Section 6.1. It is followed by validation for the developed computer script, as described in Section 6.2. The subsequent section of this chapter presents the results for the optimization tuning work.

6.1. Global Optimization Methods

For the thesis work, global optimum transfer and abort trajectory solutions are to be computed, which would utilize the design space in the best possible ways to reduce the ΔV cost and/or the transit duration of the Mars mission. Therefore, it is required to use global optimization methods, and such methods should be implemented in the form of computer algorithms by the selected optimization tool *PaGMO*.

A survey of global optimization methods implemented within *PaGMO* has revealed that all available algorithms are meta-heuristics algorithms such as the genetic algorithm. Even though these nature-inspired population-based methods do not guarantee convergence to a truly global solution, they are robust and do not require the existence of differentials [37]. They also do not need an in-depth understanding of the physics of the problem to accurately formulate a mathematical model. Moreover, such methods have been successfully used for the optimization of similar trajectory design problems in the past [27] [34] [35] [38] [39] [40] .

It has been decided to use the meta-heuristic algorithm(s) in the thesis work based on the above reasons. Through validation of the optimization script, it can be ensured that these algorithms are working as expected for the problem at hand. Moreover, with different initialization of the quasi-random numbers generator[1] used in these algorithms, the performance of the optimization process can be tested to check the robustness of the obtained solutions.

As mentioned earlier, transfer and abort trajectories are required to be optimized for the total ΔV requirement and total TOF. Thus, the concerned problem is a multi-objective optimization, and the

[1] A particular initialization of the quasi-random numbers generator can be achieved with a particular value for the random seed number. It is important to document such values of the random seed number to reproduce the exact same results.

following two[2] meta-heuristic global optimization algorithms have been implemented in *PaGMO* tool that offer such a multi-objective optimization capability.

- Multi-objective Evolutionary Algorithm by Decomposition (MOEA/D)
- Non-dominated Sorting Genetic Algorithm (NSGA-II)

A short description of these algorithms is presented in the following sections.

6.1.1. MOEA/D

As described in [41], the MOEA/D algorithm decomposes the multi-objective optimization problem into a number of scalar optimization sub-problems that approximate the Pareto front (explained in Section 6.2.2). Each of these sub-problems is then optimized simultaneously using an evolutionary algorithm. The methods by which the aggregation/decomposition of/into such sub-problems is achieved are called decomposition methods.

The counterpart of the MOEA/D algorithm - multi-objective evolutionary algorithms - do not associate every solution with any specific scalar optimization problem. These algorithms have issues such as fitness assignment and diversity maintenance which are eliminated by decomposition in MOEA/D. Moreover, MOEA/D has a lower complexity compared to other algorithms such as NSGA-II [41]. According to another research [42], this algorithm has a promising performance while dealing with complicated Pareto set shapes.

The implementation of this algorithm with the chosen toolbox *PaGMO* has the following characteristics [43]:

- rand/2/exp Differential Evolution (DE) operator
- polynomial mutation to create off-springs
- Tchebycheff, weighted or boundary intersection decomposition methods
- A diversity-preservation mechanism

6.1.2. NSGA-II

NSGA-II is a genetic algorithm that uses the crowding distance function to compute the fitness value for each individual in the population. Over the years since the original proposal of this algorithm, many improvements have been made such as in [44] where a local search strategy is added to the original method. However, the documentation [45] for implemented algorithm in *PaGMO* refers to the original work of Deb and others, published as [46] in 2002.

As described in [46], the traditional counterpart of NSGA-II - the non-dominated sorting algorithm - has a computational complexity of $O(MN^3)$ where M and N represent the number of objectives and population size respectively. This complexity is reduced to $O(MN^2)$ with NSGA-II with a faster approach for non-dominated sorting. Moreover, with this algorithm, a crowded comparison approach is used instead of the sharing function approach which eliminates the need to specify the sharing parameter by the user.

Optimization scripts have been developed that use both of these algorithms to find the relevant optimum transfer and/or abort trajectory solutions. Such scripts are first required to be validated and the optimization process might be tuned to improvise the performance. This will be discussed in the subsequent two sections of this chapter. During the process of validation or tuning, one of the algorithms might prove inferior to the other and further use of this algorithm can be avoided to save the computational efforts.

[2] A survey and selection of these algorithms have been performed during the literature study phase. As of January 2020, there are two more additions to this list of relevant algorithms in *PaGMO* viz. Multi-objective Hypervolume-based Ant Colony Optimization and Non-dominated Sorting Particle Swarm Optimization.

6.2. Validation

Before using the optimization algorithms considered for the thesis work, we need to validate the use of such algorithms by computing a solution to the problem whose true solution is already known. Mathematical test functions, having multiple local minima and maxima over the design space can be used for this benchmarking purpose. During the early phase of optimization, a validation of the solution to one such test function, the Schaffer's f_6 function, using the selected algorithms has been performed. The results for this validation of the optimization process can be found in Appendix B.

The static optimization problem of the Schaffer's f_6 test function is a good starting point. However, the trajectory design problems to be considered in the thesis work have more complexity and uncertainty than the Schaffer's f_6 test function. The trajectory design problems of this thesis work also have a number of constraints imposed on the design and the objective space as mentioned in Section 3.4 and have more than one objective to be optimized. Therefore, there is a need to validate the use of multi-objective optimization algorithms to find the solution(s) for more complex trajectory design problems (that resemble the optimization problems of this thesis work considering nature and complexity), whose solution(s) is/are available in literature.

For this purpose, the test case TC_2 (mentioned earlier in Chapter 4) can be utilized. As discussed before while validating the Lambert targeting script for this test case, the design variables - the date of departure and the date of arrival - have values the same as the reference values. In other words, the conditions for the best fitness individual have been directly selected during such an earlier validation. The deviation of the resulting fitness from the reference values was then computed for the purpose of validating only the Lambert targeting script.

For the validation of the optimization script, the same test case is solved by the optimization algorithms to *identify* the best fitness individuals. The design space chosen is the same as the reference design space and the performance of both the optimization algorithms has been analyzed. Two other launch opportunities of TC_2, subsequent to those used in Chapter 4, are used for this purpose viz. the 2014 and 2016 launch opportunities for Earth-to-Mars ballistic transfer trajectories.

For both launch opportunities, minimum departure excess velocity trajectory solutions have been used for the comparison with the reference values. Two constraints are associated with these solutions: i. Only type-I transfer trajectories are valid. ii. The transfer trajectory has a constant TOF (180 days for the 2014 launch opportunity and 181 days for the 2016 launch opportunity). These constraints can be marked with identifiers C_1 and C_2 respectively. The allowed designed space is reduced as these constraints are imposed on the optimization problem.

Since there is no direct mathematical way to implement constraints when the meta-heuristics algorithms are used for the optimization, these constraints are incorporated using penalties for their violation added to the values of the objectives of the optimization problem. Such penalties for violation of these constraints can be computed as given by Equations 6.1 and 6.2. W_1 and W_2 in these equations are weighing factors, which are optimization parameters used to scale the values of the penalty violations correctly while adding them to the primary objective function value(s). With these computations for the penalty functions, the mathematical formulation of the multi-objective optimization problem is given by Equation 6.3. Two objectives of this problem - objective I (Obj_1) and objective II (Obj_2) - are to be minimized.

$$\text{Penalty for violation of } C_1 \text{ constraint} = W_1 \times (\Delta\theta - 180^\circ), \text{ if } \Delta\theta > 180^\circ \tag{6.1}$$

$$\begin{aligned}\text{Penalty for violation of } C_2 \text{ constraint} &= W_2 \times \text{ abs(TOF} - 180), \text{ if 2014 launch opportunity} \\ &= W_2 \times \text{ abs(TOF} - 181), \text{ if 2016 launch opportunity}\end{aligned} \tag{6.2}$$

$$\begin{aligned}\text{Minimize} \quad Obj_1 &= V_{\infty \text{ at departure}} + \text{Penalty for violation of } C_1 \text{ constraint} \\ &\quad + \text{Penalty for violation of } C_2 \text{ constraint} \\ \text{Minimize} \quad Obj_2 &= V_{\infty \text{ at arrival}} + \text{Penalty for violation of } C_1 \text{ constraint} \\ &\quad + \text{Penalty for violation of } C_2 \text{ constraint}\end{aligned} \tag{6.3}$$

Here $\Delta\theta$ represents the heliocentric transfer angle associated with a particular individual of the population. The function $abs(x)$ computes the absolute value of a variable x.

6.2.1. Selected Solutions

Both optimization algorithms have been used five times (with five different values for the random seed number) and the sets of optimum trajectory solutions have been obtained. From each solution set, the trajectory solution having the minimum value for the first objective (i.e. minimum departure excess velocity trajectory) has been selected and compared with the reference trajectory solution. The results for this comparison are presented in Tables 6.1 and 6.2 for the 2014 and 2016 opportunity, respectively.

#	Date of departure		Date of arrival		V_∞ at departure		V_∞ at arrival	
	Comp. value [MJD2000]	% Error	Comp. value [MJD2000]	% Error	Comp. value [m/s]	% Error	Comp. value [m/s]	% Error
MOEA/D algorithm								
1	5116.80	$-3.90 \cdot 10^{-3}$	5296.80	$-3.76 \cdot 10^{-3}$	3313.08	$-2.88 \cdot 10^{-1}$	6809.01	$3.54 \cdot 10^{-1}$
2	5116.82	$-3.60 \cdot 10^{-3}$	5296.82	$-3.47 \cdot 10^{-3}$	3312.88	$-2.94 \cdot 10^{-1}$	6807.62	$3.33 \cdot 10^{-1}$
3	5116.64	$-7.05 \cdot 10^{-3}$	5296.64	$-6.81 \cdot 10^{-3}$	3312.66	$-3.01 \cdot 10^{-1}$	6820.83	$5.28 \cdot 10^{-1}$
4	5116.85	$-2.99 \cdot 10^{-3}$	5296.85	$-2.88 \cdot 10^{-3}$	3313.10	$-2.87 \cdot 10^{-1}$	6805.46	$3.02 \cdot 10^{-1}$
5	5116.61	$-7.64 \cdot 10^{-3}$	5296.61	$-7.38 \cdot 10^{-3}$	3312.73	$-2.99 \cdot 10^{-1}$	6823.15	$5.62 \cdot 10^{-1}$
$\bar{x}$	**of % error**	$5.04 \cdot 10^{-3}$		$4.86 \cdot 10^{-3}$		$2.94 \cdot 10^{-1}$		$4.16 \cdot 10^{-1}$
σ	**of % error**	$2.14 \cdot 10^{-3}$		$2.07 \cdot 10^{-3}$		$6.02 \cdot 10^{-3}$		$1.20 \cdot 10^{-1}$
NSGA-II algorithm								
1	5132.81	$3.09 \cdot 10^{-1}$	5312.81	$2.99 \cdot 10^{-1}$	3857.99	$1.61 \cdot 10^{1}$	5656.43	$-1.66 \cdot 10^{1}$
2	5115.94	$-2.06 \cdot 10^{-2}$	5295.94	$-1.99 \cdot 10^{-2}$	3314.16	$-2.55 \cdot 10^{-1}$	6873.43	$1.30 \cdot 10^{0}$
3	5114.47	$-4.95 \cdot 10^{-2}$	5294.47	$-4.78 \cdot 10^{-2}$	3325.65	$9.03 \cdot 10^{-2}$	6984.63	$2.94 \cdot 10^{0}$
4	5115.99	$-1.97 \cdot 10^{-2}$	5295.99	$-1.91 \cdot 10^{-2}$	3313.62	$-2.72 \cdot 10^{-1}$	6869.58	$1.25 \cdot 10^{0}$
5	5126.32	$1.82 \cdot 10^{-1}$	5306.32	$1.76 \cdot 10^{-1}$	3530.06	$6.24 \cdot 10^{0}$	6110.33	$-9.94 \cdot 10^{0}$
$\bar{x}$	**of % error**	$1.16 \cdot 10^{-1}$		$1.12 \cdot 10^{-1}$		$4.59 \cdot 10^{0}$		$6.41 \cdot 10^{0}$
σ	**of % error**	$1.58 \cdot 10^{-1}$		$1.53 \cdot 10^{-1}$		$7.12 \cdot 10^{0}$		$8.64 \cdot 10^{0}$

Table 6.1: Validation of the optimum transfer trajectory (minimum C_3) solution for the 2014 launch opportunity of TC_2. Using two algorithms, the optimum solutions to a Lambert targeting problem are found. The optimization process is repeated five times for each algorithm (#1 to #5), using five values for the random seed number as 12345, 466, 8000, 22, and 500000, respectively. A population of 200 individuals has been used and the results presented above are obtained after 200 generations. Computed (Comp.) values for the four variables are compared with the reference values [24]. The mean ($\bar{x}$) and standard deviation (σ) for the percent (%) errors are computed to check the robustness of an algorithm.

As seen in these tables, when the MOEA/D algorithm is used the mean values of percentage error associated with the design variables of the problem (i.e the date of departure and date the arrival) have an order of magnitude (-2) to (-3). The mean values of percentage error associated with the arrival and departure V_∞ have an order of magnitude (-1). In order to check for the sensitivity of this optimization algorithm to the value of random seed number (i.e to check the robustness of any obtained solution with the algorithm), the standard deviations of the percentage errors have been computed. It can be seen that the standard deviations of the percentage errors associated with the design variables and V_∞ at departure have an order of magnitude (-2) to (-3). In the case of V_∞ at arrival, this standard deviation has an order of magnitude (-1).

When the NSGA-II algorithm is used instead of the MOEA/D to solve the same trajectory optimization problems, the order of magnitude associated with mean values of all the percentage errors has increased by one or two, while the order of magnitude of the standard deviations of the error values has increased by one to three. Thus, if the optimization parameters have the same values[3], the MOEA/D

[3]Relevant optimization parameters in these cases are the population size, the number of generations used to find the best fitness

#	Date of departure		Date of arrival		V_∞ at departure		V_∞ at arrival	
	Comp. value [MJD2000]	% Error	Comp. value [MJD2000]	% Error	Comp. value [m/s]	% Error	Comp. value [m/s]	% Error
				MOEA/D algorithm				
1	5893.83	$-2.95 \cdot 10^{-3}$	6074.83	$-2.86 \cdot 10^{-3}$	2989.26	$3.69 \cdot 10^{-1}$	5282.02	$-2.83 \cdot 10^{-1}$
2	5894.17	$2.81 \cdot 10^{-3}$	6075.17	$2.73 \cdot 10^{-3}$	2989.60	$3.81 \cdot 10^{-1}$	5260.74	$-6.85 \cdot 10^{-1}$
3	5894.19	$3.19 \cdot 10^{-3}$	6075.19	$3.10 \cdot 10^{-3}$	2989.62	$3.81 \cdot 10^{-1}$	5259.32	$-7.11 \cdot 10^{-1}$
4	5893.28	$-1.22 \cdot 10^{-2}$	6074.28	$-1.18 \cdot 10^{-2}$	2989.36	$3.73 \cdot 10^{-1}$	5316.34	$3.65 \cdot 10^{-1}$
5	5893.78	$-3.76 \cdot 10^{-3}$	6074.78	$-3.65 \cdot 10^{-3}$	2989.40	$3.74 \cdot 10^{-1}$	5285.21	$-2.23 \cdot 10^{-1}$
$\bar{x}$	**of % error**	$4.98 \cdot 10^{-3}$		$4.83 \cdot 10^{-3}$		$3.76 \cdot 10^{-1}$		$4.53 \cdot 10^{-1}$
σ	**of % error**	$6.24 \cdot 10^{-3}$		$6.05 \cdot 10^{-3}$		$5.28 \cdot 10^{-3}$		$4.37 \cdot 10^{-1}$
				NSGA-II algorithm				
1	5887.15	$-1.16 \cdot 10^{-1}$	6068.16	$-1.13 \cdot 10^{-1}$	3040.55	$2.09 \cdot 10^{0}$	5719.85	$7.98 \cdot 10^{0}$
2	5900.47	$1.10 \cdot 10^{-1}$	6081.47	$1.06 \cdot 10^{-1}$	3043.13	$2.18 \cdot 10^{0}$	4885.61	$-7.77 \cdot 10^{0}$
3	5891.39	$-4.43 \cdot 10^{-2}$	6072.39	$-4.30 \cdot 10^{-2}$	2995.61	$5.83 \cdot 10^{-1}$	5438.68	$2.67 \cdot 10^{0}$
4	5907.40	$2.27 \cdot 10^{-1}$	6088.39	$2.20 \cdot 10^{-1}$	3208.06	$7.72 \cdot 10^{0}$	4520.42	$-1.47 \cdot 10^{1}$
5	5891.14	$-4.85 \cdot 10^{-2}$	6072.14	$-4.71 \cdot 10^{-2}$	2996.30	$6.06 \cdot 10^{-1}$	5454.21	$2.97 \cdot 10^{0}$
$\bar{x}$	**of % error**	$1.09 \cdot 10^{-1}$		$1.06 \cdot 10^{-1}$		$2.63 \cdot 10^{0}$		$7.21 \cdot 10^{0}$
σ	**of % error**	$1.40 \cdot 10^{-1}$		$1.36 \cdot 10^{-1}$		$2.94 \cdot 10^{0}$		$9.21 \cdot 10^{0}$

Table 6.2: Validation of the optimum transfer trajectory (minimum C_3) solution for the 2016 launch opportunity of TC_2. Using two algorithms, the optimum solutions to a Lambert targeting problem are found. The optimization process is repeated five times for each algorithm (#1 to #5), using five values for the random seed number as 12345, 466, 8000, 22, and 500000, respectively. A population of 200 individuals has been used and the results presented above are obtained after 100 generations. Computed (Comp.) values for the four variables are compared with the reference values [24]. The mean ($\bar{x}$) and standard deviation (σ) for the percent (%) errors are computed to check the robustness of an algorithm.

algorithm outperforms the NSGA-II algorithm based on the accuracy of the computed solution with respect to the reference solution and the robustness of this computed solution.

It should be noted that the errors associated with the computed solutions can be further reduced through the process of local refinement, after performing the global optimization using meta-heuristic algorithms. However, such a process is not performed during the validation phase of the thesis work due to time constraints. Values of the errors and their standard deviations shown in Tables 6.1 and 6.2 have been deemed as acceptable to validate the use of optimization algorithms.

6.2.2. Pareto Front Formation

The quantitative comparison has been performed for the computed minimum departure excess velocity solutions for test case TC_2 as the reference values are provided only for this particular solution type in [24]. However, the optimization problem solved has multiple objectives as it is evident from its formulation given by Equation 6.3. Such a multi-objective optimization would result in a solution set, which would have solutions with values of both objectives ranging from minimum to maximum. In other words, along with the minimum departure excess velocity solution, the solution set would also contain a solution that has minimum arrival excess velocity and all other solutions having a performance in between these two extremes.

The points from the design space are called Pareto optimal if any improvement in the associated value for one of the objectives leads to a deterioration of the value of at least one other objective [41]. The set of Pareto optimal points is referred to as the Pareto set and the corresponding set of all Pareto optimal objective vectors is called the Pareto front. Thus, a solution set obtained through the con-

individual and the weighing factors W_1 and W_2.

verged generation of a multi-objective optimization process should ideally lead to a Pareto front of the objective values. Therefore, in this report, the terms solution set and Pareto front are sometimes used interchangeably.

It is required to validate the formation of a Pareto front for an optimization problem as it ensures that the multi-objective optimization is working as expected. Such a validation is shown in Figures 6.1 and 6.2.

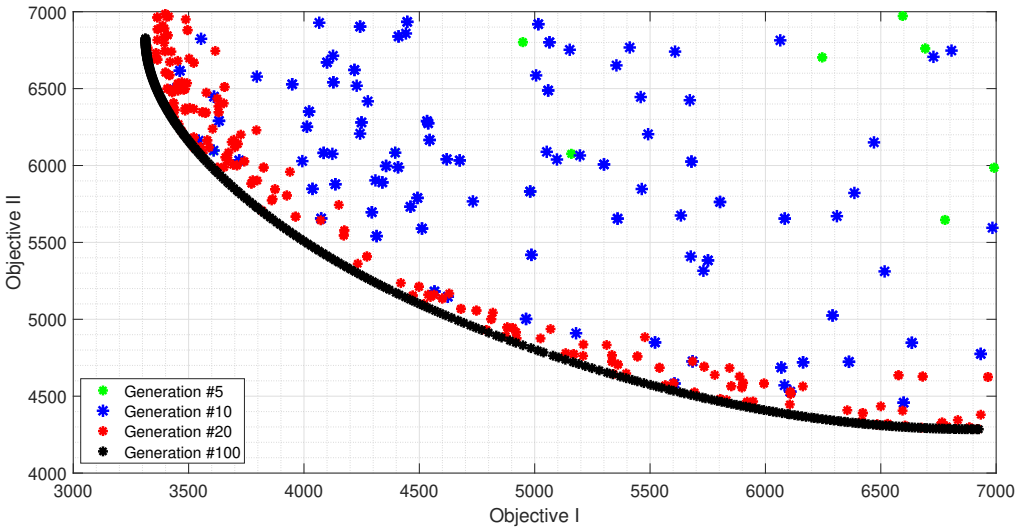

Figure 6.1: Formation of the Pareto front for the multi-objective optimization problem when solved using the MOEA/D algorithm. Earth-to-Mars transfer trajectory solutions with the 2014 launch opportunity of the test case TC_2 are optimized. Points marked in black indicate the formation of the Pareto front as the number of generation reaches 100.

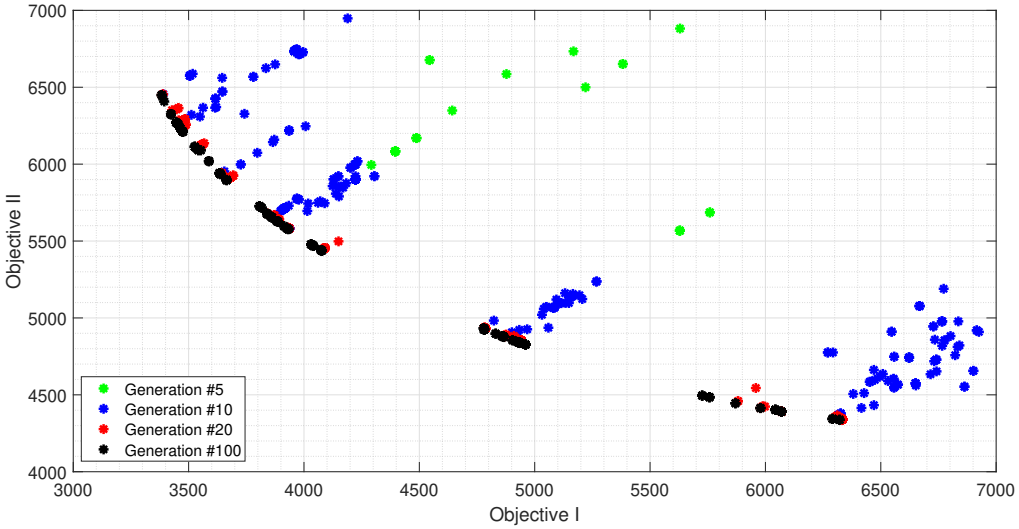

Figure 6.2: Formation of the Pareto front for the multi-objective optimization problem when solved using the NSGA-II algorithm. Earth-to-Mars transfer trajectory solutions with the 2014 launch opportunity of the test case TC_2 are optimized. Points marked in black indicate the formation of the Pareto front as the number of generation reaches 100.

As seen in Figures 6.1 and 6.2, the formation of a Pareto front can be validated by visually inspecting the behavior of objective-function values of the individuals in the population at different generations. As the number of generations reaches 100, both algorithms lead to a solution set having a trade-off between the values of two objectives. While the MOEA/D algorithm has resulted in a solution set

that has a regular/uniform collection of the Pareto optimal points between two extreme solutions, the NSGA-II algorithm has failed to include all such points. Keeping this issue with the NSGA-II algorithm in mind, it can be concluded that a better Pareto front is formed with successive generations of the optimization process using the MOEA/D algorithm.

Until now, a fixed number of generations has been used in the optimization process for obtaining the solution set. It is possible to improvise the quantitative results presented for minimum departure excess velocity solutions in the previous section and those presented for the formation of the Pareto front in this section, by increasing the number of generations. Moreover, a number of other parameters exist to which the optimization process of an optimization algorithm is sensitive. The procedure of determining values for such parameters is referred to as optimization tuning and through such a procedure, the performance of an optimization process can be further improvised. In the next section, optimization tuning performed for this thesis work will be described.

6.3. Optimization Tuning

Two optimization parameters that clearly require tuning procedure are the population size (number of individuals) for the meta-heuristic algorithm and the number of generations executed before stopping the optimization process. The formulation of a penalty function (used to penalize the objectives in case of a constraint violation) can also have an influence on the performance of the optimization process. In this section, results for the optimization tuning procedure performed to find the best values for all such parameters are presented.

The optimization problem selected to perform such a tuning is the optimization of Earth-to-Mars ballistic transfer trajectories during the 2014 launch opportunity, as presented in [24] and marked with an identifier TC_2 earlier.

6.3.1. Number of Generations

While validating the use of multi-objective optimization methods earlier, the number of generations (i.e. the number of iterations with a meta-heuristic algorithm) had been set to values such as 100 or 200, deemed sufficiently high to show the validity of the process. However, such a random setting for this optimization parameter might lead to either inferior solutions or the overuse of computational capability. To analyze the influence of changing the number of generations, the best fitness value of objective I and the best fitness value of objective II over the population, at each generation, have been observed. Additionally, average fitness values for the objectives I and II have also been observed.

Results for the MOEA/D algorithm when the number of generations increases from 100 to 600 are presented in Figures 6.3 and 6.4. It has been observed that the best fitness value for either objective fluctuates with the increasing number of generations and this behavior is not expected at all. The evolutionary nature of the meta-heuristic algorithm is supposed to retain the solutions which have the best fitness value in the population as the population evolves through iterations.

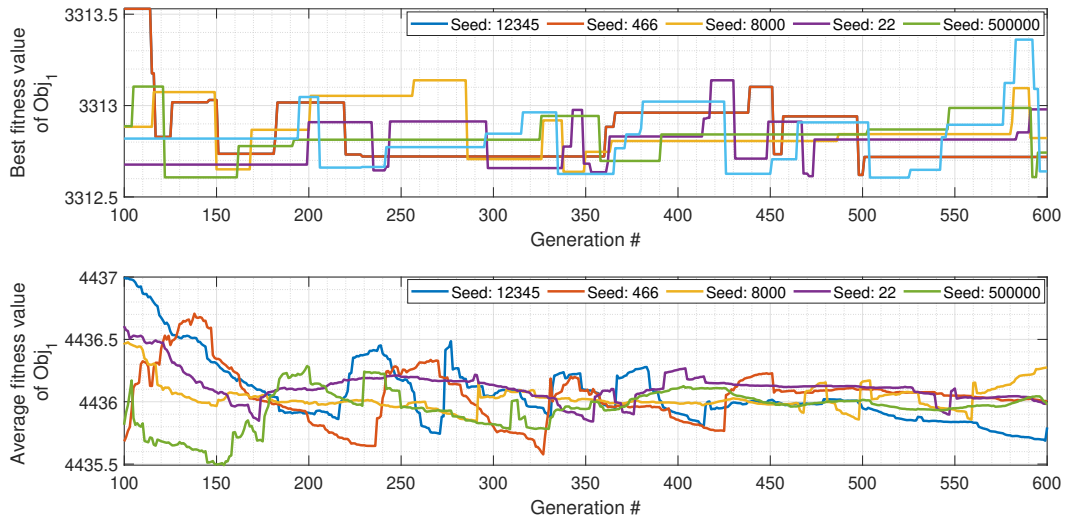

Figure 6.3: Variation of the objective I fitness value with the MOEA/D algorithm using the Tchebycheff decomposition method. The Earth-to-Mars ballistic transfer trajectory optimization problem has been solved for the 2014 launch opportunity of TC_2. The variation of both best fitness in the population and average fitness of the population is shown over 600 generations for five different initializations of the quasi-random numbers generator. A population of 300 individuals has been used.

Observing the default values for the parameters of the MOEA/D algorithm in the selected optimization library *PaGMO*, it was noticed that the tool is set to use the Tchebycheff decomposition method unless specified otherwise. Apart from this particular method, two other options are available in the toolbox. In the next phase of optimization tuning, such decomposition methods have been selected instead of the default choice of the Tchebycheff decomposition method and the results of this analysis are presented in the subsequent section to check whether the issue regarding best fitness value still persists.

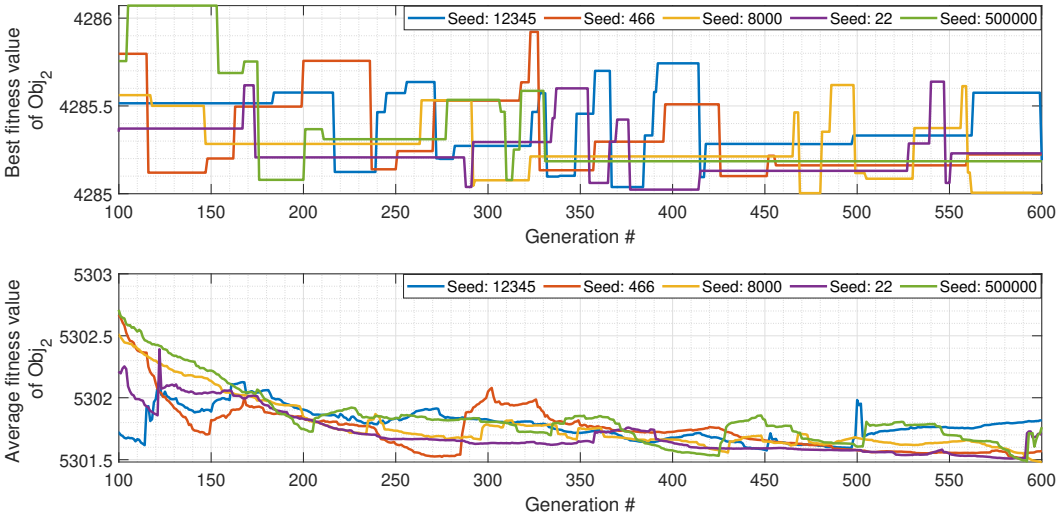

Figure 6.4: Variation of the objective II fitness value with the MOEA/D algorithm using the Tchebycheff decomposition method. The Earth-to-Mars ballistic transfer trajectory optimization problem has been solved for the 2014 launch opportunity of TC_2. The variation of both best fitness in the population and average fitness of the population is shown over 600 generations for five different initializations of the quasi-random numbers generator. A population of 300 individuals has been used.

Results for the NSGA-II algorithm are presented in Figures 6.5 and 6.6 for the fitness values of objectives I and II respectively. It is observed that unlike the MOEA/D algorithm with the Tchebycheff decomposition method, the best fitness values of both the objectives always decrease as the number of generations increases. However, the best fitness values and average fitness values for both objectives show a larger variation with different values for the random seed number. This implies that the solution set obtained lacks robustness even when generations as high as 600 are executed, and the results obtained for the trajectory optimization are highly sensitive to the chosen initialization of the random generator.

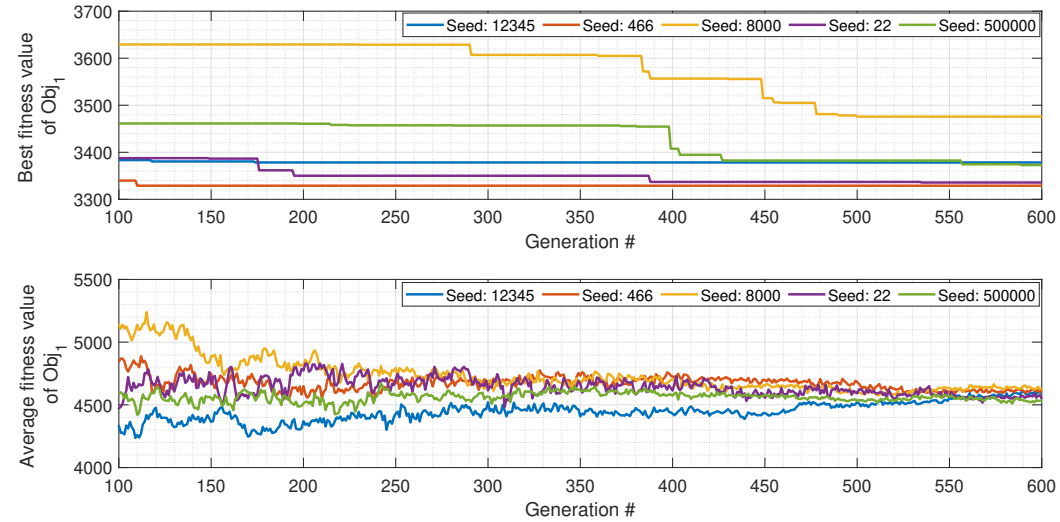

Figure 6.5: Variation of the objective I fitness value with the NSGA-II algorithm. The Earth-to-Mars ballistic transfer trajectory optimization problem has been solved for the 2014 launch opportunity of TC_2. The variation of both best fitness in the population and average fitness of the population is shown over 600 generations for five different initializations of the quasi-random numbers generator. A population of 300 individuals has been used.

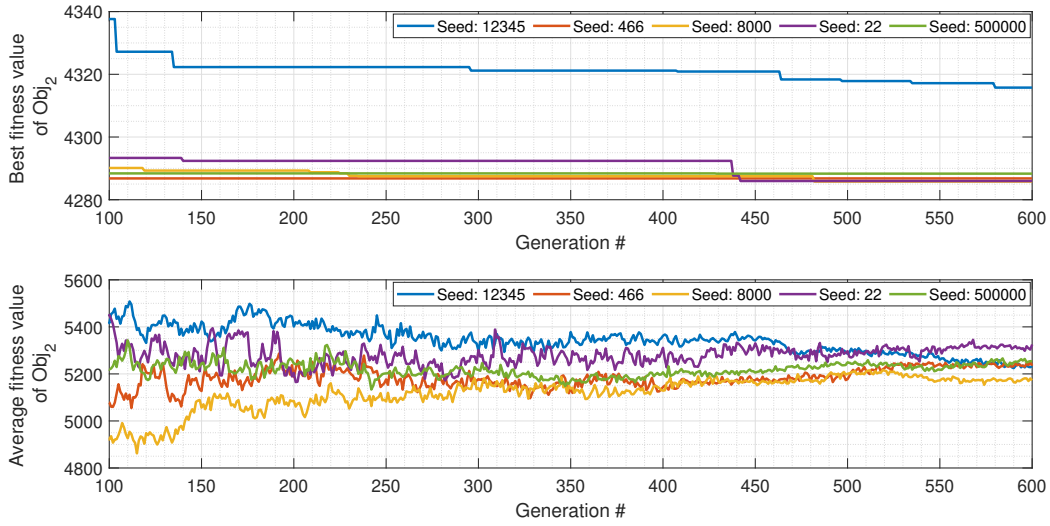

Figure 6.6: Variation of the objective II fitness value with the NSGA-II algorithm. The Earth-to-Mars ballistic transfer trajectory optimization problem has been solved for the 2014 launch opportunity of TC_2. The variation of both best fitness in the population and average fitness of the population is shown over 600 generations for five different initializations of the quasi-random numbers generator. A population of 300 individuals has been used.

Due to the inferior performance of the NSGA-II algorithm observed until this phase of the optimization tuning procedure, it has been decided that this particular algorithm will not be used for the thesis work and no further analysis has been performed using this algorithm. Moreover, due to the fluctuations of the best fitness values obtained through the MOEA/D algorithm with the Tchebycheff decomposition method, a fixed number of generations based on the best fitness value of either objective can not be decided upon yet.

However, deciding upon a fixed number of generations based on the best fitness value for the optimization process might be disadvantageous, as certain initializations of the quasi-random numbers generator would lead to a different evolutionary path, requiring a different level of the computational effort than another initialization to reach the same accuracy. If a convergence criterion is used instead, each run of the optimization process can then be stopped once the fluctuations of the fitness value stay within pre-defined limits.

Such convergence criterion can be defined for either the best fitness value of the objective I or objective II or even sum of the best fitness values of both objectives. However, as the aim of the optimization process for the thesis work is to obtain a solution set that ideally captures all Pareto optimal points between two extremes, it has been decided to define the convergence criterion based on the sum of the average fitness value for the objective I and the average fitness value for the objective II, over the population. This is a more *conservative* approach for stopping the optimization process compared to the one based on the best fitness values, but it strives to obtain a uniformly-spread Pareto front even if the extremes of such a Pareto front do not show a considerable variation over additional iterations/generations.

Each run of the optimization process will be executed for a certain minimum number of generations (to permit the minimum evolution for the population) and will also be limited by a maximum number of generations (to keep the computational efforts within limit). Between these two limits, the process will be stopped according to the convergence of the parameter mentioned above. To ensure that the convergence is indeed reached, a certain number of generations will still be executed after the first detection of convergence.

6.3.2. Decomposition Methods for MOEA/D

Even though the procedure to determine the number of generations for the optimization has been decided through the previous phase of the optimization tuning, the issue regarding retention of the best fitness individuals is still present. Out of a number that changed the default values for the parameters of the selected MOEA/D algorithm[4], the most promising effect has been observed for the decomposition method settings. Results for two more decomposition methods implemented in the *PaGMO* library are presented as follows.

Weighted Sum Decomposition Method

Results for the fitness values of objectives I and II, when the weighted sum decomposition method is used for the MOEA/D algorithm, are presented in Figures 6.7 and 6.8 respectively.

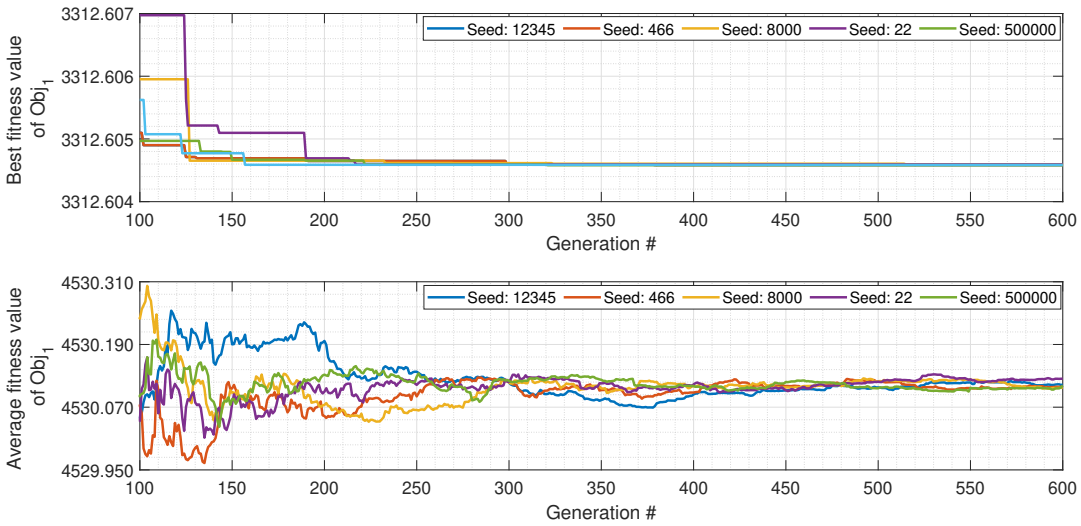

Figure 6.7: Effect of using the weighted sum decomposition method for MOEA/D algorithm on the objective I fitness values. The Earth-to-Mars ballistic transfer trajectory optimization problem has been solved for the 2014 launch opportunity of TC_2. Variation of the objective I values (both the best fitness in the population and the average fitness of the population) over 600 generations is shown for five different initializations of the quasi-random numbers generator. The population size is 300.

Unlike for the default choice of decomposition method, values of the best fitness for both objectives always decrease with the weighted sum decomposition method as seen in Figures 6.7 and 6.8. Additionally, the range of variation of the best fitness and average fitness values for both objectives after 100 generations is smaller compared to the results presented for the Tchebycheff decomposition method, let alone after 600 generations.

Boundary Intersection Decomposition Method

Results for the fitness values of the objectives I and II, when the boundary intersection decomposition method is used for the MOEA/D algorithm, are presented in Figures 6.9 and 6.10 respectively.

From Figures 6.9 and 6.10, it can be observed that with this decomposition method, the best fitness value is not retained in the population and this individual is often lost during next iterations/generations of the optimization. The reason behind such a strange behavior is unknown but it has been clear that without further investigation, this decomposition method proves inferior to the weighted sum decomposition method.

Based on the results presented in this and previous sections for three decomposition methods of the MOAE/D algorithm, it has been decided to use the weighted sum decomposition method for the thesis

[4]The values other than the default value for the maximum number of copies reinserted in the population were used. The algorithm was also tested with and without the use of the diversity preservation mechanisms.

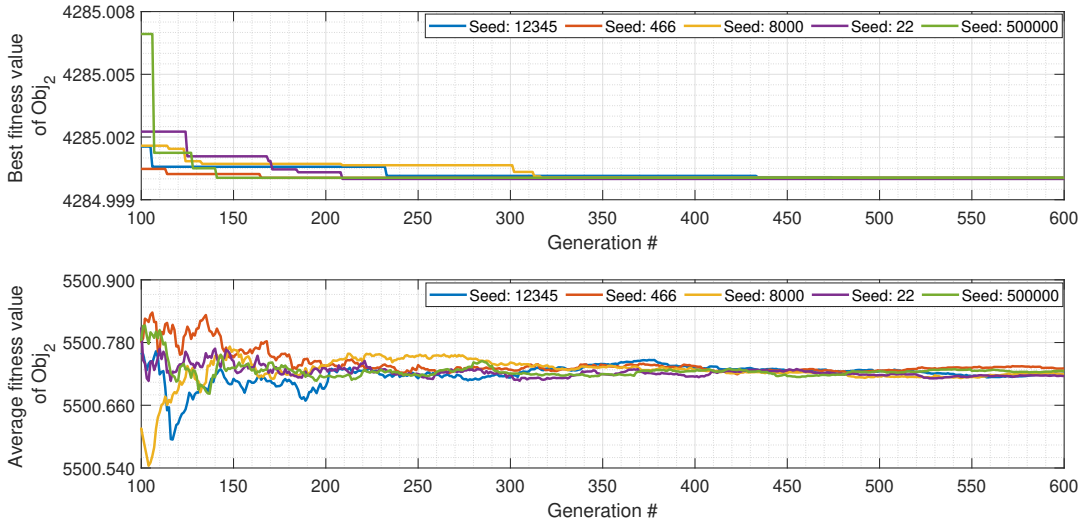

Figure 6.8: Effect of using the weighted sum decomposition method for MOEA/D algorithm on the objective II fitness values. The Earth-to-Mars ballistic transfer trajectory optimization problem has been solved for the 2014 launch opportunity of TC_2. Variation of the objective II values (both the best fitness in the population and the average fitness of the population) over 600 generations is shown for five different initializations of the quasi-random numbers generator. The population size is 300.

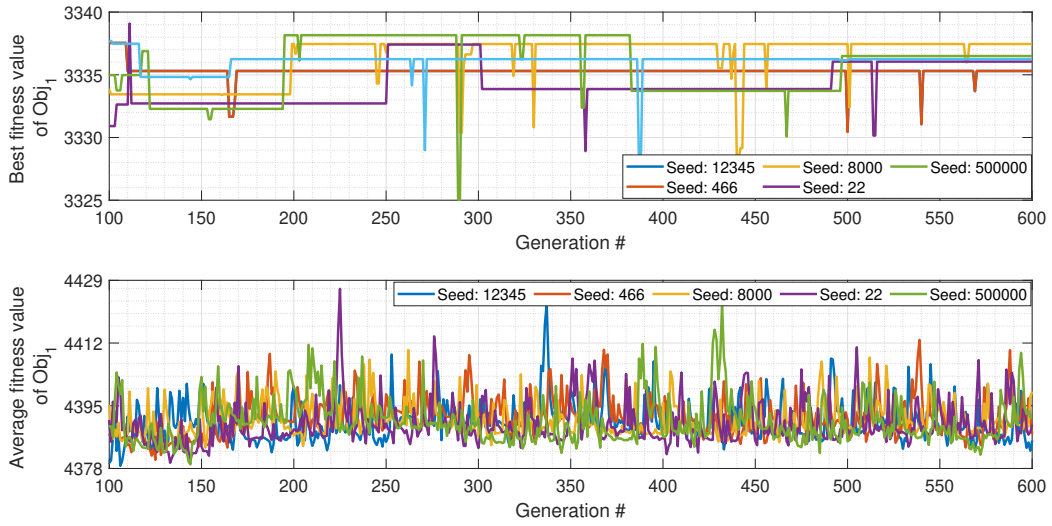

Figure 6.9: Effect of using the boundary intersection decomposition method for MOEA/D algorithm on the objective I fitness values. The Earth-to-Mars ballistic transfer trajectory optimization problem has been solved for the 2014 launch opportunity of TC_2. Variation of the objective I values (both the best fitness in the population and the average fitness of the population) over 600 generations is shown for five different initializations of the quasi-random numbers generator. The population size is 300.

work[5]. With this selection, the next phase of the optimization tuning procedure will investigate the effect of population size on the results and it is described in the subsequent section.

[5]In-depth analysis of why one particular method outperforms the others has not been performed due to the time constraints of the research work. One of the potential reasons behind the superiority of this decomposition method might be that it is more suitable for the nature of the trajectory design problem at hand than other.

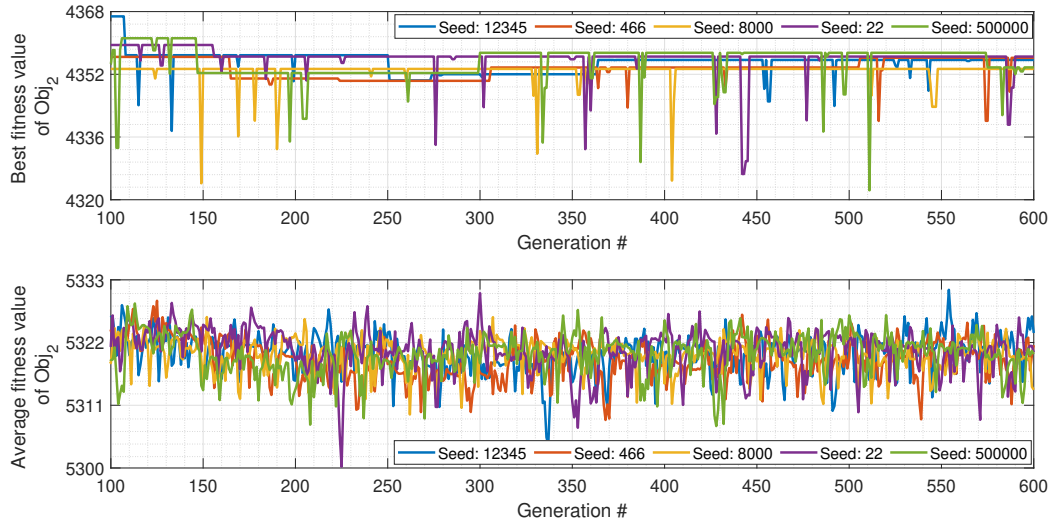

Figure 6.10: Effect of using the boundary intersection decomposition method for MOEA/D algorithm on the objective II fitness values. The Earth-to-Mars ballistic transfer trajectory optimization problem has been solved for the 2014 launch opportunity of TC_2. Variation of the objective II values (both the best fitness in the population and the average fitness of the population) over 600 generations is shown for five different initializations of the quasi-random numbers generator. The population size is 300.

6.3.3. Population Size

For earlier analyses, a population size of 300 individuals has been used in the optimization process. However, such a population size might be too small requiring more generations to generate and retain better solutions within the population. Such a population size might be too large as well, generating undesired (from a fitness perspective) individuals in the population and then requiring more generations so that more desirable individuals eventually replace these undesired individuals. Figure 6.11 shows the effect of changing the population size on the sum of the average fitness values for objective I and the average fitness value for objective II, which is to be used for detecting the convergence.

Considering the performance of the optimization process for five different values of the random seed number, it can be concluded from Figure 6.11 that population sizes of 100, 150 and 250 usually require more generations before the process reaches convergence, compared to the number of generations required with the population size of 300 individuals. On the other hand, the usage of more individuals in the population - 400 or 500 - would often lead to a quicker convergence. It has been decided to use the population size of 400 individuals for the thesis work, to reduce the computational effort with respect to the population size of 500 individuals, as a clear advantage of the latter (with respect to the former) is not evident through a visual inspection of Figure 6.11.

It should be noted that for the actual trajectory analysis to be performed in this thesis, the number of design variables is higher than the test case TC_2 currently used in this analysis. This will lead to a larger search (design) space and having a small number of individuals in the population would not help in the exploration of this larger design space. However, the usage of a convergence criterion instead of a fixed number of generations ensures that if the problem becomes too complex (than currently anticipated) and the population size has an underestimated value, the optimization process would simply be continued for more generations, until a pre-defined upper limit on the number of generations is reached.

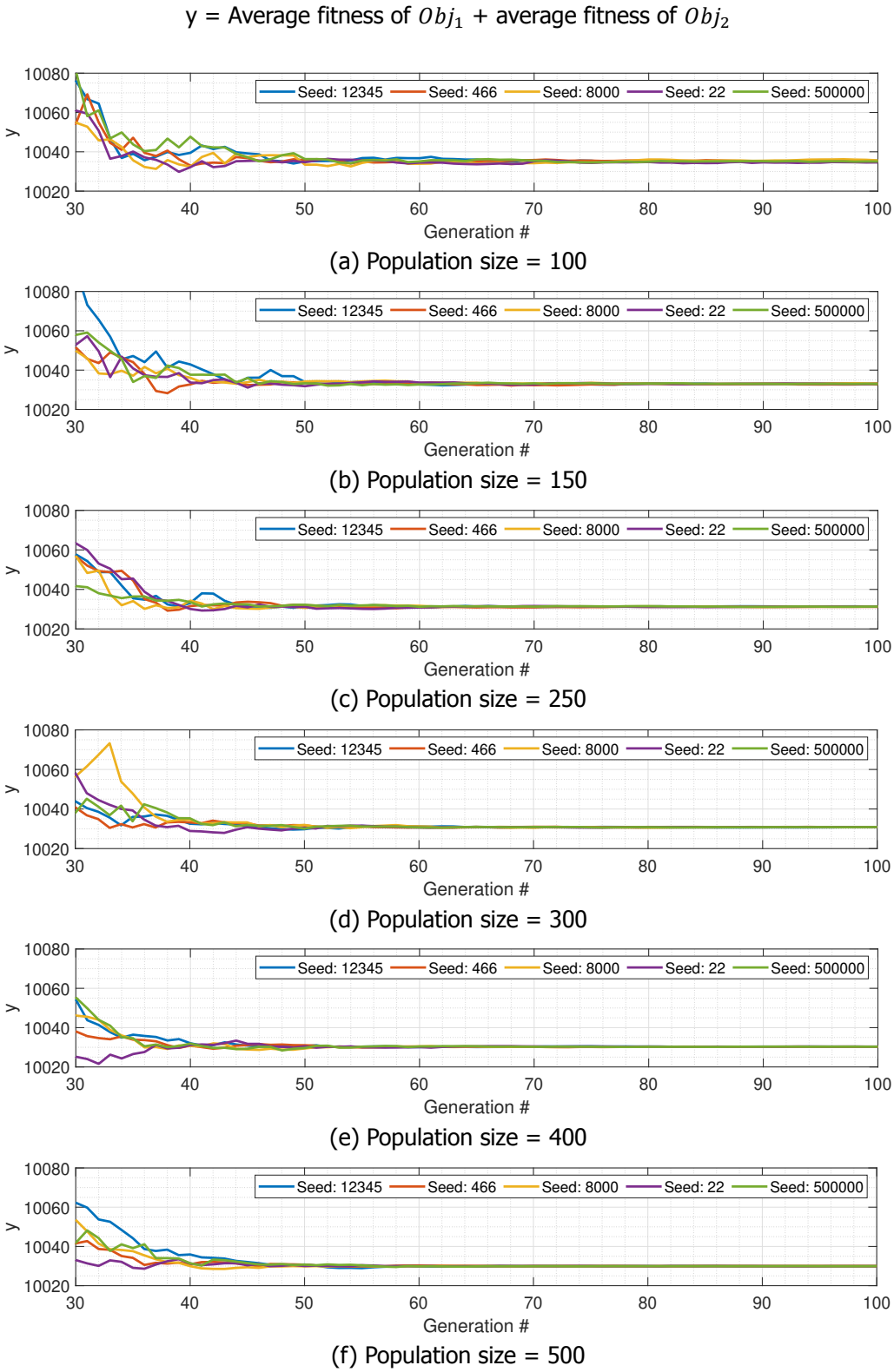

Figure 6.11: Effect of the change in the population size on the sum of averages of the objective I and objective II fitness values. The Earth-to-Mars ballistic transfer trajectory optimization problem has been solved for the 2014 launch opportunity of TC_2. Six different population sizes are used with the MOEAD/D algorithm having the weighted sum decomposition method and each optimization problem has been solved for five different initializations of the quasi-random numbers generator.

6.3.4. Penalty Function Formulation

As mentioned in Section 3.4, the optimization problems to be solved for various mission scenarios have one or more constraints concerning the trajectory parameters. As described in Section 6.2, violation of such constraints would lead to the addition of extra terms in the computed objective values. The penalty functions given by Equations 6.1 and 6.2 can be termed as a linear formulation as the penalty is linearly proportional to the deviation from the constraining value.

In order to quickly eliminate the trajectory solutions which do not meet the imposed constraints, another formulation can be used for the penalty functions as given by Equations 6.4 and 6.5. Here, the penalty values are also quadratically proportional to the deviation from the constraining value.

$$\begin{aligned}\text{Penalty for violation of } C_1 \text{ constraint} = {} & W_1 * (\Delta\theta - 180^\circ) \\ & + W_3 * (\Delta\theta - 180^\circ)^2, \text{ if } \Delta\theta > 180^\circ\end{aligned} \tag{6.4}$$

$$\begin{aligned}\text{Penalty for violation of } C_2 \text{ constraint} = {} & W_2 \times \text{ abs(TOF} - 180) \\ & + W_4 \times \text{ abs(TOF} - 180)^2, \text{ if 2014 launch opportunity} \\ = {} & W_2 \times \text{ abs(TOF} - 181) \\ & + W_4 \times \text{ abs(TOF} - 181)^2, \text{ if 2016 launch opportunity}\end{aligned} \tag{6.5}$$

Here W_1 to W_4 are the weighing factors that scale the deviations of the different trajectory parameters ($\Delta\theta$, TOF) from their constraining values (180°, 180/181 days) while adding them to the corresponding penalty functions. Such penalty functions are then added to the objectives, as shown before in Equation 6.3. The choice of specific values for the weighing factors defines a particular formulation for the penalty function. Six such formulations have been studied during this phase of the optimization tuning procedure and they are marked with identifiers S_1 to S_6. The values of the weighing factors for these formulations are given in Table 6.3.

Weighing Factor	S_1	S_2	S_3	S_4	S_5	S_6
W_1	$\frac{20000}{180}$	$\frac{20000}{180}$	$\frac{2000}{180}$	$\frac{200}{180}$	$\frac{20000}{180}$	$\frac{20000}{180}$
W_2	1000	1000	10	1	1000	1000
W_3	0	$\frac{2000}{180}$	$\frac{20000}{180}$	$\frac{200000}{180}$	$\frac{200000}{180}$	$\frac{20000}{180}$
W_4	0	10	1000	10000	10000	1000

Table 6.3: Values of the weighing factors for six different formulations of the penalty function. A set of values for the weighing factors (W_1 to W_4) defines a formulation (S_1 to S_6) of the penalty function.

As seen in Table 6.3, S_1 is a linear formulation of the penalty function and has been used during earlier phases of the optimization tuning. The other five formulations - S_2 to S_6 - are quadratic formulations introduced to test the hypothesis regarding the elimination of solutions violating constraints. The effect of different formulations on the sum of the average fitness value of objective I and the average fitness value of objective II, with the progression of the optimization process is shown in Figure 6.12. As seen in this figure, the formulation S_3 performs better compared to other formulations as all five values of the random seed number lead to quicker convergence.

Quicker convergence with this particular formulation implies that the computational effort can be reduced to reach the same accuracy level. This is confirmed by checking the number of generations required with each formulation to reach a converged state in the optimization process and the sum of average fitness values for the objectives over the population of such a converged generation. Results for this analysis are shown in Figure 6.13. It can be observed that with the S_3 formulation, often the least number of generations are required to reach the converged state. Moreover, the sum of the average fitness values for the objectives over the population of the converged generation is smaller for

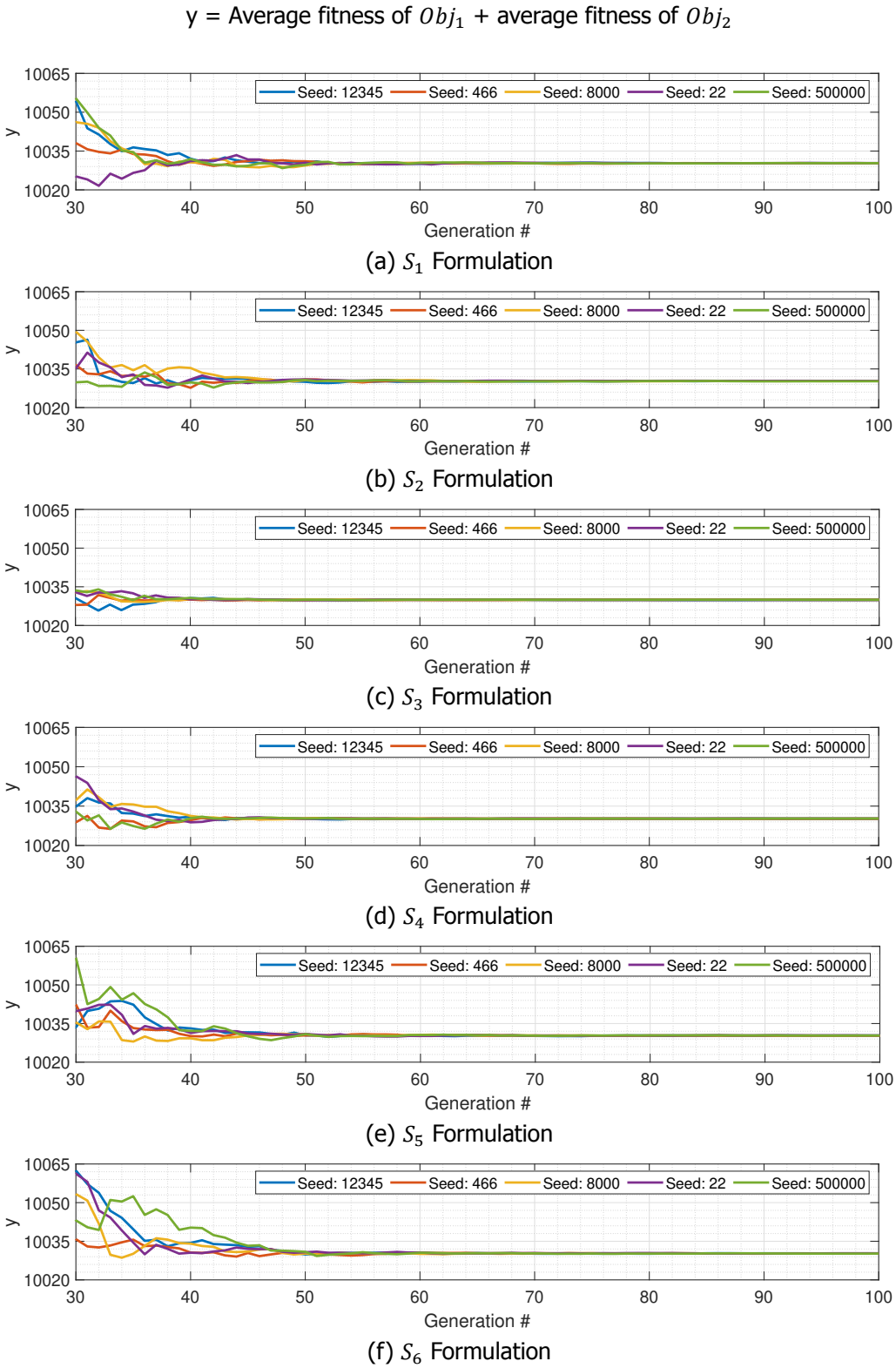

Figure 6.12: Effect of the change in the formulation of penalty function on the sum of averages of the objective I and objective II fitness values. The Earth-to-Mars ballistic transfer trajectory optimization problem has been solved for the 2014 launch opportunity of TC_2. Six different formulations - S_1 to S_6 - each defined by a set of weighting factor values are used with the MOEAD/D algorithm having the weighted sum decomposition method. Each optimization problem has been solved for five different initializations of the quasi-random numbers generator.

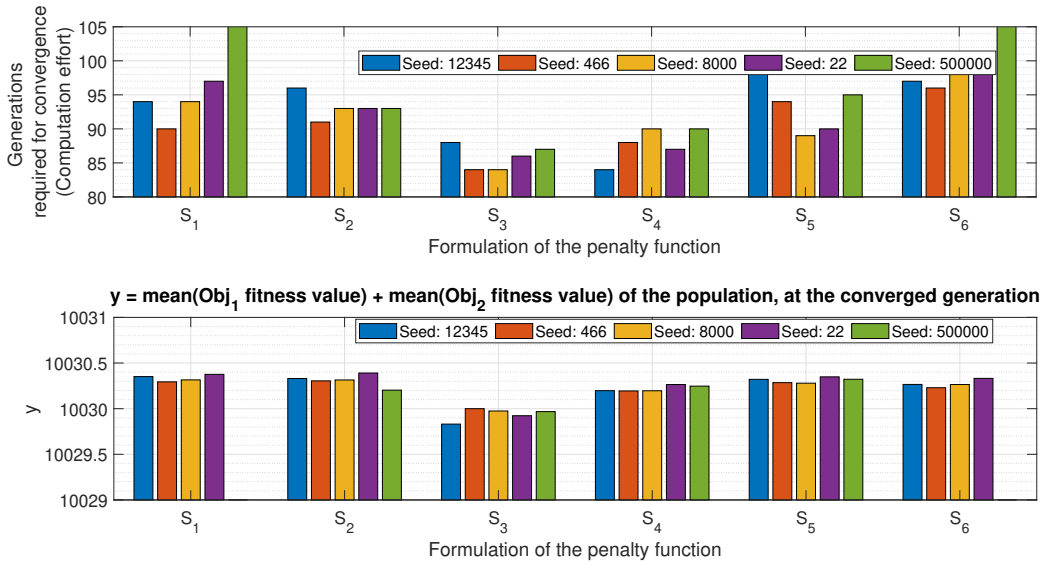

Figure 6.13: Effect of change in the formulation of penalty function on the computational effort and total average fitness value of the converged generation. Dynamic convergence based on the sum of the average fitness value of objective I and the average fitness value of objective II is utilized. Results for parameter y are not shown when more than 100 generations are required to reach a converged solution set.

S_3 formulation compared to that associated with any other formulation. Based on these results, the formulation S_3 appears to outperform all others. Before choosing this penalty function formulation for the thesis work, some additional checks have been made as shown in Figures 6.14 and 6.15.

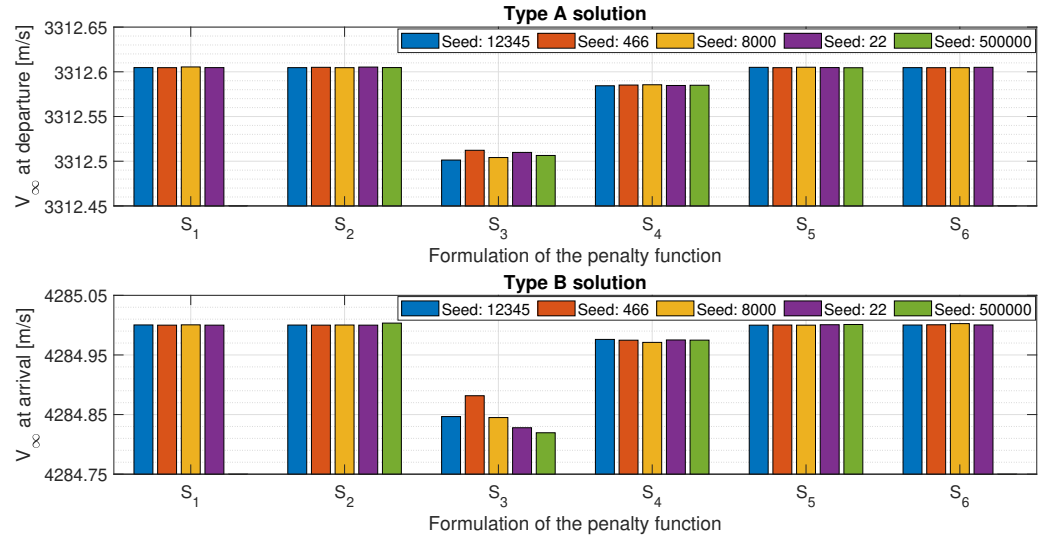

Figure 6.14: Effect of change in the formulation of penalty function on the excess velocity values of the Type A and Type B solutions. Convergence criterion based on the sum of the average fitness value of objective I and the average fitness value of objective II is utilized. Results are not analyzed when more than 100 generations are required to reach a converged solution set.

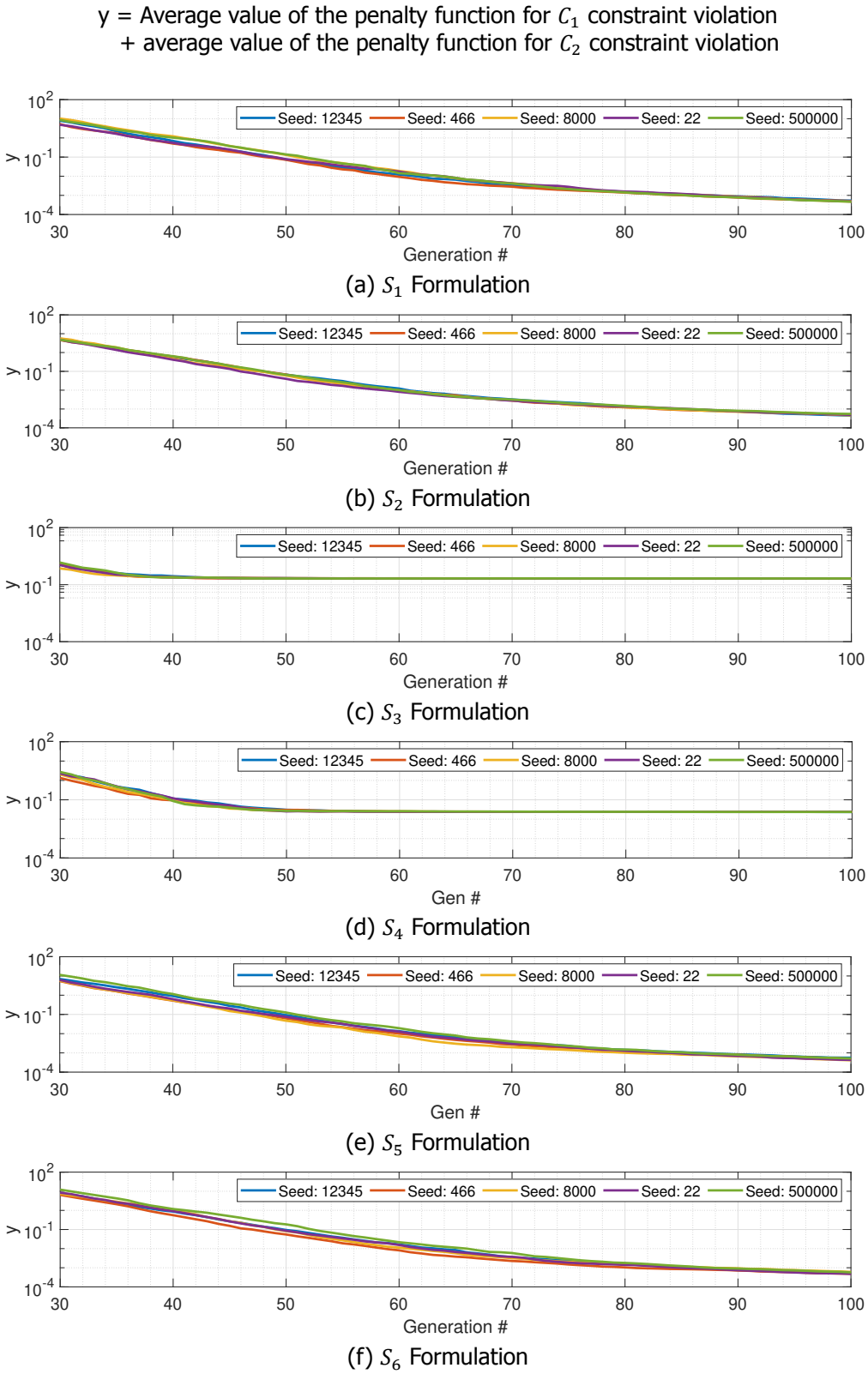

Figure 6.15: Effect of the change in the formulation of penalty function on the average value of the penalty function. The Earth-to-Mars ballistic transfer trajectory optimization problem has been solved for the 2014 launch opportunity of TC_2. Six different formulations - S_1 to S_6 - each defined by a set of weighting factor values are used with the MOEAD/D algorithm having the weighted sum decomposition method. Each optimization problem has been solved for five different initializations of the quasi-random numbers generator.

From the solution set obtained with the converged generation of the multi-objective optimization process, two solution types have been identified viz. type A solution and type B solution. These solutions respectively represent the best fitness values for objective I and objective II. For the optimization problem used, the best fitness values for these objectives indicate that the solutions correspond to minimum V_∞ at departure and minimum V_∞ at arrival, provided that the value of the penalty function reduces to zero (Equation 6.3).

As seen in Figure 6.14, formulation S_3 leads to type A and type B solutions which are marginally better compared to the similar solutions obtained with other formulations. In other words, formulation S_3 produces more optimum extreme ends for the Pareto front than others by the time convergence is detected during the optimization process.

Figure 6.15 shows how the sum of average penalty function values for the C_1 constraint violation and average penalty function value for the C_2 constraint violation changes with the progression of optimization process. Except for the formulation S_4, all other formulations reduce this value to a smaller order of magnitude than the formulation S_3. However, as seen in Figure 6.1, the values of the objective functions have an order of magnitude (3) or (4) i.e. in thousands. Therefore, residual penalty function values having an order of magnitude (-1) can be accepted for the formulation S_3, given it has other considerable advantages discussed so far in this section.

With this choice of the S_3 formulation, the phase of optimization tuning undertaken for the optimization problems of this thesis was completed. It should be noted that more extensive and rigorous analysis for determining the settings for the optimization process can be performed but it might not affect the results presented in this research by a large margin. Due to time constraints, analyses performed so far have been deemed sufficient and results of this analysis are summarized in the next section of this chapter.

6.3.5. Selected Optimization Parameters

In this section, the results of the optimization tuning phase are summarized. This section can be used for quick reference to the values of optimization parameters used in the thesis work.

- **Number of generations(i)**
  Maximum number of generations(i_{max}) = 600
  Minimum number of generations(i_{min}) = 30
  Minimum number of generations to be executed, even after detecting the convergence(i_{buffer}) = 50
- **Convergence criterion**
  Parameter used to detect the convergence (y):

  y = Average fitness value of the objective I + average fitness value of the objective II

  Check for convergence if $i > i_{min}$
  - Stop the optimization process after i generations if
    - $i \geq i_{max}$
      OR
    - $i > (i_{min} + i_{buffer})$ and
    - |Value of y for (i)th generation - Value of y for $(i-1)$th generation| ≤ 1.0
- **Optimization algorithm:** MOEA/D with the weighted decomposition method
- **Population size:** 400
- **Penalty function formulation:** S_3 - quadratic formulation with $W_3 = 10 \times W_1$ and $W_4 = 100 \times W_2$

In the next chapter, results obtained by solving the optimization problems for the thesis work using the above settings for the optimization parameters will be presented.

7

Results

Based on the methodology described in Chapters 4, 5 and 6 for solving the trajectory optimization problems under consideration, solution sets of a number of relevant trajectory optimization problems for the transfer and abort mission scenarios are obtained. Out of these solution sets, a number of trajectory solutions are selected and compared with other solutions of that particular mission scenario. These results are presented and discussed in this chapter to answer the research questions of this thesis work.

Results obtained for various ballistic transfer trajectory solutions are presented in Section 7.1. Trajectory solutions, when the abort of the mission occurs during the nominal Earth-to-Mars transfer, are presented in the subsequent section. Section 7.3 includes the results for abort trajectories when the mission is aborted during the nominal Mars surface stay period. All the trajectory solutions obtained in this thesis work are then compared with each other in Section 7.4.

7.1. Transfer Trajectories: *MS-1* and *MS-2*

In this thesis work, two mission scenarios viz. *MS-1* and *MS-2* have been investigated to find optimum transfer trajectory solutions for a reconnaissance human Mars mission (Table 3.3). These two mission scenarios use ballistic transfer trajectories (trajectories without any DSM) for outbound (Earth-to-Mars) and inbound (Mars-to-Earth) legs of the mission but they differ in the choice of the parking orbit around Mars. A solution set, in the form of a Pareto front of the two objectives of the problem, is obtained for each of these mission scenarios and presented in Section 7.1.1. From this solution set, two particular solutions are selected which represent two transfer trajectory pairs (Earth-to-Mars and Mars-to-Earth) having minimum total TOF and minimum total ΔV requirement. These selected solutions are discussed in Section 7.1.2.

7.1.1. Solution Sets

Pareto fronts of the solutions for the optimization problems of mission scenarios *MS-1* and *MS-2* are presented in Figures 7.1 and 7.2. As mentioned earlier, five different values of the random seed number are used to change the initialization of the quasi-random numbers generator of the optimization algorithm and solutions obtained are plotted together to check the robustness of the solution set. It has been observed that the objective values of the solutions are in agreement when the population of the evolutionary optimization algorithm is initialized differently.

As expected, an increase in the total TOF for the interplanetary transfer results in decreasing values of total ΔV required for the mission. Thus, if potential problems with a prolonged duration of human interplanetary spaceflight are solved, the reduction of about 1850 m/s (at least) in total ΔV requirement is possible, which will lead to a considerable reduction in IMLEO. Moreover, the comparison of solution sets for *MS-1* and *MS-2*, as shown in Figure 7.3, clearly reveals the advantage of using an elliptical parking orbit around Mars (*MS-2*) instead of a circular parking orbit (*MS-1*). The total ΔV of the mission can be reduced by about 2370 m/s if the interplanetary transfer vehicle is captured into

and departed from an elliptical parking orbit around Mars.

The TOF of the outbound leg and the inbound leg of the mission are constrained to have a value between 180 days and 270 days. Therefore, the total minimum possible TOF is 360 days and solutions are obtained for both *MS-1* and *MS-2* corresponding to this total TOF value. These solutions are marked with identifiers A_N^c and A_N^e respectively. The other ends of the Pareto fronts for the two mission scenarios represent trajectory solutions which have minimum total ΔV values. These solutions are marked with identifiers B_N^c and B_N^e respectively. These selected solutions for transfer trajectories are listed in Table 7.1 and also marked in Figures 7.1 and 7.2.

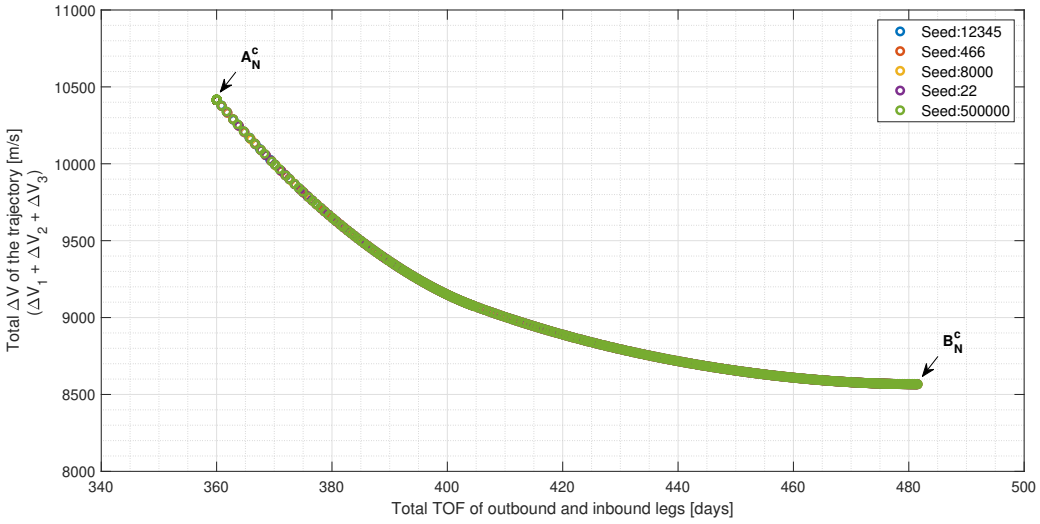

Figure 7.1: Solution set for the ballistic transfer trajectory solutions with a circular parking orbit around Mars (*MS-1*).

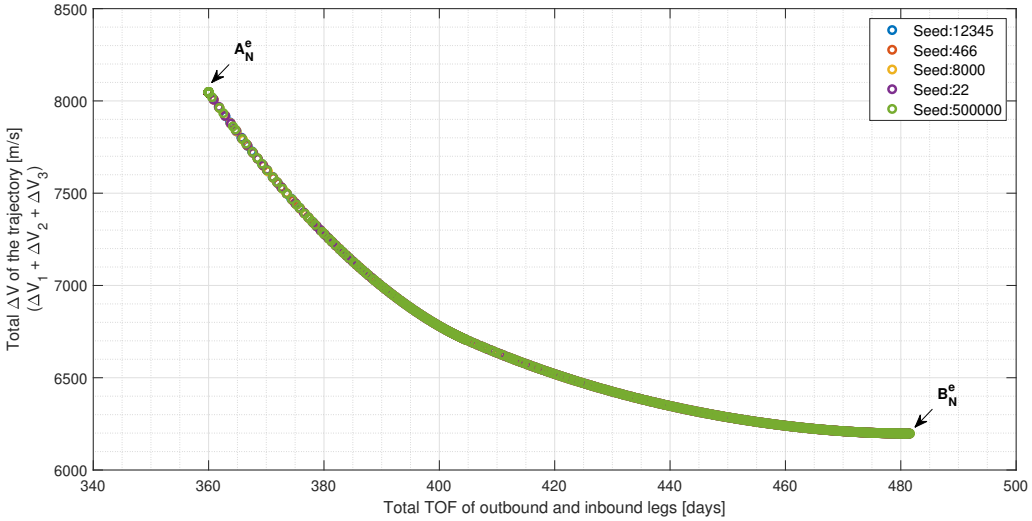

Figure 7.2: Solution set for the ballistic transfer trajectory solutions with an elliptical parking orbit around Mars (*MS-2*).

It should be noted that unlike solutions A_N^c and A_N^e, solutions B_N^c and B_N^e do not lie on the boundaries of the constrained design space. Observation of the solution sets implies the possibility that a further increase of the total TOF might lead to solutions with (slightly) smaller total ΔV requirement. Such points should be present on the Pareto front of objective values but the optimization process misses

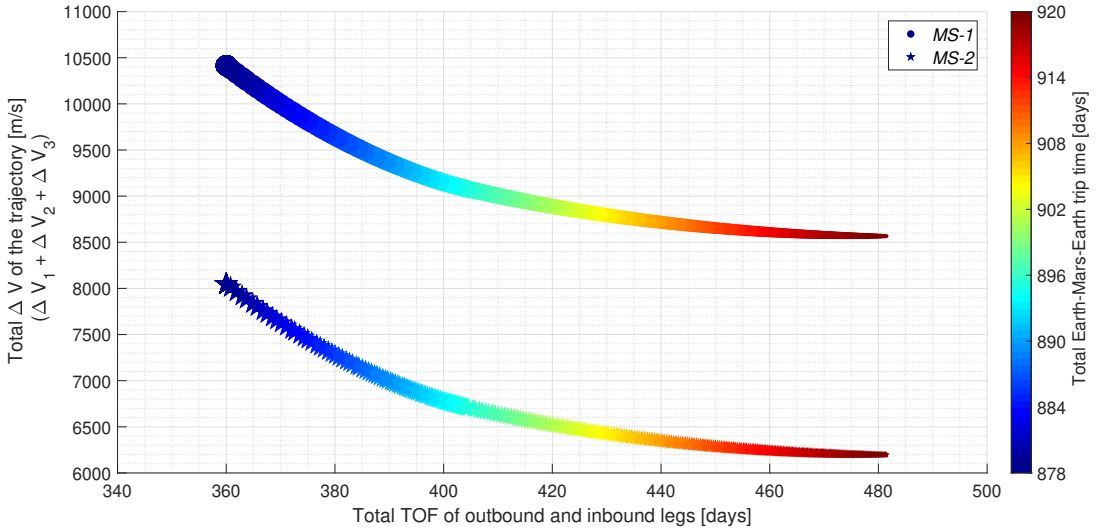

Figure 7.3: Comparison of the solution sets for *MS-1* and *MS-2*, where ballistic transfer trajectory solutions are investigated with a circular and an elliptical parking orbit around Mars respectively. Relative sizes of the marker indicate Mars surface stay period.

Mission Scenario	**Solution Identifier**	**Description**
MS-1	A_N^c	minimum total TOF
	B_N^c	minimum total ΔV of three propulsive maneuvers
MS-2	A_N^e	minimum total TOF
	B_N^e	minimum total ΔV of three propulsive maneuvers

Table 7.1: Selected solutions from the solution sets of the ballistic transfer trajectories (*MS-1* and *MS-2*).

such points[1]. However, the gradient of the Pareto front has reduced towards the minimum total ΔV end, causing a relatively less decrease in the total ΔV with a relatively higher increase in the total TOF. Therefore, even though the solutions B_N^c and B_N^e can be sub-optimal in terms of the total ΔV requirement, they can be considered sufficient to represent the minimum total ΔV solutions.

7.1.2. Selected Solutions

Details of the transfer trajectory solutions listed in Table 7.1 are presented in Tables 7.2 and 7.3. These selected solutions are the best solutions (in terms of total ΔV or total TOF) when the solution sets obtained with all five different values of the random seed number are considered together. In other words, A_N^c is one of the five best solutions (in terms of total TOF) that are obtained with five different values of the random seed number. To reflect upon the robustness of the value of a mission parameter, the associated standard deviation (σ) is computed using the results that are obtained at these five different seed number values. As expected, the trajectories A_N^c and A_N^e have almost the same values for the departure and arrival epochs. Earth-departure ΔVs of these solutions differ[2] only by about 5 m/s. A similar result can be observed when details of the trajectory solutions B_N^c and B_N^e are compared with each other. All four selected transfer trajectory solutions satisfy the constraints on the values of arrival V_∞ at both Earth and Mars.

[1] In this thesis work it has been observed that the optimization process misses a part of the ideal/expected Pareto front as the population is evolved to find optimum solutions to the problem. While the exact reason behind this is unknown, the author suspects that further tuning the optimization algorithm (such that two objectives are equally/proportionally weighed) or changing the optimization algorithm can resolve this issue.

[2] It is not possible to obtain exactly the same values for these mission parameters due to random initialization of the population in a meta-heuristic algorithm, and the resulting different evolution path when the number of generations/iterations are also limited by a convergence criterion.

Mission Scenario	***MS-1***			
Solution	A_N^c	-	B_N^c	-
Parameter	Value	σ	Value	σ
Earth-departure epoch [MJD2000]	10609.25	$3.78 \cdot 10^{-1}$	10590.05	$1.70 \cdot 10^{-2}$
Mars-arrival epoch [MJD2000]	10789.25	$3.78 \cdot 10^{-1}$	10823.90	$1.00 \cdot 10^{-2}$
Mars-departure epoch [MJD2000]	11308.07	$1.01 \cdot 10^{0}$	11262.15	$3.15 \cdot 10^{-2}$
Earth-arrival epoch [MJD2000]	11488.07	$1.01 \cdot 10^{0}$	11509.79	$3.20 \cdot 10^{-2}$
TOF of the outbound leg [days]	180.00	$2.26 \cdot 10^{-5}$	233.86	$1.29 \cdot 10^{-2}$
TOF of the inbound leg [days]	180.00	$1.78 \cdot 10^{-5}$	247.64	$3.68 \cdot 10^{-2}$
Earth-Mars-Earth trip time [days]	878.81	$1.38 \cdot 10^{0}$	919.74	$1.94 \cdot 10^{-2}$
Earth-departure ΔV [m/s]	4360.32	$1.56 \cdot 10^{1}$	3848.67	$2.15 \cdot 10^{-1}$
Mars-capture ΔV [m/s]	3639.94	$1.61 \cdot 10^{1}$	2739.62	$2.14 \cdot 10^{-1}$
Mars-departure ΔV [m/s]	2415.31	$1.47 \cdot 10^{0}$	1978.44	$1.05 \cdot 10^{-3}$
Total ΔV [m/s]	10415.57		8566.74	
V_∞ at Mars-arrival [m/s]	5142.38	$2.20 \cdot 10^{1}$	3816.49	$3.45 \cdot 10^{-1}$
V_∞ at Earth-arrival [m/s]	8350.27	$1.39 \cdot 10^{2}$	5635.35	$2.39 \cdot 10^{0}$

Table 7.2: Details of the selected ballistic transfer trajectory solutions , when parking orbit around Mars is circular (*MS-1*).

Mission Scenario	***MS-2***			
Solution	A_N^e	-	B_N^e	-
Parameter	Value	σ	Value	σ
Earth-departure epoch [MJD2000]	10609.14	$5.85 \cdot 10^{-2}$	10590.05	$1.44 \cdot 10^{-2}$
Mars-arrival epoch [MJD2000]	10789.14	$6.00 \cdot 10^{-2}$	10823.90	$3.00 \cdot 10^{-2}$
Mars-departure epoch [MJD2000]	11309.78	$7.37 \cdot 10^{-1}$	11262.15	$9.01 \cdot 10^{-2}$
Earth-arrival epoch [MJD2000]	11489.78	$7.37 \cdot 10^{-1}$	11509.79	$3.44 \cdot 10^{-2}$
TOF of the outbound leg [days]	180.00	$2.25 \cdot 10^{-5}$	233.86	$1.25 \cdot 10^{-2}$
TOF of the inbound leg [days]	180.00	$1.28 \cdot 10^{-4}$	247.64	$6.10 \cdot 10^{-2}$
Earth-Mars-Earth trip time [days]	880.64	$7.94 \cdot 10^{-1}$	919.74	$2.26 \cdot 10^{-2}$
Earth-departure ΔV [m/s]	4355.42	$2.45 \cdot 10^{0}$	3848.67	$2.95 \cdot 10^{-1}$
Mars-capture ΔV [m/s]	2460.26	$2.46 \cdot 10^{0}$	1555.01	$2.96 \cdot 10^{-1}$
Mars-departure ΔV [m/s]	1232.48	$7.94 \cdot 10^{-1}$	793.83	$1.02 \cdot 10^{-3}$
Total ΔV [m/s]	8048.16		6197.52	
V_∞ at Mars-arrival [m/s]	5149.14	$3.37 \cdot 10^{0}$	3816.49	$4.76 \cdot 10^{-1}$
V_∞ at Earth-arrival [m/s]	8112.61	$1.02 \cdot 10^{2}$	5635.35	$2.57 \cdot 10^{0}$

Table 7.3: Details of the selected ballistic transfer trajectory solutions, when parking orbit around Mars is elliptical (*MS-2*).

Two-dimensional trajectory visualizations for the solutions A_N^c and B_N^c are shown in Figure 7.4 for the analysis in the HECRF. Trajectory visualizations for solutions A_N^e and B_N^e are not shown because the interplanetary transfer trajectories associated with these solutions are almost identical to those with the solutions A_N^c and B_N^c respectively. The trajectory visualizations clearly show that the heliocentric transfer angle associated with the minimum total TOF trajectory solution A_N^c is smaller than the minimum total ΔV trajectory solution B_N^c, for both outbound and inbound legs of the mission.

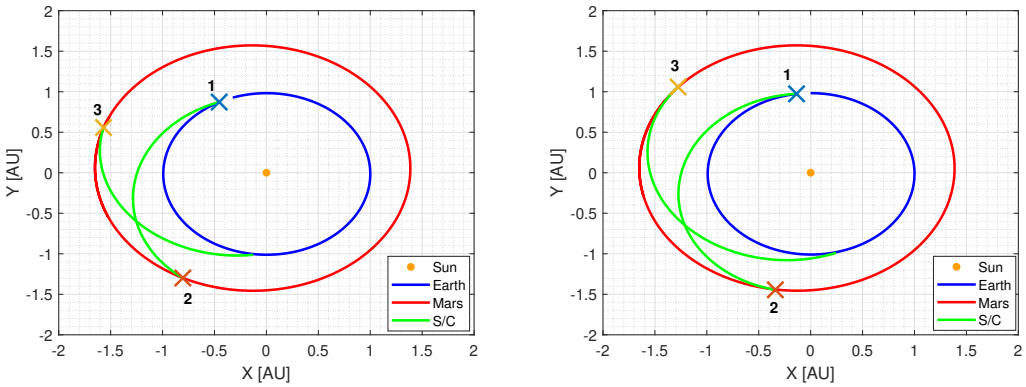

(a) Solution A_N^c (b) Solution B_N^c

Figure 7.4: Visualization for the selected ballistic transfer trajectory solutions, when parking orbit around Mars is circular (*MS-1*). Numbers 1 to 3 represent propulsive maneuvers performed by the spacecraft (S/C) for departure from the parking orbit around Earth (TMI), capture into the parking orbit around Mars and departure from the parking orbit around Mars (TEI), respectively.

Out of these four selected transfer trajectory solutions, solution A_N^c is recommended for a reconnaissance human Mars mission. This solution has the shortest possible TOF for the outbound and inbound legs of the mission, for the given constraints on the design space. A shorter interplanetary transit duration, under nominal (non-abort) mission conditions, implies fewer problems associated with human interplanetary spaceflight.

Even though with the use of an elliptical parking orbit at Mars the total ΔV requirement of the mission can be reduced, designing a mission for insertion into/departure from a circular parking orbit around Mars has an important advantage from a mission abort point of view. Having a higher ΔV capability onboard S/C is likely to allow more abort trajectory options. Thus, the recommended trajectory solution A_N^c, despite having a higher total ΔV requirement than B_N^c, A_N^e and B_N^e, is used for the nominal outbound transfer trajectory while various abort scenarios have been investigated in this thesis work. With this particular transfer trajectory solution, the results obtained for the associated abort trajectories are presented in the subsequent sections.

7.2. Abort Trajectories: *MS-3* and *MS-4*

Two mission scenarios viz. *MS-3* and *MS-4* have been investigated in this thesis work to find Earth-return trajectory options when the mission is aborted during the Earth-to-Mars transfer phase. This investigation is performed when the S/C has already completed 20 or 40 or 60 or 80% of its nominal Earth-to-Mars transfer (outbound leg). With *MS-3*, the S/C continues to travel toward Mars after this abort epoch and performs a swing-by maneuver at Mars before returning to Earth. Such a swing-by can be a powered swing-by maneuver and additionally, the *MS-3* abort trajectory can have two other DSMs after the abort maneuver. On the other hand, the S/C returns directly to Earth with *MS-4* using an abort maneuver and a DSM. In the subsequent sections, solution sets and a few selected solutions for both the mission scenarios are discussed as per the abort fraction that relates to the Earth-departure epoch as mentioned earlier in Table 5.2. Out of the selected solutions, one abort trajectory solution is recommended at each abort fraction. The reader can refer to Section 7.4 for a quick comparison between the selected and recommended solutions at various abort fractions.

7.2.1. Abort Fraction 0.2

The nominal outbound transfer trajectory solution chosen for the abort analysis is A_N^c, which has a TOF of about 180 days. Therefore, at an abort fraction of 0.2, the abort decision is taken about 36 days after the S/C leaves the SOI of Earth.

Solution Set

The Pareto fronts of the solutions for the optimization problems of *MS-3* and *MS-4* are presented in Figures 7.5 and 7.6 respectively.

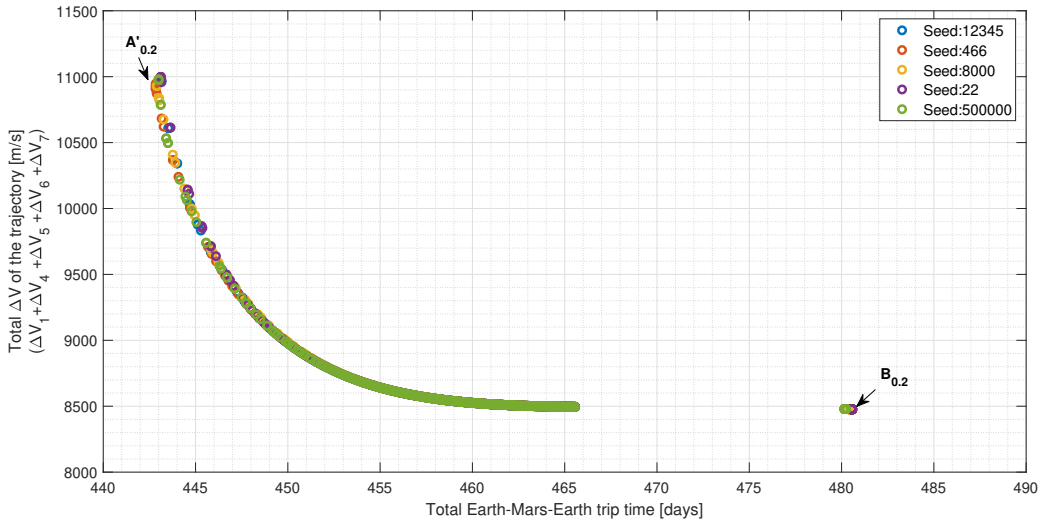

Figure 7.5: Solution set for the propulsive abort trajectories when the abort occurs during the nominal Earth-to-Mars transfer at abort fraction 0.2 and a Mars swing-by is performed (*MS-3*).

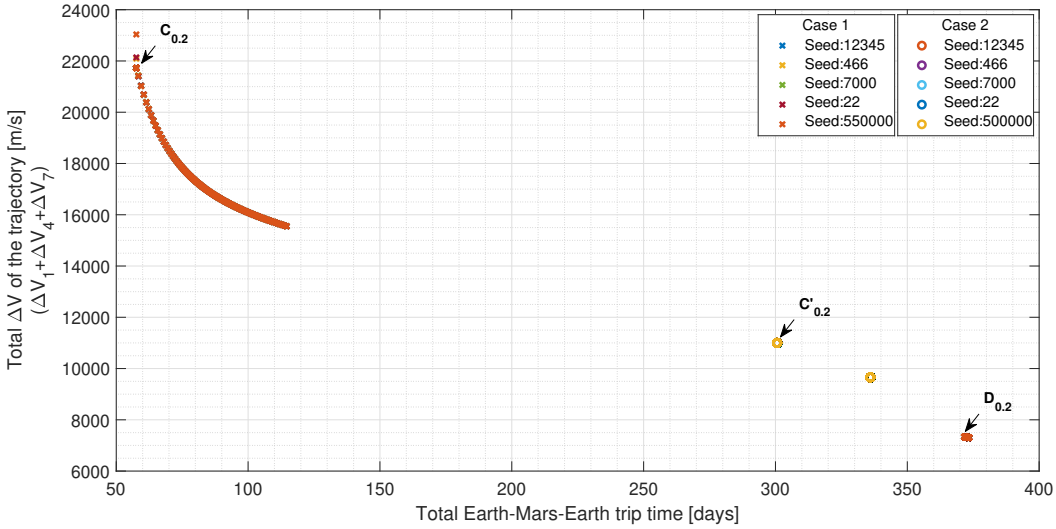

Figure 7.6: Solution set for the propulsive abort trajectories when the abort occurs during the nominal Earth-to-Mars transfer at abort fraction 0.2 and a Mars swing-by is not performed (*MS-4*).

For a number of optimization problems solved in this thesis work, it has been observed that the optimization process subjected to particular design space and applied constraints, failed to retain/identify all the important points of the solution set. To obtain different parts and important points of the solution set despite this problem, a few cases have been solved, each at five different values of the random

seed number[3]. Cases 1 and 2 have been solved for obtaining the solution set depicted in Figure 7.6. The robustness of the solution is reflected through the agreement between the solution sets (or parts of a solution set) obtained with different values for the random seed number.

Two solutions - $A'_{0.2}$ and $B_{0.2}$ - have been selected from the solution set obtained for the *MS-3* optimization problem. Three solutions have been selected from the solution set obtained for the *MS-4* optimization problem viz. $C_{0.2}$, $C'_{0.2}$ and $D_{0.2}$. Table 7.4 lists the most important details of these selected solutions, and their trajectory visualizations are shown in Figure 7.7.

Mission Scenario	**Solution Identifier**	**Description**	**Constraint on total ΔV**
MS-3	$A'_{0.2}$	minimum total TOF (sub-optimal)	≤ 11000 m/s
	$B_{0.2}$	minimum total ΔV of five propulsive maneuvers, including the nominal Earth-departure ΔV (sub-optimal, TOF of inbound leg ≤ 300 days)	-
MS-4	$C_{0.2}$	minimum total TOF	-
	$C'_{0.2}$	minimum total TOF (sub-optimal)	≤ 11000 m/s
	$D_{0.2}$	minimum total ΔV of three propulsive maneuvers, including the nominal Earth-departure ΔV	-

Table 7.4: Selected solutions from the solution sets of the propulsive abort trajectories when the abort occurs during the nominal Earth-to-Mars transfer at abort fraction 0.2 (*MS-3* and *MS-4*).

Selected Solutions

Important trajectory parameters of the five selected abort trajectory solutions are presented in Figure 7.8, while all trajectory parameter values and associated standard deviation can be found in Appendix C. Important trajectory parameters include the arrival excess velocity at Earth (to ensure safe re-entry of the Earth return taxi vehicle), the minimum distance of the trajectory to the Sun and the interplanetary transit duration (both relate with the radiation protection, thermal system, life-support system, etc. requirements of the crewed S/C). It can be observed that all the selected solutions meet the constraint on the arrival excess velocity at Earth.

While trajectory solutions involving a Mars swing-by (i.e $A'_{0.2}$ and $B_{0.2}$) have a moderate total ΔV requirement, the associated interplanetary transit durations for these trajectories are higher than the nominal mission. If there does not exist any scientific benefit of pursuing a Mars flyby mission when it is to be aborted after about 36 days into the Earth-to-Mars transfer, these trajectory solutions do not present any advantage compared to other solutions. Moreover, the minimum distance to the Sun with both trajectory solutions is smaller than the perihelion distance of Venus, which might lead to challenging requirements for the radiation protection and thermal management subsystems of the crewed S/C.

From Figures 7.6 and 7.7, it is clear that solution $C_{0.2}$ is the fastest abort trajectory option that has been computed. Although with this solution, the crewed S/C can return to Earth in about 58 days, it requires a ΔV as high as about 21700 m/s. Considering the infeasibility of providing such a high ΔV capability to the S/C, this trajectory solution is not recommended. On the other hand, solution $D_{0.2}$ has the smallest ΔV requirement (about 7309 m/s) compared to the other solutions. However, this ΔV requirement is smaller than what the crewed S/C is capable of providing for the nominal mission (about 10415 m/s). Therefore, despite its interplanetary transit duration being close to the nominal mission, the solution $D_{0.2}$ is not recommended.

The solution $C'_{0.2}$ is recommended for this abort fraction because the total mission duration (total trip time) is reduced by about 578 days with this abort trajectory solution when compared to that of the nominal mission and this is a significant benefit. The interplanetary transit duration of $C'_{0.2}$ is smaller than that of the transfer trajectory solution A^c_N by about 60 days at the total ΔV cost of 11000 m/s,

[3]Refer to Appendix B for more details about all such optimization problem cases of this work.

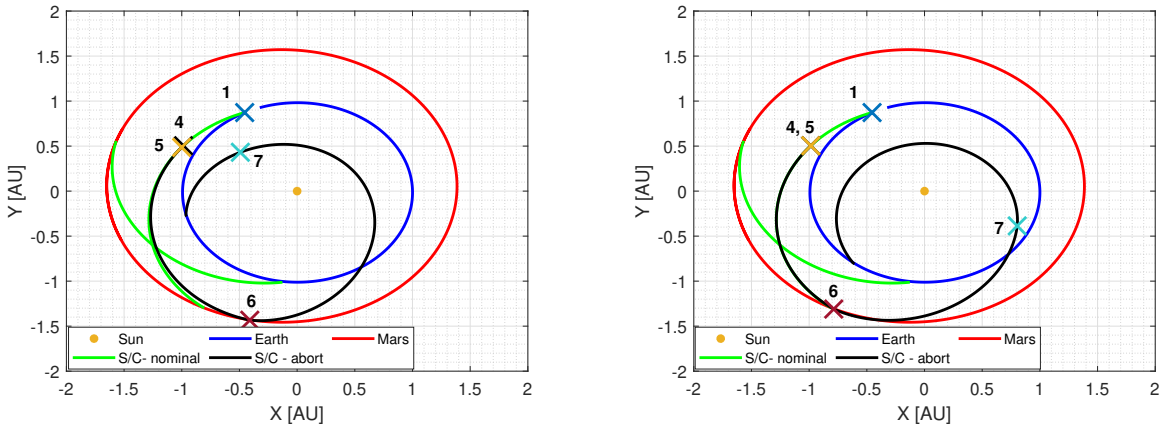

(a) Solution $A'_{0.2}$

(b) Solution $B_{0.2}$

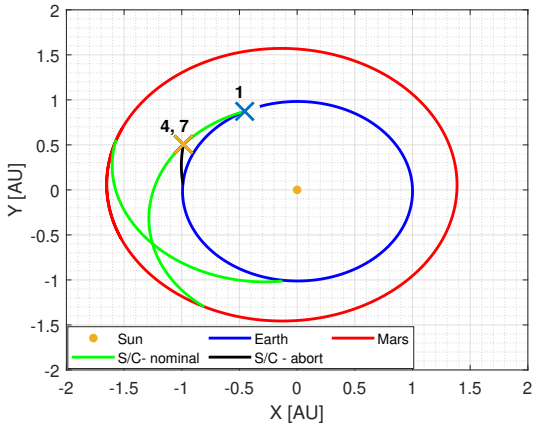

(c) Solution $C_{0.2}$

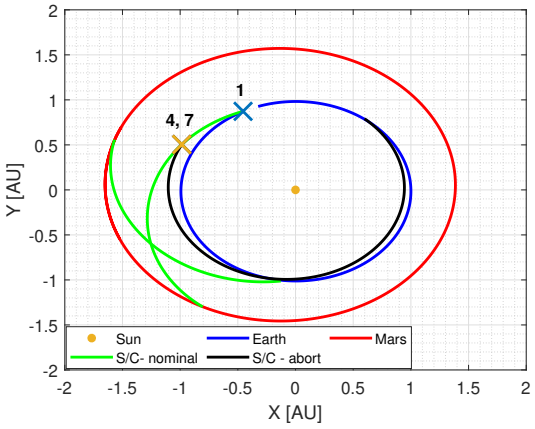

(d) Solution $C'_{0.2}$

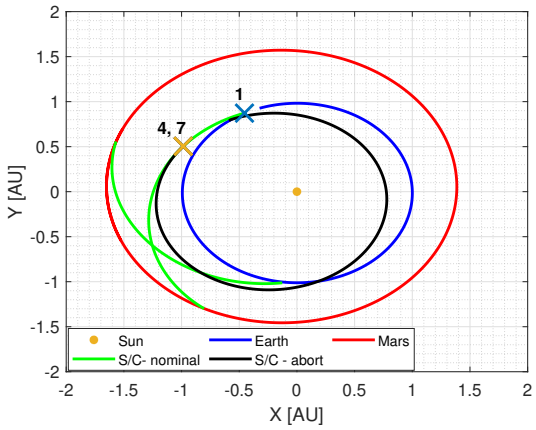

(e) Solution $D_{0.2}$

Figure 7.7: Visualizations for the selected propulsive abort trajectory solutions, when the abort occurs during the nominal Earth-to-Mars transfer (*MS-3* and *MS-4*), at abort fraction 0.2. Numbers 1, 4 to 7 represent propulsive maneuvers performed by the S/C for departure from the parking orbit around Earth, aborting from the nominal Earth-to-Mars transfer trajectory, a DSM of the outbound leg after the abort, a powered Mars swing-by and a DSM of the inbound leg, respectively.

which is only about 6% higher than that of the latter. Moreover, the Earth arrival excess velocity is the smallest for this particular solution compared to the other selected solutions.

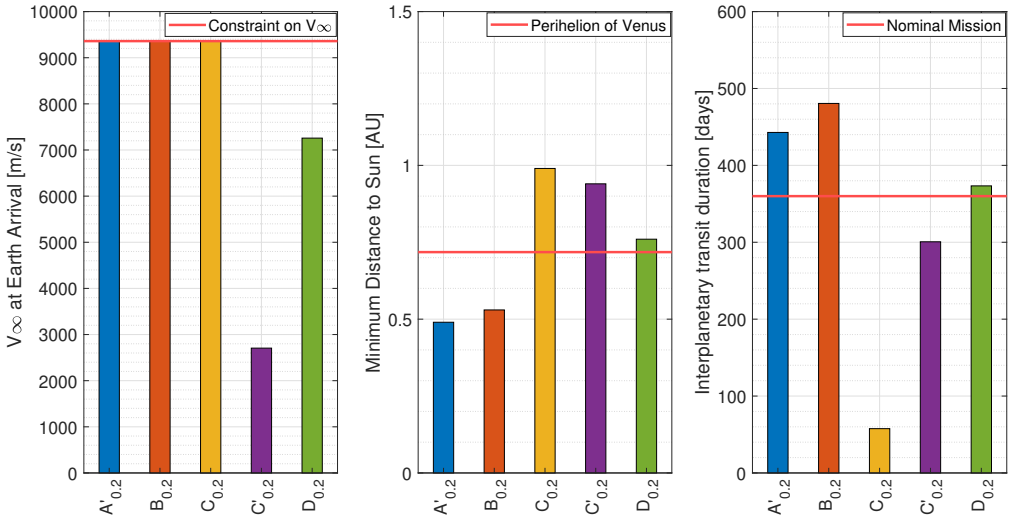

Figure 7.8: Important parameters for the selected propulsive abort trajectory solutions when the abort occurs during the nominal Earth-to-Mars transfer (*MS-3* and *MS-4*), at abort fraction 0.2.

7.2.2. Abort Fraction 0.4

At an abort fraction of 0.4, the crewed S/C has traveled for 72 days toward Mars after leaving the SOI of Earth.

Solution Set

The Pareto fronts of the solutions for the optimization problems of *MS-3* and *MS-4* are shown in Figures 7.9 and 7.10 respectively. For the latter, two cases of the optimization problem (viz. Case 3 and Case 4) have been solved to obtain important parts and solutions of the Pareto front. The agreement between results obtained with different values for the random seed number indicates that the solution sets obtained are robust.

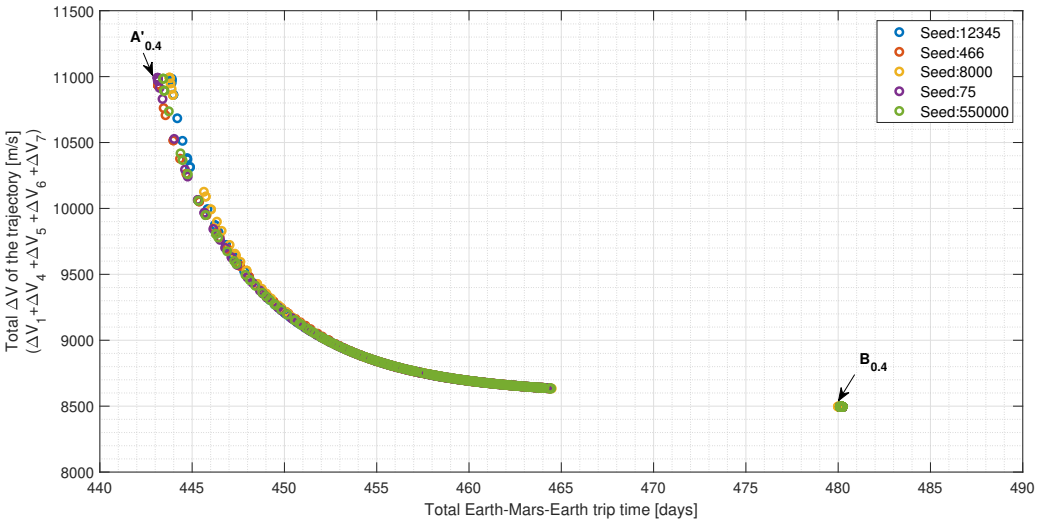

Figure 7.9: Solution set for the propulsive abort trajectories when the abort occurs during the nominal Earth-to-Mars transfer at abort fraction 0.4 and a Mars swing-by is performed (*MS-3*).

Similar to the results at abort fraction of 0.2, two solutions - $A'_{0.4}$ and $B_{0.4}$ - have been selected from the solution set obtained for the *MS-3* optimization problem. Three solutions have been selected from

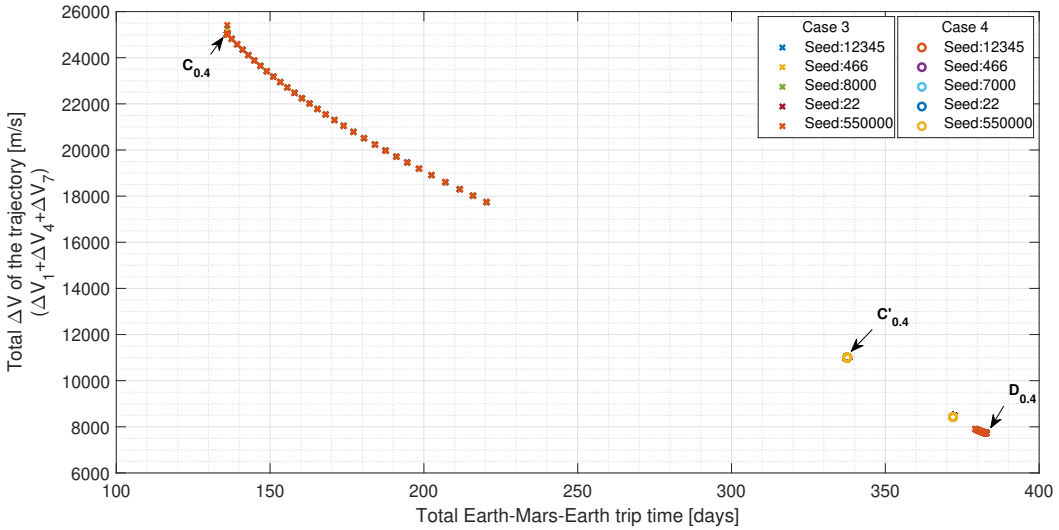

Figure 7.10: Solution set for the propulsive abort trajectories when the abort occurs during the nominal Earth-to-Mars transfer at abort fraction 0.4 and a Mars swing-by is not performed (*MS-4*).

the solution set obtained for the *MS-4* optimization problem viz. $C_{0.4}$, $C'_{0.4}$ and $D_{0.4}$. Table 7.5 lists the most important details for these selected solutions and their trajectory visualizations are shown in Figure 7.11.

Mission Scenario	**Solution Identifier**	**Description**	**Constraint on total ΔV**
MS-3	$A'_{0.4}$	minimum total TOF (sub-optimal)	≤ 11000 m/s
	$B_{0.4}$	minimum total ΔV of five propulsive maneuvers, including the nominal Earth-departure ΔV (sub-optimal, TOF of inbound leg ≤ 300 days)	-
MS-4	$C_{0.4}$	minimum total TOF	-
	$C'_{0.4}$	minimum total TOF (sub-optimal)	≤ 11000 m/s
	$D_{0.4}$	minimum total ΔV of three propulsive maneuvers, including the nominal Earth-departure ΔV	-

Table 7.5: Selected solutions from the solution sets of the propulsive abort trajectories when the abort occurs during the nominal Earth-to-Mars transfer at abort fraction 0.4 (*MS-3* and *MS-4*).

Selected Solutions

Important trajectory parameters for the five selected solutions are presented in Figure 7.12 while all trajectory parameter values and associated standard deviations can be found in Appendix C. Similar to the selected Earth-return trajectories when the abort fraction is 0.2, all the current solutions also satisfy the constraint on arrival excess velocity at Earth.

For the reasons similar to not recommending the trajectory solutions $A'_{0.2}$ and $B_{0.2}$, the solutions $A'_{0.4}$ and $B_{0.4}$ are not recommended for this abort fraction. From Figures 7.10 and 7.11, it can be concluded that the fastest Earth-return trajectory solution obtained is $C_{0.4}$. A total mission duration or an interplanetary transit time of about 136 days for this particular solution comes at the cost of ΔV as high as about 25000 m/s. On the other hand, the solution $D_{0.4}$ does not utilize the complete ΔV capability of the S/C, similar to the solution $D_{0.2}$. It has an interplanetary transit duration higher than the nominal mission (by about 23 days). Due to these reasons, the solutions $C_{0.4}$ and $D_{0.4}$ are not recommended.

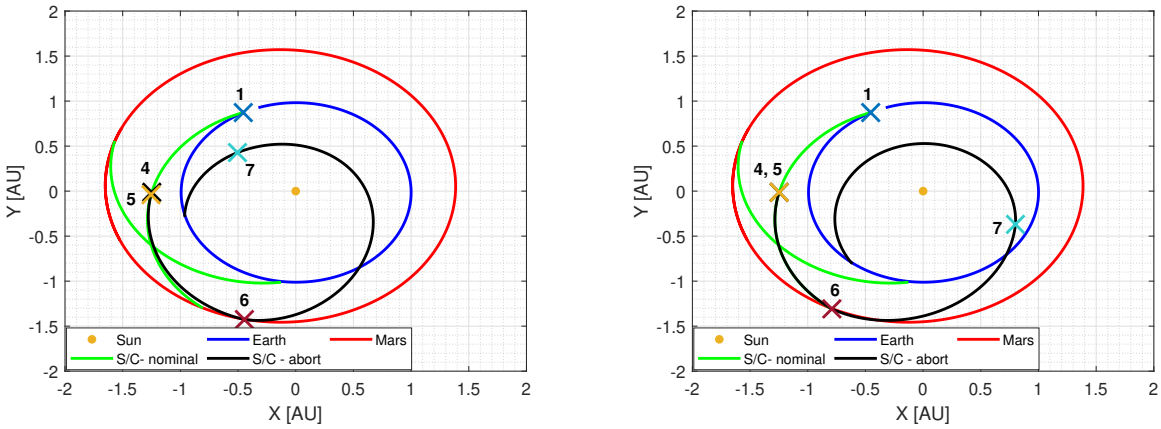

(a) Solution $A'_{0.4}$

(b) Solution $B_{0.4}$

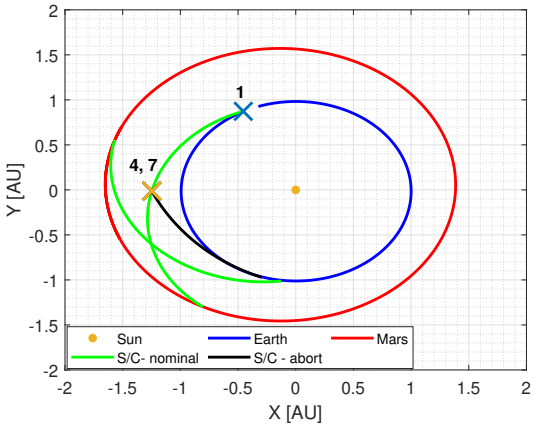

(c) Solution $C_{0.4}$

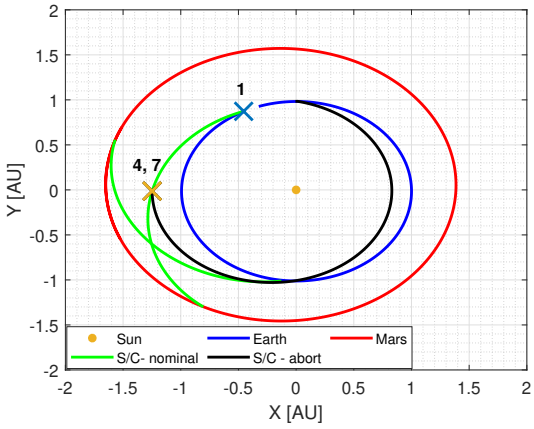

(d) Solution $C'_{0.4}$

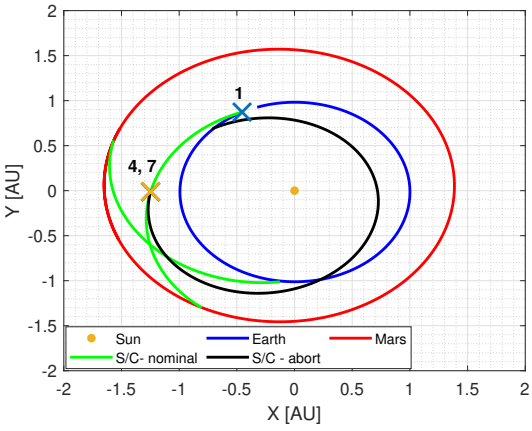

(e) Solution $D_{0.4}$

Figure 7.11: Visualizations for the selected propulsive abort trajectory solutions, when the abort occurs during the nominal Earth-to-Mars transfer (*MS-3* and *MS-4*), at abort fraction 0.4. Numbers 1, 4 to 7 represent propulsive maneuvers performed by the S/C for departure from the parking orbit around Earth, aborting from the nominal Earth-to-Mars transfer trajectory, a DSM of the outbound leg after abort, a powered Mars swing-by and a DSM of the inbound leg, respectively.

The solution with the smallest excess velocity at Earth-arrival - $C'_{0.4}$ - is recommended for this abort fraction during the nominal Earth-to-Mars transfer. Similar to the solution $C'_{0.2}$, it offers a significant (about 541 days) reduction in the total mission duration compared to the nominal mission. The interplanetary transit duration for this solution is smaller than that of the nominal mission by about 22 days

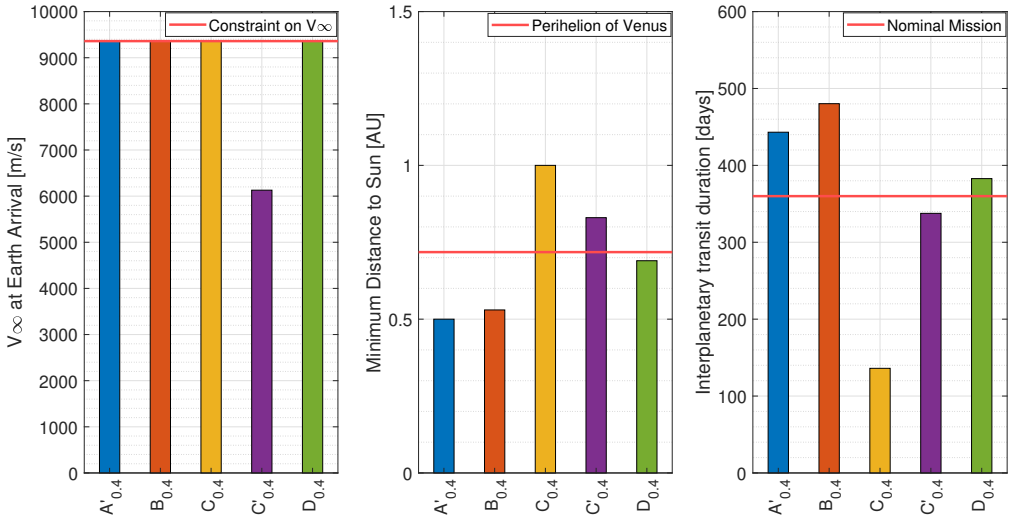

Figure 7.12: Important parameters for the selected propulsive abort trajectory solutions when the abort occurs during the nominal Earth-to-Mars transfer (*MS-3* and *MS-4*), at abort fraction 0.4.

while the total ΔV requirement is only 6% higher than that of the nominal mission.

7.2.3. Abort Fraction 0.6

At an abort fraction of 0.6, the crewed S/C has traveled for more than half of its nominal TOF of the Earth-to-Mars transfer leg. It is interesting to investigate whether performing a Mars swing-by is more advantageous now than directly returning to Earth at this abort fraction.

Solution Set

The Pareto fronts of the solutions for the optimization problems of *MS-3* and *MS-4* are shown in Figures 7.13 and 7.14 respectively. For the latter, two cases of the optimization problem (viz. Case 5 and Case 6) have been solved to obtain important parts and solutions of the Pareto front.

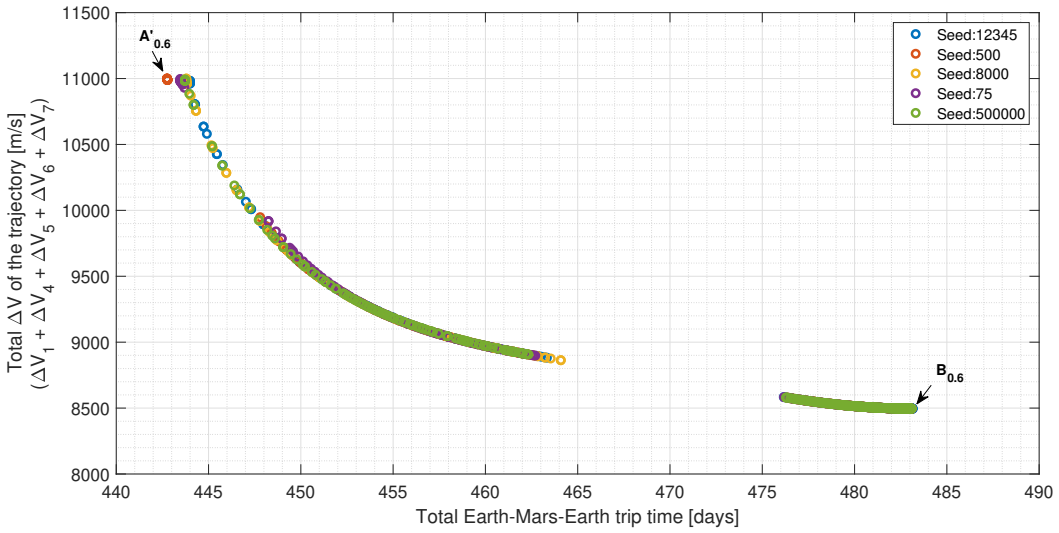

Figure 7.13: Solution set for the propulsive abort trajectories when the abort occurs during the nominal Earth-to-Mars transfer at abort fraction 0.6 and a Mars swing-by is performed (*MS-3*).

Apart from the optimum Earth-Mars-Earth trip time solutions from the *MS-4* solution set, there is a strong agreement between the results obtained with different values for the random seed number.

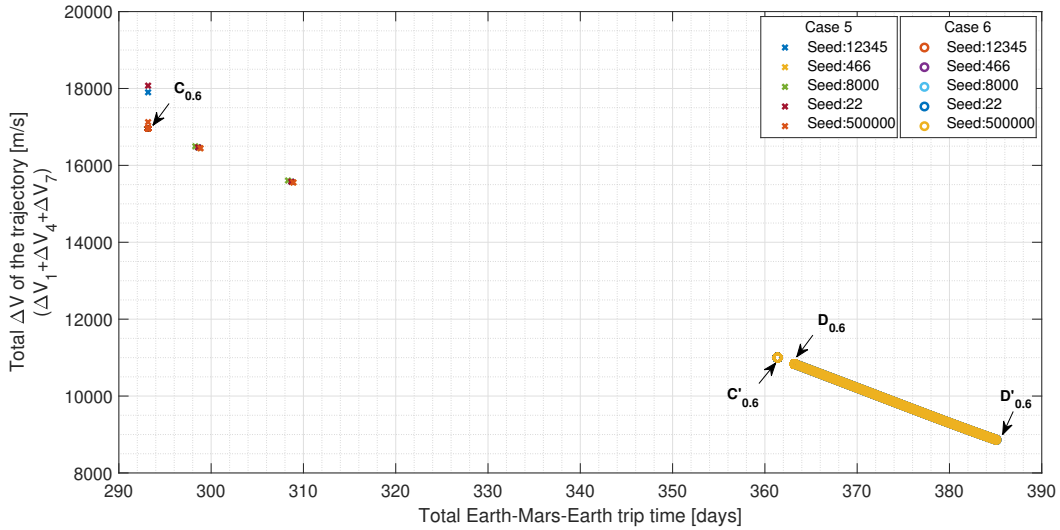

Figure 7.14: Solution set for the propulsive abort trajectories when the abort occurs during the nominal Earth-to-Mars transfer at abort fraction 0.6 and a Mars swing-by is not performed (*MS-4*).

This reflects the robustness of the solutions for the most part of the solution set. Two solutions - $A'_{0.6}$ and $B_{0.6}$ - have been selected from the solution set obtained for the *MS-3* optimization problem. Four solutions have been selected from the solution set obtained for the *MS-4* optimization problem viz. $C_{0.6}$, $C'_{0.6}$, $D_{0.6}$ and $D'_{0.6}$. Table 7.6 lists the most important details for these selected solutions and as usual, their trajectory visualizations are shown in Figure 7.15.

Mission Scenario	**Solution Identifier**	**Description**	**Constraint on total ΔV**
MS-3	$A'_{0.6}$	minimum total TOF (sub-optimal)	≤ 11000 m/s
	$B_{0.6}$	minimum total ΔV of five propulsive maneuvers, including the nominal Earth-departure ΔV	-
MS-4	$C_{0.6}$	minimum total TOF	-
	$C'_{0.6}$	minimum total TOF (sub-optimal)	≤ 11000 m/s
	$D_{0.6}$	minimum total ΔV of three propulsive maneuvers, including the nominal Earth-departure ΔV (sub-optimal)	-
	$D'_{0.6}$	minimum total ΔV of three propulsive maneuvers, including the nominal Earth-departure ΔV	-

Table 7.6: Selected solutions from the solution sets of the propulsive abort trajectories when the abort occurs during the nominal Earth-to-Mars transfer at an abort fraction 0.6 (*MS-3* and *MS-4*).

Selected Solutions

Important trajectory parameters for the six selected solutions are presented in Figure 7.16 while all trajectory parameter values and associated standard deviations can be found in Appendix C. All these solutions except $D'_{0.6}$ satisfy the constraint on arrival excess velocity at Earth. Compared to the nominal mission, solution $D'_{0.6}$ does offer a smaller total mission duration, but it does not utilize the complete ΔV capability of the S/C. Moreover, the interplanetary transit duration for this solution is about 25 days more than the nominal mission. Due to these reasons, this particular abort trajectory solution is not recommended.

Trajectory solutions involving a Mars swing-by maneuver - $A'_{0.6}$ and $B_{0.6}$ - are still not recommended at this abort fraction as their total mission durations (or interplanetary transit times) are still higher than

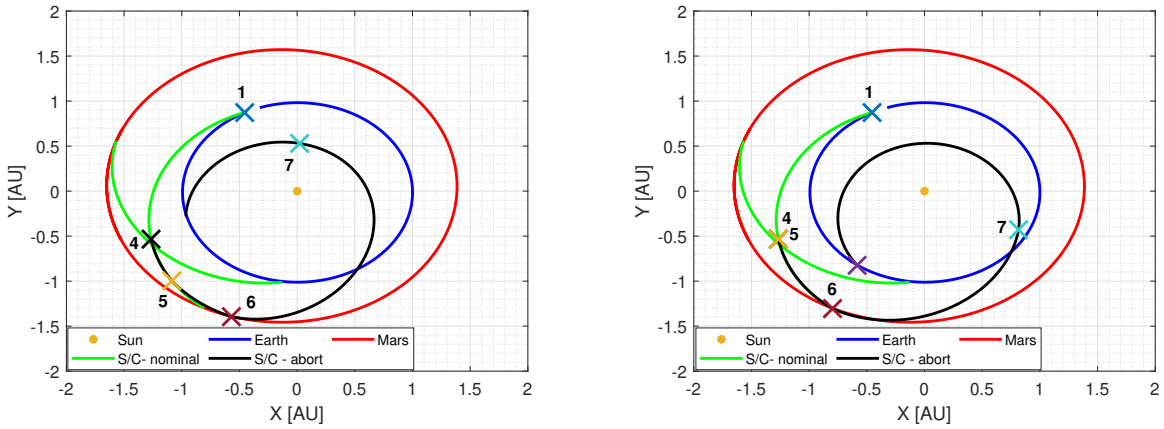

(a) Solution $A'_{0.6}$ (b) Solution $B_{0.6}$

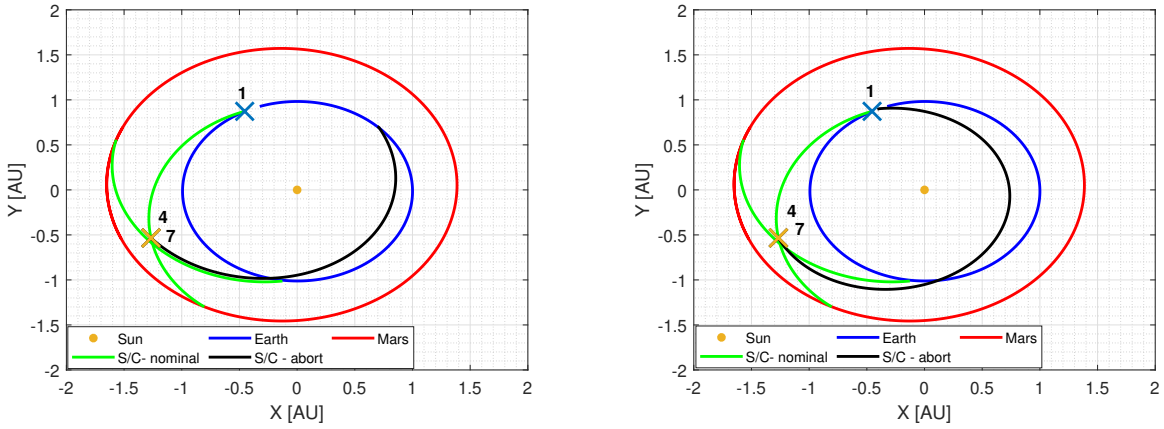

(c) Solution $C_{0.6}$ (d) Solution $C'_{0.6}$

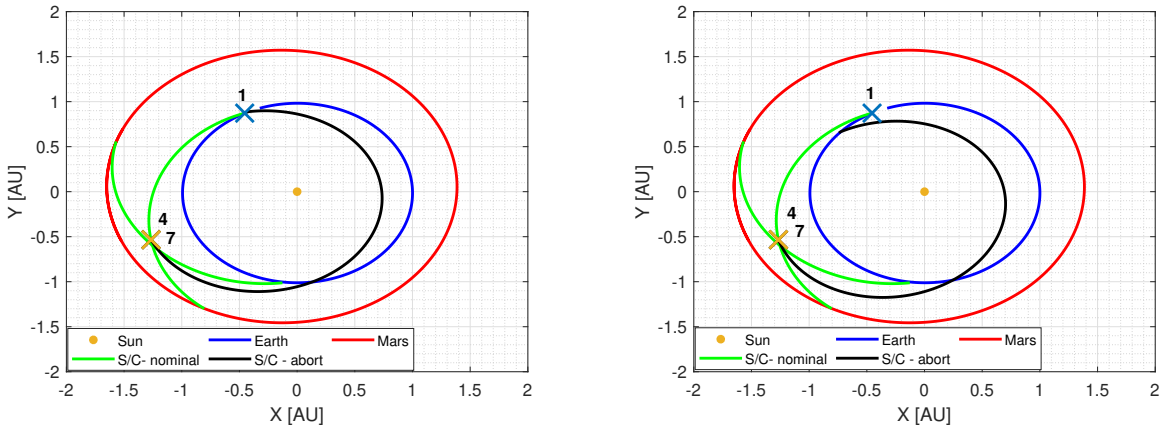

(e) Solution $D_{0.6}$ (f) Solution $D'_{0.6}$

Figure 7.15: Visualizations for the selected propulsive abort trajectory solutions, when the abort occurs during the nominal Earth-to-Mars transfer (*MS-3* and *MS-4*), at abort fraction 0.6. Numbers 1, 4 to 7 represent propulsive maneuvers performed by the S/C for departure from the parking orbit around Earth, aborting from the nominal Earth-to-Mars transfer trajectory, a DSM of the outbound leg after abort, a powered Mars swing-by and a DSM of the inbound leg, respectively.

other four trajectory solutions without a Mars swing-by. Trajectory solution $C_{0.6}$ is not recommended, despite its attractive mission duration compared to the nominal mission, as it requires a total ΔV about 63% higher than the nominal mission. Additionally, it is also obtained from the optimization problem

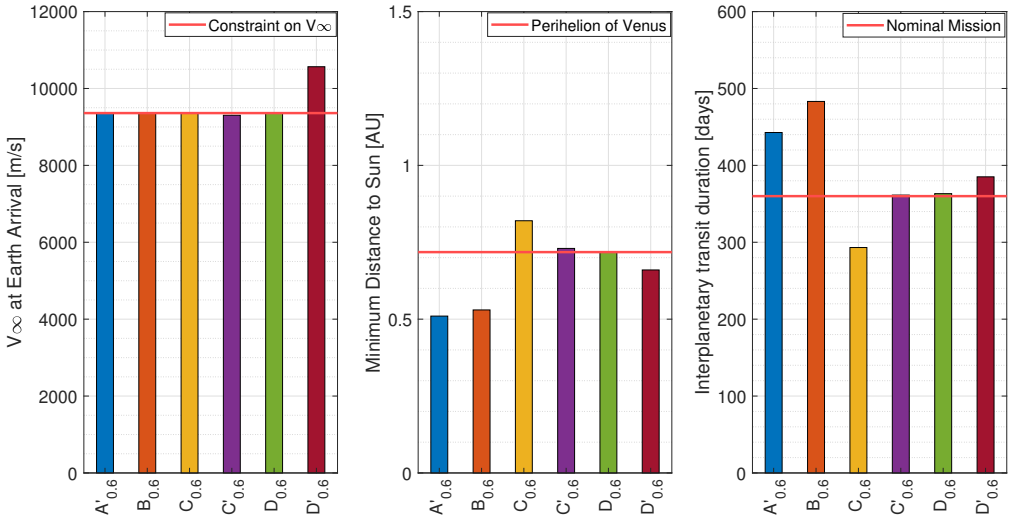

Figure 7.16: Important parameters for the selected propulsive abort trajectory solutions when the abort occurs during the nominal Earth-to-Mars transfer (*MS-3* and *MS-4*), at abort fraction 0.6.

Case 5 which has not resulted in a continuous and robust part of the Pareto front.

Both the trajectory solutions $C'_{0.6}$ and $D_{0.6}$ have a total ΔV higher by only about 5.62% and 4.02% than the nominal mission. They also have comparable values for the interplanetary transit time, about the same as the nominal mission. However, compared to $D_{0.6}$, $C'_{0.6}$ results in a smaller arrival excess velocity at Earth (by about 57 m/s) and the minimum heliocentric distance of this trajectory is slightly higher (by about 0.01 AU). Due to these advantages, solution $C'_{0.6}$ is recommended at this abort fraction. Compared to the nominal mission, a reduction of about 517 days in the total mission duration is achieved with this solution, again highlighting the importance of an abort option.

7.2.4. Abort Fraction 0.8

At the abort fraction of 0.8, the crewed S/C has already traveled for 144 days on its nominal Earth-to-Mars transfer trajectory. Similar to the analysis performed at the abort fraction of 0.6, it is expected that Earth-return trajectories involving a Mars swing-by might be advantageous at this abort fraction.

Solution Set

The Pareto fronts of the solutions for the optimization problems of *MS-3* and *MS-4* are shown in Figures 7.17 and 7.18. For the solution set of *MS-4*, optimization problem Case 7 to Case 9 have been solved to obtain important parts and points of the Pareto front. The robustness of the solution sets is reflected through the agreement between the results obtained with different values for the random seed number.

In total six trajectory solutions are selected for comparison at this abort fraction, from the solution sets of *MS-3* and *MS-4* optimization problems, as listed in Table 7.7. Out of these six abort trajectory solutions, solution $E_{0.8}$ seems an outlier of the Pareto front, as seen in Figure 7.18. However, this solution is likely to belong to another Pareto front that has not been completely retained/identified during the optimization process. Nevertheless, this solution is considered for an inclusive analysis of the abort trajectory options.

Selected Solutions

Important trajectory parameters for the six selected solutions are presented in Figure 7.19 while all trajectory parameter values and associated standard deviations can be found in Appendix C. Trajectory visualizations for these solutions are presented in Figure 7.20. As seen in Figure 7.19, three out of four trajectory solutions without a Mars swing-by maneuver (viz. $C''_{0.8}$, $C'_{0.8}$ and $D_{0.8}$) do not satisfy the constraint on the Earth-arrival excess velocity. Therefore, these solutions are not recommended.

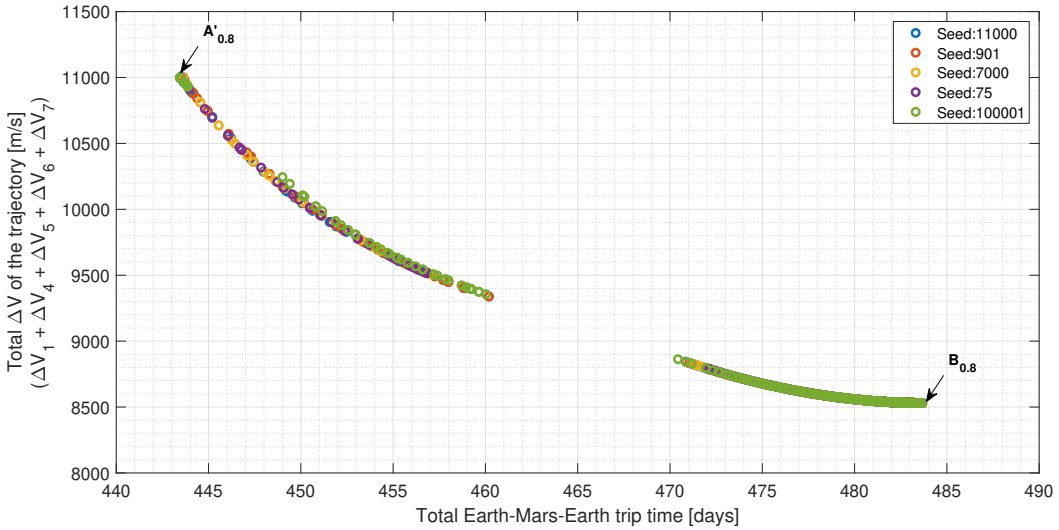

Figure 7.17: Solution set for the propulsive abort trajectories when the abort occurs during the nominal Earth-to-Mars transfer at abort fraction 0.8 and a Mars swing-by is performed (*MS-3*).

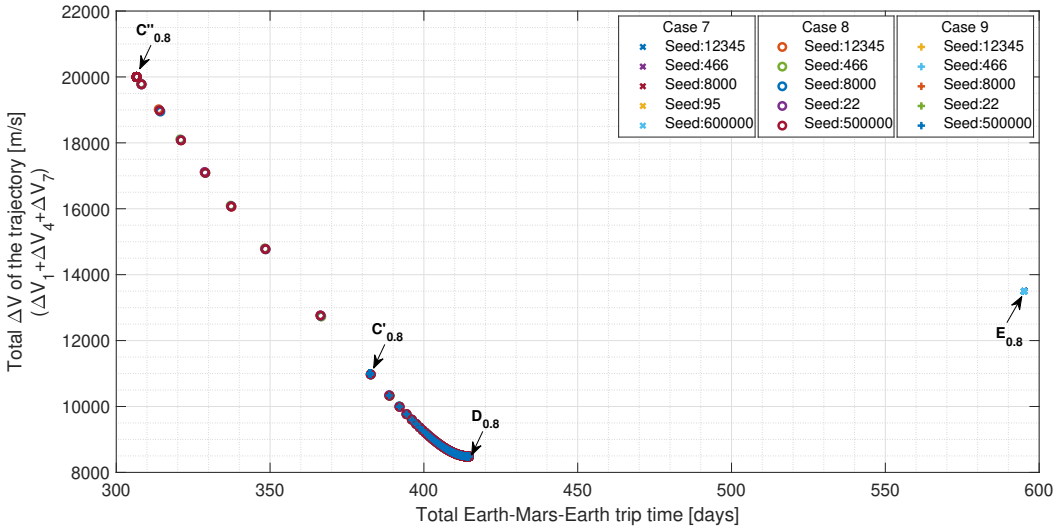

Figure 7.18: Solution set for the propulsive abort trajectories when the abort occurs during the nominal Earth-to-Mars transfer at abort fraction 0.8 and a Mars swing-by is not performed (*MS-4*).

Trajectory solution $E_{0.8}$ which satisfies the constraint on the Earth-arrival excess velocity is an outlier of the solution set as mentioned earlier. The total mission duration (or the interplanetary transit time) with this abort trajectory solution is about 595 days, which is still shorter than the total mission duration of the nominal mission by about 283 days. However, when compared to the interplanetary transit time of the nominal mission (360 days), there is an increase of 65% in such a transit time while passing close to the Sun at a distance of 0.41 AU. Due to these reasons, this abort trajectory solution is not recommended.

Mission Scenario	Solution Identifier	Description	Constraint on total ΔV
MS-3	$A'_{0.8}$	minimum total TOF (sub-optimal)	≤ 11000 m/s
	$B_{0.8}$	minimum total ΔV of five propulsive maneuvers, including the nominal Earth-departure ΔV	-
MS-4	$C''_{0.8}$	minimum total TOF (sub-optimal)	≤ 20000 m/s
	$E_{0.8}$	minimum total ΔV of three propulsive maneuvers, including the nominal Earth-departure ΔV (sub-optimal)	-
	$C'_{0.8}$	minimum total TOF (sub-optimal)	≤ 11000 m/s
	$D_{0.8}$	minimum total ΔV of three propulsive maneuvers, including the nominal Earth-departure ΔV	-

Table 7.7: Selected solutions from the solution sets of the propulsive abort trajectories when the abort occurs during the nominal Earth-to-Mars transfer at abort fraction 0.8 (*MS-3* and *MS-4*).

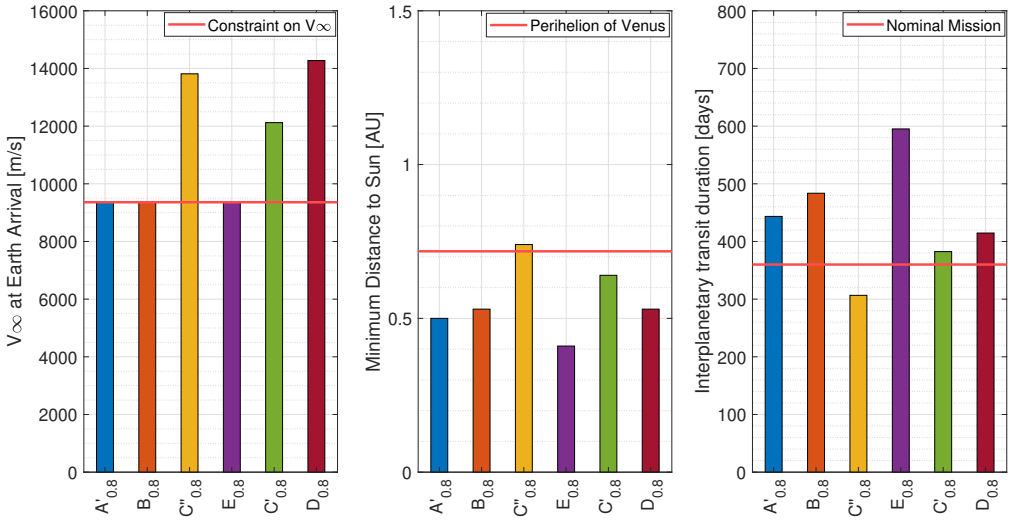

Figure 7.19: Important parameters for the selected propulsive abort trajectory solutions when the abort occurs during the nominal Earth-to-Mars transfer (*MS-3* and *MS-4*), at abort fraction 0.8.

On the other hand, trajectory solutions $A'_{0.8}$ and $B_{0.8}$ have a total mission duration (or an interplanetary transit duration) about 444 days and 484 days respectively. The minimum heliocentric distances of these trajectory solutions are also higher than that of $E_{0.8}$. Therefore, compared to $E_{0.8}$, these two trajectory solutions involving a Mars swing-by maneuver are preferable solutions. Out of these two, $B_{0.8}$ does not utilize the complete on-board total ΔV capability of the crewed S/C and has a higher trip time compared to $A'_{0.8}$. Thus, the trajectory solution $A'_{0.8}$ is recommended for this abort fraction. With this abort trajectory solution, a reduction of about 334 days in the total mission duration is achieved and a Mars swing-by is performed unlike the recommended solutions at other abort fractions, discussed earlier.

In the next section, results for the Earth-return trajectories when the abort occurs during the nominal Mars surface stay period are presented.

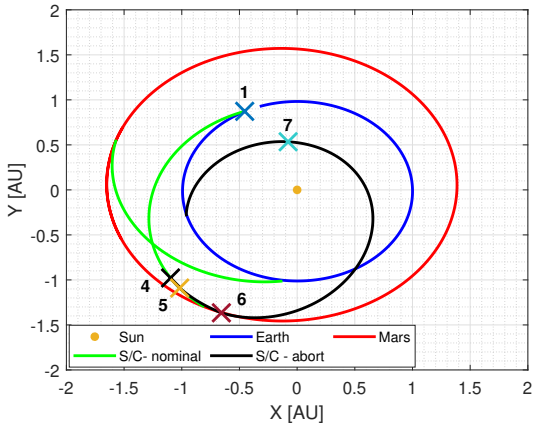

(a) Solution $A'_{0.8}$

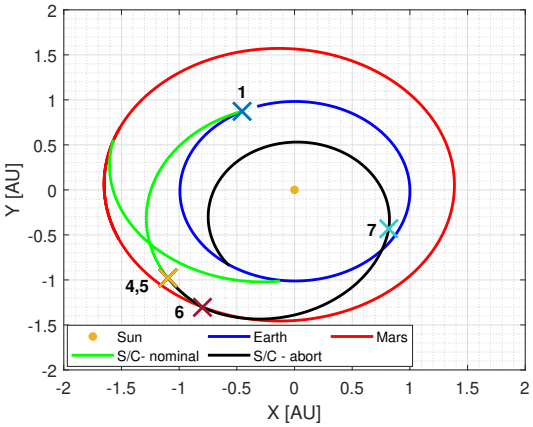

(b) Solution $B_{0.8}$

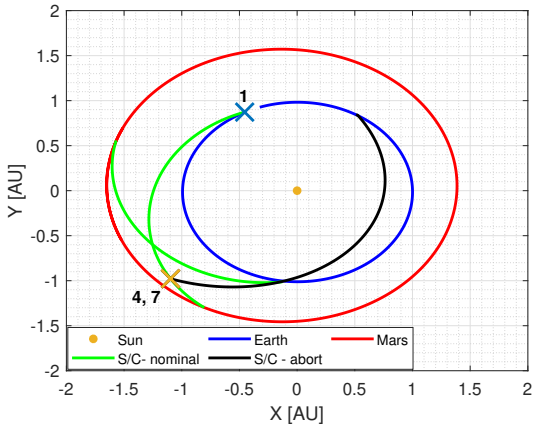

(c) Solution $C''_{0.8}$

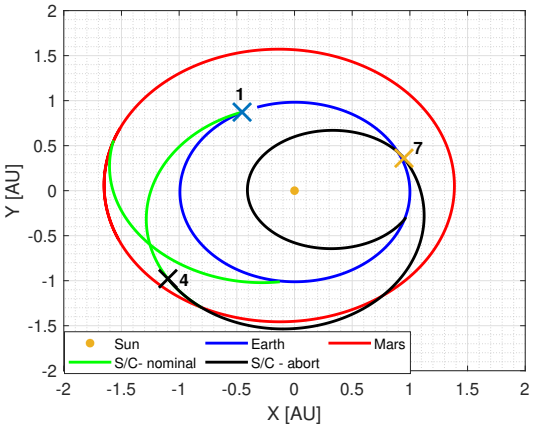

(d) Solution $E_{0.8}$

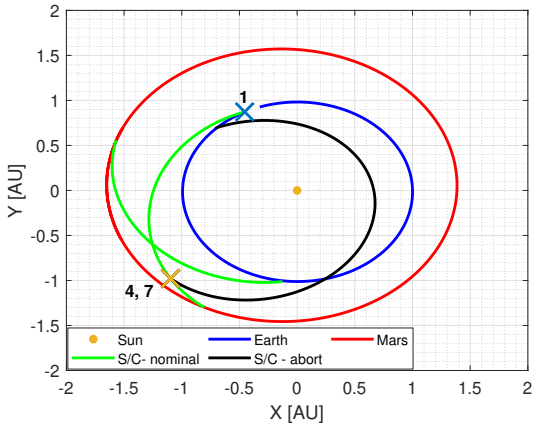

(e) Solution $C'_{0.8}$

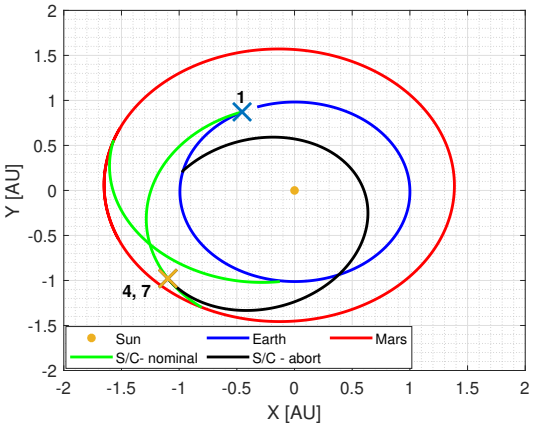

(f) Solution $D_{0.8}$

Figure 7.20: Visualizations for the selected propulsive abort trajectory solutions, when the abort occurs during the nominal Earth-to-Mars transfer (*MS-3* and *MS-4*), at abort fraction 0.8. Numbers 1, 4 to 7 represent propulsive maneuvers performed by the S/C for departure from the parking orbit around Earth, aborting from the nominal Earth-to-Mars transfer trajectory, a DSM of the outbound leg after the abort, a powered Mars swing-by and a DSM of the inbound leg, respectively.

7.3. Abort Trajectories: *MS-5*

MS-5 investigated in this thesis work refers to finding Mars-to-Earth trajectory solutions when the mission abort decision is taken during the nominal (planned) Mars surface stay. Similar to *MS-3* and *MS-4*, such abort trajectories are computed for 20, 40, 60, and 80% of the nominal Mars surface stay period. For such trajectories, along with a departure maneuver from the parking orbit around Mars (TEI), a DSM is included to expand the design space of the problem. In the subsequent sections, solutions for this mission scenario are discussed as per the abort fraction, which relates to the Mars-arrival epoch as mentioned earlier in Table 5.2. At each abort fraction, the obtained solution set is presented and a few selected solutions from this set are discussed. Based on this discussion, one abort trajectory solution is recommended. As mentioned earlier, the reader should refer to Section 7.4 for quickly comparing the different selected and recommended solutions with each other.

7.3.1. Abort Fraction 0.2

An abort fraction of 0.2 with *MS-5* refers to the departure epoch at 20% of the nominal Mars surface stay period. For the selected ballistic transfer trajectory solution A_N^c, the Mars surface stay period is about 519 days. Therefore, for the current analysis, the Mars-departure epoch is about 104 days after the nominal Mars-arrival epoch.

Solution Set

The Pareto front of the solutions obtained for the optimization problem of mission scenario *MS-5* is presented in Figure 7.21. Multiple cases of the optimization problem have been solved (viz. Case 10 to Case 13), each for five different values of the random seed number, to obtain different parts of the solution set. As depicted in Figure 7.21, results obtained with these optimization problem cases are in good agreement with each other for all the five values of random seed number, whenever there is an overlap between the parts of the Pareto front.

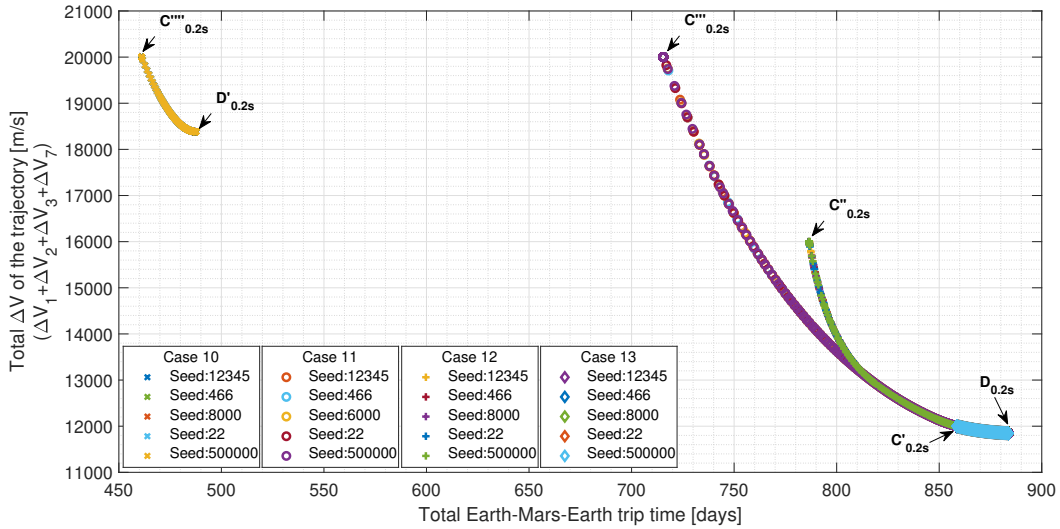

Figure 7.21: Solution set for the propulsive abort trajectories when the abort occurs during the nominal Mars surface stay period (*MS-5*) at abort fraction 0.2.

Two parts of the solution set are clearly separated in Figure 7.21. A number of abort trajectories exist, which can bring the crewed S/C back to Earth within a shorter duration, but require a total ΔV higher than 18000 m/s. Two trajectory solutions have been selected from this part of the solution set and marked with identifiers $C''''_{0.2s}$ and $D'_{0.2s}$. Trajectory visualizations for these trajectories are shown in Figure 7.22. From these visualizations, it can be inferred that this part of the solution set contains abort trajectories which cross Earth's (average) orbital distance while coming back to Earth, in order to achieve shorter trip times.

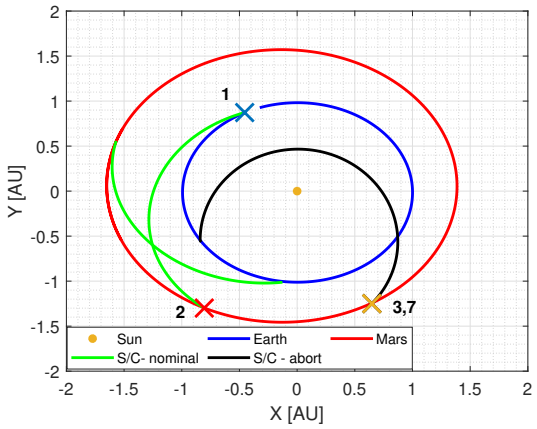

(a) Solution $C''''_{0.2s}$

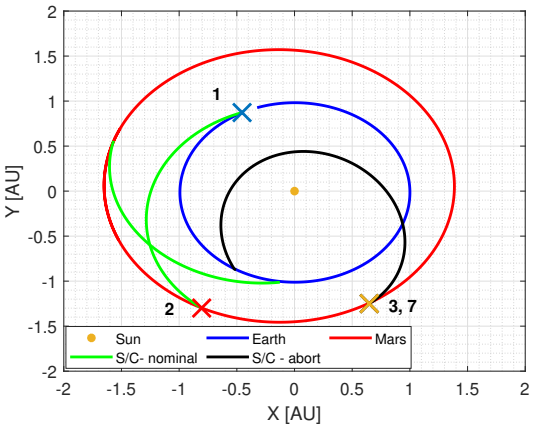

(b) Solution $D'_{0.2s}$

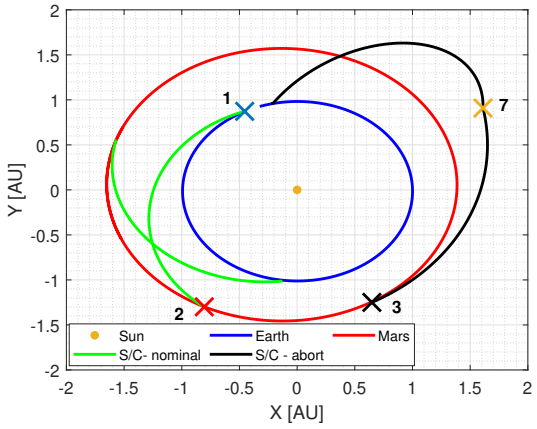

(c) Solution $C'''_{0.2s}$

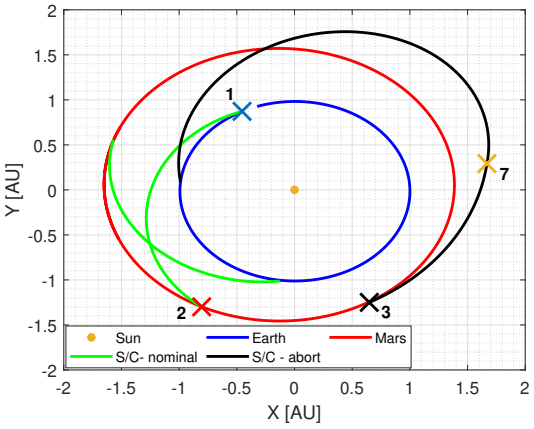

(d) Solution $C''_{0.2s}$

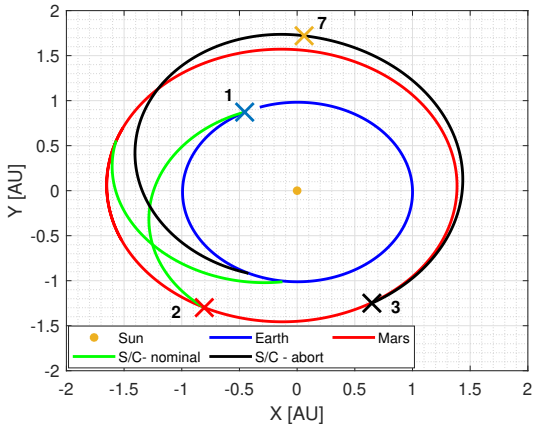

(e) Solution $C'_{0.2s}$

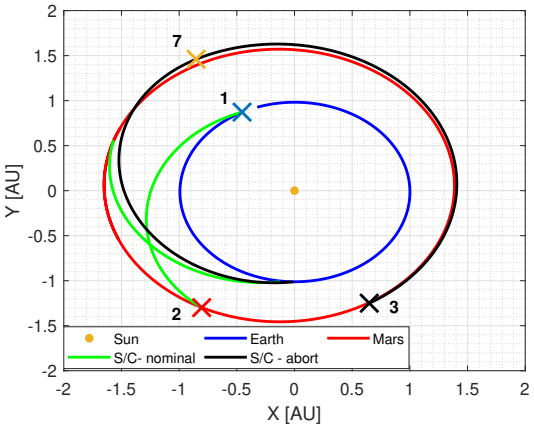

(f) Solution $D_{0.2s}$

Figure 7.22: Visualizations for the selected propulsive abort trajectory solutions, when the abort occurs during the nominal Mars surface stay period (*MS-5*), at abort fraction 0.2. Numbers 1 to 3 and 7 represent propulsive maneuvers performed by the S/C for departure from the parking orbit around Earth, capture into the parking orbit around Mars, departure from the parking orbit around Mars and a DSM of the inbound leg, respectively.

Another part of the solution set contains abort trajectories that have relatively longer trip times but relatively more feasible total ΔV requirement. Four trajectories solutions - $C''''_{0.2s}$, $C'''_{0.2s}$, $C'_{0.2s}$ and $D_{0.2s}$ - are selected from this part of the solution set and their trajectory visualizations are also shown in Figure 7.22. From these visualizations, it can be inferred that this part of the solution set contains abort

trajectories that do not cross Earth's (average) orbital distance while coming back to Earth, leading to higher trip times. Table 7.8 lists the most important details of all selected abort trajectories and these trajectories are compared with each other in the following section.

Mission Scenario	**Solution Identifier**	**Description**	**Constraint on total ΔV**
MS-5	$C''''_{0.2s}$	minimum total TOF (sub-optimal)†	≤ 20000 m/s
	$D'_{0.2s}$	minimum total ΔV of four propulsive maneuvers, including the nominal Earth-departure and Mars-capture ΔVs (sub-optimal)	-
	$C'''_{0.2s}$	minimum total TOF (sub-optimal)†	≤ 20000 m/s
	$C''_{0.2s}$	minimum total TOF (sub-optimal)	≤ 16000 m/s
	$C'_{0.2s}$	minimum total TOF (sub-optimal)	≤ 12000 m/s
	$D_{0.2s}$	minimum total ΔV of four propulsive maneuvers, including the nominal Earth-departure and Mars-capture ΔVs (sub-optimal, total trip time $\leq$ 884 days)	-

Table 7.8: Selected solutions from the solution sets of the propulsive abort trajectories when the abort occurs during the nominal Mars surface stay period, at abort fraction 0.2 (*MS-5*). † Even though trajectories $C''''_{0.2s}$ and $C'''_{0.2s}$ have a similar value for the constraint on total ΔV, they have different values for the TOF of the inbound leg of the mission and different values for the minimum distance to the Sun.

Selected Solutions

Important trajectory parameters of the six selected abort trajectory solutions are presented in Figure 7.23 while all trajectory parameter values and associated standard deviations can be found in Appendix C. The total mission duration of the abort trajectory options has been constrained to be smaller than that of the nominal mission. Out of the six selected solutions, three solutions - $C''''_{0.2s}$, $D'_{0.2s}$ $C'''_{0.2s}$ - do not meet the constraint on excess velocity at Earth-arrival and have a total ΔV requirement greater than the nominal mission (by at least 75%). Therefore, none of these solutions is recommended at this abort fraction.

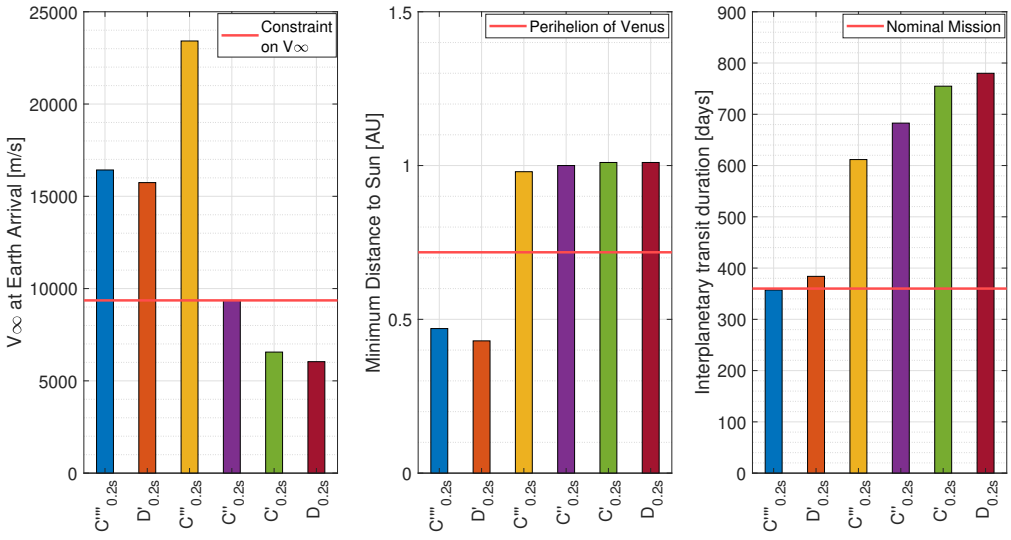

Figure 7.23: Important parameters for the selected propulsive abort trajectory solutions when the abort occurs during the nominal Mars surface stay period (*MS-5*), at abort fraction 0.2.

Out of the remaining trajectory solutions, $C''_{0.2s}$ has the smallest interplanetary transit duration (about 683 days). However, its total ΔV requirement (about 16000 m/s) is more than 150% of that associated

with the nominal mission. Due to this higher ΔV requirement, even this solution is not recommended at this abort fraction. For the solutions $C'_{0.2s}$ and $D_{0.2s}$, the requirement of total ΔV is higher by 15.22 and 13.75% than the nominal mission, respectively. The latter trajectory solution has an interplanetary transit duration of about 25 days longer than the former. Assuming that it is possible to provide 15.22% extra total ΔV capability to the crewed S/C, trajectory solution $C'_{0.2s}$ is recommended at this abort fraction. With this solution, total mission duration is reduced by about 20 days compared to that of the nominal mission and such an advantage of the abort trajectory option is marginal compared to the advantage obtained with the recommended solutions for *MS-3* and *MS-4*.

7.3.2. Abort Fraction 0.4

An abort fraction of 0.4 with *MS-5* refers to the departure epoch at 40% of the nominal Mars surface stay period, which translates to about 208 days after the nominal Mars-arrival epoch. As the Earth-to-Mars trajectory for this mission scenario has a TOF of 180 days, the abort epoch (off-nominal Mars-departure epoch) occurs 388 days (about an year) after the S/C would have left Earth for its interplanetary transit.

Solution Set

The Pareto front of the solutions for the optimization problem of *MS-5* at 0.4 abort fraction, obtained through multiple cases is shown in 7.24. Case 14 to Case 17 are solved, each for five different values of the seed number. As seen in this figure, results of these optimization problem cases are in perfect agreement whenever there is an overlap between parts of the Pareto front.

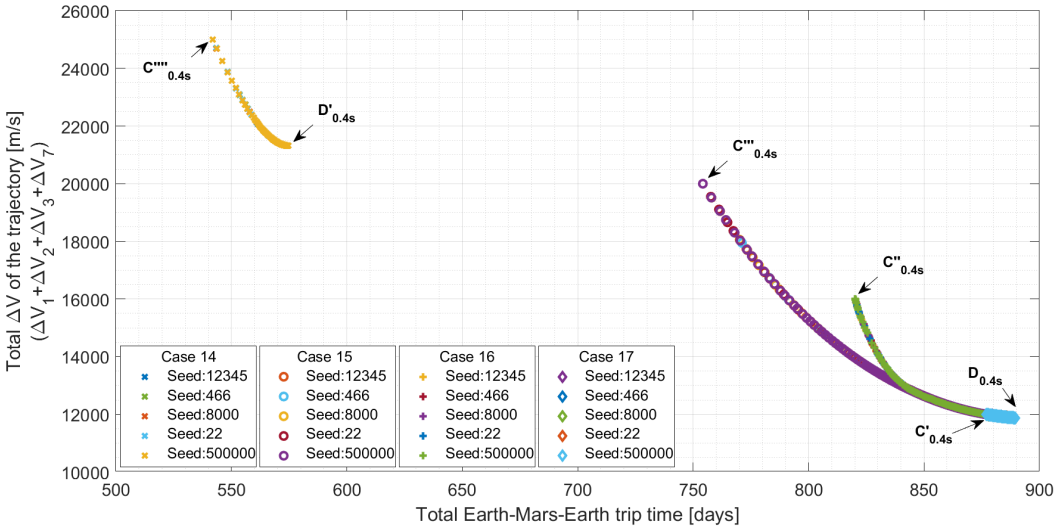

Figure 7.24: Solution set for the propulsive abort trajectories when the abort occurs during the nominal Mars surface stay period (*MS-5*) at abort fraction 0.4.

The complete solution set has two clearly separated parts similar to the solution set obtained at abort fraction of 0.2 with *MS-5*. From the part containing trajectory solutions with shorter trip time values, two solutions - $C''''_{0.4s}$ and $D'_{0.4s}$ - have been selected. From the other part of solution set, four trajectory solutions have been selected viz. $C'''_{0.4s}$, $C''_{0.4s}$, $C'_{0.4s}$ and $D'_{0.4s}$. Trajectory visualizations for all these selected solutions are presented in Figure 7.25, and Table 7.9 provides most important details for these solutions.

Unlike for the analysis presented in the previous section, the total mission duration was allowed to be higher than the nominal mission's duration. By allowing an increase in the total mission duration by only about 10 days, the minimum total ΔV cost of any possible abort solution was checked. A similar increase in the total mission duration has been allowed for the abort trajectory solutions when the abort fraction is 0.6 or 0.8.

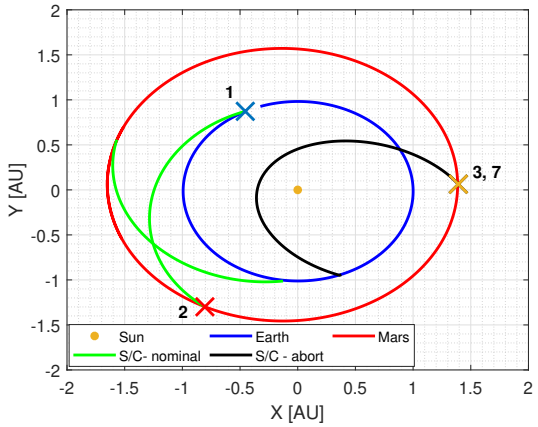

(a) Solution $C''''_{0.4s}$

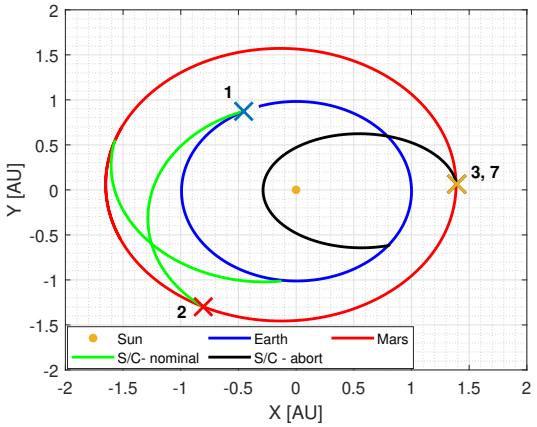

(b) Solution $D'_{0.4s}$

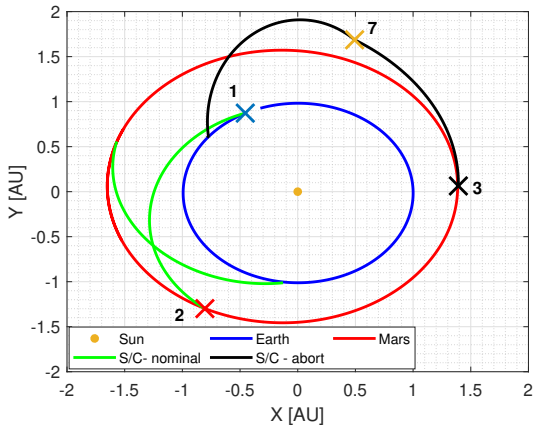

(c) Solution $C'''_{0.4s}$

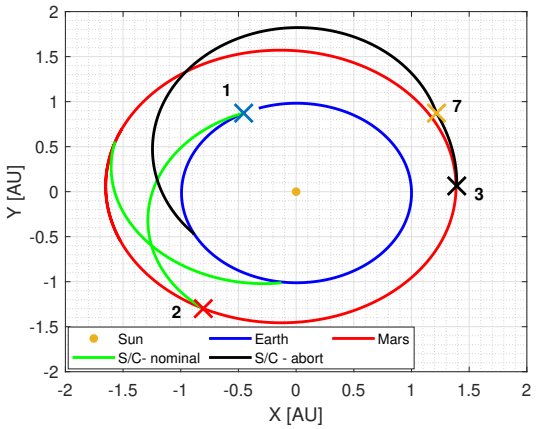

(d) Solution $C''_{0.4s}$

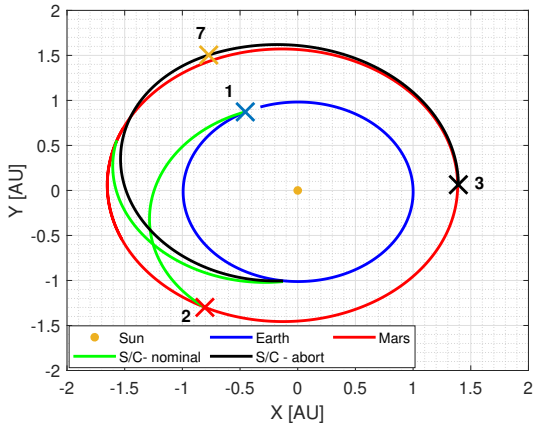

(e) Solution $C'_{0.4s}$

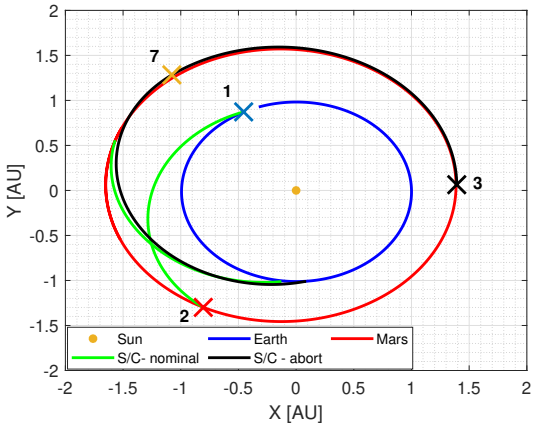

(f) Solution $D_{0.4s}$

Figure 7.25: Visualizations for the selected propulsive abort trajectory solutions, when the abort occurs during the nominal Mars surface stay period (*MS-5*), at abort fraction 0.4. Numbers 1 to 3 and 7 represent propulsive maneuvers performed by the S/C for departure from the parking orbit around Earth, capture into the parking orbit around Mars, departure from the parking orbit around Mars and a DSM of the inbound leg, respectively.

Mission Scenario	Solution Identifier	Description	Constraint on total ΔV
MS-5	$C''''_{0.4s}$	minimum total TOF (sub-optimal)	≤ 25000 m/s
	$D'_{0.4s}$	minimum total ΔV of four propulsive maneuvers, including the nominal Earth-departure and Mars-capture ΔVs (sub-optimal)	-
	$C'''_{0.4s}$	minimum total TOF (sub-optimal)	≤ 20000 m/s
	$C''_{0.4s}$	minimum total TOF (sub-optimal)	≤ 16000 m/s
	$C'_{0.4s}$	minimum total TOF (sub-optimal)	≤ 12000 m/s
	$D_{0.4s}$	minimum total ΔV of four propulsive maneuvers, including the nominal Earth-departure and Mars-capture ΔVs (sub-optimal, total trip time $\leq$ 890 days)	-

Table 7.9: Selected solutions from the solution sets of the propulsive abort trajectories when the abort occurs during the nominal Mars surface stay period, at abort fraction 0.4 (*MS-5*).

Selected Solutions

Important trajectory parameters of the six selected abort trajectory solutions are presented in Figure 7.26 while all trajectory parameter values and associated standard deviations can be found in Appendix C. The Earth-return trajectory solutions $C''''_{0.4s}$, $D'_{0.4s}$, $C'''_{0.4s}$ and $C''_{0.4s}$ are not recommended at the abort fraction of 0.4 for the similar reasons (high values of V_∞ and total ΔV) due to which the solutions $C''''_{0.2s}$, $D'_{0.2s}$, $C'''_{0.2s}$ and $C''_{0.2s}$ have not been recommended at abort fraction of 0.2 for *MS-5*.

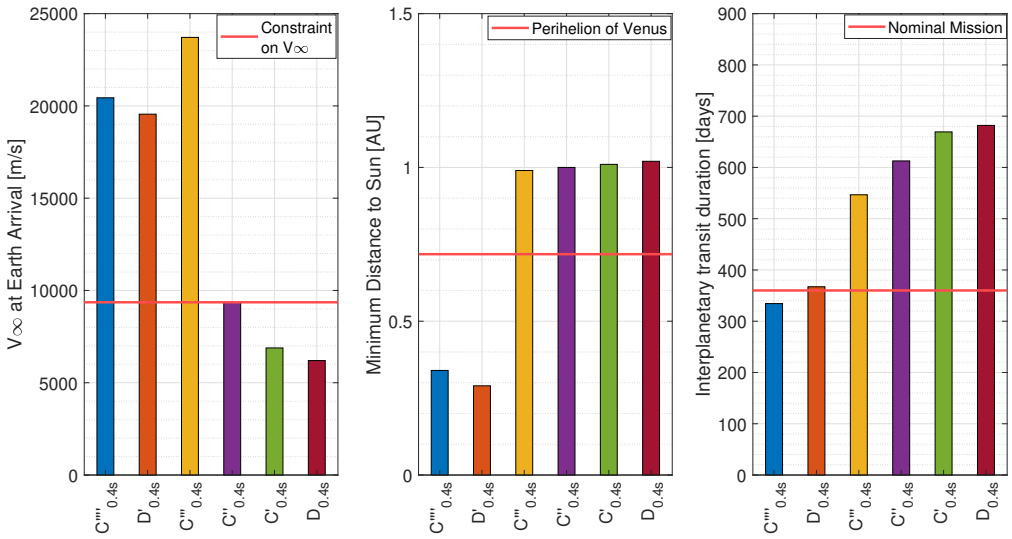

Figure 7.26: Important parameters for the selected propulsive abort trajectory solutions when the abort occurs during the nominal Mars surface stay period (*MS-5*), at an abort fraction 0.4.

The remaining two trajectory solutions - $C'_{0.4s}$ and $D_{0.4s}$- have an interplanetary transit duration of about 669 and 682 days respectively. The former solution has a total ΔV requirement 15.22% higher than that of the nominal mission, while for the latter solution this increase is 14.02%. As assumed earlier for $C'_{0.2s}$, the increase of 15.22% in total ΔV is accepted and thus, the solution $C'_{0.4s}$ is recommended at this abort fraction. It should be noted that the total mission duration of this recommended abort trajectory solution is about the same as that of the nominal mission.

7.3.3. Abort Fraction 0.6

An abort fraction of 0.6 with *MS-5* refers to the off-nominal departure of the crewed S/C from the parking orbit around Mars when more than half (60%) of the nominal Mars surface stay period has passed.

Solution Set

The Pareto front of the solutions for the optimization problem of *MS-5* at 0.6 abort fraction, obtained through Case 18 to Case 21, is shown in Figure 7.27. Similar to earlier analyses, the solution sets obtained show robustness. However, unlike the Pareto front obtained at earlier abort fractions of *MS-5*, there are no clearly separated parts of the solution set[4].

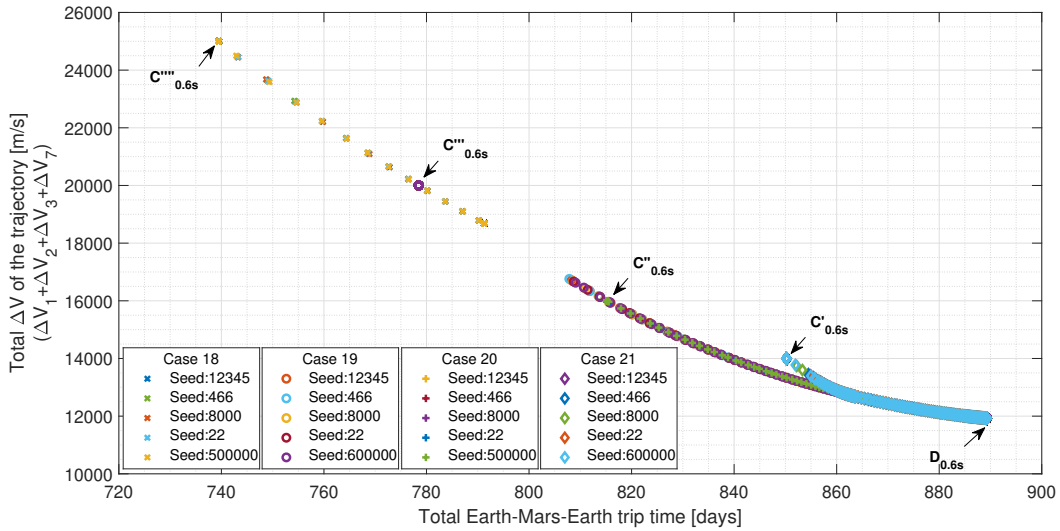

Figure 7.27: Solution set for the propulsive abort trajectories when the abort occurs during the nominal Mars surface stay period (MS-5) at abort fraction 0.6.

From this solution set, five trajectory solutions are selected viz. $C''''_{0.6s}$, $C'''_{0.6s}$, $C''_{0.6s}$, $C'_{0.6s}$ and $D_{0.6s}$. The trajectory visualizations for these solutions are shown in Figure 7.28 while important details about these solutions are presented in Table 7.10. Comparison of Figures 7.25 and 7.28 indicates that unlike selected trajectory solutions for the abort fraction of 0.4, none of the selected trajectory solutions for the abort fraction of 0.6 involve crossing of the (average) orbital distance of Earth when the crewed S/C returns back to Earth after the abort epoch.

[4]Any Earth-return trajectory solutions with a total ΔV requirement more than 25000 m/s have not been investigated because such solutions would not have been recommended owing to the at least 140% increase in the total ΔV compared to the nominal mission.

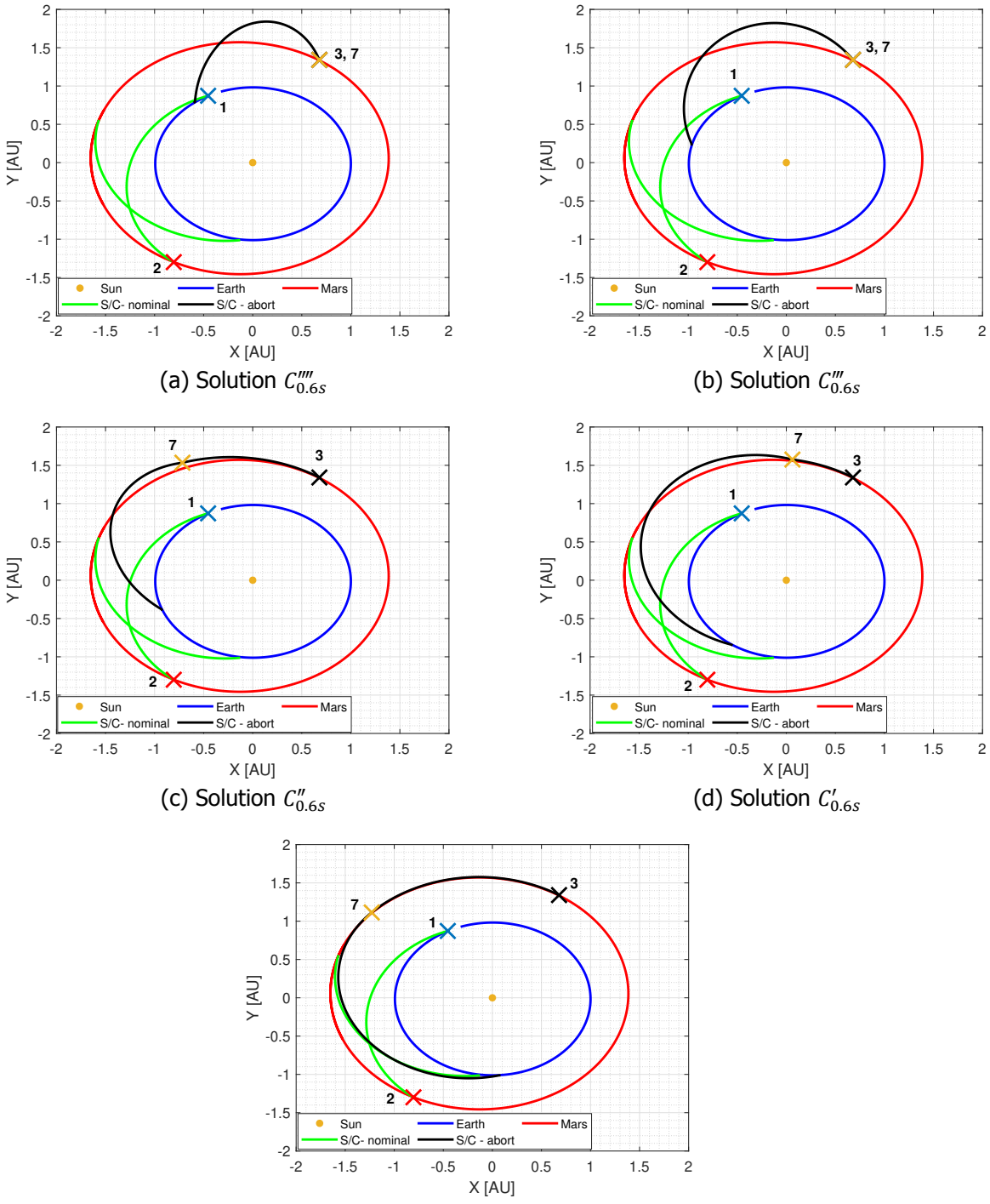

(a) Solution $C''''_{0.6s}$ (b) Solution $C'''_{0.6s}$

(c) Solution $C''_{0.6s}$ (d) Solution $C'_{0.6s}$

(e) Solution $D_{0.6s}$

Figure 7.28: Visualizations for the selected propulsive abort trajectory solutions, when the abort occurs during the nominal Mars surface stay period (*MS-5*), at abort fraction 0.6. Numbers 1 to 3 and 7 represent propulsive maneuvers performed by the S/C for departure from the parking orbit around Earth, capture into the parking orbit around Mars, departure from the parking orbit around Mars and a DSM of the inbound leg, respectively.

Selected Solutions

Important trajectory parameters of the five selected abort trajectory solutions are presented in Figure 7.29 while all trajectory parameter values and associated standard deviations can be found in Appendix C. The trajectory solutions $C''''_{0.6s}$, $C'''_{0.6s}$ and $C''_{0.6s}$ are not recommended because they do not

Mission Scenario	Solution Identifier	Description	Constraint on total ΔV
MS-5	$C''''_{0.6s}$	minimum total TOF (sub-optimal)	≤ 25000 m/s
	$C'''_{0.6s}$	minimum total TOF (sub-optimal)	≤ 20000 m/s
	$C''_{0.6s}$	minimum total TOF (sub-optimal)	≤ 16000 m/s
	$C'_{0.6s}$	minimum total TOF (sub-optimal)	≤ 14000 m/s
	$D_{0.6s}$	minimum total ΔV of four propulsive maneuvers, including the nominal Earth-departure and Mars-capture ΔVs (sub-optimal, total trip time $\leq$ 890 days)	-

Table 7.10: Selected solutions from the solution sets of the propulsive abort trajectories when the abort occurs during the nominal Mars surface stay period, at abort fraction 0.6 (*MS-5*).

meet the constraint on arrival excess velocity at Earth and the total ΔV requirement of these solutions is at least 153% of the total ΔV associated with the nominal mission.

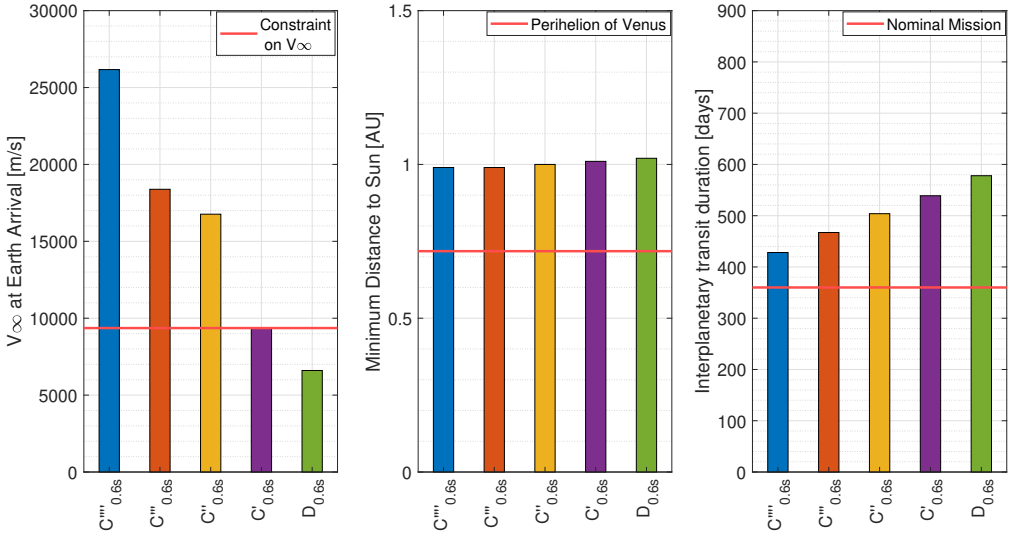

Figure 7.29: Important parameters for the selected propulsive abort trajectory solutions when the abort occurs during the nominal Mars surface stay period (*MS-5*), at abort fraction 0.6.

Trajectory solution $C'_{0.6s}$ meets the constraint on arrival excess velocity at Earth, but the required total ΔV for this solution is about 14000 m/s. This is about 34% higher than the value associated with the nominal mission. On the other hand, the total ΔV required by the solution $D_{0.6s}$ is about 11930 m/s (about 15% higher than that of the nominal mission). In earlier sections, it has been assumed that an increase in total ΔV by 15.22% is accepted. Therefore, solution $D_{0.6s}$ is recommended for the current abort fraction value.

From the trajectory visualizations shown in Figure 7.28, it appears that with the Earth-return trajectory solution $D_{0.6s}$ the crewed S/C stays in an interplanetary heliocentric orbit similar to the orbit of Mars before a DSM maneuver is performed. Moreover, the total Earth-Mars-Earth trip time associated with this particular solution is about 889 days while the nominal mission has a total trip time of about 879 days. As mentioned earlier, such a slightly longer mission duration was allowed in this analysis to check the minimum total ΔV requirement of abort trajectory options. However, compared to the nominal transfer trajectory solution A_N^c, this abort trajectory solution does not provide any advantage in terms of the interplanetary transit duration or the total ΔV requirement.

Thus, if the Mars surface mission is aborted at the fraction of 0.6, the crew can stay in the TV (the

crewed S/C) which had been parked in a circular parking orbit around Mars until the nominal Mars-departure epoch. If the mission architecture can support such an arrangement, then the crewed S/C can follow the nominal inbound transfer trajectory after the nominal Mars-departure epoch. Abort trajectory option $D_{0.6s}$ is not recommended under such a scenario.

7.3.4. Abort Fraction 0.8

The abort fraction of 0.8 corresponds to a mission abort scenario closest to the nominal Mars-departure epoch. With a nominal Mars surface stay period of 519 days (the transfer solution A_N^c), the off-nominal Mars-departure epoch with this abort fraction is about 415 days after the nominal Mars-arrival epoch or 104 days before the nominal Mars-departure epoch.

Solution Set

The Pareto front of the solutions for the optimization problem of *MS-5* at 0.8 abort fraction, obtained through Case 22 to Case 25, is shown in Figure 7.30. Similar to other analyses of this thesis work, the solution set obtained shows robustness for the different values of random seed number and with different problem cases.

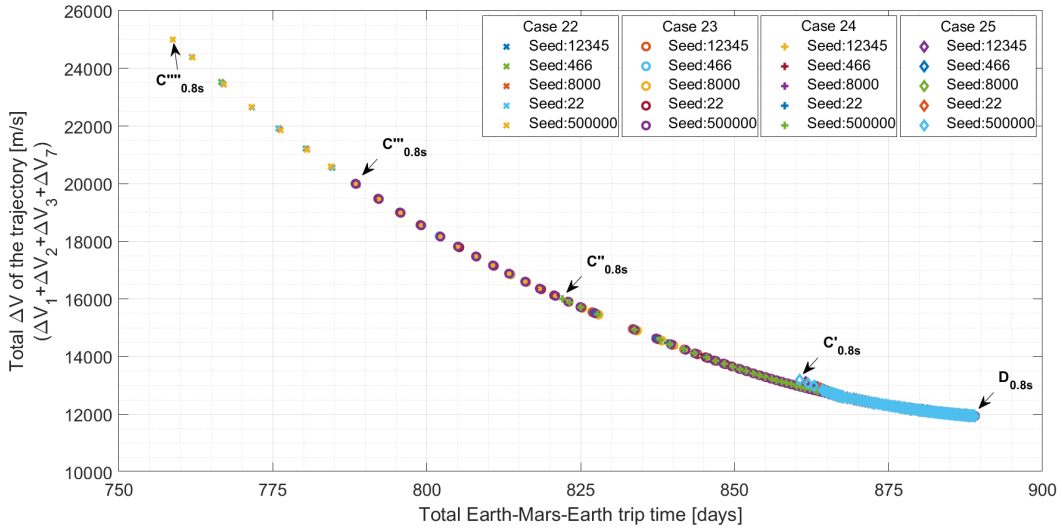

Figure 7.30: Solution set for the propulsive abort trajectories when the abort occurs during the nominal Mars surface stay period *(MS-5)* at abort fraction 0.8.

From this solution set, five trajectory solutions are selected for comparison viz. $C''''_{0.8s}$, $C'''_{0.8s}$, $C''_{0.8s}$, $C'_{0.8s}$ and $D_{0.8s}$. The trajectory visualizations for these solutions are shown in Figure 7.31, while important details about these solutions are presented in Table 7.11. From these trajectory visualizations, it is clear that none of the selected solutions for the abort fraction of 0.8 have Earth-return trajectories that cross the (average) orbital distance of Earth.

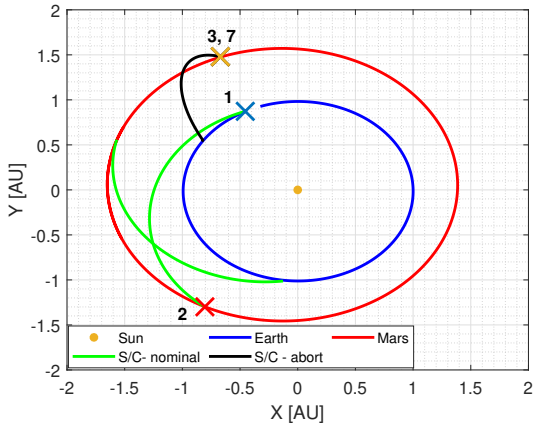

(a) Solution $C''''_{0.8s}$

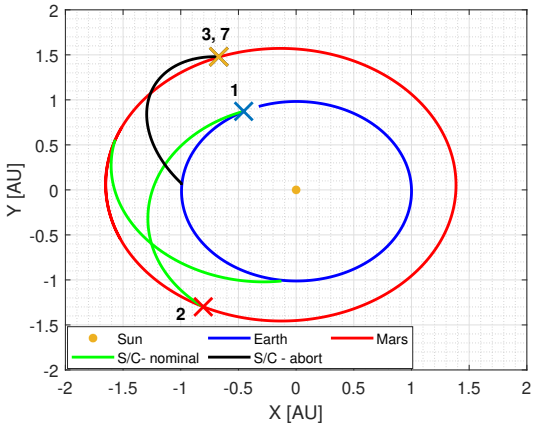

(b) Solution $C'''_{0.8s}$

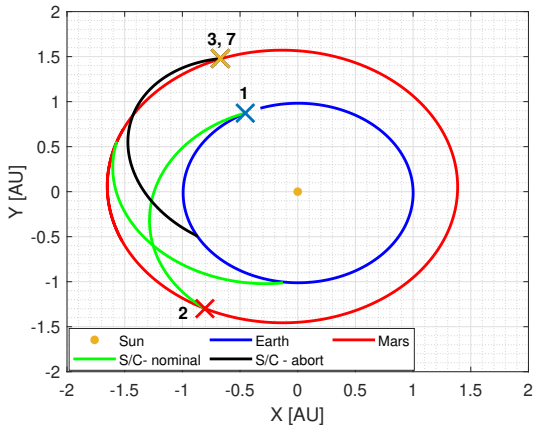

(c) Solution $C''_{0.8s}$

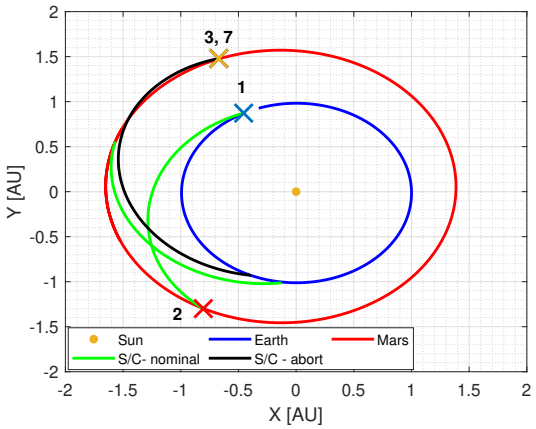

(d) Solution $C'_{0.8s}$

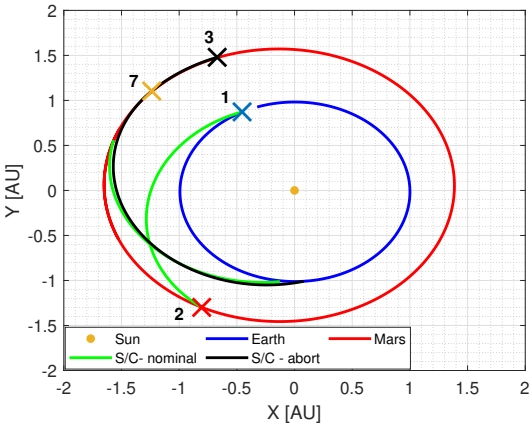

(e) Solution $D_{0.8s}$

Figure 7.31: Visualizations for the selected propulsive abort trajectory solutions, when the abort occurs during the nominal Mars surface stay period (*MS-5*), at abort fraction 0.8. Numbers 1 to 3 and 7 represent propulsive maneuvers performed by the S/C for departure from the parking orbit around Earth, capture into the parking orbit around Mars, departure from the parking orbit around Mars and a DSM of the inbound leg, respectively.

Mission Scenario	Solution Identifier	Description	Constraint on total ΔV
MS-5	$C''''_{0.8s}$	minimum total TOF (sub-optimal)†	≤ 25000 m/s
	$C'''_{0.8s}$	minimum total TOF (sub-optimal)	≤ 20000 m/s
	$C''_{0.8s}$	minimum total TOF (sub-optimal)	≤ 16000 m/s
	$C'_{0.8s}$	minimum total TOF (sub-optimal)†	≤ 25000 m/s
	$D_{0.8s}$	minimum total ΔV of four propulsive maneuvers, including the nominal Earth-departure and Mars-capture ΔVs (sub-optimal, total trip time $\leq$ 890 days)	-

Table 7.11: Selected solutions from the solution sets of the propulsive abort trajectories when the abort occurs during the nominal Mars surface stay period, at abort fraction 0.8 (*MS-5*). † Even though trajectories $C''''_{0.8s}$ and $C'_{0.8s}$ have a similar value for the constraint on total ΔV, the latter has a smaller value of the actual total ΔV requirement and satisfies the constraint on arrival excess velocity at Earth.

Selected Solutions

Important trajectory parameters of the five selected abort trajectory solutions are presented in Figure 7.32, while all trajectory parameter values and associated standard deviations can be found in Appendix C. The trajectory solutions $C''''_{0.8s}$, $C'''_{0.8s}$ and $C''_{0.8s}$ are not recommended because they do not meet the constraint on arrival excess velocity at Earth and the associated total ΔV with these solutions is at least 53% higher than that of the nominal mission.

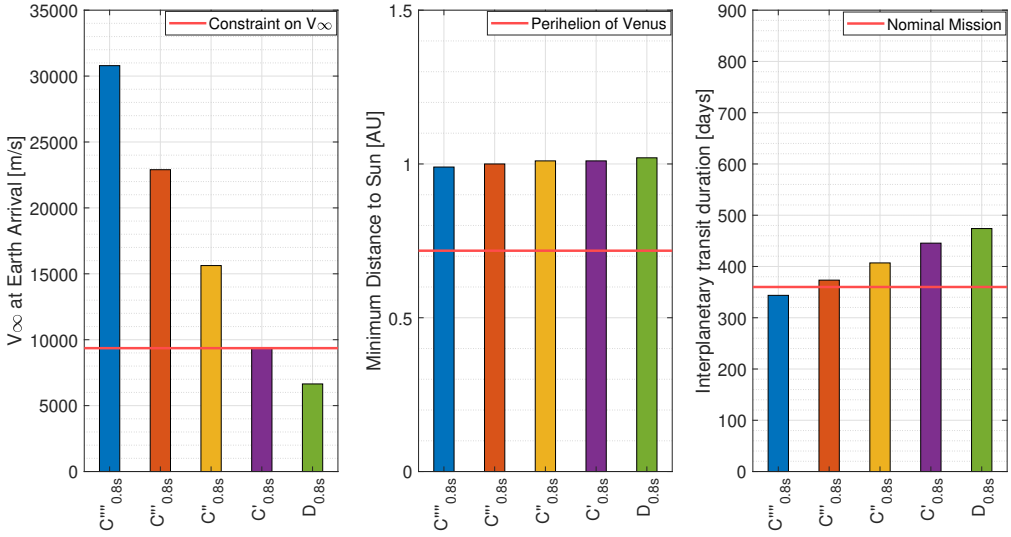

Figure 7.32: Important parameters for the selected propulsive abort trajectory solutions when the abort occurs during the nominal Mars surface stay period (*MS-5*), at abort fraction 0.8.

Trajectory solution $C'_{0.8s}$ meets the constraint on arrival excess velocity at Earth but the required total ΔV for this solution is 13194.25 m/s, about 27% higher than the value associated with the nominal mission. On the other hand, for the solution $D_{0.8s}$, this increase in the total ΔV with respect to the nominal mission is 14.67% while satisfying the constraint on arrival excess velocity at Earth. As per the earlier assumption that an increase in total ΔV up to 15.22% is accepted, the solution $D_{0.8s}$ is recommended at this abort fraction.

From the trajectory visualizations shown in Figure 7.28 and 7.31, it can be concluded that the trajectory solution $D_{0.8s}$ has characteristics similar to that of the trajectory solution $D_{0.6s}$. The total trip time of the $D_{0.8s}$ solution is about 889 days while the nominal mission has a total trip time of 879 days. Therefore, by following the similar rationale mentioned in the earlier section for the solution $D_{0.6s}$, the nominal

Mars-to-Earth trajectory might be a better option to return the crewed S/C back to Earth compared to the trajectory solution $D_{0.8s}$.

7.4. Comparative Analysis

The first research sub-question of this thesis work was aimed at obtaining the optimum ballistic transfer trajectory solutions for a reconnaissance human Mars mission, launched from Earth during the 2028 opportunity. By investigating the mission scenarios *MS-1* and *MS-2*, four transfer trajectory solutions - A_N^c, B_N^c, A_N^e and B_N^e - were computed and out of these solutions, the solution A_N^c was then chosen for the Earth-to-Mars and Mars-to-Earth transfers of the nominal mission. The total ΔV requirement, total mission duration, and the interplanetary transit duration associated with this solution define the baseline requirements for the reconnaissance human Mars mission of interest.

However, as mentioned earlier, it is important to include a fail-safe provision of returning the crew back to Earth in such a mission, in case it is aborted during the journey of the crew to Mars or during the nominal Mars surface stay period. The second and third research sub-questions of this thesis work investigated such Earth-return abort trajectory options through the mission scenarios *MS-3*, *MS-4*, and *MS-5*. A number of abort trajectory options were presented in earlier sections of this chapter. Out of the five to six solutions selected at every abort fraction (i.e. for different abort epochs), one abort trajectory solution was recommended due to its superiority over others.

It follows naturally that if possible, the mission architecture and relevant system elements should be designed to support (ideally) all the recommended abort trajectory options. Therefore, the important mission parameters of these options should be first compared with each other to observe the change in the baseline requirements and to comment upon the feasibility of incorporating the abort trajectory options. The fourth research sub-question of this thesis focuses on such a comparative analysis, which is presented in Table 7.12. In this table, the recommended transfer and abort trajectory solutions are listed along with the computed values of the associated important mission parameters. The reader can quickly compare the total ΔV requirements and the total trip times for these solutions through a visual inspection of Figure 7.33.

Abort fraction	Recom. solution	Inclusion of a Mars swing-by	Total ΔV [m/s]	Total trip time [days]	Transit time in space [days]	V_∞ at Earth arrival [m/s]	Minimum distance to the Sun [AU]
Nominal mission (Earth-to-Mars and Mars-to-Earth ballistic transfers)							
-	A_N^c	No	10415.57	878.81	360.00	8350.27	1.00
Mission abort during the nominal Earth-to-Mars transfer							
0.2	$C'_{0.2}$	No	11000.00	300.63	300.63	2705.70	0.94
0.4	$C'_{0.4}$	No	11000.00	337.62	337.62	6129.13	0.83
0.6	$C'_{0.6}$	No	11000.00	361.37	361.37	9303.25	0.73
0.8	$A'_{0.8}$	Yes	10999.56	443.46	443.46	9359.69	0.50
Mission abort during the nominal Mars surface stay period							
0.2	$C'_{0.2s}$	No	12000.00	858.58	754.82	6558.94	1.01
0.4	$C'_{0.4s}$	No	12000.00	876.84	669.31	6886.60	1.01
0.6	$D_{0.6s}$	No	11927.46	889.29	578.00	6601.44	1.02
0.8	$D_{0.8s}$	No	11941.54	889.05	474.00	6645.60	1.02

Table 7.12: Important mission parameters for all the recommended transfer and abort trajectory solutions for a reconnaissance human Mars mission. Mission scenarios *MS-3* and *MS-4* investigate the abort trajectory solutions when the mission abort occurs during the nominal Earth-to-Mars transfer. Mission scenario *MS-5* investigates the abort trajectory solutions when such an abort occurs during the nominal Mars surface stay period.

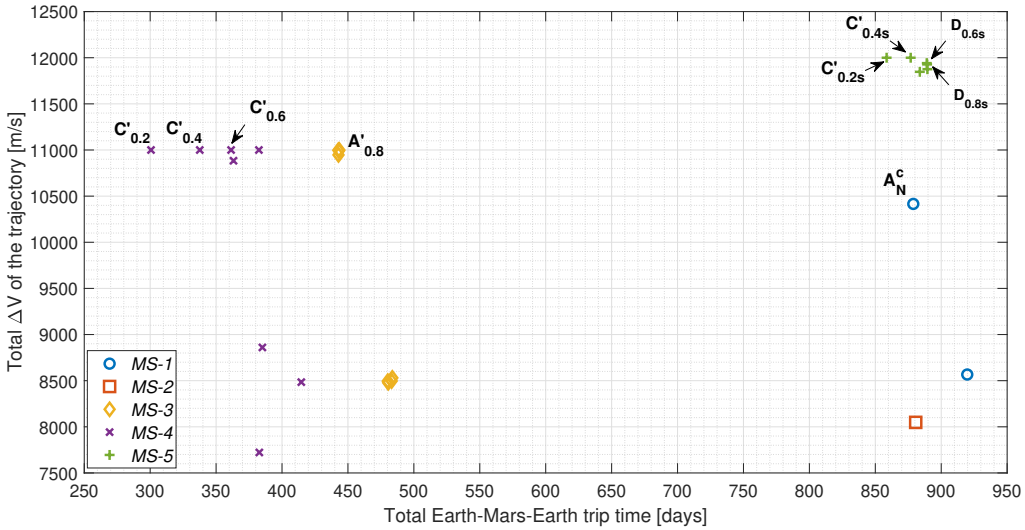

Figure 7.33: Comparison of the recommended transfer and abort trajectory solutions for a reconnaissance human Mars mission. Solution identifiers are provided only for such recommended trajectory solutions. The markers without identifiers represent a few of the selected trajectory solutions which have not been recommended but have a total ΔV and trip time close to those for the recommended solutions.

Based on the information presented in Table 7.12 and Figure 7.33, the architecture of a reconnaissance human Mars mission should have the following characteristics to support the recommended transfer and abort trajectory solutions.

- Total ΔV capacity of at least 12000 m/s is essential for the TV and it should be utilized for the Earth-departure, Mars capture/departure/powered swing-by, abort maneuvers and DSM(s).
- Different elements of the mission architecture should support an Earth-Mars-Earth trip duration of at least 890 days. Any physical/mental health considerations of the crew for this duration of the mission should be considered.
- For the TV, adequate measures for radiation protection and mitigation of adverse effects of the prolonged weightlessness condition and a functioning life-support system (including the consumables) should be provided for the in-space duration of at least 755 days.
- The taxi vehicle to be used by the crew to return to the surface of Earth and the associated Earth-capture trajectory design should be compatible with the maximum Earth-arrival excess velocity value of 9360 m/s.
- For the TV, the radiation protection system and thermal management system should be able to function effectively for a minimum heliocentric distance of 0.5 AU.

The above characteristics of the mission architecture are based on the recommended solutions of this chapter. The reader can refer to Figure 7.34 for an overview of all the selected transfer and abort trajectory solutions presented in this chapter.

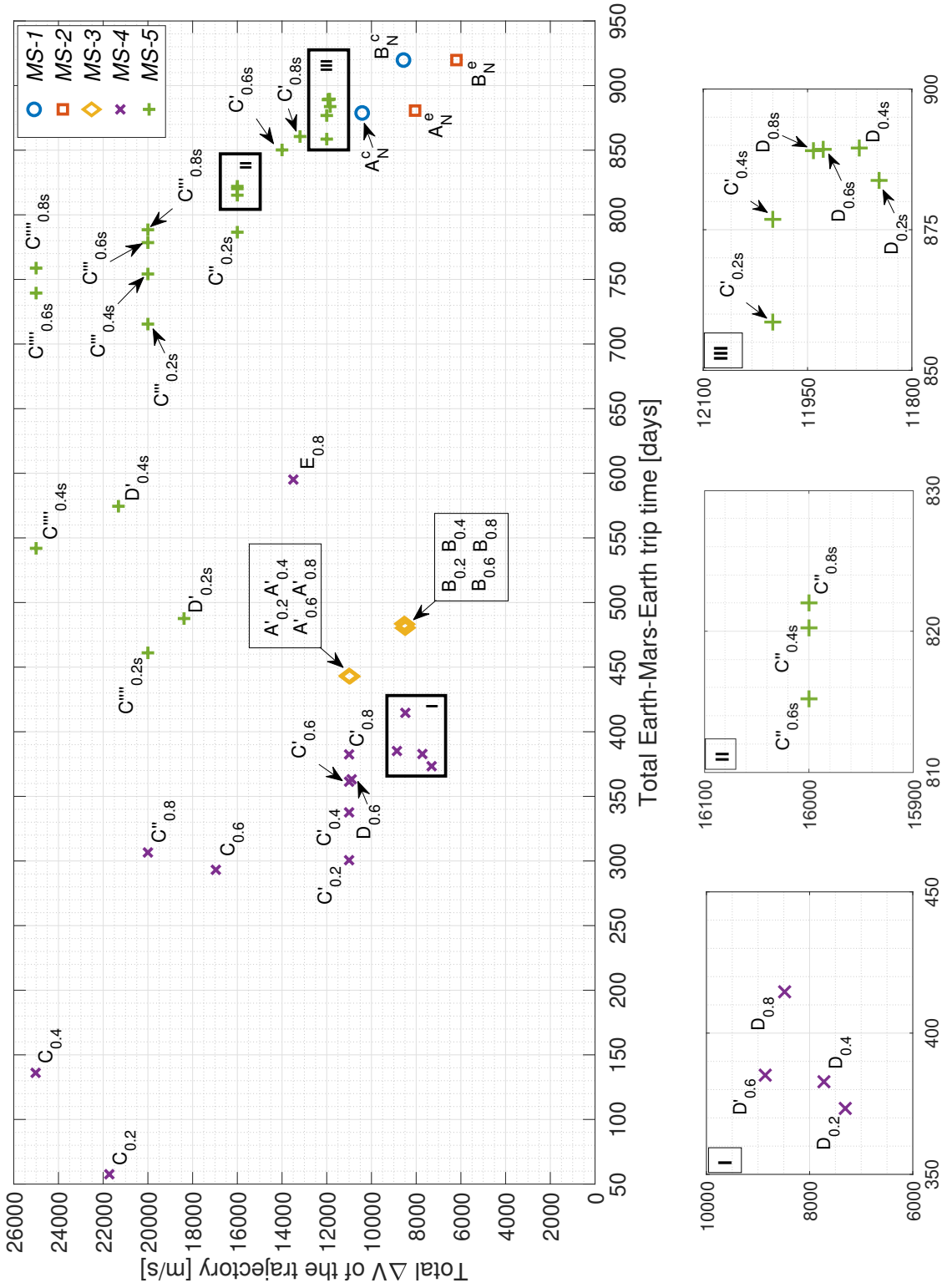

Figure 7.34: All transfer and abort trajectory solutions selected from the associated solution sets for the five mission scenarios.

7.5. Estimation of the IMLEO

Based on the results presented in the previous section, it is now possible to estimate the IMLEO for the TV of a reconnaissance human Mars mission. As mentioned before in Section 3.1, the payload mass of 70 metric tons has been assumed for such a mission. Using Equations 7.1 and 7.2 [1], the mass ratio (q) and the gear ratio (G)[5] can be computed for the TV, for a given ΔV requirement. In Equation 7.1, g_0 refers to the standard acceleration due to gravity.

$$q = \frac{\text{Initial mass}}{\text{Final mass}} = e^{\frac{\Delta V}{g_0 \cdot I_{sp}}} \tag{7.1}$$

$$G = \frac{\text{Initial mass}}{\text{Payload mass}} = \frac{q}{1 - K \cdot (q - 1)} \tag{7.2}$$

When a single-stage propulsion system is used by the TV, the IMLEO of the mission can become unrealistically high. In fact, for a number of values for the I_{sp} and K, it is not possible to obtain the total ΔV of 10415.57 m/s as required by the nominal mission, using a single-stage propulsion system for the S/C. It makes sense to utilize a multi-stage propulsion system in such a case and jettison the unnecessary elements. As three propulsive maneuvers are associated with the nominal mission (adding up to the total ΔV of 10415.57 m/s), a three-stage propulsion system can be used. The estimated IMLEO for the S/C, using one of the two different propellant combinations, is shown in Table 7.13.

CH_4/O_2						**H_2/O_2**					
I_{sp}	K					I_{sp}	K				
	0.04	**0.06**	**0.08**	**0.1**	**0.12**		**0.08**	**0.1**	**0.12**	**0.14**	**0.16**
360	1667	1872	2113	2400	2744	420	1248	1372	1515	1679	1868
370	1524	1702	1910	2154	2445	435	1122	1227	1346	1481	1636
380	1400	1556	1736	1947	2195	450	1016	1106	1206	1320	1449

Table 7.13: Estimation of the IMLEO (in metric tons) considering the ΔV requirements for a nominal reconnaissance human Mars mission when the crewed S/C has a three-stage chemical propulsion system. Either CH_4/O_2 or H_2/O_2 propellant combination is used for all three stages. The assumed payload mass is 70 metric tons.

The IMLEO values shown in Table 7.13 are computed by multiplying the gear ratios of individual stages and the payload mass of the TV. Due to an uncertainty in the exact values for the parameters of the propulsion system, the analysis is performed for a number of values within the typical range of values found in literature (refer to Table 3.2). Cryogenic propellants such as H_2/O_2 have a higher value for K compared to space storable propellants such as CH_4/O_2, due to the extra insulation mass or the mass of a cryocooler system. Moreover, as it is expected that for a large-scale propulsion system, such as those to be used for the TV of a reconnaissance human Mars mission, the value of K will reduce [1]. Therefore, the computations are also performed for the values of K equal to 0.04 and 0.08 for CH_4/O_2 and H_2/O_2 propellants, respectively.

As seen in Table 7.13, the estimated values for the IMLEO are in thousands of metric tons. The order of magnitude for these values is in agreement with that of the expected wet mass (1320 metric ton [22]) for the *Starship* S/C in-development by the *SpaceX Cooperation* for its proposed human Mars mission. It should be noted that the human Mars exploration mission proposed by the *SpaceX Cooperation* uses the ISRU technology for the propellant production at Mars, which will reduce the mass to be launched from Earth. For the reconnaissance mission of this thesis work, no such dependence on the ISRU technology has been assumed.

With the most optimistic values for the I_{sp} and K, the estimated IMLEO for the nominal mission is about 1016 metric tons, using the H_2/O_2 propellants. On the other hand, the more conservative values lead

[5]The terminology of the gear ratio has been used in [1] for a direct estimation of the initial rocket mass from the known values of the payload mass, q and K. It is the inverse of the payload ratio (λ), which is a common terminology for the multi-stage rocket [47].

to an estimated IMLEO of about 2744 metric tons with the CH_4/O_2 propellant combination. Thus, the uncertainty in the performance of a propulsion system and the choice of propellants can change the minimum estimated value of IMLEO by 170%.

However, the TV should be capable of providing a total ΔV of at least 12000 m/s, in order to support all the recommended abort trajectory options of this thesis work. When the individual ΔV requirements of possible propulsive maneuvers are considered, it can be seen that only the TMI maneuver (having a ΔV of about 4360 m/s) is common to all such trajectories and the subsequent maneuvers have different ΔV values. In such a case, it is logical to design a two-stage propulsion system for the TV that is capable of providing ΔVs of about 4360 and 7640 m/s, respectively through two stages. The estimated IMLEO values of the TV equipped with such a two-stage propulsion system are shown in Table 7.14.

CH_4/O_2						H_2/O_2					
I_{sp}	K					I_{sp}	K				
	0.04	**0.06**	**0.08**	**0.1**	**0.12**		**0.08**	**0.1**	**0.12**	**0.14**	**0.16**
360	3367	4583	6824	12179	40262	420	2678	3460	4741	7187	13580
370	2971	3930	5577	8993	19952	435	2272	2844	3717	5193	8183
380	2645	3416	4668	7013	12847	450	1959	2394	3021	3998	5707

Table 7.14: Estimation of the IMLEO (in metric tons) considering the ΔV requirements of the recommended Earth-return abort trajectories for a reconnaissance human Mars mission. The crewed S/C has a two-stage chemical propulsion system that uses either CH_4/O_2 or H_2/O_2 as propellants for both stages. The assumed payload mass is 70 metric tons.

As seen in Table 7.14, there is a considerable increase in the estimated IMLEO values for the TV when all the recommended abort-trajectory solutions are to be supported by the S/C (through an increase of about 15.22 % in the total ΔV capability). For example, a propulsion system that uses H_2/O_2 as the propellants and has the most optimistic values for the I_{sp} and K, the minimum estimated IMLEO is about 1959 metric tons. This is about 93% increase in the minimum estimated IMLEO when a two-stage propulsion system is to be used (instead of a three-stage propulsion system) with an extra ΔV capability to support the abort trajectories.

On the other hand, with more conservative values for the I_{sp} and K with either CH_4/O_2 or H_2/O_2 propellants, the estimated IMLEO values are unrealistically high. For example, when the I_{sp} of 360 s and K of 0.12 is assumed for the CH_4/O_2 based two-stage propulsion system, the estimated IMLEO is more than 40000 tons, which is certainly impossible to achieve with the current or near-future technologies. Such a higher estimated values for the IMLEO emphasize on the necessity to develop more efficient chemical propulsion systems and/or to increase the TRLs of other beneficial technologies such as the in-situ propellant production or the re-usability of the launch vehicles for the human Mars mission to have more feasible requirements.

It is important to realize that when the Earth-return abort trajectory options are provided for a reconnaissance human Mars mission, the in-situ produced resources such as the propellants can not be utilized for the off-nominal mission operations. In such a case, the TV needs to carry all required propellant mass to support the abort trajectory options. Comparison of Tables 7.13 and 7.14 clearly shows how the provision of fail-safe provisions such as the abort trajectories will significantly impact the IMLEO (and in turn, the launch cost) of a human Mars mission.

For the two-stage propulsion system under consideration, it is also possible to utilize two different sets of the propellants for each stage. To avoid the unnecessary propellant boil-off losses associated with the cryogenic propellants (H_2/O_2), the second stage of the propulsion system can utilize CH_4/O_2 propellants. On the other hand, the more efficient H_2/O_2 propellants can still be used for the first stage of the propulsion system, without providing any long-term provisions against the propellant boil-off losses. The estimated IMLEO values of the TV equipped with such a two-stage propulsion system, that uses different sets of the propellants, are shown in Table 7.15.

Estimation approach	Stage	Propellants	I_{sp} [s]	K	Gear ratio	Total gear ratio	IMLEO [t]
Optimistic	Stage I Stage II	H_2/O_2 CH_4/O_2	450 380	0.08 0.04	3.11 10.67	33.17	**2322**
Conservative	Stage I Stage II	H_2/O_2 CH_4/O_2	420 360	0.16 0.12	4.13 118.16	487.97	**34158**

Table 7.15: Estimation of the IMLEO (in metric tons) when the crewed S/C has a two-stage chemical propulsion system that uses H_2/O_2 and CH_4/O_2 as the propellants for the first and second stages, respectively. The ΔV requirements of the recommended Earth-return abort trajectories for a reconnaissance human Mars mission are taken into account. The payload mass assumed is 70 metric tons.

As seen in Table 7.15, the IMLEO is estimated for the optimistic and conservative values for the parameters I_{sp} and K. The most optimistic values for such parameters of the two-stage propulsion system leads to an IMLEO value of about 2322 metric tons. This value is higher by 18.53% than the minimum estimated IMLEO for the best performance of H_2/O_2 based two-stage propulsion system. On the other hand, the conservative estimation approach will lead to an estimated IMLEO of about 34158 metric tons, which is highly unlikely to be achieved in near future.

All the estimations presented in this section are based on a number of assumptions and are quite sensitive to the exact performance characteristics of the propulsion system. Nevertheless, such first-order analysis clearly highlights the challenge of having a considerably high (if not unrealistically high) IMLEO value for a reconnaissance human Mars mission that provides a fail-safe provision of returning to Earth.

The estimated values of the IMLEO have been presented for the mission architecture that supports all the recommended abort trajectory solutions. The exact values of the trajectory parameters and the choice of such solutions is sensitive to a number of assumptions and constraints. The sensitivity of the results of this thesis work to a few such important assumptions and constraints is discussed in the subsequent chapter.

8

Sensitivity Analysis

Results for various transfer and Earth-return abort trajectory scenarios derived from the solution sets obtained by solving the optimization problems for *MS-1* to *MS-5* were presented in the previous chapter. While selecting or recommending the transfer trajectory solution(s) for the reconnaissance human Mars mission, assumptions have been made regarding the launch opportunities for both legs of this mission, parameters of the planetary parking orbits, etc. For the trade-off and selection of the abort trajectory solutions, assumptions have been made regarding various constraints on the capability of a crewed S/C and the mission architecture. This chapter discusses the sensitivity of the results for various mission scenarios investigated in this thesis to the important assumptions.

Results of the sensitivity analysis are quantitatively and/or qualitatively described in this chapter, in two sections. Section 8.1 describes the sensitivity of the results for the transfer trajectories to three important parameters: the launch opportunity, the altitude of the parking orbit, and the date of departure. Section 8.2 describes the sensitivity of recommended abort trajectory solutions to two important constraints - the constraint on the excess velocity at Earth-arrival and the constraint on the minimum distance to the Sun.

8.1. Transfer Trajectories

Three important parameters for which a sensitivity analysis is performed for the transfer trajectory solution/solution set are the choice of launch opportunity for the outbound and inbound legs of the mission, the actual altitude of the circular parking orbit where the crewed S/C is departed from/captured into, and the actual date of departure from Earth/Mars for an interplanetary transfer.

8.1.1. Launch Opportunity

While investigating the transfer trajectory options with *MS-1* and *MS-2*, both Earth-to-Mars and Mars-to-Earth transfer legs have been considered together and the solution set has been optimized for the total ΔV and the total TOF of these two trajectories. The nominal launch opportunity (from Earth) considered for the outbound leg is 2028. The inbound leg of the mission is assumed to be during the subsequent launch opportunity from Mars in 2030, leading to a conjunction-class transfer. The solution set obtained is sensitive to these assumptions regarding the launch opportunities.

Figures 8.1 and 8.2 show how the solution set changes for the off-nominal launch opportunities for the mission scenarios *MS-1* and *MS-2* respectively. Results for two off-nominal launch opportunities - 2026 and 2031 - for the Earth-to-Mars transfer are shown in these figures, along with the results for the nominal launch opportunity (2028). Similar to the nominal case, it has been assumed that the corresponding Mars-to-Earth transfer will be a conjunction-class transfer, taking place during the subsequent possible launch opportunity from Mars. This assumption leads to the launch opportunities (from Mars) in 2028 and 2033 respectively, for the off-nominal conditions.

As seen in Figure 8.1, the launch of the reconnaissance mission in 2026 requires a higher total ΔV for the same interplanetary transit duration if such a duration is less than about 450 days. The minimum TOF solution obtained for the 2026 launch opportunity has a total interplanetary transit duration of 360 days similar to the nominal transfer trajectory solution A_N^c, due to the same constraints on the design space. However, there is an increase of about 7% in the total ΔV requirement to achieve this same interplanetary transit duration. The minimum total ΔV solution obtained for the 2026 launch opportunity[1] requires a total ΔV of about 7% smaller compared to the B_N^c solution for the nominal launch opportunity, at the cost of an increase in the total TOF by about 11%.

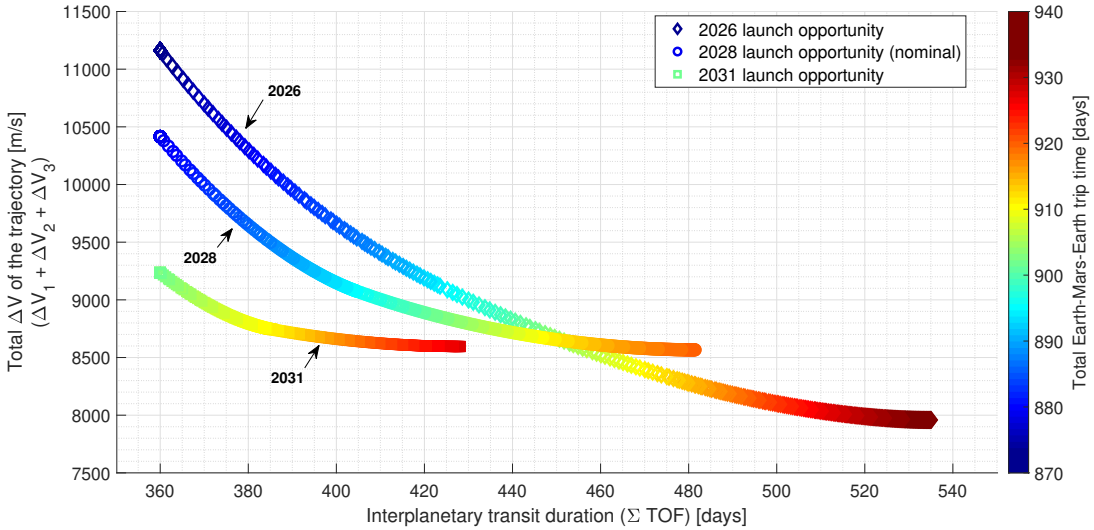

Figure 8.1: Sensitivity of the solution set for *MS-1* to the launch opportunity of the Earth-to-Mars leg. Solution sets at three such launch opportunities - 2026, 2028, and 2031 - are shown. Launch opportunities for the associated inbound legs are 2028, 2030, and 2033 respectively.

On the other hand, if the human reconnaissance Mars mission uses the 2031 launch opportunity instead of the 2028 launch opportunity, the total ΔV required to achieve an interplanetary transit duration of 360 days reduces by about 11%. The minimum total ΔV solution obtained through the optimization process has a total TOF value of about 428 days (smaller by about 11%) with a less than 1% increase in the total ΔV with respect to the nominal launch opportunity.

From Figure 8.1, it is clear that if a minimum total TOF transfer trajectory is used within the 2031 Earth-launch (2033 Mars-launch) opportunity, it will lead to a longer reconnaissance mission. The total Earth-Mars-Earth trip time associated with such trajectories is about 23 days longer than that associated with the A_N^c solution (nominal launch opportunity). This change in the total trip time is only about a week for the minimum total TOF trajectories of the 2026 launch opportunity compared to the A_N^c solution.

Sensitivity analyses of the solution sets obtained at off-nominal launch opportunities with *MS-2* show similar trends. This is expected because the use of an elliptical parking orbit around Mars will only lead to an effective reduction in the total ΔV values, while the optimum planetary departure and arrival epochs remain almost the same as those obtained for the solution set of *MS-1*.

It can be concluded that the choice of launch opportunity will affect the important mission parameters of the transfer trajectories of a reconnaissance human Mars mission by non-negligible amounts. Additionally, some of the launch opportunities might present a better set of propulsive abort trajectory

[1]It should be noted that unlike for the optimization problem of the nominal launch opportunity, the optimization process has explored (or retained the solutions from) a greater portion of the design space while obtaining the solution set for the 2026 launch opportunity. This is evident from the total TOF value of the minimum total ΔV solution at the 2026 launch opportunity: about 535 days. This is very close to the value allowed by the constraints on the design space: 540 days.

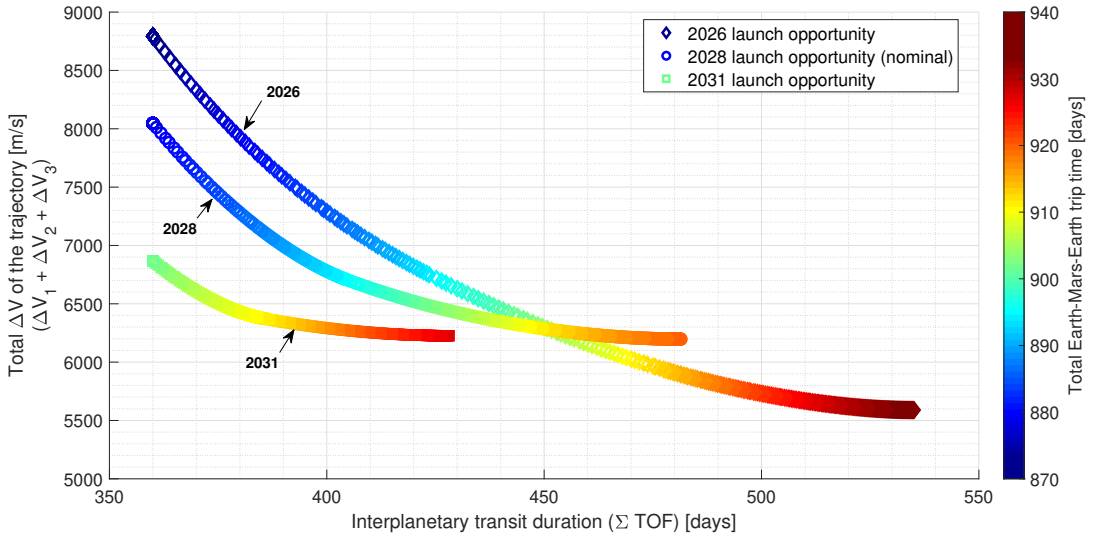

Figure 8.2: Sensitivity of the solution set for *MS-2* to the launch opportunity of the Earth-to-Mars leg. Solution sets at three such launch opportunities - 2026, 2028 and 2031 - are shown. Launch opportunities for the associated inbound legs are 2028, 2030, and 2033 respectively.

options during different phases of the mission than others. Eventually, the choice of the launch window at which the first reconnaissance Mars mission will be executed in reality is driven by a number of technical and non-technical factors. Even though it is not included in this thesis work, it is important to evaluate the effect of potential choices for the nominal launch opportunity on the abort trajectory options.

8.1.2. Altitude of Parking Orbit

Assumed values of the parking orbit parameters viz. altitude of the circular parking orbits or periapsis altitude/period of the elliptical parking orbit result into particular values of the departure and capture ΔV maneuvers for the same excess velocities at departure or arrival (V_∞). Even though the parameters of a parking orbit are pre-defined in the mission design, there can be errors in the orbit insertion process, leading to off-nominal parking orbit altitudes in reality. Tables 8.1 and 8.2 show the effect of such errors on the values of various ΔV maneuvers for the solutions A_N^c and B_N^c, respectively.

For this sensitivity analysis, it has been assumed that the maximum increase or decrease in the altitude of the circular parking orbit around Earth is 5 km. Similarly, the increase or decrease in the altitude of the circular parking orbit altitude around Mars is assumed to be three times higher. A larger possible change (due to a larger possible error) in the altitude of the parking orbit around Mars is assumed because the orbit insertion is now performed at about 400 million km from Earth, where the lack of a navigation system such as the Global Positioning System (GPS) might result into a less accurate navigation.

Moreover, it has been assumed that apart from the altitudes of the parking orbits, all other mission parameters such as the departure epochs and the TOF have their nominal values. Thus, only values of the ΔV for the three propulsive maneuvers of the transfer trajectory solutions A_N^c and B_N^c will be affected. With these assumptions, eight possible combinations of changes in the altitudes of the parking orbits have been analyzed for both solutions, as presented in Tables 8.1 and 8.2, respectively, along with results for the nominal case.

From these tables, it is clear that the A_N^c solution is less sensitive to the changes in the altitude of the parking orbit than the solution B_N^c. The maximum possible changes in the total ΔV values for these solutions are about ± 1.8 and ± 3.6 m/s respectively. These effective changes are very small (less than 0.04% in magnitude) compared to the nominal total ΔV of the mission. Since there will be a design

Nominal altitude of the circular LEO [km]	Nominal altitude of the circular LMO [km]	ΔV_1 [m/s]	ΔV_2 [m/s]	ΔV_3 [m/s]	Total ΔV [m/s]
200.0	300.0	4360.3245	3639.9366	2415.3125	10415.5735
Change in the nominal altitude of the circular LEO [km]	Change in the nominal altitude of the circular LMO [km]	Change in ΔV_1 [m/s]	Change in ΔV_2 [m/s]	Change in ΔV_3 [m/s]	Change in the total ΔV [m/s]
-5.0	0.0	0.8368	0.0000	0.0000	0.8368
-5.0	**-15.0**	**0.8368**	**-0.2259**	**1.1859**	**1.7968**
-5.0	15.0	0.8368	0.2318	-1.1735	-0.1050
0.0	-15.0	0.0000	-0.2259	1.1859	0.9600
0.0	15.0	0.0000	0.2318	-1.1735	-0.9418
5.0	0.0	-0.8356	0.0000	0.0000	-0.8356
5.0	-15.0	-0.8356	-0.2259	1.1859	0.1244
5.0	**15.0**	**-0.8356**	**0.2318**	**-1.1735**	**-1.7773**
Standard deviation of the change in ΔV (Based on the absolute values)		0.3871	0.1060	0.5461	0.6344

Table 8.1: Sensitivity of the transfer trajectory solution A_N^c to the altitudes of the parking orbits. ΔV_1, ΔV_2 and ΔV_3 represent the propulsive maneuvers performed by the S/C for departure from the parking orbit around Earth, capture into the parking orbit around Mars, departure from the parking orbit around Mars, respectively. LMO refers to a low Mars orbit.

Nominal altitude of the circular LEO [km]	Nominal altitude of the circular LMO [km]	ΔV_1 [m/s]	ΔV_2 [m/s]	ΔV_3 [m/s]	Total ΔV [m/s]
200.0	300.0	3848.6746	2739.6227	1978.4378	8566.7351
Change in the nominal altitude of the circular LEO [km]	Change in the nominal altitude of the circular LMO [km]	Change in ΔV_1 [m/s]	Change in ΔV_2 [m/s]	Change in ΔV_3 [m/s]	Change in the total ΔV [m/s]
-5.0	0.0	1.0039	0.0000	0.0000	1.0039
-5.0	**-15.0**	**1.0039**	**0.7574**	**1.8446**	**3.6059**
-5.0	15.0	1.0039	-0.7468	-1.8299	-1.5728
0.0	-15.0	0.0000	0.7574	1.8446	2.6020
0.0	15.0	0.0000	-0.7468	-1.8299	-2.5766
5.0	0.0	-1.0026	0.0000	0.0000	-1.0026
5.0	-15.0	-1.0026	0.7574	1.8446	1.5995
5.0	**15.0**	**-1.0026**	**-0.7468**	**-1.8299**	**-3.5792**
Standard deviation of the change in ΔV (Based on the absolute values)		0.4644	0.3482	0.8505	1.0556

Table 8.2: Sensitivity of the transfer trajectory solution B_N^c to the altitudes of the parking orbits. ΔV_1, ΔV_2 and ΔV_3 represent the propulsive maneuvers performed by the S/C for departure from the parking orbit around Earth, capture into the parking orbit around Mars, departure from the parking orbit around Mars, respectively.

margin in any ΔV budget (especially considering the fact that an extra ΔV capability is required to allow the abort trajectory options), these effects can be considered as negligible.

8.1.3. Departure Date

Optimization of the Lambert targeting problem to find solution sets for the mission scenarios *MS-1* and *MS-2* results in finding such combinations of the planetary departure and arrival epochs that the two objectives of the problem - the total TOF and total ΔV - are minimized. Such optimal planetary departure and arrival epochs were listed for the solutions A_N^c and B_N^c in Section 7.1.

Due to the reasons such as the delay in the launch operations, the actual planetary departure might take place at an epoch before or after the optimal epoch obtained through the trajectory design. This will change the values of the propulsive maneuvers associated with the transfer trajectories. In this section, the results of a sensitivity analysis of the nominal ΔV values to the planetary departure epochs are presented, assuming that such off-nominal epochs are 5 days before or 5 days after the nominal departure epochs. Tables 8.3 and 8.4 show how the values of ΔV change for solutions A_N^c and B_N^c respectively, when the departure epochs for the outbound and inbound legs have off-nominal values.

Nominal Earth-departure epoch [MJD2000]	Nominal Mars-departure epoch [MJD2000]	ΔV_1 [m/s]	ΔV_2 [m/s]	ΔV_3 [m/s]	Total ΔV [m/s]
10609.2528	11308.0651	4360.3245	3639.9366	2415.3125	10415.5735
Change in the nominal Earth-departure epoch [days]	**Change in the nominal Mars-departure epoch [days]**	**Change in ΔV_1 [m/s]**	**Change in ΔV_2 [m/s]**	**Change in ΔV_3 [m/s]**	**Change in the total ΔV [m/s]**
-5.0	0.0	-191.4476	224.9599	0.0000	33.5123
-5.0	**-5.0**	**-191.4476**	**224.9599**	**17.3691**	**50.8813**
-5.0	5.0	-191.4476	224.9599	15.4040	48.9163
0.0	-5.0	0.0000	0.0000	17.3691	17.3691
0.0	5.0	0.0000	0.0000	15.4040	15.4040
5.0	0.0	225.2481	-193.5603	0.0000	31.6878
5.0	-5.0	225.2481	-193.5603	17.3691	49.0568
5.0	5.0	225.2481	-193.5603	15.4040	47.0918
Standard deviation of the change in ΔV (Based on the absolute values)		97.7073	97.9530	7.6398	14.5086

Table 8.3: Sensitivity of the transfer trajectory solution A_N^c to the departure epochs of the outbound and inbound legs. ΔV_1, ΔV_2 and ΔV_3 represent the propulsive maneuvers performed by the S/C for departure from the parking orbit around Earth, capture into the parking orbit around Mars, departure from the parking orbit around Mars, respectively.

For this sensitivity analysis, it has been assumed that all other mission parameters including the TOF for both outbound and inbound legs have their nominal values. Similar to the earlier analysis, eight possible combinations of changes in the Earth-departure and Mars-departure epochs have been analyzed. From Tables 8.3 and 8.4, it is clear that the trajectory solution A_N^c is more sensitive to the changes in the planetary departure epochs compared to the solution B_N^c.

As expected, a change in ΔV_3 is only driven by a change in the Mars-departure epoch but it smaller by one order of magnitude compared to the changes in ΔV_1 and ΔV_2. For the solution A_N^c, if the Earth-departure epoch changes by 5 days, ΔV_1 and ΔV_2 can change as much as by about 225 m/s. However, as an increase in ΔV_1 is accompanied by a decrease in ΔV_2 and vice versa, the effective maximum change in the total ΔV is observed to be about 51 m/s for this particular solution. A similar trend is observed concerning the changes in the ΔV_1 and ΔV_2 for the solution B_N^c and the effective maximum change in the total ΔV is observed to be about 27 m/s.

When compared with the nominal total ΔV requirement of the solutions A_N^c and B_N^c, these maximum changes are only about 0.5 and 0.3%, respectively. If there exists a design margin in the total ΔV budget, it should also account for these estimated changes due to the off-nominal planetary departure epochs.

Nominal Earth-departure epoch [MJD2000]	Nominal Mars-departure epoch [MJD2000]	ΔV_1 [m/s]	ΔV_2 [m/s]	ΔV_3 [m/s]	Total ΔV [m/s]
10590.0487	11262.1482	3848.6746	2739.6227	1978.4378	8566.7351
Change in the nominal Earth-departure epoch [days]	**Change in the nominal Mars-departure epoch [days]**	**Change in ΔV_1 [m/s]**	**Change in ΔV_2 [m/s]**	**Change in ΔV_3 [m/s]**	**Change in the total ΔV [m/s]**
-5.0	0.0	-73.0018	90.8479	0.0000	17.8460
-5.0	-5.0	-73.0018	90.8479	8.9015	26.7476
-5.0	5.0	-73.0018	90.8479	8.6623	26.5083
0.0	-5.0	0.0000	0.0000	8.9015	8.9015
0.0	5.0	0.0000	0.0000	8.6623	8.6623
5.0	0.0	87.6527	-69.7226	0.0000	17.9301
5.0	**-5.0**	**87.6527**	**-69.7226**	**8.9015**	**26.8317**
5.0	5.0	87.6527	-69.7226	8.6623	26.5924
Standard deviation of the change in ΔV (Based on the absolute values)		37.7977	38.4299	4.0667	7.9162

Table 8.4: Sensitivity of the transfer trajectory solution B_N^c to the departure epochs of the outbound and inbound legs. ΔV_1, ΔV_2 and ΔV_3 represent the propulsive maneuvers performed by the S/C for departure from the parking orbit around Earth, capture into the parking orbit around Mars, departure from the parking orbit around Mars, respectively.

8.2. Abort Trajectories

In the previous chapter, five to six Earth-return abort trajectory solutions were selected for comparison at the various abort fractions with mission scenarios *MS-3*, *MS-4* and *MS-5*. One of these abort trajectory solutions was then recommended at that abort fraction considering important trajectory parameters such as the total ΔV requirement, total mission duration or arrival excess velocity at Earth. If the assumptions regarding the feasible values of a number of these parameters are changed, the analysis might result in a different set of recommended abort trajectory options.

This section describes the sensitivity of the abort trajectory solutions to two important possible constraints, that can determine the feasibility of a trajectory solution. These two constraints are the constraint on the excess velocity at Earth-arrival and the constraint on the minimum distance of the S/C to the Sun while following an abort trajectory.

8.2.1. Constraint on Excess Velocity at Arrival

As mentioned in Section 3.1, the mission architecture considered for this thesis work assumes that the crewed S/C has an Earth return taxi vehicle which will perform a near-ballistic re-entry on Earth-arrival. As mentioned in Section 2.3, this implies that a constraint on the hyperbolic excess velocity at Earth-arrival should be applied and the chosen value of such a constraint for this thesis work is 9360 m/s.

While presenting the important parameters of the selected propulsive abort trajectory solutions in Chapter 7, this particular value of such a constraint has been marked in the plots. In reality, the re-entry trajectory and structural/thermal design characteristics of an Earth return taxi vehicle might allow a higher or lower value for the V_∞ than the assumed constraining value. This can change the recommended solution for an abort scenario.

For example, at the abort fraction of 0.6 when the abort occurs during the Earth-to-Mars transfer (*MS-3* and *MS-4*), one of the reasons for not recommending the Earth-return trajectory solution $D'_{0.6}$ despite its lowest total ΔV value (among all the selected solutions) has been that its V_∞ value is greater than 9360 m/s. Similarly for the abort fraction of 0.8 analyzed with *MS-3* and *MS-4*, three Earth-return trajectory solutions without a Mars swing-by - $C''_{0.8}$, $C'_{0.8}$, and $D_{0.8}$ - have not been recommended because

their V_∞ values are greater than 9360 m/s. Out of these three trajectory solutions, $C'_{0.8}$ and $D_{0.8}$ have an attractive mission duration length and more feasible total ΔV requirement.

In case of an abort during the nominal Mars surface stay period (*MS-5*), the first three Earth-return trajectory solutions from the set of selected solutions at every abort fraction have not been considered further because their V_∞ values are greater than 9360 m/s. As the associated values of the total ΔV with such solutions are greater than at least 16000 m/s, the decision about not recommending these solutions is unlikely to be changed. However, such observations highlight the fact that better Earth-return abort trajectory solutions can be recommended given the exact known value of the possible constraint on V_∞ through in-depth mission and trajectory design. Such trajectory solutions might gain performance with respect to the other mission parameters if higher values of V_∞ are allowed.

The range of arrival excess velocity at Earth, that the Earth-return taxi vehicle has to experience with all the possible mission abort scenarios is another important factor to be accounted for in the design of Earth re-entry system and trajectory. As seen in Table 7.12, this range for the recommended interplanetary transfer and abort trajectories of this thesis work is about 2706 to 9360 m/s.

Finally, it has been observed that the optimization process has failed to retain/identify all the expected points on the Pareto front for the optimization problems of *MS-3* and *MS-4*. Multiple cases of such optimization problems have been solved to obtain the important points of the solution sets, some of which are the selected trajectory solutions of this thesis work. A number of these optimization problem cases have been solved with the assumed value of 9360 m/s for the constraint on V_∞. Changing the exact value of this constraint might change the solution set obtained (through retention/identification of new points) and might provide new solutions that are superior compared to those selected and recommended in this thesis work.

8.2.2. Constraint on Minimum Distance to the Sun

Effective radiation protection for an interplanetary human space mission such as the reconnaissance human Mars mission considered in this thesis work remains a critical challenge to be solved in the upcoming decade. Space radiation has two major components: the electromagnetic radiation and charged particles. There are two sources of the charged particles: Solar Particle Events (SPE) and Galactic Cosmic Rays (GCR) [48]. Charged particle radiation due to SPE can define how close the crewed S/C can travel to the Sun with the provided radiation shielding measures. The design of sufficient protection measures against both sources of the charged particles, with minimum possible impact on the mass of the S/C, is another problem in itself.

Protons released during the SPE have usually have energies below hundreds of MeV even though the current models available to predict such events are described as inadequate [49]. Due to such low energies, [48] has concluded that the localized passive radiation shielding approaches are adequate for the protection against the SPE radiation. Some of the passive radiation shielding materials are high-density polyethylene and liquid water.

Even though the passive radiation shielding approach is claimed as effective, it can add excessive structural mass to the crewed S/C if designed with a conservative approach considering the inaccurate models and insufficient prediction capabilities. With a higher ΔV requirement of a reconnaissance mission supporting a number of abort trajectory options, this increased structural mass can translate into a very high (possibly unrealistic) IMLEO. Moreover, the placement of such radiation shielding measures should be optimized while ensuring that a sufficient livable volume of the S/C is available to the crew on a long-duration space mission, considering their psychological health [48].

Interestingly, during the period of solar maximum, the number of SPE increases, but due to the increased solar wind intensity during such a period the incoming GCR flux decreases [48]. This complex relationship between GCR flux, solar wind and SPE has also to be taken into account along with the phase of the solar cycle during the period of interplanetary voyage. Based on all these factors, a constraint on the minimum distance to the Sun might have to be introduced.

Another reason for introducing such a constraint or preferring one Earth-return abort trajectory solution over another based on the minimum distance to the Sun is the thermal management of a crewed S/C. To understand the requirements of a thermal management subsystem, preliminary computations of the equilibrium temperature of a body (such as the crewed S/C) in the Solar System at various distances are performed for a number of Bond albedo [2] (A_B) values. Results of such computations are presented in Figure 8.3. The S/C is assumed to behave like a black body and Equation 8.1 is used to estimate its equilibrium or effective black-body temperature (T_{eq}).

$$T_{eq} = \left[\frac{I_0(1 - A_B)}{4\sigma}\right]^{\frac{1}{4}} \tag{8.1}$$

In the above equation, I_0 is the incident solar radiation at 1 AU (solar constant) and it has value of 1366 W/m^2 [18]. σ is the Stefan–Boltzmann constant.

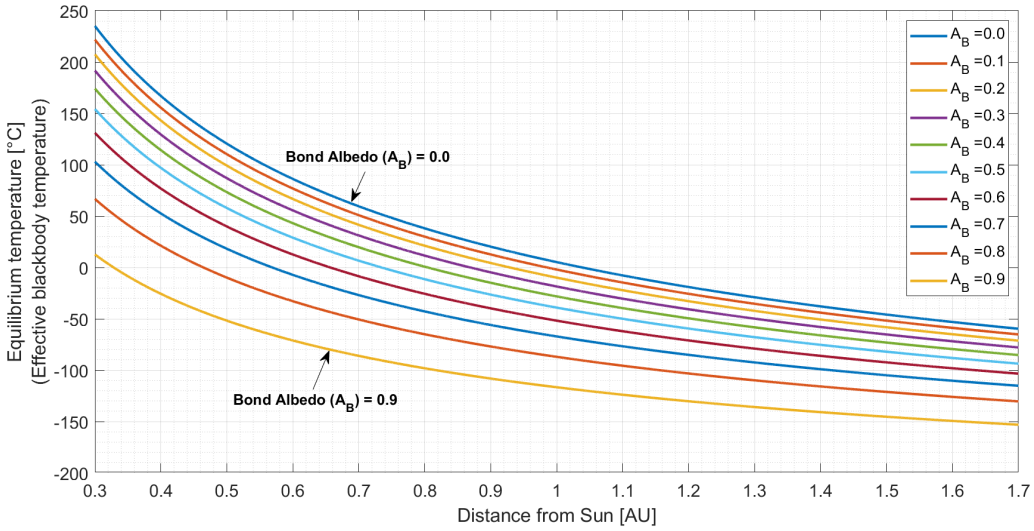

Figure 8.3: Equilibrium temperature as a function of distance from the Sun, for various values of the Bond albedo (A_B).

While obtaining solution sets for the abort trajectory options, which have been presented in Chapter 7, *no constraint has been imposed* for the minimum distance to the Sun due to uncertainty in the exact value of such a constraint. The average perihelion distance of the Venus was marked for reference in all plots for this mission parameter[3]. Depending upon the radiation protection and thermal management system's requirements, some of the recommended abort trajectory solutions might require special attention. For example, for the abort trajectory solution $A'_{0.8}$ which performs a Mars swing-by maneuver, the closest approach to the Sun is at 0.50 AU. The equilibrium temperature at this distance will be somewhere between $120°$ and $-50°$ depending upon exact Bond albedo for the S/C. The maximum distance of the S/C from the Sun would also have an effect on the design of the thermal management system in addition to other considerations such as power generation.

Therefore, it can be concluded that the exact value of the constraint on the minimum distance to the Sun is likely to change the set of recommended solutions for the abort scenarios. Due to the large uncertainty in the available literature and the lack of expertise by the author himself, an in-depth sensitivity analysis in this regard is considered as future scope of this thesis work.

In Chapter 9, conclusions based on the results presented in this and the previous chapter are listed.

[2] The definition of Bond albedo as per [18] is "the ratio of the total radiation reflected or scattered by the object to the total incident light from the Sun."

[3] The perihelion distance of Venus has been marked because reaching such a distance with the crewed S/C of a Mars mission has been mentioned as one of the problems of the opposition class mission architecture, from the perspective of radiation hazards, in literature such as [3].

9

Conclusions

The research objective of this thesis work has been to investigate the ballistic transfer and propulsive abort trajectory options for a reconnaissance human Mars mission. In earlier chapters of this report, important aspects of such an investigation have been described. The solutions obtained for the high-thrust transfer and abort trajectories have been presented in Chapter 7. Chapter 8 presented the results of the sensitivity analyses of such solutions to a number of important parameters and assumptions. Conclusions based on all such results can now be summarized as follows.

1. Solution sets for the ballistic Earth-to-Mars (outbound) transfer and ballistic Mars-to-Earth (inbound) transfer belonging to the conjunction class mission architecture have been presented assuming either a circular or an elliptical parking around Mars. A reconnaissance human Mars mission, that uses the 2028 opportunity for a 180-day outbound transfer and uses the 2030 opportunity for a 180-day inbound transfer, would require a total ΔV of about 10416 m/s if the parking orbit around Mars is circular.

2. For a similar value of the transit duration, the total ΔV requirement of the ballistic outbound and inbound transfer trajectories is highly sensitive to the chosen launch opportunity. For example, the total ΔV requirement of the minimum transit time solutions can either increase by about 7% or decrease by about 11% if the launch from Earth is scheduled in 2026 or 2031 respectively, instead of the nominal launch in 2028.

3. For the nominal launch opportunity, the minimum total ΔV solution is more sensitive to the orbit-insertion errors compared to the minimum total transit duration solution. With a ± 5 km variation in the altitude of the circular parking orbit around Earth and with a ± 15 km variation in the altitude of the circular parking orbit around Mars, the maximum total ΔV change can be 3.6 m/s. Compared to the nominal ΔV requirement, such changes can are negligible (less than 0.04%).

4. If instead of the optimum planetary-departure epochs, the actual departure epochs change by ± 5 days, then a maximum effective increase of about 51 m/s in the total ΔV is required to maintain the nominal transit duration of 180 days for both outbound and inbound transfers. This 0.5% increase indicates that the ballistic transfer trajectories have a higher sensitivity to the departure epoch than to the parking orbit parameters but the sensitivity is highest to the launch opportunity, compared to these two parameters.

5. It is possible to provide the Earth-return abort trajectory options for the reconnaissance human Mars mission if such a mission is aborted after 20%, 40%, 60%, and 80% of the nominal Earth-to-Mars transit time or the Mars surface stay period. With a 15.21% increase in the nominal ΔV requirement, at least one Earth-return abort trajectory exists at all such abort epochs that meets the imposed constraint of 9360 m/s on the hyperbolic excess velocity (V_∞) at Earth-arrival.

6. Changing the value of such a constraint on the V_∞ at Earth-arrival might lead to superior abort trajectory options. However, the feasibility of such interplanetary trajectories should be analyzed considering the re-entry characteristics of Earth return taxi vehicle that is employed in the mission architecture.

7. The recommended Earth-return abort trajectories of this thesis work differ significantly from each other with respect to the trajectory parameters such as the total mission duration, total time in space (total transit duration), V_∞ at Earth-arrival. The transfer vehicle and associated Earth return taxi vehicle should be designed to meet the relevant worse-case requirements if the mission abort scenario is to be supported at all the considered epochs during the nominal duration of the mission.

8. The nominal mission duration for the chosen transfer trajectory solution is about 879 days. The recommended abort trajectory options for an abort during the Mars surface period result in a total trip time that approaches the nominal value. Thus, under such circumstances, the crew might have to wait for a similar period of time, as they would have waited in the nominal scenario, before they can return to Earth. If the cause of an abort relates to health issues of the crew or the failure of any life-support systems, such an abort situation can prove fatal.

9. At least until 60% of the nominal Earth-to-Mars transfer duration, it is possible to abort the mission and return safely to Earth along the trajectories having a transit duration less than or almost the same as the nominal mission. With the subsequent abort epochs, all the recommended abort trajectory solutions have a higher total transit duration than the selected trajectories for the nominal mission.

10. In case the mission is aborted at 20% of the nominal Mars surface period, the recommended abort trajectory solution has the highest transit duration (of about 755 days). Such a high transit duration is expected because the relative positions of Earth and Mars would force the TV to take a longer path if the imposed constraints are to be satisfied. Any radiation shielding measures and the provisions to mitigate the adverse effects of the prolonged weightlessness should be provided on-board the TV for this worse case requirement of about 755 days.

11. The radiation protection system and thermal management system might limit the distance of the closest approach of the TV to the Sun. For the recommended abort trajectories, the closest approach to the Sun occurs at the distance of 0.5 AU while utilizing a Mars swing-by (after the abort at 80% of the nominal Earth-to-Mars transfer period). If solutions such as these are deemed infeasible, then some of the other imposed constraints or the values of the parameters for the abort trajectory design might have to be changed.

12. While recommending a solution from the set of selected abort trajectory solutions, an increase in the total ΔV requirement (compared to the nominal transfer trajectories) has been limited to 15.21%, leading to a limiting total ΔV of 12000 m/s. If any other trajectory parameter such as the total transit duration is to be improvised, then a higher ΔV capability might have to be allocated for a reconnaissance human Mars mission that provides the abort trajectory options.

13. However, any further increase in the total ΔV capability of the S/C will result in the IMLEO requirement, which might be very difficult to achieve with the current technologies in near future. The minimum possible IMLEO for the TV that can support all the investigated abort trajectory options was estimated to be 1959 metric tons, by assuming the best performance of the H_2/O_2 based two-stage propulsion system. Considering the launch capabilities of various super heavy-lift launchers, more than one launch will be required to assemble and re-fuel such a heavy TV in a parking orbit around Earth. Therefore, further improvement in the performance of available abort trajectories and/or reduction of IMLEO needs the development of efficient propulsion technology.

14. If the computed propulsive abort trajectory solutions (for the mission abort at the various epochs of interest) are compared with the propulsive abort trajectory solutions presented in [2] (for a mission abort at the Mars-arrival epoch), the values for the total mission duration of the abort trajectories are consistent. When the mission abort occurs after 80% of the nominal Earth-to-Mars transfer duration, the recommended trajectory solution has a trip time of about 444 days. On the other hand, with the mission abort after 20% of the Mars surface stay period, the recommended abort trajectory solution has a total mission duration of about 859 days. Even though the values of the total ΔV requirements are not provided in [2], the listed propulsive abort trajectory solutions with a different abort ΔV during the Mars swing-by have trip times between 700 to 800 days for the 2028 Earth-departure opportunity (refer to Figure 2.7).

During the thesis work, a number of aspects for the optimization of transfer and abort trajectory solutions have been identified which have the potential to improvise the results of this work and modify the conclusions listed above. Due to time constraints, such aspects were not worked upon but they are listed as the recommendations for future work in the next chapter.

10

Recommendations

The recommendations for a research work in future, investigating the abort trajectory options for a human Mars mission, can be listed as follows.

1. While studying the mission heritage during the literature study phase, a number of technologies were identified that can influence the characteristics of a human Mars mission. Two such technologies - aeroassist and propellant production through the ISRU - have been summarized in Section 2.2. Performing aerobraking or aerocapture maneuvers at Mars would reduce the ΔV requirement from the propulsion system of the transfer vehicle. Propellants such as the liquid methane-liquid oxygen (CH_4/O_2), produced through an ISRU system on the Martian surface, can be used to eliminate the propellant mass to be carried by the TV for the Mars ascent taxi vehicle. To maintain the applicability of results produced during this thesis research in the near future, such technologies are not considered for the selected mission architecture. However, if these technologies achieve the required TRL before an actual reconnaissance human Mars mission is executed in the future, they should be considered for the mission architecture. Such inclusion of these technologies will definitely lead to superior solutions that have more feasible IMLEO estimates than those presented in this thesis.

2. Two more technologies that can be used to reduce the ΔV budget for a reconnaissance human Mars mission are - aero-gravity assist maneuvers during a Mars swing-by and Lunar gravity assist maneuvers. Moreover, if the abort trajectories crossing the (average) orbital distance of Venus are allowed, a powered/unpowered gravity assist at Venus (before the TV comes back to Earth) can help to reduce the ΔV cost of a mission.

3. For the ballistic transfer trajectory solutions of the mission, the conjunction-class architecture was selected. As this architecture utilizes the best configuration of relative positions of Earth and Mars for sending the TV on an interplanetary voyage, the epochs other than the optimum epochs for the interplanetary transfers, such as the abort epochs do not have an equally attractive configuration for the relative positions of the planets. This was evident from the obtained abort trajectory solutions, which often have a longer transit duration after the mission is aborted. Use of a longer Earth-to-Mars *transfer* obtained through an conjunction-class architecture might improvise the available *abort* trajectory solutions, at the cost of deteriorating performance of the former in terms of transit duration and/or the ΔV requirement. A trade-off analysis might lead to the best combination of sub-optimal transfer and optimal abort trajectory solutions.

4. Instead of using the ballistic transfer trajectories, the trajectories having one or more DSM(s) can be used for the nominal transfer to/from Mars. By including the DSM(s), the problems regarding a longer transit duration of the ballistic transfer trajectories of the opposition-class mission might be eliminated while ensuring that the abort trajectories benefit from more attractive relative positions of Earth and Mars. Similarly, the inclusion of more than one or two DSMs for the propulsive abort trajectories would expand the design space and might lead to superior abort trajectory solutions.

5. To find the optimum transfer and abort trajectory solutions in this thesis, the ΔV costs of all the propulsive maneuvers of the mission scenario are added together and then used as one of the objectives. However, depending on the exact distribution of mass elements within the mission architecture and the configuration of a multi-stage propulsion system, some of the propulsive maneuvers would be costly (in terms of the actual propellant mass required) than others. For example, having a smaller value for the TMI ΔV is often more desired than having a smaller value for the TEI ΔV. In such a case, appropriate weighing factors can be applied for different ΔV costs of the transfer and abort trajectories and better solutions can be obtained for the given configuration of mass elements and/or the stages of a propulsion system.

6. The computed optimum abort trajectory solutions are also limited by the chosen boundaries of the design space, for various design variables such as the in-plane angle (θ) for hyperbolic excess velocity in the MGA-1DSM-VF model. For the design variables related to the TOF, broad design spaces have been usually explored through multiple optimization problem cases. However, comparatively narrower design spaces have been explored for the other design variables of the thesis work. An expansion of the design space might lead to better trajectory solutions than those presented in this report.

7. The optimization process followed in this thesis is not perfect considering the fact that not all important points or portions of the Pareto front were naturally identified/retained with the progression of the process. As mentioned in the case of the solution sets obtained for mission scenarios *MS-4* and *MS-5*, a number of optimization problem cases (with different boundaries for the design space and different values for the imposed constraints) have been solved to obtain the important points on the Pareto front. Instead of this, the optimization process itself can be improvised to fix this issue and two potential solutions are - the fine-tuning of various parameters for a particular optimization algorithm and the change of the algorithm itself.

8. A meta-heuristic global optimization algorithm has been used for finding the solutions to the optimization problems. While such an algorithm tries to explore all the points in design space, minor or sometimes even major improvements in the obtained solutions are possible. Through the use of local optimization techniques or Monte-Carlo analysis, the obtained solutions can be subjected to a local-refinement process to check for any improvements and to ensure the optimality of the computed results.

9. Unlike the transfer trajectory solutions, the abort trajectory solutions have not been subjected to an extensive quantitative sensitivity analysis. By investigating how the sensitivity of the nominal transfer trajectory solution (to parameters such as the launch opportunity, departure epochs, TOF) translates into the sensitivity of associated abort trajectory solutions, a more comprehensive analysis can be performed in the future.

10. Finally, the computed high-thrust trajectory solutions of this thesis work are the solutions to a low-fidelity case where the orbital perturbations have been totally neglected and analytical or semi-analytical methods such as the Lambert targeting problem, the trajectory model have been used to find the interplanetary trajectories. While this is a good first-order approximation of the problem, it should be followed by a high-fidelity analysis that accounts for relevant orbital perturbations, to increase the accuracy of the obtained results. Numerical propagation scheme(s) and numerical integration routine(s) should be used for such a high-fidelity analysis.

A

Appendix: Lambert Targeting Problem

Classification of Formulations

Classification of various formulations for a solution of the the Lambert targeting problem is described below, with the names of researchers or authors indicating various approaches. This classification can be found in [30] and it uses the choice of the free parameter and the major lines of research as a basis to categorize the various formulations.

- Universal variables
  - Lancaster & Blanchard, Gooding, Izzo.
  - Bate, Vallado, Luo, Thomson, Arora.
  - Battin-Vaughan, Loechler, Shen, MacLellan.
- Semi-major axis
  - Lagrange, Thorne, Prussing, Chen, Wailliez.
- Semi-latus rectum (p-iteration)
  - Herrick-Liu, Boltz.
  - Bate
- Eccentricity vector
  - Avanzini, He, Zhang, Wen.
- Kustaanheimo-Stiefel (K-S) regularized coordinates
  - Simó.
  - Kriz, Jezewsky.

The interested reader is advised to refer [30] for more information on this classification and the references for various formulations mentioned above.

Izzo's Algorithm

Izzo's algorithm to find a solution to the Lambert targeting problem is shown in Figure A.1. This algorithm needs an evaluation of the supporting function $find(\lambda, T)$. The algorithm for this supporting function is presented in Figure A.2.

(MS-4)

Algorithm 1 Lambert solver: inputs, $\mathbf{r}_1 = [r_{11}, r_{12}, r_{13}]$, $\mathbf{r}_2 = [r_{21}, r_{22}, r_{23}]$, t and μ

Require: $t > 0, \mu > 0$
$\mathbf{c} = \mathbf{r}_2 - \mathbf{r}_1$
$c = |\mathbf{c}|, r_1 = |\mathbf{r}_1|, r_2 = |\mathbf{r}_2|$
$s = \frac{1}{2}(r_1 + r_2 + c)$
$\hat{\mathbf{i}}_{r,1} = \mathbf{r}_1/r_1, \hat{\mathbf{i}}_{r,2} = \mathbf{r}_2/r_2$
$\hat{\mathbf{i}}_h = \hat{\mathbf{i}}_{r,1} \times \hat{\mathbf{i}}_{r,2}$
$\lambda^2 = 1 - c/s, \lambda = \sqrt{\lambda^2}$
if $(r_{11}r_{22} - r_{12}r_{21}) < 0$ **then**
  $\lambda = -\lambda$
  $\hat{\mathbf{i}}_{t,1} = \hat{\mathbf{i}}_{r,1} \times \hat{\mathbf{i}}_h, \hat{\mathbf{i}}_{t,2} = \hat{\mathbf{i}}_{r,2} \times \hat{\mathbf{i}}_{r,2}$
else
  $\hat{\mathbf{i}}_{t,1} = \hat{\mathbf{i}}_h \times \hat{\mathbf{i}}_{r,1}, \hat{\mathbf{i}}_{t,2} = \hat{\mathbf{i}}_h \times \hat{\mathbf{i}}_h$
end if
$T = \sqrt{\frac{2\mu}{s^3}}t$
$x_{list}, y_{list} = \text{findxy}(\lambda, T)$
$\gamma = \sqrt{\frac{\mu s}{2}}, \rho = \frac{r_1 - r_2}{c}, \sigma = \sqrt{(1 - \rho^2)}$
for each x, y in x_{list}, y_{list} **do**
  $V_{r,1} = \gamma[(\lambda y - x) - \rho(\lambda y + x)]/r_1$
  $V_{r,2} = -\gamma[(\lambda y - x) + \rho(\lambda y + x)]/r_2$
  $V_{t,1} = \gamma\sigma(y + \lambda x)/r_1$
  $V_{t,2} = \gamma\sigma(y + \lambda x)/r_2$
  $\mathbf{v}_1 = V_{r,1}\hat{\mathbf{i}}_{r,1} + V_{t,1}\hat{\mathbf{i}}_{t,1}$
  $\mathbf{v}_2 = V_{r,2}\hat{\mathbf{i}}_{r,2} + V_{t,2}\hat{\mathbf{i}}_{t,2}$
end for

Figure A.1: Izzo's algorithm for solving the Lambert tageting problem [31].

Algorithm 2 findxy(λ, T): computes all x, y for single and muti-rev solutions

Require: $|\lambda| < 1, T < 0$
$M_{max} = floor(T/\pi)$
$T_{00} = \arccos\lambda + \lambda\sqrt{1 - \lambda^2}$
if $T < T_{00} + M_{max}\pi$ and $M_{max} > 0$ **then**
  start Halley iterations from $x = 0, T = T_0$ and find $T_{min}(M_{max})$
  if $T_{min} > T$ **then**
    $M_{max} = M_{max} - 1$
  end if
end if
$T_1 = \frac{2}{3}(1 - \lambda^3)$
compute x_0 from Eq. (30)
start Householder iterations from x_0 and find x, y
while $M_{max} > 0$ **do**
  compute x_{0l} and x_{0r} from Eq. (31) with $M = M_{max}$
  start Householder iterations from x_{0l} and find x_r, y_r
  start Householder iterations from x_{0r} and find x_l, y_l
  $M_{max} = M_{max} - 1$
end while

Figure A.2: Algorithm for the *find(λ, T)* function in the Izzo's algorithm for a solution of the Lambert targeting problem [31].

B

Appendix: Optimization

Schaffer's f_6 Function

Schaffer's f_6 function can be used as a test function to solve a static optimization problem using the optimization algorithm(s) under consideration. One dimensional ($n = 1$) form of this test function is given by Equation B.1 and its value is plotted in Figure B.1, over the interval $x\epsilon[-5, 5]$.

$$f(x) = 1 + (x^2)^{0.25} * \left([\sin(50 * (x^2)^{0.1})]^2 + 1\right) \tag{B.1}$$

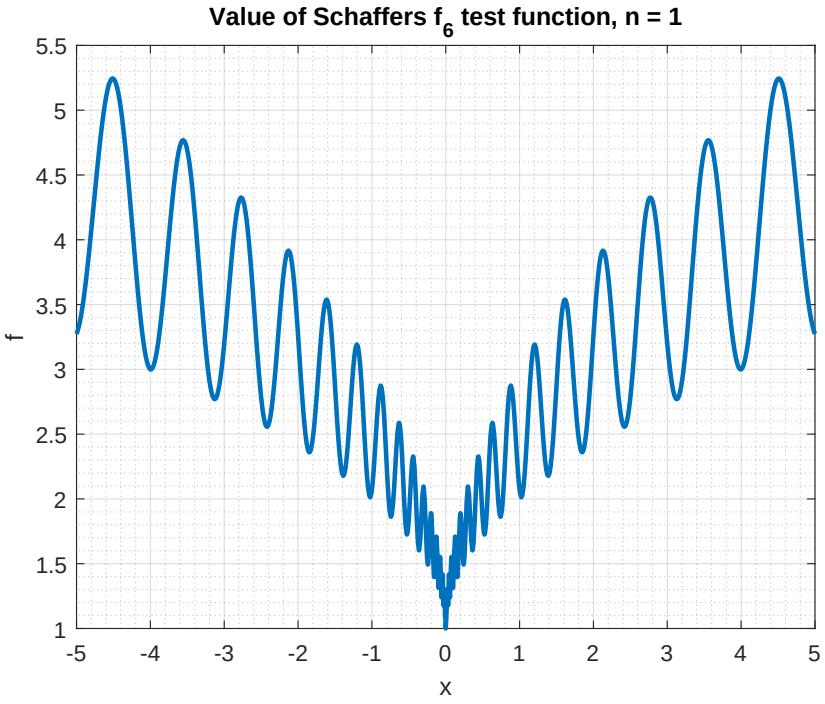

Figure B.1: Schaffer's f_6 test function ($n = 1$) over the interval $x\epsilon[-5, 5]$.

In the early phases of thesis work, the global optimum values (both minima and maxima) of the one dimensional Schaffer's f_6 function are found using the meta-heuristics algorithms - the MOEA/D and the NSGA-II. The interval of the independent variable (x) considered for this purpose is [1,4] which includes a few local minima and maxima. As the true global solutions to the Schaffer's f_6 function are known in this chosen design space, the deviation of the best fitness value and the average fitness value of the generation from the true optimum can be computed for successive generations of the population. Such results are shown in Figures B.2 and B.3 for the minimization and maximization problems respectively.

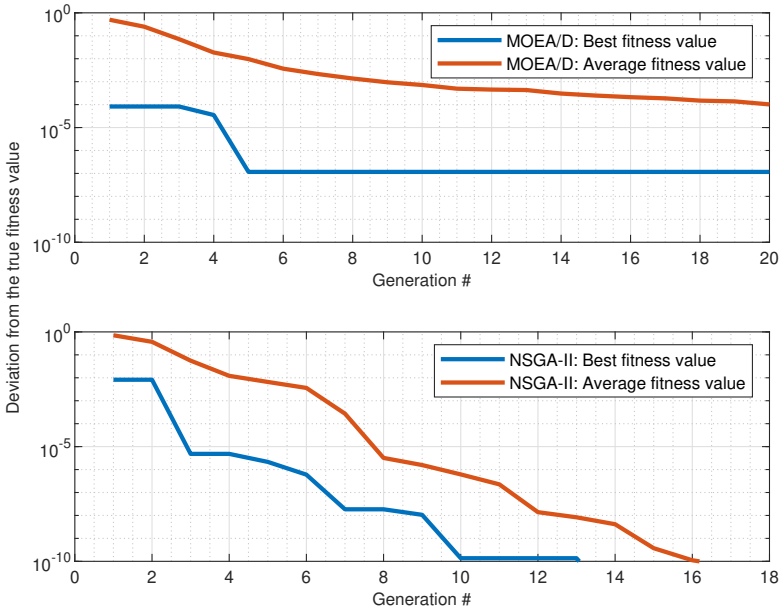

Figure B.2: Minimization of the Schaffer's f_6 test function using the MOEA/D and NSGA-II algorithms (population size = 100). Deviation of the best fitness value and the average fitness value from the true fitness value is plotted on a logarithmic scale. The design space chosen is: $x\epsilon[1,4]$.

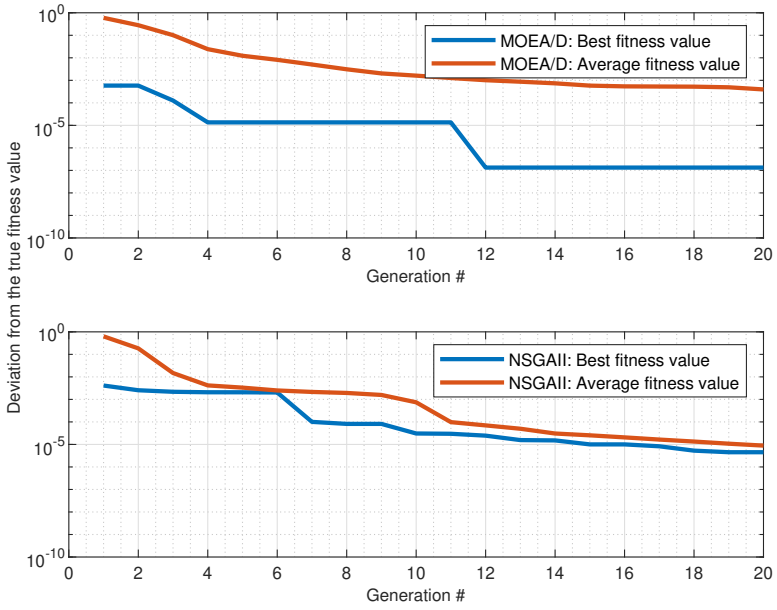

Figure B.3: Maximization of the Schaffer's f_6 test function using the MOEA/D and NSGA-II algorithms (population size = 100). Deviation of the best fitness value and the average fitness value from the true fitness value is plotted on a logarithmic scale. The design space chosen is: $x\epsilon[1,4]$.

It can be concluded that both the optimization algorithms are leading to the solutions which are in good agreement with the true optimum solutions. During the early phases of thesis work, such agreement has validated the use of optimization algorithms. The error might be further reduced by fine-tuning the optimization algorithms to solve this static optimization problem.

Optimization Problem Cases

For a number of optimization problems for the mission scenarios *MS-4* and *MS-5* solved in this thesis work, multiple problem cases have been solved to obtain the important parts/points of the solution set. Details of such optimization problem cases have been presented in Tables B.1 and B.2.

Abort Fraction	Case	Solutions Obtained	**Design Space**		**Constraints**	
			Minimum (TOF_{in}) [days]	Maximum (TOF_{in}) [days]	Constraint on total ΔV [m/s]	Constraint on V_∞ at Earth arrival [m/s]
0.2	1	$C_{0.2}$,$D_{0.2}$	10	406	-	9360.0
	2	$C'_{0.2}$	120	300	11000.0	9360.0
0.4	3	$C_{0.4}$,$D_{0.4}$	10	406	-	9360.0
	4	$C'_{0.4}$	120	300	11000.0	9360.0
0.6	5	$C_{0.6}$,$D_{0.6}$	10	406	-	9360.0
	6	$C'_{0.6}$,$D'_{0.6}$	200	300	11000.0	9360.0
0.8	7	$E_{0.8}$	10	500	-	9360.0
	8	$C''_{0.8}$	10	500	20000.0	-
	9	$C'_{0.8}$, $D_{0.8}$	200	300	11000.0	-

Table B.1: Various optimization problem cases solved to obtain important abort trajectory solutions, when the abort occurs during outbound ballistic transfer and Mars swing-by is not performed *(MS-4)*.

Abort Fraction	Case	Solutions Obtained	**Design Space**		**Constraints**	
			Minimum (TOF_{in}) [days]	Maximum (TOF_{in}) [days]	Constraint on total ΔV [m/s]	Constraint on V_∞ at Earth arrival [m/s]
0.2	10	$C''''_{0.2s}$,$D'_{0.2s}$	120	360	20000.0	-
	11	$C'''_{0.2s}$,$D_{0.2s}$	270	600	20000.0	-
	12	$C''_{0.2s}$	270	600	16000.0	-
	13	$C'_{0.2s}$	270	600	12000.0	9360.0
0.4	14	$C''''_{0.4s}$,$D'_{0.4s}$	120	270	25000.0	-
	15	$C'''_{0.4s}$	120	490	20000.0	-
	16	$C''_{0.4s}$	120	502	16000.0	9360.0
	17	$C'_{0.4s}$, $D_{0.4s}$	120	502	12000.0	-
0.6	18	$C''''_{0.6s}$	120	300	25000.0	-
	19	$C'''_{0.6s}$	120	398	20000.0	-
	20	$C''_{0.6s}$,$D_{0.6s}$	120	398	16000.0	-
	21	$C'_{0.6s}$	120	398	14000.0	9360.0
0.8	22	$C''''_{0.8s}$, $D_{0.8s}$	120	294	25000.0	-
	23	$C'''_{0.8s}$	120	294	20000.0	-
	24	$C''_{0.8s}$	120	294	16000.0	-
	25	$C'_{0.8s}$	120	294	25000.0	9360.0

Table B.2: Various optimization problem cases solved to obtain important abort trajectory solutions, when the abort occurs during Mars surface stay period *(MS-5)*.

C

Appendix: Results

In this appendix, the detailed results for all the selected abort trajectory solutions associated with the mission scenarios - *MS-3*, *MS-4*, and *MS-5* - are presented. Tables C.1 to C.8 provide the computed values of the trajectory parameters for the relevant abort trajectory solutions. In these tables, following symbols are used for the various parameters apart from the those listed in the previous chapters of this report.

Symbol	Parameter
h_p	Altitude of the pericenter
$V_{\infty-EA}$	V_∞ when the S/C arrives at Earth
$r_{Sun-min}$	Minimum distance to the Sun
$T_{mission}$	Total duration of the mission
$\Sigma\Delta V$	Sum of all the relevant ΔVs

Mission Scenario		MS-3				MS-4					
Solution		$A'_{0.2}$	-	$B_{0.2}$	-	$C_{0.2}$	-	$C'_{0.2}$	-	$D_{0.2}$	-
Parameter	**Unit**	**Value**	σ	**Value**	σ	**Value**	σ	**Value**	σ	**Value**	σ
t_{nom-ED}	[MJD2000]	10609.25	-	10609.25	-	10609.25	-	10609.25	-	10609.25	-
t_0	[MJD2000]	10645.25	-	10645.25	-	10645.25	-	10645.25	-	10645.25	-
t_0 - t_{nom-ED}	[days]	36.00	-	36.00	-	36.00	-	36.00	-	36.00	-
T_1	[days]	172.85	$3.39 \cdot 10^{0}$	144.57	$3.69 \cdot 10^{-2}$	21.61	$1.04 \cdot 10^{-3}$	264.63	$6.49 \cdot 10^{-10}$	337.34	$1.29 \cdot 10^{-4}$
T_2	[days]	233.99	$3.40 \cdot 10^{0}$	300.00	$1.09 \cdot 10^{-1}$	-	-	-	-	-	-
$T_{mission}$	[days]	442.84	$1.32 \cdot 10^{-1}$	480.56	$1.37 \cdot 10^{-1}$	57.61	$1.04 \cdot 10^{-3}$	300.63	$6.49 \cdot 10^{-10}$	373.34	$1.29 \cdot 10^{-4}$
η_1	[-]	0.01	$3.71 \cdot 10^{-2}$	0.00	$1.03 \cdot 10^{-5}$	0.00	$1.88 \cdot 10^{-5}$	0.00	$9.45 \cdot 10^{-13}$	0.00	$4.99 \cdot 10^{-11}$
V_∞	[m · s^{-1}]	33.73	$1.33 \cdot 10^{1}$	0.00	$4.90 \cdot 10^{-4}$	0.04	$5.43 \cdot 10^{2}$	0.00	$3.95 \cdot 10^{-9}$	0.00	$1.25 \cdot 10^{-8}$
θ	[degree]	14.68	$1.02 \cdot 10^{1}$	-2.63	$1.02 \cdot 10^{1}$	14.18	$4.92 \cdot 10^{0}$	-6.50	$7.23 \cdot 10^{0}$	15.00	$9.16 \cdot 10^{0}$
ϕ	[degree]	1.67	$3.85 \cdot 10^{0}$	2.81	$3.31 \cdot 10^{0}$	-4.30	$3.55 \cdot 10^{0}$	4.83	$4.13 \cdot 10^{0}$	-4.99	$4.39 \cdot 10^{0}$
η_2	[-]	0.79	$1.55 \cdot 10^{-2}$	0.53	$7.81 \cdot 10^{-4}$	-	-	-	-	-	-
b_{incl}	[degree]	74.47	$3.03 \cdot 10^{0}$	86.65	$3.39 \cdot 10^{-1}$	-	-	-	-	-	-
h_p	[km]	259.77	$1.65 \cdot 10^{1}$	257.00	$3.13 \cdot 10^{-4}$	-	-	-	-	-	-
ΔV_{GA}	[m · s^{-1}]	2664.78	$8.00 \cdot 10^{1}$	247.42	$1.70 \cdot 10^{1}$	-	-	-	-	-	-
ΔV_1	[m · s^{-1}]	4360.32	-	4360.32	-	4360.32	-	4360.32	-	4360.32	-
ΔV_4	[m · s^{-1}]	33.73	$1.33 \cdot 10^{1}$	0.00	$4.90 \cdot 10^{-4}$	0.04	$5.43 \cdot 10^{2}$	0.00	$3.95 \cdot 10^{-9}$	0.00	$1.25 \cdot 10^{-8}$
ΔV_5	[m · s^{-1}]	512.12	$2.83 \cdot 10^{1}$	19.12	$5.71 \cdot 10^{-1}$	-	-	-	-	-	-
ΔV_6	[m · s^{-1}]	2664.78	$8.00 \cdot 10^{1}$	247.42	$1.70 \cdot 10^{1}$	-	-	-	-	-	-
ΔV_7	[m · s^{-1}]	3375.76	$1.17 \cdot 10^{2}$	3850.60	$1.59 \cdot 10^{1}$	17365.36	$2.15 \cdot 10^{1}$	6639.68	$8.77 \cdot 10^{-9}$	2948.43	$3.39 \cdot 10^{-7}$
$\Sigma\Delta V$	[m · s^{-1}]	10946.71	-	8477.46	-	21725.73	-	11000.00	-	7308.75	-
$V_{\infty-EA}$	[m · s^{-1}]	9355.08	$1.86 \cdot 10^{1}$	9360.00	$5.33 \cdot 10^{-2}$	9359.86	$1.97 \cdot 10^{-1}$	2705.70	$2.65 \cdot 10^{-8}$	7257.67	$3.10 \cdot 10^{-2}$
$r_{Sun-min}$	[AU]	0.49	$2.95 \cdot 10^{-3}$	0.53	$2.36 \cdot 10^{-4}$	0.99	$3.02 \cdot 10^{-7}$	0.94	$9.79 \cdot 10^{-13}$	0.76	$1.05 \cdot 10^{-6}$

Table C.1: Trajectory parameters for the selected propulsive abort trajectory solutions, when the abort occurs during the nominal Earth-to-Mars transfer (*MS-3* and *MS-4*), at abort fraction 0.2.

Mission Scenario		***MS-3***				***MS-4***					
Solution		$A'_{0.4}$	-	$B_{0.4}$	-	$C_{0.4}$	-	$C'_{0.4}$	-	$D_{0.4}$	-
Parameter	**Unit**	**Value**	σ	**Value**	σ	**Value**	σ	**Value**	σ	**Value**	σ
t_{nom-ED}	[MJD2000]	10609.25	-	10609.25	-	10609.25	-	10609.25	-	10609.25	-
t_0	[MJD2000]	10681.25	-	10681.25	-	10681.25	-	10681.25	-	10681.25	-
t_0 - t_{nom-ED}	[days]	72.00	-	72.00	-	72.00	-	72.00	-	72.00	-
T_1	[days]	134.38	$2.77 \cdot 10^{0}$	108.24	$5.29 \cdot 10^{-3}$	64.07	$9.43 \cdot 10^{-8}$	265.62	$1.79 \cdot 10^{-7}$	310.79	$0.00 \cdot 10^{0}$
T_2	[days]	236.75	$3.08 \cdot 10^{0}$	300.00	$6.92 \cdot 10^{-5}$	-	-	-	-	-	-
$T_{mission}$	[days]	443.13	$3.50 \cdot 10^{-1}$	480.24	$5.28 \cdot 10^{-3}$	136.07	$9.43 \cdot 10^{-8}$	337.62	$1.79 \cdot 10^{-7}$	382.79	$0.00 \cdot 10^{0}$
η_1	[-]	0.01	$1.52 \cdot 10^{-1}$	0.00	$6.51 \cdot 10^{-6}$	0.00	$1.79 \cdot 10^{-10}$	0.00	$8.80 \cdot 10^{-10}$	0.00	$5.75 \cdot 10^{-16}$
V_∞	[m · s^{-1}]	0.67	$5.45 \cdot 10^{1}$	0.00	$2.27 \cdot 10^{-4}$	0.00	$7.13 \cdot 10^{1}$	0.00	$8.56 \cdot 10^{-8}$	0.00	$2.55 \cdot 10^{-13}$
θ	[degree]	-5.65	$7.64 \cdot 10^{0}$	13.09	$1.05 \cdot 10^{1}$	2.15	$4.00 \cdot 10^{0}$	-14.38	$1.13 \cdot 10^{1}$	-2.96	$1.05 \cdot 10^{1}$
ϕ	[degree]	-4.52	$2.74 \cdot 10^{0}$	3.26	$3.75 \cdot 10^{0}$	-2.89	$3.97 \cdot 10^{0}$	-3.08	$2.46 \cdot 10^{0}$	-2.61	$4.44 \cdot 10^{0}$
η_2	[-]	0.79	$2.66 \cdot 10^{-2}$	0.53	$6.59 \cdot 10^{-5}$	-	-	-	-	-	-
b_{incl}	[degree]	76.79	$2.96 \cdot 10^{0}$	86.77	$1.67 \cdot 10^{-2}$	-	-	-	-	-	-
h_p	[km]	261.15	$2.30 \cdot 10^{1}$	257.00	$4.13 \cdot 10^{-5}$	-	-	-	-	-	-
ΔV_{GA}	[m · s^{-1}]	2637.20	$4.65 \cdot 10^{1}$	314.22	$9.63 \cdot 10^{-1}$	-	-	-	-	-	-
ΔV_1	[m · s^{-1}]	4360.32	-	4360.32	-	4360.32	-	4360.32	-	4360.32	-
ΔV_4	[m · s^{-1}]	0.67	$5.45 \cdot 10^{1}$	0.00	$2.27 \cdot 10^{-4}$	0.00	$7.13 \cdot 10^{1}$	0.00	$8.56 \cdot 10^{-8}$	0.00	$2.55 \cdot 10^{-13}$
ΔV_5	[m · s^{-1}]	734.08	$2.91 \cdot 10^{2}$	23.58	$1.41 \cdot 10^{-1}$	-	-	-	-	-	-
ΔV_6	[m · s^{-1}]	2637.20	$4.65 \cdot 10^{1}$	314.22	$9.63 \cdot 10^{-1}$	-	-	-	-	-	-
ΔV_7	[m · s^{-1}]	3258.46	$3.58 \cdot 10^{2}$	3797.24	$8.22 \cdot 10^{-1}$	20661.12	$1.09 \cdot 10^{1}$	6639.68	$3.61 \cdot 10^{-7}$	3361.79	$8.95 \cdot 10^{-12}$
$\Sigma\Delta V$	[m · s^{-1}]	10990.73	-	8495.37	-	25021.44	-	11000.00	-	7722.12	-
$V_{\infty-EA}$	[m · s^{-1}]	9354.59	$4.91 \cdot 10^{0}$	9360.00	$2.74 \cdot 10^{-4}$	9360.00	$5.81 \cdot 10^{-6}$	6129.13	$2.13 \cdot 10^{-5}$	9360.00	$9.35 \cdot 10^{-11}$
$r_{Sun-min}$	[AU]	0.50	$4.40 \cdot 10^{-3}$	0.53	$2.08 \cdot 10^{-5}$	1.00	$5.41 \cdot 10^{-11}$	0.83	$6.95 \cdot 10^{-10}$	0.69	$7.15 \cdot 10^{-15}$

Table C.2: Trajectory parameters for the selected propulsive abort trajectory solutions, when the abort occurs during the nominal Earth-to-Mars transfer (*MS-3* and *MS-4*), at abort fraction 0.4.

Mission Scenario		***MS-3***				***MS-4***							
Solution		$A'_{0.6}$	-	$B_{0.6}$	-	$C_{0.6}$	-	$C'_{0.6}$	-	$D_{0.6}$	-	$D'_{0.6}$	-
Parameter	**Unit**	**Value**	σ	**Value**	σ	**Value**	σ	**Value**	σ	**Value**	σ	**Value**	σ
t_{nom-ED}	[MJD2000]	10609.25	-	10609.25	-	10609.25	-	10609.25	-	10609.25	-	10609.25	-
t_0	[MJD2000]	10717.25	-	10717.25	-	10717.25	-	10717.25	-	10717.25	-	10717.25	-
t_0 - t_{nom-ED}	[days]	108.00	-	108.00	-	108.00	-	108.00	-	108.00	-	108.00	-
T_1	[days]	89.26	$4.41 \cdot 10^{0}$	71.72	$1.05 \cdot 10^{-2}$	185.17	$2.06 \cdot 10^{-9}$	253.37	$4.08 \cdot 10^{-8}$	255.21	$1.31 \cdot 10^{-12}$	277.11	$3.00 \cdot 10^{-3}$
T_2	[days]	245.49	$4.01 \cdot 10^{0}$	303.43	$3.93 \cdot 10^{-2}$	-	-	-	-	-	-	-	-
$T_{mission}$	[days]	442.75	$4.82 \cdot 10^{-1}$	483.15	$3.65 \cdot 10^{-2}$	293.17	$2.06 \cdot 10^{-9}$	361.37	$4.08 \cdot 10^{-8}$	363.21	$8.14 \cdot 10^{-13}$	385.11	$3.00 \cdot 10^{-3}$
η_1	[-]	0.42	$2.09 \cdot 10^{-1}$	0.00	$4.69 \cdot 10^{-6}$	0.00	$4.34 \cdot 10^{-14}$	0.00	$5.28 \cdot 10^{-11}$	0.00	$1.47 \cdot 10^{-17}$	0.00	$2.31 \cdot 10^{-10}$
V_∞	[m · s^{-1}]	127.17	$5.94 \cdot 10^{1}$	0.01	$6.67 \cdot 10^{-3}$	0.00	$4.23 \cdot 10^{2}$	0.00	$5.09 \cdot 10^{-7}$	0.00	$4.54 \cdot 10^{-12}$	0.00	$6.83 \cdot 10^{-6}$
θ	[degree]	15.00	$1.31 \cdot 10^{1}$	14.80	$1.09 \cdot 10^{1}$	-13.26	$1.03 \cdot 10^{1}$	-10.67	$1.24 \cdot 10^{1}$	-12.67	$1.28 \cdot 10^{1}$	-15.00	$7.24 \cdot 10^{0}$
ϕ	[degree]	3.75	$3.86 \cdot 10^{0}$	-3.08	$2.27 \cdot 10^{0}$	1.99	$3.35 \cdot 10^{0}$	1.89	$3.44 \cdot 10^{0}$	-2.47	$3.04 \cdot 10^{0}$	-4.80	$3.06 \cdot 10^{0}$
η_2	[-]	0.72	$1.98 \cdot 10^{-2}$	0.52	$3.22 \cdot 10^{-4}$	-	-	-	-	-	-	-	-
b_{incl}	[degree]	83.40	$1.95 \cdot 10^{0}$	86.84	$6.41 \cdot 10^{-2}$	-	-	-	-	-	-	-	-
h_p	[km]	259.84	$7.30 \cdot 10^{0}$	257.00	$1.40 \cdot 10^{-4}$	-	-	-	-	-	-	-	-
ΔV_{GA}	[m · s^{-1}]	2648.32	$3.68 \cdot 10^{1}$	15.23	$4.21 \cdot 10^{0}$	-	-	-	-	-	-	-	-
ΔV_1	[m · s^{-1}]	4360.32	-	4360.32	-	4360.32	-	4360.32	-	4360.32	-	4360.32	-
ΔV_4	[m · s^{-1}]	127.17	$5.94 \cdot 10^{1}$	0.01	$6.67 \cdot 10^{-3}$	0.00	$4.23 \cdot 10^{2}$	0.00	$5.09 \cdot 10^{-6}$	0.00	$4.54 \cdot 10^{-12}$	0.00	$6.83 \cdot 10^{-6}$
ΔV_5	[m · s^{-1}]	1691.87	$2.46 \cdot 10^{2}$	19.91	$1.79 \cdot 10^{-2}$	-	-	-	-	-	-	-	-
ΔV_6	[m · s^{-1}]	2648.32	$3.68 \cdot 10^{1}$	15.23	$4.21 \cdot 10^{0}$	-	-	-	-	-	-	-	-
ΔV_7	[m · s^{-1}]	2171.70	$2.73 \cdot 10^{2}$	4100.60	$4.20 \cdot 10^{0}$	12599.43	$1.35 \cdot 10^{2}$	6639.68	$3.11 \cdot 10^{-6}$	6473.35	$1.14 \cdot 10^{-10}$	4499.79	$2.50 \cdot 10^{-1}$
$\Sigma\Delta V$	[m · s^{-1}]	10999.38	-	8496.07	-	16959.75	-	11000.00	-	10833.67	-	8860.11	-
$V_{\infty-EA}$	[m · s^{-1}]	9359.93	$5.97 \cdot 10^{0}$	9360.00	$3.28 \cdot 10^{-3}$	9360.00	$4.53 \cdot 10^{-8}$	9303.25	$1.92 \cdot 10^{-6}$	9360.00	$3.25 \cdot 10^{-11}$	10565.83	$2.50 \cdot 10^{-1}$
$r_{Sun-min}$	[AU]	0.51	$6.03 \cdot 10^{-3}$	0.53	$4.77 \cdot 10^{-5}$	0.82	$2.09 \cdot 10^{-12}$	0.73	$1.01 \cdot 10^{-10}$	0.72	$1.44 \cdot 10^{-14}$	0.66	$1.07 \cdot 10^{-5}$

Table C.3: Trajectory parameters for the selected propulsive abort trajectory solutions, when the abort occurs during the nominal Earth-to-Mars transfer (*MS-3* and *MS-4*), at abort fraction 0.6.

Mission Scenario		***MS-3***				***MS-4***							
Solution		$A'_{0.8}$	-	$B_{0.8}$	-	$C''_{0.8}$	-	$E_{0.8}$	-	$C'_{0.8}$	-	$D_{0.8}$	-
Parameter	**Unit**	**Value**	σ	**Value**	σ	**Value**	σ	**Value**	σ	**Value**	σ	**Value**	σ
t_{nom-ED}	[MJD2000]	10609.25	-	10609.25	-	10609.25	-	10609.25	-	10609.25	-	10609.25	-
t_0	[MJD2000]	10753.25	-	10753.25	-	10753.25	-	10753.25	-	10753.25	-	10753.25	-
t_0 - t_{nom-ED}	[days]	144.00	-	144.00	-	144.00	-	144.00	-	144.00	-	144.00	-
T_1	[days]	46.72	$2.69 \cdot 10^{0}$	35.69	$7.64 \cdot 10^{-4}$	162.59	$1.04 \cdot 10^{-6}$	451.14	$7.14 \cdot 10^{-6}$	238.47	$3.30 \cdot 10^{-8}$	270.62	$1.76 \cdot 10^{-4}$
T_2	[days]	252.74	$2.67 \cdot 10^{0}$	303.97	$3.25 \cdot 10^{-3}$	-	-	-	-	-	-	-	-
$T_{mission}$	[days]	443.46	$7.88 \cdot 10^{-2}$	483.66	$3.74 \cdot 10^{-3}$	306.59	$1.04 \cdot 10^{-6}$	595.14	$7.14 \cdot 10^{-6}$	382.47	$3.30 \cdot 10^{-8}$	414.62	$1.76 \cdot 10^{-4}$
η_1	[-]	0.23	$8.30 \cdot 10^{-2}$	0.00	$1.54 \cdot 10^{-6}$	0.00	$1.08 \cdot 10^{-9}$	0.62	$2.42 \cdot 10^{-7}$	0.00	$1.63 \cdot 10^{-10}$	0.00	$1.17 \cdot 10^{-10}$
V_∞	[m · s^{-1}]	321.11	$1.44 \cdot 10^{2}$	0.00	$1.70 \cdot 10^{-3}$	0.00	$1.03 \cdot 10^{-4}$	0.00	$3.37 \cdot 10^{-8}$	0.00	$4.22 \cdot 10^{-7}$	0.00	$4.77 \cdot 10^{-7}$
θ	[degree]	14.59	$1.33 \cdot 10^{1}$	3.62	$7.58 \cdot 10^{0}$	-14.01	$1.16 \cdot 10^{1}$	6.56	$8.83 \cdot 10^{0}$	3.69	$1.24 \cdot 10^{1}$	13.59	$1.01 \cdot 10^{1}$
ϕ	[degree]	-4.77	$3.94 \cdot 10^{0}$	2.31	$2.19 \cdot 10^{0}$	5.00	$4.97 \cdot 10^{0}$	-2.47	$3.61 \cdot 10^{0}$	-3.46	$4.08 \cdot 10^{0}$	-0.73	$2.07 \cdot 10^{0}$
η_2	[-]	0.74	$6.55 \cdot 10^{-3}$	0.52	$2.98 \cdot 10^{-5}$	-	-	-	-	-	-	-	-
b_{incl}	[degree]	85.02	$7.91 \cdot 10^{-1}$	86.73	$5.89 \cdot 10^{-2}$	-	-	-	-	-	-	-	-
h_p	[km]	262.80	$2.55 \cdot 10^{0}$	257.00	$3.43 \cdot 10^{-4}$	-	-	-	-	-	-	-	-
ΔV_{GA}	[m · s^{-1}]	2634.05	$3.36 \cdot 10^{1}$	0.00	$5.35 \cdot 10^{-3}$	-	-	-	-	-	-	-	-
ΔV_1	[m · s^{-1}]	4360.32	-	4360.32	-	4360.32	-	4360.32	-	4360.32	-	4360.32	-
ΔV_4	[m · s^{-1}]	321.11	$1.44 \cdot 10^{2}$	0.00	$1.70 \cdot 10^{-3}$	0.00	$1.03 \cdot 10^{-4}$	0.00	$3.37 \cdot 10^{-8}$	0.00	$4.22 \cdot 10^{-7}$	0.00	$4.77 \cdot 10^{-7}$
ΔV_5	[m · s^{-1}]	1408.66	$1.39 \cdot 10^{2}$	38.79	$2.23 \cdot 10^{-2}$	-	-	-	-	-	-	-	-
ΔV_6	[m · s^{-1}]	2634.05	$3.36 \cdot 10^{1}$	0.00	$5.35 \cdot 10^{-3}$	-	-	-	-	-	-	-	-
ΔV_7	[m · s^{-1}]	2275.42	$6.43 \cdot 10^{1}$	4131.38	$1.43 \cdot 10^{-2}$	15639.68	$1.00 \cdot 10^{-4}$	9134.32	$5.30 \cdot 10^{-6}$	6639.68	$1.24 \cdot 10^{-6}$	4123.83	$8.58 \cdot 10^{-7}$
$\Sigma\Delta V$	[m · s^{-1}]	10999.56	-	8530.50	-	20000.00	-	13494.65	-	11000.00	-	8484.15	-
$V_{\infty-EA}$	[m · s^{-1}]	9359.69	$1.61 \cdot 10^{0}$	9360.00	$8.66 \cdot 10^{-4}$	13814.58	$5.77 \cdot 10^{-5}$	9360.00	$7.92 \cdot 10^{-5}$	12122.14	$3.20 \cdot 10^{-6}$	14273.82	$2.24 \cdot 10^{-2}$
$r_{Sun-min}$	[AU]	0.50	$3.90 \cdot 10^{-3}$	0.53	$8.79 \cdot 10^{-6}$	0.74	$1.28 \cdot 10^{-9}$	0.41	$1.19 \cdot 10^{-7}$	0.64	$1.18 \cdot 10^{-10}$	0.53	$8.38 \cdot 10^{-7}$

Table C.4: Trajectory parameters for the selected propulsive abort trajectory solutions, when the abort occurs during the nominal Earth-to-Mars transfer (*MS-3* and *MS-4*), at abort fraction 0.8.

Mission Scenario Solution		***MS-5***											
		$C'''_{0.2s}$	-	$D'_{0.2s}$	-	$C'''_{0.2s}$	-	$C''_{0.2s}$	-	$C'_{0.2s}$	-	$D_{0.2s}$	-
Parameter	**Unit**	**Value**	σ	**Value**	σ	**Value**	σ	**Value**	σ	**Value**	σ	**Value**	σ
t_{nom-ED}	[MJD2000]	10609.25	-	10609.25	-	10609.25	-	10609.25	-	10609.25	-	10609.25	-
t_{nom-MA}	[MJD2000]	10789.25	-	10789.25	-	10789.25	-	10789.25	-	10789.25	-	10789.25	-
t_0	[MJD2000]	10893.02	-	10893.02	-	10893.02	-	10893.02	-	10893.02	-	10893.02	-
t_0 - t_{nom-MA}	[days]	103.76	-	103.76	-	103.76	-	103.76	-	103.76	-	103.76	-
T_1	[days]	177.30	$6.67 \cdot 10^{-7}$	203.85	$3.02 \cdot 10^{-4}$	431.67	$5.57 \cdot 10^{-4}$	502.78	$4.90 \cdot 10^{-2}$	574.82	$4.58 \cdot 10^{-5}$	600.00	$6.39 \cdot 10^{-7}$
$T_{mission}$	[days]	461.06	$6.67 \cdot 10^{-7}$	487.61	$3.02 \cdot 10^{-4}$	715.44	$5.57 \cdot 10^{-4}$	786.54	$4.90 \cdot 10^{-2}$	858.58	$4.58 \cdot 10^{-5}$	883.76	$6.39 \cdot 10^{-7}$
η_1	[-]	0.00	$2.80 \cdot 10^{-10}$	0.00	$4.02 \cdot 10^{-11}$	0.38	$7.55 \cdot 10^{-4}$	0.24	$2.90 \cdot 10^{-3}$	0.48	$3.33 \cdot 10^{-5}$	0.56	$2.17 \cdot 10^{-6}$
V_∞	[m · s^{-1}]	0.00	$5.14 \cdot 10^{-5}$	0.00	$7.23 \cdot 10^{-7}$	3169.86	$1.96 \cdot 10^{0}$	3519.96	$8.26 \cdot 10^{0}$	623.56	$1.33 \cdot 10^{-1}$	210.84	$1.20 \cdot 10^{-2}$
θ	[degree]	-14.87	$1.10 \cdot 10^{1}$	-1.93	$6.74 \cdot 10^{0}$	-15.00	$9.29 \cdot 10^{-4}$	-15.00	$1.97 \cdot 10^{-2}$	-15.00	$6.35 \cdot 10^{-5}$	-15.00	$1.39 \cdot 10^{-6}$
ϕ	[degree]	0.51	$4.37 \cdot 10^{0}$	0.08	$4.02 \cdot 10^{0}$	-0.07	$3.30 \cdot 10^{-1}$	4.95	$2.88 \cdot 10^{-2}$	-5.00	$6.90 \cdot 10^{-5}$	-5.00	$3.63 \cdot 10^{-6}$
ΔV_1	[m · s^{-1}]	4360.32	-	4360.32	-	4360.32	-	4360.32	-	4360.32	-	4360.32	-
ΔV_2	[m · s^{-1}]	3639.94	-	3639.94	-	3639.94	-	3639.94	-	3639.94	-	3639.94	-
ΔV_3	[m · s^{-1}]	1411.25	$4.47 \cdot 10^{-12}$	1411.25	$0.00 \cdot 10^{0}$	2360.45	$1.08 \cdot 10^{0}$	2560.04	$4.87 \cdot 10^{0}$	1451.43	$1.71 \cdot 10^{-2}$	1415.86	$5.24 \cdot 10^{-4}$
ΔV_7	[m · s^{-1}]	10588.49	$3.46 \cdot 10^{-5}$	8972.07	$1.29 \cdot 10^{-6}$	9639.29	$1.09 \cdot 10^{0}$	5439.22	$4.82 \cdot 10^{0}$	2548.30	$1.74 \cdot 10^{-2}$	2430.98	$5.27 \cdot 10^{-4}$
$\Sigma\Delta V$	[m · s^{-1}]	20000.00	-	18383.58	-	20000.00	-	15999.52	-	12000.00	-	11847.11	-
$V_{\infty-EA}$	[m · s^{-1}]	16426.95	$3.87 \cdot 10^{-5}$	15742.50	$5.27 \cdot 10^{-3}$	23416.25	$1.65 \cdot 10^{1}$	9358.23	$2.94 \cdot 10^{0}$	6558.94	$4.60 \cdot 10^{-1}$	6039.67	$4.69 \cdot 10^{-2}$
$r_{Sun-min}$	[AU]	0.47	$6.10 \cdot 10^{-10}$	0.43	$6.41 \cdot 10^{-7}$	0.98	$2.63 \cdot 10^{-9}$	1.00	$1.29 \cdot 10^{-5}$	1.01	$6.43 \cdot 10^{-9}$	1.01	$2.58 \cdot 10^{-11}$

Table C.5: Trajectory parameters for the selected propulsive abort trajectory solutions, when the abort occurs during the nominal Mars surface stay period (*MS-5*), at abort fraction 0.2.

Mission		***MS-5***											
Scenario		$C'''_{0.4s}$	-	$D'_{0.4s}$	-	$C'''_{0.4s}$	-	$C''_{0.4s}$	-	$C'_{0.4s}$	-	$D_{0.4s}$	-
Solution													
Parameter	**Unit**	**Value**	σ	**Value**	σ	**Value**	σ	**Value**	σ	**Value**	σ	**Value**	σ
t_{nom-ED}	[MJD2000]	10609.25	-	10609.25	-	10609.25	-	10609.25	-	10609.25	-	10609.25	-
t_{nom-MA}	[MJD2000]	10789.25	-	10789.25	-	10789.25	-	10789.25	-	10789.25	-	10789.25	-
t_0	[MJD2000]	10996.78	-	10996.78	-	10996.78	-	10996.78	-	10996.78	-	10996.78	-
t_0 - t_{nom-MA}	[days]	207.52	-	207.52	-	207.52	-	207.52	-	207.52	-	207.52	-
T_1	[days]	154.40	$4.96 \cdot 10^{-6}$	187.26	$1.97 \cdot 10^{-4}$	366.68	$5.44 \cdot 10^{-3}$	432.69	$5.74 \cdot 10^{-2}$	489.31	$2.71 \cdot 10^{-5}$	502.00	$9.46 \cdot 10^{-9}$
$T_{mission}$	[days]	541.93	$4.96 \cdot 10^{-6}$	574.79	$1.97 \cdot 10^{-4}$	754.20	$5.44 \cdot 10^{-3}$	820.22	$5.74 \cdot 10^{-2}$	876.84	$2.71 \cdot 10^{-5}$	889.52	$9.46 \cdot 10^{-9}$
η_1	[-]	0.00	$1.68 \cdot 10^{-8}$	0.00	$6.78 \cdot 10^{-11}$	0.35	$1.00 \cdot 10^{-3}$	0.12	$2.00 \cdot 10^{-3}$	0.45	$6.28 \cdot 10^{-5}$	0.49	$2.33 \cdot 10^{-6}$
V_∞	[m · s^{-1}]	0.00	$8.83 \cdot 10^{-4}$	0.00	$3.15 \cdot 10^{-8}$	2428.76	$2.03 \cdot 10^{1}$	2465.21	$1.42 \cdot 10^{2}$	298.52	$1.79 \cdot 10^{-1}$	110.32	$8.42 \cdot 10^{-3}$
θ	[degree]	4.17	$1.14 \cdot 10^{1}$	-0.86	$1.23 \cdot 10^{1}$	-15.00	$1.73 \cdot 10^{-4}$	-14.95	$1.96 \cdot 10^{-2}$	-15.00	$4.10 \cdot 10^{-5}$	-15.00	$3.34 \cdot 10^{-7}$
ϕ	[degree]	1.54	$3.58 \cdot 10^{0}$	-0.79	$3.97 \cdot 10^{0}$	-2.12	$9.27 \cdot 10^{-1}$	4.92	$4.71 \cdot 10^{-2}$	-5.00	$5.06 \cdot 10^{-5}$	-5.00	$5.02 \cdot 10^{-7}$
ΔV_1	[m · s^{-1}]	4360.32	-	4360.32	-	4360.32	-	4360.32	-	4360.32	-	4360.32	-
ΔV_2	[m · s^{-1}]	3639.94	-	3639.94	-	3639.94	-	3639.94	-	3639.94	-	3639.94	-
ΔV_3	[m · s^{-1}]	1411.25	$1.71 \cdot 10^{-10}$	1411.25	$0.00 \cdot 10^{0}$	1988.77	$9.06 \cdot 10^{0}$	2005.28	$6.44 \cdot 10^{1}$	1420.49	$1.11 \cdot 10^{-2}$	1412.52	$1.93 \cdot 10^{-4}$
ΔV_7	[m · s^{-1}]	15588.49	$1.57 \cdot 10^{-4}$	11905.30	$4.08 \cdot 10^{-7}$	10010.97	$9.01 \cdot 10^{0}$	5994.25	$6.54 \cdot 10^{1}$	2579.25	$1.11 \cdot 10^{-2}$	2462.84	$1.91 \cdot 10^{-4}$
$\Sigma\Delta V$	[m · s^{-1}]	25000.00	-	21316.81	-	20000.00	-	15999.79	-	12000.00	-	11875.61	-
$V_{\infty-EA}$	[m · s^{-1}]	20439.85	$4.06 \cdot 10^{-4}$	19552.89	$1.52 \cdot 10^{-2}$	23713.05	$2.45 \cdot 10^{1}$	9354.21	$3.96 \cdot 10^{0}$	6886.60	$4.79 \cdot 10^{-1}$	6202.00	$1.93 \cdot 10^{-2}$
$r_{Sun-min}$	[AU]	0.34	$4.92 \cdot 10^{-9}$	0.29	$7.51 \cdot 10^{-7}$	0.99	$9.95 \cdot 10^{-7}$	1.00	$1.46 \cdot 10^{-5}$	1.01	$2.11 \cdot 10^{-9}$	1.02	$6.73 \cdot 10^{-14}$

Table C.6: Trajectory parameters for the selected propulsive abort trajectory solutions, when the abort occurs during the nominal Mars surface stay period (*MS-5*), at abort fraction 0.4.

Mission Scenario Solution		**MS-5**									
		$C'''_{0.6s}$	-	$D_{0.6s}$	-	$C''_{0.6s}$	-	$C'_{0.6s}$	-	$D_{0.6s}$	-
Parameter	**Unit**	**Value**	σ	**Value**	σ	**Value**	σ	**Value**	σ	**Value**	σ
t_{nom-ED}	[MJD2000]	10609.25	-	10609.25	-	10609.25	-	10609.25	-	10609.25	-
t_{nom-MA}	[MJD2000]	10789.25	-	10789.25	-	10789.25	-	10789.25	-	10789.25	-
t_0	[MJD2000]	11100.54	-	11100.54	-	11100.54	-	11100.54	-	11100.54	-
t_0 - t_{nom-MA}	[days]	311.29	-	311.29	-	311.29	-	311.29	-	311.29	-
T_1	[days]	248.18	$1.49 \cdot 10^{-5}$	300.00	$0.00 \cdot 10^{0}$	323.91	$1.86 \cdot 10^{-3}$	358.90	$2.33 \cdot 10^{-2}$	398.00	$5.63 \cdot 10^{-13}$
$T_{mission}$	[days]	739.46	$1.49 \cdot 10^{-5}$	791.29	$0.00 \cdot 10^{0}$	815.19	$1.86 \cdot 10^{-3}$	850.19	$2.33 \cdot 10^{-2}$	889.29	$9.98 \cdot 10^{-13}$
η_1	[-]	0.00	$1.07 \cdot 10^{-7}$	0.00	1.34E-16	0.32	$1.21 \cdot 10^{-3}$	0.13	$2.92 \cdot 10^{-4}$	0.39	$1.29 \cdot 10^{-9}$
V_∞	[m $\cdot$ s^{-1}]	0.00	$3.99 \cdot 10^{-3}$	0.00	$1.60 \cdot 10^{-13}$	1025.93	$7.74 \cdot 10^{0}$	639.35	$3.01 \cdot 10^{1}$	0.00	$1.14 \cdot 10^{-12}$
θ	[degree]	-3.85	$1.00 \cdot 10^{1}$	-14.11	$9.34 \cdot 10^{0}$	-15.00	$8.09 \cdot 10^{-4}$	-14.97	$1.26 \cdot 10^{-2}$	-10.10	$7.89 \cdot 10^{0}$
ϕ	[degree]	-2.04	$2.45 \cdot 10^{0}$	3.54	$4.34 \cdot 10^{0}$	-4.00	$1.18 \cdot 10^{0}$	-4.94	$2.42 \cdot 10^{0}$	-3.57	$1.25 \cdot 10^{0}$
ΔV_1	[m $\cdot$ s^{-1}]	4360.32	-	4360.32	-	4360.32	-	4360.32	-	4360.32	-
ΔV_2	[m $\cdot$ s^{-1}]	3639.94	-	3639.94	-	3639.94	-	3639.94	-	3639.94	-
ΔV_3	[m $\cdot$ s^{-1}]	1411.25	$3.89 \cdot 10^{-9}$	1411.25	$0.00 \cdot 10^{0}$	1519.26	$1.60 \cdot 10^{0}$	1453.49	$4.17 \cdot 10^{0}$	1411.25	$0.00 \cdot 10^{0}$
ΔV_7	[m $\cdot$ s^{-1}]	15588.49	$7.28 \cdot 10^{-4}$	9271.26	$0.00 \cdot 10^{0}$	6480.47	$1.58 \cdot 10^{0}$	4546.24	$4.23 \cdot 10^{0}$	2515.94	$8.38 \cdot 10^{-12}$
$\Sigma\Delta V$	[m $\cdot$ s^{-1}]	25000.00	-	18682.77	-	16000.00	-	13999.99	-	11927.46	-
$V_{\infty-EA}$	[m $\cdot$ s^{-1}]	26168.27	$2.55 \cdot 10^{-3}$	16166.76	$2.03 \cdot 10^{-12}$	16765.02	$1.46 \cdot 10^{1}$	9359.89	$1.67 \cdot 10^{0}$	6601.44	$3.07 \cdot 10^{-6}$
$r_{Sun-min}$	[AU]	0.99	$1.73 \cdot 10^{-9}$	1.00	$1.02 \cdot 10^{-13}$	1.00	$4.90 \cdot 10^{-7}$	1.01	$4.19 \cdot 10^{-6}$	1.02	$4.39 \cdot 10^{-14}$

Table C.7: Trajectory parameters for the selected propulsive abort trajectory solutions, when the abort occurs during the nominal Mars surface stay period (*MS-5*), at abort fraction 0.6.

Mission Scenario Solution											
		$C_{0.8s}^{'''}$	-	$C_{0.8s}^{''}$	-	$C_{0.8s}^{'}$	-	$C_{0.8s}$	-	$D_{0.8s}$	-
Parameter	**Unit**	**Value**	σ	**Value**	σ	**Value**	σ	**Value**	σ	**Value**	σ
t_{nom-ED}	[MJD2000]	10609.25	-	10609.25	-	10609.25	-	10609.25	-	10609.25	-
t_{nom-MA}	[MJD2000]	10789.25	-	10789.25	-	10789.25	-	10789.25	-	10789.25	-
t_0	[MJD2000]	11204.30	-	11204.30	-	11204.30	-	11204.30	-	11204.30	-
t_0 - t_{nom-MA}	[days]	415.05	-	415.05	-	415.05	-	415.05	-	415.05	-
T_1	[days]	163.70	$2.11 \cdot 10^{-4}$	193.38	$4.34 \cdot 10^{-5}$	226.96	$3.90 \cdot 10^{-6}$	265.53	$4.85 \cdot 10^{-11}$	294.00	$0.00 \cdot 10^{0}$
$T_{mission}$	[days]	758.75	$2.11 \cdot 10^{-4}$	788.43	$4.34 \cdot 10^{-5}$	822.01	$3.90 \cdot 10^{-6}$	860.58	$4.85 \cdot 10^{-11}$	889.05	$0.00 \cdot 10^{0}$
η_1	[-]	0.00	$3.39 \cdot 10^{-6}$	0.00	$6.29 \cdot 10^{-8}$	0.00	$7.54 \cdot 10^{-7}$	0.00	$1.46 \cdot 10^{-13}$	0.18	$4.00 \cdot 10^{-9}$
V_∞	[m · s^{-1}]	0.00	$9.63 \cdot 10^{-3}$	0.00	$1.70 \cdot 10^{-4}$	0.00	$1.12 \cdot 10^{-4}$	0.00	$1.59 \cdot 10^{-7}$	0.00	$4.44 \cdot 10^{-13}$
θ	[degree]	14.98	$3.43 \cdot 10^{0}$	-9.62	$7.81 \cdot 10^{0}$	10.43	$1.34 \cdot 10^{1}$	1.31	$7.58 \cdot 10^{0}$	-13.18	$1.29 \cdot 10^{1}$
ϕ	[degree]	1.22	$2.19 \cdot 10^{0}$	-4.46	$5.04 \cdot 10^{0}$	-0.29	$3.81 \cdot 10^{0}$	3.82	$3.67 \cdot 10^{0}$	-3.60	$3.20 \cdot 10^{0}$
ΔV_1	[m · s^{-1}]	4360.32	-	4360.32	-	4360.32	-	4360.32	-	4360.32	-
ΔV_2	[m · s^{-1}]	3639.94	-	3639.94	-	3639.94	-	3639.94	-	3639.94	-
ΔV_3	[m · s^{-1}]	1411.25	$2.18 \cdot 10^{-8}$	1411.25	$8.95 \cdot 10^{-12}$	1411.25	$5.49 \cdot 10^{-12}$	1411.25	$0.00 \cdot 10^{0}$	1411.25	$0.00 \cdot 10^{0}$
ΔV_7	[m · s^{-1}]	15588.49	$7.73 \cdot 10^{-3}$	10588.49	$5.93 \cdot 10^{-3}$	6588.49	$3.21 \cdot 10^{-5}$	3782.73	$1.18 \cdot 10^{-7}$	2530.03	$5.48 \cdot 10^{-12}$
$\Sigma\Delta V$	[m · s^{-1}]	25000.00	-	20000.00	-	16000.00	-	13194.25	-	11941.54	-
$V_{\infty-EA}$	[m · s^{-1}]	30791.61	$6.09 \cdot 10^{-3}$	22897.82	$9.90 \cdot 10^{-3}$	15625.43	$6.20 \cdot 10^{-3}$	9360.00	$5.63 \cdot 10^{-9}$	6645.60	$7.36 \cdot 10^{-6}$
$r_{Sun-min}$	[AU]	0.99	$4.23 \cdot 10^{-8}$	1.00	$1.15 \cdot 10^{-8}$	1.01	$9.77 \cdot 10^{-10}$	1.01	$4.73 \cdot 10^{-14}$	1.02	$1.48 \cdot 10^{-14}$

Table C.8: Trajectory parameters for the selected propulsive abort trajectory solutions, when the abort occurs during the nominal Mars surface stay period (*MS-5*), at abort fraction 0.8.

Bibliography

[1] D. Rapp, *Human Missions to Mars: Enabling Technologies for Exploring the Red Planet*, Springer Praxis Books (Springer International Publishing, 2016).

[2] P. Wooster, R. Braun, J. Ahn, and Z. Putnam, *Trajectory Options for Human Mars Missions,* in *AIAA/AAS Astrodynamics Specialist Conference and Exhibit* (Keystone, Colorado, USA, 2006).

[3] B. Mattfeld, C. Stromgren, H. Shyface, D. R. Komar, W. Cirillo, and K. Goodliff, *Trades Between Opposition and Conjunction Class Trajectories for Early Human Missions to Mars*, Tech. Rep. (NASA, 2014).

[4] D. F. Landau and J. M. Longuski, *Comparative Assessment of Human Mars Mission Technologies and Architectures,* Acta Astronautica **65**, 893 (2009).

[5] D. V. Byrnes, J. M. Longuski, and B. Aldrin, *Cycler orbit between Earth and Mars,* Journal of Spacecraft and Rockets **30**, 334 (1993).

[6] D. F. Landau and J. M. Longuski, *Trajectories for Human Missions to Mars, Part I: Impulsive Transfers,* Journal of Spacecraft and Rockets **43**, 1035 (2006).

[7] M. Okutsu, D. F. Landau, B. A. Rogers, and J. M. Longuski, *Low-thrust Roundtrip Trajectories to Mars with One-synodic-period Repeat Time,* Acta Astronautica **110**, 191 (2015).

[8] L. M. Burke, R. D. Falck, and M. L. McGuire, *Interplanetary Mission Design Handbook: Earth-to-Mars Mission Opportunities 2026 to 2045*, Tech. Rep. (2010).

[9] D. Landau, J. Longuski, and B. Aldrin, *Continuous Mars Habitation with a Limited Number of Cycler Vehicles,* Journal of the British Interplanetary Society **60**, 122 (2007).

[10] D. F. Landau and J. M. Longuski, *Human Exploration of Mars via Earth-Mars Semicyclers,* Journal of Spacecraft and Rockets **44**, 203 (2007).

[11] P. Penzo and K. Nock, *Earth-Mars Transportation Using Stop-Over Cyclers,* in *AIAA/AAS Astrodynamics Specialist Conference and Exhibit* (Monterey, California, USA, 2002).

[12] A. S. W. Thomas, C. A. Ocampo, and D. F. Landau, *A Crewed Mars Exploration Architecture Using Flyby and Return Trajectories,* American Astronomical Society Prepint (2015).

[13] D. Landau, *Comparative Assessment of Human Missions to Mars*, Tech. Rep. (Purdue University, USA, 2009).

[14] D. F. Landau and J. M. Longuski, *Trajectories for Human Missions to Mars, Part II: Low-thrust Transfers,* Journal of Spacecraft and Rockets **43**, 1043 (2006).

[15] R. G. Merrill, N. Strange, Min Qu, and N. Hatten, *Mars Conjunction Crewed Missions with a Reusable Hybrid Architecture,* in *2015 IEEE Aerospace Conference* (Big Sky, MT, USA, 2015).

[16] C. L. Moore, *Technology Development for Human Exploration of Mars,* Acta Astronautica **67**, 1170 (2010).

[17] R. H. Frisbee, *Advanced Space Propulsion for the 21st Century,* Journal of Propulsion and Power **19**, 1129 (2003).

[18] J. Lissauer and I. de Pater, *Fundamental Planetary Science: Physics, Chemistry and Habitability* (Cambridge University Press, 2013).

[19] J. Wilson, *Nasa: Mars Overview,* Webpage (2015), http://www.nasa.gov/mission_pages/mars/overview/index.html. Date of access: January 09, 2020.

[20] M. Pontani and B. A. Conway, *Optimal Trajectories for Hyperbolic Rendezvous with Earth–Mars Cycling Spacecraft,* Journal of Guidance, Control, and Dynamics **41**, 360 (2018).

[21] Wikipedia, *List of crewed Mars mission plans,* Webpage (2019), https://en.wikipedia.org/wiki/List_of_crewed_Mars_mission_plans. Date of access: January 09, 2020.

[22] Wikipedia, *SpaceX Mars transportation infrastructure,* Webpage (2020), https://en.wikipedia.org/wiki/SpaceX_Mars_transportation_infrastructure. Date of access: January 23, 2020.

[23] SpaceX, *Spacex: Starship,* Webpage (2020), https://www.spacex.com/starship. Date of access: January 09, 2020.

[24] L. E. George and L. D. Kos, *Interplanetary Mission Design Handbook: Earth-to-Mars Mission Opportunities and Mars-Earth Return Opportunities 2009-2024*, Tech. Rep. (1998).

[25] J. Wertz, *Mission Geometry: Orbit and Constellation Design and Management: Spacecraft Orbit and Attitude Systems*, Space Technology Library (Springer, Netherlands, 2002).

[26] P. Patole, *Literature Study (AE4020): Interplanetary Trajectory Design for a Reconnaissance Human Mars Mission,* Report (2018).

[27] J. Melman, *Trajectory Optimization for a Mission to Neptune and Triton*, Master's thesis, Delft University of Technology, The Netherlands (2007).

[28] ESA, *Rosetta Media factsheet,* Webpage (2014), https://www.esa.int/Science_Exploration/Space_Science/Rosetta/Rosetta_Media_factsheet. Date of access: January 11, 2020.

[29] K. Wakker, *Fundamentals of Astrodynamics* (TU Delft Library, Delft, The Netherlands, 2015).

[30] D. De La Torre Sangrà and E. Fantino, *Review of Lambert's Problem,* in *25th International Symposium on Space Flight Dynamics* (Munich, Germany, 2015).

[31] D. Izzo, *Revisiting Lambert's problem,* Celestial Mechanics and Dynamical Astronomy **121** (2014).

[32] R. H. Gooding, *A procedure for the solution of Lambert's orbital boundary-value problem,* Celestial Mechanics and Dynamical Astronomy **48**, 145 (1990).

[33] T. A. Leite Pinto Secretin, *Design of a Combinatorial Tool for Preliminary Space Mission Analysis applied to the GTOC2 Problem*, Master's thesis, Delft University of Technology, The Netherlands (2012).

[34] P. Musegaas, *Optimization of Space Trajectories including Multiple Gravity Assists and Deep Space Maneuvers*, Master's thesis, Delft University of Technology, The Netherlands (2012).

[35] S. Molenaar, *Optimization of Interplanetary Trajectories with Deep Space Maneuvers - Model Development and Application to a Uranus Orbiter Mission*, Master's thesis, Delft University of Technology, The Netherlands (2009).

[36] Delft University of Technology, *TU Delft Astrodynamic Toolbox documentation: Trajectory Design,* Webpage (2018), https://tudat.tudelft.nl/tutorials/tudatFeatures/astroTools/trajectoryDesign. Date of access: January 16, 2020.

[37] A. Nardi, *Orbit Modelling of Galilean Moons Flybys*, Master's thesis, Delft University of Technology, The Netherlands (2017).

[38] J. Spaans, *Improving Global Optimization Methods for Low Thrust Trajectories*, Master's thesis, Delft University of Technology, The Netherlands (2009).

[39] A. Pagano, *Global Launcher Trajectory Optimization for Lunar Base Settlement*, Master's thesis, Delft University of Technology, The Netherlands (2010).

[40] R. Oldenhuis, *Trajectory Optimization of a Mission to the Solar Bow Shock and Minor Planets*, Master's thesis, Delft University of Technology, The Netherlands (2010).

[41] Q. Zhang and H. Li, *MOEA/D: A Multiobjective Evolutionary Algorithm Based on Decomposition,* IEEE Transactions on Evolutionary Computation **11**, 712 (2007).

[42] H. Li and Q. Zhang, *Multiobjective Optimization Problems With Complicated Pareto Sets, MOEA/D and NSGA-II,* IEEE Transactions on Evolutionary Computation **13**, 284 (2009).

[43] PaGMO Development Team, *Multi-objective Evolutionary Algorithm by Decomposition (MOEA/D-DE),* Webpage (2020), https://esa.github.io/pagmo2/docs/cpp/algorithms/moead. Date of access: January 15, 2020.

[44] R. Wang, *An Improved Nondominated Sorting Genetic Algorithm for Multiobjective Problem,* Mathematical Problems in Engineering **2016** (2016), 10.1155/2016/1519542.

[45] PaGMO Development Team, *Non dominated sorting genetic algorithm (NSGA-II),* Webpage (2020), https://esa.github.io/pagmo2/docs/cpp/algorithms/nsga2. Date of access: January 15, 2020.

[46] K. Deb, A. Pratap, S. Agarwal, and T. Meyarivan, *A fast and elitist multiobjective genetic algorithm: NSGA-II,* IEEE Transactions on Evolutionary Computation **6**, 182 (2002).

[47] J. Cornelisse, H. Schöyer, and K. Wakker, *Rocket Propulsion and Spaceflight Dynamics*, Aerospace Engineering Series (Pitman, 1979).

[48] J. Barthel and N. Sarigul-Klijn, *A review of radiation shielding needs and concepts for space voyages beyond Earth's magnetic influence,* Progress in Aerospace Sciences **110**, 100553 (2019).

[49] J. W. Norbury, T. C. Slaba, S. Aghara, F. F. Badavi, S. R. Blattnig, M. S. Clowdsley, L. H. Heilbronn, K. Lee, K. M. Maung, C. J. Mertens, J. Miller, R. B. Norman, C. A. Sandridge, R. Singleterry, N. Sobolevsky, J. L. Spangler, L. W. Townsend, C. M. Werneth, K. Whitman, J. W. Wilson, S. X. Xu, and C. Zeitlin, *Advances in space radiation physics and transport at NASA,* Life Sciences in Space Research **22**, 98 (2019).